Robert L. Price
W. Gray (Jay) Jerome
Editors

Basic Confocal Microscopy

Springer

Basic Confocal Microscopy

Robert L. Price • W. Gray (Jay) Jerome
Editors

Basic Confocal Microscopy

Springer

Editors
Robert L. Price
Department of Cell and
Developmental Biology
School of Medicine
University of South Carolina
6439 Garner's Ferry Road
Columbia, SC
USA
Bob.Price@uscmed.sc.edu

W. Gray (Jay) Jerome
Department of Pathology
Vanderbilt University Medical Center
U-2206 MCN, 1161 21st Avenue,
South Nashville, TN
USA
jay.jerome@vanderbilt.edu

ISBN 978-0-387-78174-7 e-ISBN 978-0-387-78175-4
DOI 10.1007/978-0-387-78175-4
Springer New York Dordrecht Heidelberg London

Library of Congress Control Number: 2011925553

Printed on acid-free paper

Springer is part of Springer Science+Business Media (www.springer.com)

Preface

Biological confocal microscopy is still a relatively young field. Most researchers in the field would date the modern era of biological confocal microscopy from the 1985 description of a particularly useful confocal design published by White and Amos in the Journal of Cell Biology. Since that time, the use of confocal microscopes by biologists has increased phenomenally, with new converts joining the ranks daily; many with little or no previous microscopy training. For this reason, in 2001 when we were asked to organize a 1 day session on "basic confocal microscopy" for attendees at the Southeastern Microscopy Society annual meeting in Clemson, SC, we decided to focus not only on the confocal microscope itself, but also on ancillary subjects that are critical for getting the most from confocal microscopy.

Our initial effort seemed to meet a growing need to train new students, technologists, and faculty wishing to use confocal microscopy in their research. Evidence for this need is that each year since 2001, we have been invited by several meeting organizers and microscopy core facility Directors to present our take on what is important to use confocal microscopy successfully for biological exploration. In 2005, we also began teaching a 5-day intensive, hands-on workshop at the University of South Carolina each year. As that course evolved, we invited various colleagues to help with the course. This book is a direct outgrowth of that course and follows the general structure of the didactic portion of the course. In line with the course philosophy, we have not attempted to cover each topic in depth. However, we have maintained a focus on basic information and we have endeavored to cover information that is important for designing, carrying out, and interpreting the results of basic confocal microscopy-based biological experiments completely. We were very fortunate that two of the other course instructors, Drs. Ralph Albrecht and Tom Trusk, have provided chapters for this volume and have embraced the overall philosophy of presenting a basic knowledge base in a complete but concise manner.

Although the forums have been different and the course lengths have varied anywhere from 1 to 5 days, we have always based the workshops on the original concept that there is a group of core issues that must be understood before one can efficiently get the best results from the use of a confocal microscope. The early chapters in this book address these core issues and it is not by accident that after an initial introductory chapter on confocal microscopy, the chapters describing the components of the confocal microscope and how to set the various operating

parameters correctly are located toward the end of the book. Without a well-designed research plan and properly prepared specimen, the data collected by the microscope will not be optimum. Thus, we have devoted Chaps. 2 and 3 to fluorescence and understanding the use of fluorescent microscopy, and Chaps. 4 and 5 to specimen preparation and labeling strategies. These chapters are essential since regardless of the quality of the confocal microscope, if the sample is not prepared properly, the data collected will not be optimal.

Most modern confocal microscope images are digital. Thus, many of the basic operating parameters for confocal microscopy involve setting up the analog to digital conversion of specimen information. It is essential that a confocal microscope operator have a thorough understanding of how digital images for scientific purposes should be collected and analyzed. For this reason, following the chapters on specimen preparation, Chaps. 6 and 7 discuss digital microscopy with respect to confocal imaging.

Although it might seem odd that a book on confocal microscopy contains only two chapters directly devoted to the actual operation of the confocal microscope, these chapters are packed with practical information and, taking advantage of the preliminary information presented in preceding chapters, they provide all that is necessary to begin doing confocal microscopy and optimizing the information obtained. After Chaps. 8 and 9, which discuss the types of confocal instruments and setting up proper operating parameters, the final set of chapters provide information on the 3D analysis and reconstruction of data sets and some ethical considerations in confocal imaging, and provide some resources that we have found useful in our own use of confocal microscopes. After mastering the basic information presented in this book, these resources are great guides for continuing your education into more advanced forms of confocal microscopy.

This book has benefited from our association with numerous colleagues who have challenged and informed us. In particular, numerous debates with one of the course instructors, Dr. John MacKenzie, Jr., have helped hone the information on digital image processing to the most important concepts. We are also grateful to Drs. K. Sam Wells, David Piston, and John Fuseler for stimulating and challenging conversations that have made us better microscopists. We also owe a huge debt to the many students over the years whose enthusiasm and questions have guided our decisions regarding what to include and exclude from the workshops and chapters in this book. We are also thankful to the many companies that have provided resources and applications experts who have significantly enhanced our hands-on workshops at the University of South Carolina.

Finally, we must thank our lab members and families for not only putting up with our obsession for microscopy but also encouraging us in our pursuits.

Columbia, SC Robert L. Price
Nashville, TN W. Gray (Jay) Jerome

List of Abbreviations

2D	Two-dimensional
3D	Three-dimensional
AOBS	Acousto-optical beam splitter
AOTF	Acousto-optical tunable filter
A to D	Analog-to-digital conversion
AVI	Audio-video interleave
BFP	Blue fluorescent protein
CCD camera	Charge-coupled device camera
CDRs	Complementarity-determining regions
CFP	Cyan fluorescent protein
CLAHE	Contrast limited adaptive histogram equalization
CMOS	Complementary metal oxide semiconductor
CMYK	Cyan, magenta, yellow, and black images
CSLM	Confocal scanning laser microscope
CTF	Contrast transfer function
Cy	Cyanine
DABCO	1,4-Diazabicyclo[2,2,2]octane
DIC	Differential interference contrast
DPI	Dots per inch
EMCCD	Electron-multiplied charge-coupled device
EGFP	Enhanced green fluorescent protein
FITC	Fluorescein isothiocyanate
FLIM	Fluorescent lifetime imaging
FRAP	Fluorescent recovery after photobleaching
FRET	Förster resonant energy transfer
FWHM	Full-width half maximum
GFP	Green fluorescent protein
HeNe	Helium–neon laser

IgA	Immunoglobulin class A
IgD	Immunoglobulin class D
IgE	Immunoglobulin class E
IgG	Immunoglobulin class G
IgM	Immunoglobulin class M
IR	Infrared
JPEG	Joint photographic experts group
LASER	Light amplification by stimulated emission of radiation
LED	Light-emitting diode
LM	Light microscopy
LUTs	Look-up tables
MPEG	Moving picture experts group
MSDS	Material safety data sheet
NAD(H)	Nicotinamide adenine dinucleotide
NADPH	Nicotinamide adenine dinucleotide phosphate-oxidase
NA	Numerical aperture
NPG	*n*-propyl gallate
PEG	Polyethylene glycol
PerCP	Peridinin-chlorophyll protein
PDF	Portable document format
PMT	Photomultiplier tube
PPD	*p*-Phenylenediamine
PSF	Point-spread function
PPI	Pixels per inch
RESEL	Resolvable element
RFP	Red fluorescent protein
RGB	Red, green, and blue images
RGBA	Red, green, blue, alpha images
ROI	Region of interest
RSOM	Real-time scanning optical microscope
scFv	Single-chain variable fragment
TEM	Transmission electron microscopy
Tf	Transferrin
TIF(F)	Tagged image file format
TRITC	Tetramethylrhodamine-isothiocyanate
TSRLM	Tandem scanning reflected light microscope
UV	Ultraviolet
VaLaP	Vaseline, lanolin, and petroleum jelly
V_H	Variable heavy chain
V_L	Variable light chain
WGA	Wheat germ agglutinin
YFP	Yellow fluorescent protein

Contents

Contributors

Ralph M. Albrecht
Department of Animal Sciences; Pediatrics; and Pharmaceutical Sciences, University of Wisconsin – Madison, 1046 Animal Science Bldg., 1675 Observatory Drive, Madison, WI 53706, USA
albrecht@ansci.wisc.edu

John Fuseler
Department of Cell and Developmental Biology, School of Medicine, University of South Carolina, 6439 Garner's Ferry Road, Columbia, SC 29208, USA
John.Fuseler@uscmed.sc.edu

W. Gray (Jay) Jerome
Department of Pathology, Vanderbilt University Medical Center, U-2206 MCN, 1161 21st Avenue, South Nashville, TN 37232-2561, USA
jay.jerome@vanderbilt.edu

Julie A. Oliver
Department of Biological Sciences, University of Wisconsin – Milwaukee, Lapham Hall N209, 3209 N. Maryland Avenue, Milwaukee, WI 53201, USA
joliver@uwm.edu

Robert L. Price
Department of Cell and Developmental Biology, School of Medicine, University of South Carolina, 6439 Garner's Ferry Road, Columbia, SC 29208, USA
Bob.Price@uscmed.sc.edu

Thomas C. Trusk
Department of Regenerative Medicine and Cell Biology, Medical University of South Carolina, BSB 643, 173 Ashley Avenue, Charleston, SC 29425, USA
truskt@musc.edu

Chapter 1
Introduction and Historical Perspective

Robert L. Price and W. Gray (Jay) Jerome

Keywords Dichroic • Gamma • Refractive index mismatch • Resolution • Signal-to-noise ratio

1.1 Why an Introductory Text on Confocal Microscopy?

During our combined 35 plus years of operating confocal microscopes and managing core microscopy facilities, and through teaching our Basic Confocal Microscopy Workshop at several venues, we have found that students and technicians who are novice users of confocal microscopes are often instructed by their mentors to go to the confocal system and collect some images. Often the implied message is that it should be easy and quick since it is only a microscope. Unfortunately, all too often the advisor of the student or supervisor of the technician does not have a full understanding of the complexity of a confocal microscope. Unless these novice users are in a situation where others have the time and knowledge to properly train them, their initial efforts often amount to an exercise in futility because key parameters are not properly considered. This leads to specimens that are not prepared properly and a lack of understanding of how to operate the confocal microscope in a way that maintains the fidelity of the specimen information. In too many instances, this lack of user training is exacerbated further because there is little or no daily oversight of the setup and maintenance of the microscope. In this combined scenario, neither the experimental preparation nor the microscopes are capable of producing the highest quality information.

Good confocal microscopy is obviously dependent upon proper specimen preparation and the correct setup of various microscope parameters. However, even if an excellent confocal image is collected there is often a poor understanding of how to

R.L. Price (✉)
Department of Cell and Developmental Biology, School of Medicine, University of South Carolina, 6439 Garner's Ferry Road, Columbia, SC 29208, USA
e-mail: Bob.Price@uscmed.sc.edu

R.L. Price and W.G. (Jay) Jerome (eds.), *Basic Confocal Microscopy*,
DOI 10.1007/978-0-387-78175-4_1,

properly enhance and analyze two-dimensional (2-D) and 3-D confocal images. There is an abundance of good image processing and analysis software available to the user. However, these robust programs also provide the capability of inadvertently degrading the image information. A lack of understanding of basic digital imaging and image processing theory frequently results in improper image processing in 2-D programs, such as Image J (NIH freeware), Photoshop (Adobe Systems, Inc., San Jose, CA), Metamorph (Molecular Devices, Sunnyvale, CA), or others and in more advanced 3-D volumetric programs such as AMIRA (Visage Imaging, Carlsbad, CA) or Voxblast (VayTek, Inc., Fairfield, IA).

The goal of this book is to provide beginning and intermediate users of confocal microscopes a resource that can be used to address many of the frequently asked questions concerning confocal imaging and to provide a strong foundation for maximizing the data obtained from experiments involving confocal microscopy. While most of the information is directly relevant to single photon scanning laser systems, much of the information also applies to spinning disk and multiphoton confocal systems. In several chapters, specific comparisons of the technology that differentiates these systems will be made and advantages and disadvantages of each will be presented. The information presented will also provide the background information necessary when moving forward to complex imaging protocols such as Forster (or Fluorescent) resonant energy transfer (FRET), fluorescence recovery after photobleaching (FRAP), fluorescent lifetime imaging (FLIM), and other advanced techniques.

1.2 Historical Perspective

It has long been recognized by microscopists that as the thickness of the specimen increases, light emerging from scattering objects above and below the focal plane of the microscope degrade the quality of the image. This occurs primarily because of reduced image contrast. The loss of contrast is caused by impinging light produced from the out-of-focus planes. Like turning on the lights in a movie theater, this stray light reduces the signal-to-noise (S/N) ratio and obscures important image details. The various factors affecting the axial resolution (ability to distinguish two small objects as separate and distinct along the axial axis) were explored by Berek in 1927. In Berek's analysis, the three key elements affecting image quality were (1) spreading of the light beam emerging from objects in the specimen, (2) the magnification of the image, and (3) the sensitivity of the detection system. For Berek, the detection system was the observer's eye. However, in the modern age of microscopy the eye has been replaced with more sensitive detectors. With regard to Berek's item 2, microscopists have always worked with the highest magnification required for maintaining image data fidelity. This leaves the spread of out-of-focus light into the image plane as the last of Berek's parameters that needs to be minimized to obtain good axial resolution. Obviously, if one could limit the projection of out-of-focus light onto the image then a significant gain in resolution should be achieved.

The removal of the obscuring out-of-focus light is precisely what the confocal microscope is designed to do and the subsequent gain in axial resolution remains the biggest advantage of confocal microscopy. However, as described in subsequent chapters, several other advantages accrue from the confocal design, including increases in lateral resolution.

The first confocal microscope is generally credited to Marvin Minsky (1988). In his 1957 patent application, Minsky described a microscope in which the typical widefield illumination arrangement is replaced with one in which a point source is focused to a small spot within the specimen. Light arising from the illuminated spot is focused by the objective lens to a small spot at the image plane. Thus, a point source of light is in conjugate focus (confocal) at the specimen and at the image plane (Fig. 1.1a). Placing a small pinhole aperture made of an opaque material at the image plane permits only the light coming from the focal point of the specimen to pass to the detector. In contrast, light coming from above and below the plane of focus will not be in focus at the image plane and will be rejected by the opaque material surrounding the pinhole. This confocal setup can also be achieved in an epi-illumination setup (Fig. 1.1b). The confocal arrangement dramatically improves contrast by removing the out-of-focus light originating above and below the focal plane. The arrangements diagramed in Fig. 1.1 are not the only possible designs. Since its inception, various other designs have been introduced for creating the required confocality of focus at the specimen and image planes.

Of course, a single point within a specimen does not provide much information about the specimen. In order to acquire full details across the lateral focal plane of the specimen, the spot must be scanned across the image and the image information collected sequentially. In Minsky's original design, the scanning was produced by translating the specimen laterally. This method was slow and prone to vibration, both of which presented problems for biological work. A notable advance for the use of point scanning instruments in biology was made in the 1980s with the development of the ability to raster the illumination across the specimen rather than translating the stage. This allowed for faster scan rates without the introduction of vibration. The publication of images of biological samples using the beam-scanning instrument (White et al. 1987) spurred an extreme interest in confocal microscopy for biological research.

Arguably, the development of beam scanning along with concurrent advancements in laser technology, fluorescent labels, lens design, and computer processing really set the stage for the rapid deployment of laser scanning confocal microscopy as a key tool for cell biological research. However, laser scanning instruments are not the only mechanism for implementing confocal microscopy. A parallel development occurred based on Paul Nipkow's (1884) invention of a method for converting an optical image into an electrical signal that could be transmitted over a cable. Nipkow's technique converted the 2-D image information into a 1-D serial signal by scanning the image using a spinning wheel with precisely placed rectangular holes. The holes were arranged in a spiral pattern around the wheel such that when the wheel was spun the small areas being sampled changed. The moving holes filled in the gaps between the initially sampled regions. In 1967, Egger and Petráň

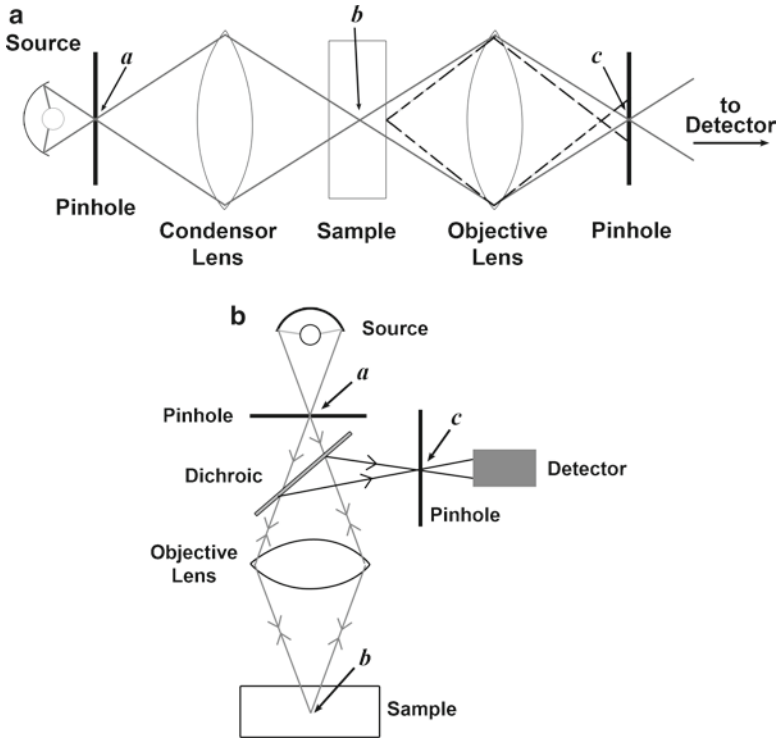

Fig. 1.1 Optical train for confocal microscope in conventional (**a**) and epi-illumination setups (**b**). The light path of the confocal beam is represented by the *gray lines*. In the conventional arrangement, light from the photon source is focused onto the entrance pinhole (***a***). This pinhole provides a bright focused point source. Light from this point source is collected by the condenser lens and focused to a spot (***b***) within the sample. The light emerging from the focused spot within the specimen is collected by the objective lens and focused at a second (exit) pinhole (***c***). Points a, b, and c are in conjugate focus (confocal). The path of light emerging outside of the focal point b is represented by the *dotted black lines* and arrives at the exit pinhole out of focus. Thus, most of this light is rejected and not transmitted to the detector. In an epi-illumination setup (**b**), the objective lens acts as both the condenser and objective lens. Light returning from the specimen is diverted by the dichroic (dichromatic beam splitter) and this diverted light (*dark gray lines*) is focused on the exit pinhole (*dark gray lines*). As with the conventional arrangement, light from above or below the focal point in the specimen arrives at the pinhole out of focus (not depicted) and so is rejected. Conventional wide field fluorescence systems lack the pinhole so all out-of-focus light becomes a component of the final image as shown in Fig. 1.3

(Petrán et al. 1968) modified the design of the Nipkow disk by including multiple spirals in a single wheel. They then used the spinning disk to provide both illuminating and imaging pinholes for a confocal microscope.

As with point scanning microscopes, over the years several different arrangements have been designed for spinning-disk confocal microscopes. Figure 1.2 illustrates one such arrangement for an epi-illumination system. In this design, light is passed through the pinholes, directed onto the specimen and the image light

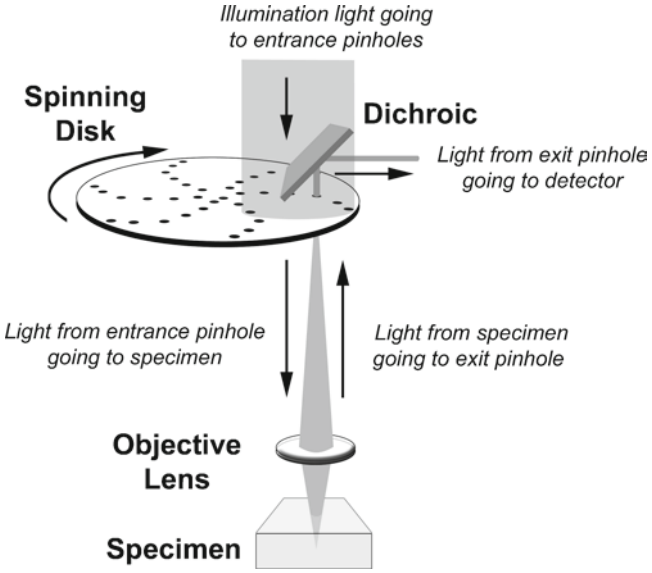

Fig. 1.2 Design of an epi-illumination spinning-disk confocal microscope. Although multiple areas of the specimen will be illuminated at once, to simplify the diagram only light from one pinhole is depicted. As in Fig. 1.1 only focused light reaches the detector. Since light emitted from all pinholes reaches the detector simultaneously image collection is rapid, but resolution and often overall signal is compromised in spinning-disk systems as discussed in Chap. 8

passes back through conjugate pinholes in the disk as it spins. By including sufficient numbers of pinholes and spinning the disk at a suitable speed, a real-time confocal image of the specimen can be obtained that can be viewed by eye or collected directly by a detector. One of the key benefits of this type of confocal microscope compared to laser scanning instruments is that spinning disks allow much faster image acquisition times. Further information on the design and use of spinning disk confocal systems is given in Chap. 8.

The Minsky and Petrán microscopes define the two principal implementations of confocal microscopy; the sequential scan (point scan) and spinning-disk (multipoint scan, area scan) microscopes, respectively. As one might imagine, however, variations on these two schemes have been designed to overcome specific limitations of each for specific applications. A nice review of some of these implementations is provided by Shinya Inoué (2006). Of course, the full power of imaging a thin plane within a specimen is best exploited by scanning multiple thin planes in succession and reconstructing a high-resolution 3-D map of the specimen by stacking the 2-D images. As described in Chaps. 6–10, key advances in digital imaging and improved computer power over the last two decades now provide a convenient method of capturing, storing, and displaying sequentially acquired image information in both 2-D and 3-D formats.

1.3 Is the Confocal Hype Legitimate?

Why has confocal microscopy revolutionized the way many laboratories image their samples? The simple answer is that the use of specific wavelengths of light, typically emitted from a laser, and the use of pinholes to eliminate out-of-focus light as described above, has significantly increased our ability to resolve and co-localize small structures and molecules in high contrast images. An example of this is shown in Fig. 1.3. Widefield images (Fig. 1.3a) contain large amounts of out-of-focus light that significantly deteriorates image resolution and contrast making it difficult to observe specific structures and detail. A confocal image (Fig. 1.3b) from the same region of the same sample clearly shows increased resolution and contrast making it much easier to discern the structures present in the section of heart muscle shown.

With the development of rapid computing capabilities and high density media for storage, confocal imaging technology grew rapidly. These advancements made it possible to collect a large number of optical sections through a sample and to rapidly reconstruct them into a high resolution high contrast projection of the sample where all detail was in focus (Fig. 1.4). Further advances in imaging software have made the use of 3-D data sets an important element in studying most biological systems. Many of these advances are discussed in subsequent chapters of this book. However, both confocal imaging hardware and digital imaging software technologies are advancing at a very rapid pace making it essential that researchers stay vigilant in determining how confocal imaging may benefit their individual research programs.

The answer to the above question about confocal hype is obviously a resounding yes. Even though commercially available systems have been available for less than 30 years, and well equipped confocal systems often cost $500K or more and can be expensive to maintain, the thousands of publications that utilize confocal imaging and the large range of applications from biological to material samples imaged clearly indicates that confocal microscopy has revolutionized the way many laboratories perform their research. Recent advances including spectral imaging, new fluorochromes and lasers, and increased imaging speed and resolution all indicate that confocal imaging will continue to be an important component of the imaging sciences in many fields of investigation.

1.4 The Ten Commandments of Confocal Imaging

As part of our Basic Confocal Microscopy Workshop we often have students create a list of Confocal Commandments, which are comprised of statements we make that might be considered unequivocal in nature. The following is a list of some of these commandments that we have collected over the years that need to be considered by all undertaking the task of learning and using confocal microscopy as a research tool. These commandments establish some general guidelines to consider

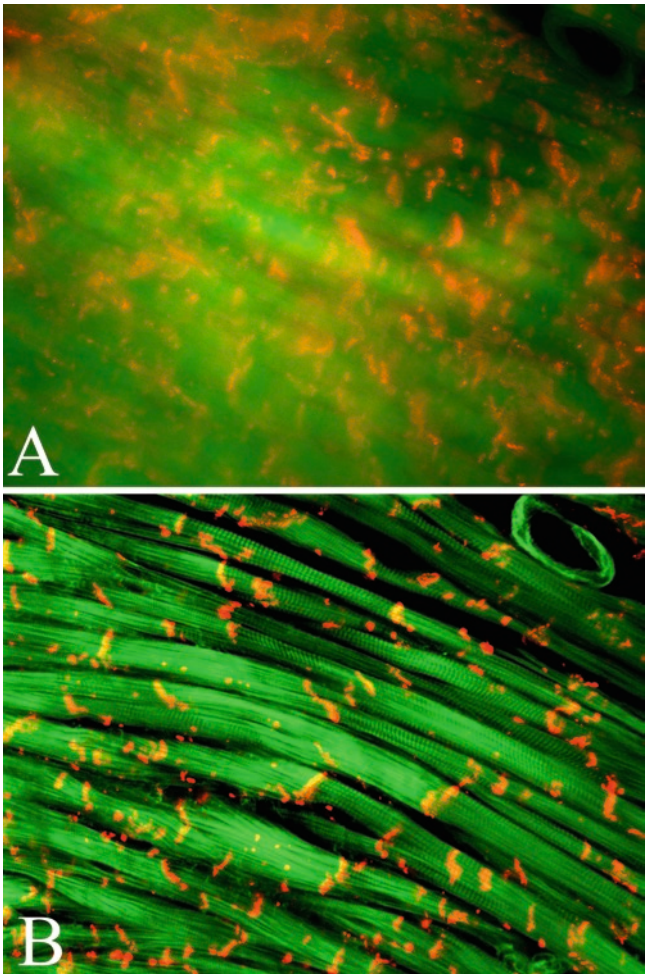

Fig. 1.3 Widefield fluorescent (*top*) and single photon confocal scanning laser microscope (CSLM) (*bottom*) images taken from a 100-μm thick vibratome section of mouse heart that has been stained for f-actin (*green*) and connexin 43 (*red*). In the widefield image out-of-focus light that contributes to the formation of the image significantly decreases the resolution and contrast of the image. Use of the pinhole in the confocal image to remove the out-of-focus light results in an image of much higher contrast and resolution as shown by the striated pattern of the myocyte sarcomeres and distinct cell: cell junctions labeled by the connexin 43 antibody

when using a confocal microscope, preparing a specimen, and handling digital images, which are all integral and equal parts of operating a confocal microscope. In fact, how we process and present the images we collect is every bit as important as how we do the initial data collection. The various chapters in this book expand on the basic principles that lead to these commandments.

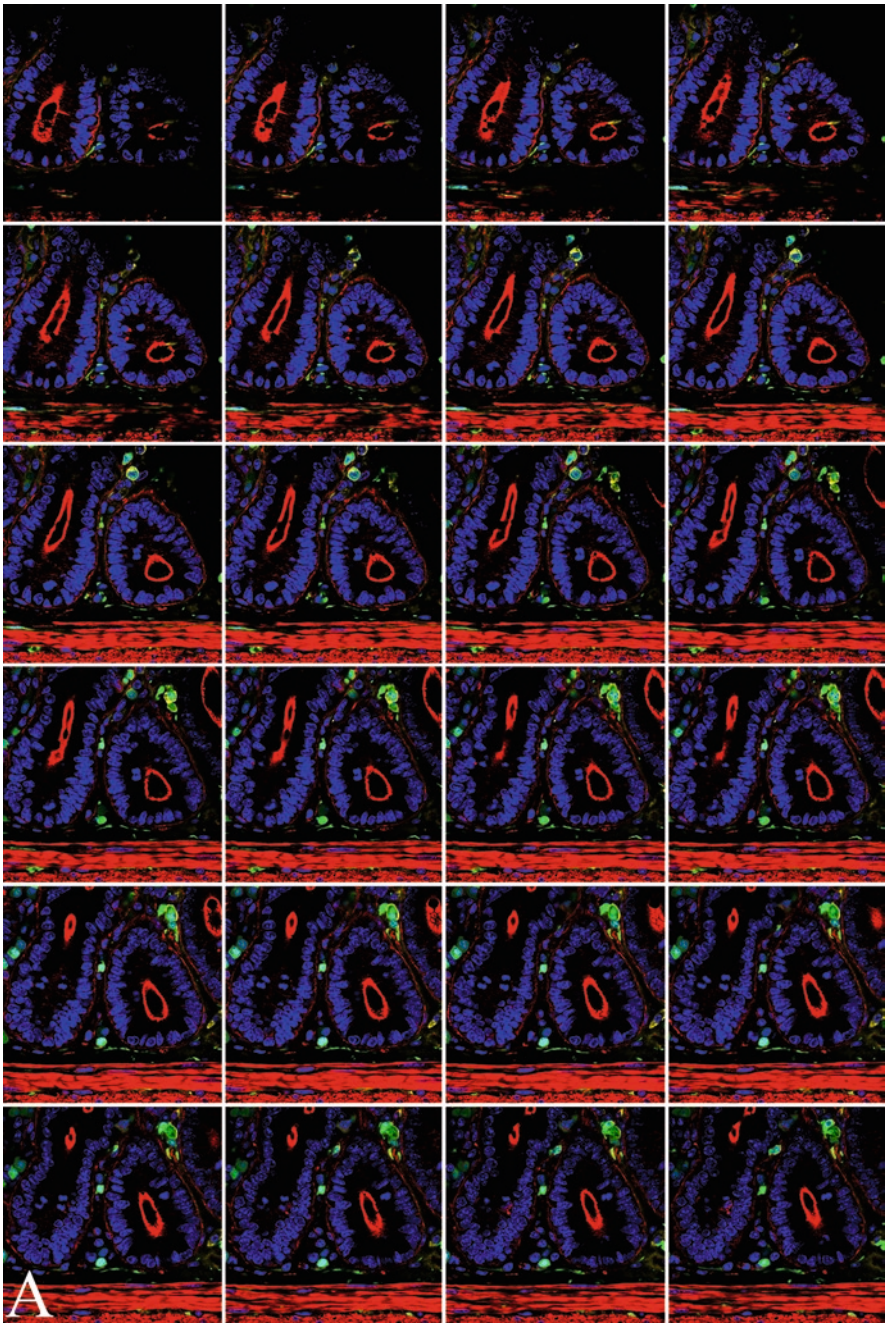

Fig. 1.4 Confocal optical sections (Z-series) through a section of intestine stained with multiple fluorescent dyes. Images were collected at 1 μm intervals through a 50-μm thick section of tissue and every other section (2 μm intervals) are shown in (**a**). All sections were then projected into a single composite image as shown in (**b**). The procedures for collection and projection of data sets are discussed in later chapters. *Blue* – DAPI stain for nuclei, *red* – f-actin stain, *green* – green fluorescent protein, *yellow* – mRNA stabilizing protein

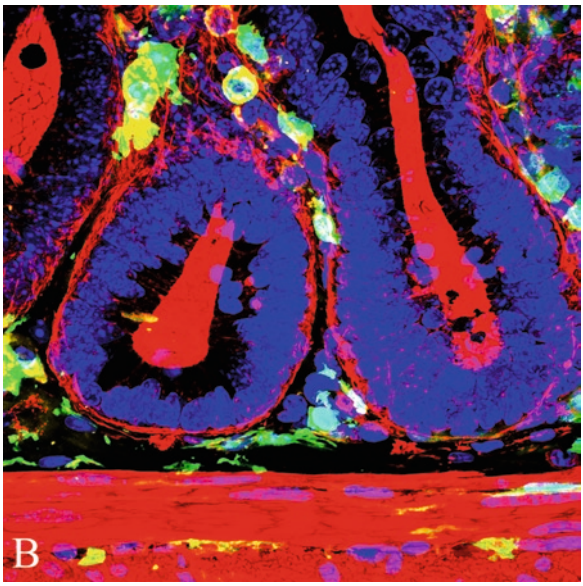

Fig. 1.4 (continued)

Our Ten Commandments of Confocal Imaging are:

1.4.1 The Perfect Microscope, and the Perfect Microscopist, Does Not Exist

As we discuss in great detail, physical factors in the design of microscopes result in image aberrations that affect the amount of light that can be collected and limits the resolution of images. Although these defects can be minimized by selection of optimal microscope components, they cannot be totally eliminated. Even with the best microscope optics available, the physical nature of light and refractive index mismatch as the light passes through the several interfaces in the optical path of the microscope and specimen will result in image defects. These defects result in the loss of signal and resolution.

Even with optimal image quality, the human element of understanding image collection and data interpretation is often a limiting factor in getting the most out of a microscope. North (2006), in a feature article for the *Journal of Cell Biology*, noted that all data are subject to interpretation and that in microscopy a great number of errors are introduced in complete innocence. A common example is the frequent interpretation that the appearance of the yellow color in a sample stained with green and red emitting fluorophores indicates co-localization. However, many factors may affect this interpretation. Without a thorough understanding of sample preparation, optics, imaging parameters, and data analysis, an incorrect conclusion of co-localization may be reached in complete innocence. Several reasons why yellow in an image generated from a sample stained with green and red fluorophores may not represent true co-localization will be discussed in subsequent chapters.

1.4.2 Confocal Microscopy Is More Than a Confocal Microscope

To effectively use a confocal microscope, investigators must have an understanding of specimen fixation and processing, antigen–antibody interactions, fluorescence theory, microscope optics and hardware components, and the handling of digital images for both image enhancement and analysis protocols. Each of these topics will be addressed in subsequent commandments and discussed in detail throughout the text.

The fact that performing confocal microscopy is much more than operating a microscope is illustrated by the sequence of the following chapters. It is essential that information on specimen preparation, fluorescence theory, and the basics of digital imaging be provided prior to material on confocal instrumentation if users are to understand the operation of a confocal microscope and be able to get the optimum amount of information from their samples.

1.4.3 During Specimen Processing the Integrity of the Specimen Must Be Maintained as Much as Possible

The integrity of the specimen includes the 3-D architecture. A major advantage of confocal imaging when compared to widefield epifluorescence imaging is the acquisition of high-resolution, high contrast images which can be obtained through the *Z*-axis of a sample, and the capability of software programs to reconstruct the 3-D nature of cells and tissues (Fig. 1.4).

Biological confocal microscopy often involves antigen staining to localize specific molecules and structures. It is essential that specimen fixation and subsequent processing maintain, as much as possible, the antigenicity of a specimen and the in vivo localization of cell and tissue antigens, analytes, structural components, etc. This may require extensive adjustment of protocols involving time, temperature, pH, and concentrations of fixatives and primary and secondary antibody solutions. Chapter 5 addresses antigen–antibody interactions, labeling strategies, and potential problems that may arise during staining of samples with various fluorochromes.

Once successful processing protocols are developed it is also essential that specimens be mounted properly to maintain the 3-D architecture of the sample. Chapter 4 presents information on various aspects of specimen preparation including the use of various fixatives, buffers, mounting media, and strategies for mounting specimens to insure maintenance of the 3-D architecture of the specimen.

1.4.4 Photons Are Your Friends and Signal-to-Noise Ratio Is King

Many factors including microscope optics and fluorochrome characteristics tend to reduce the number of photons available for formation of an image. While we are

trying to maximize the number of photons (signal) collected, microscope hardware such as detectors and electronics introduce electronic noise that may result in a poor S/N ratio. As a result, the operator must always be aware of the S/N ratio in an image in an effort to establish operating parameters that maximize image quality while minimizing specimen damage. Several chapters discuss various aspects of fluorochrome and system properties that affect the S/N ratio and provide suggestions on how to maximize the signal for optimal image quality.

1.4.5 Quantification of Fluorescence in a Confocal Micrograph Is a Challenge and at Best Is Only Semiquantitative

This is perhaps one of the most important commandments when dealing with today's competitive research environment and the need for quantitative data that is essential for funding opportunities and high impact publications. Even though a large percentage of researchers using confocal microscopes report quantitative results from their studies, one must use caution when inferring numerical data from images collected with a confocal microscope. Pawley (2000) posed the question "does a fluorescent micrograph reveal the actual location and number of labeled molecules in a cell or tissue" to members of his well-known *3D Microscopy of Living Cells* course. Based on responses collected in the course he published "The 39 Steps: A Cautionary Tale of Quantitative 3-D Fluorescence Microscopy" in *BioTechniques*. Table 1.1 is an abbreviated list of some of the factors that microscopists using confocal systems must be aware of during every imaging session. The conclusion of Pawley's paper is that "all you can really be sure of measuring with most laser-scanning confocal microscopes in the fluorescence mode is some feature of the number of photons collected at a particular time." Throughout the following chapters, we will discuss many of the issues that limit the effectiveness of confocal microscopes as a quantitative research tool and provide tips and suggestions for specimen preparation, imaging parameters, and handling digital images so that as much data as possible can be collected from each image data set.

1.4.6 Scientific Digital Imaging and Normal Digital Imaging (Family Photography) Are Not the Same

The greatest power of digital imaging is that exact copies of data can easily be made. This is excellent when archiving data and reverting to the original files when image processing does not result in the desired effect. However, while it may seem obvious that much of the processing we do on images collected with over-the-shelf digital cameras should not be done with scientific images, the innocence of the investigator again may be a problem. For example, when adjusting the contrast and brightness of a confocal image in programs, such as Photoshop, the gamma function

Table 1.1 List of some factors (adapted from Pawley 2000) that may affect the quality and quantification of confocal images

Microscope, specimen, or image component	Consideration that may affect quantitation
Laser unit	Alignment
	Instability with age
	Efficiency of optical coupling
Scanning system	Zoom magnification/Nyquist considerations
	Raster (pixel) size
	Distortions
	Environment (stray fields, vibrations)
Microscope objective characteristics	Numerical aperture
	Magnification
	Dipping/immersion lens
	Spherical/chromatic aberrations
	Cleanliness
Other optical components	Mirrors
	Excitation and emission filters
	Coverslips
	Immersion oil
Fluorochromes	Concentration
	Quantum efficiency
	Saturation state
	Loading
	Quenching
	Reaction rates
	Dye/dye interactions – FRET
Pinhole	Alignment
	Diameter
Detectors	Sensitivity
	Inherent noise
Digitization	Linearity – statistical noise

The relevance of these and other factors will be discussed in subsequent chapters with the goal of improving the confocal imaging experience of students, technologists, and principal investigators

should always be used rather than the contrast and brightness functions. Gamma corrections should also be performed only after the histogram stretch functions are completed. While rules such as this are not important in family photography applications, not applying them correctly to digital images collected for scientific applications has the potential to alter the appearance of the data.

As discussed extensively in Chaps. 6 and 11, it is essential that an original, unaltered file of the data is archived for reference. All changes in the image should be made only on a copy of the original file. There are specific guidelines that have been published by several groups, including the Microscopy Society of America (http://www.microscopy.org), that specifically state how scientific digital images should be handled. More information concerning these guidelines and the ethics of handling digital images generated for scientific studies are provided in Chaps. 6 and

9–11 on processing of confocal images and the ethics associated with the presentation of the images.

Most hardware used for the collection and display of digital images utilizes software that includes some form of image processing prior to rendering the image. Frequently, manufacturers do not make this information available resulting in images that are collected without a full understanding of how they have been processed by the hardware used in image capture. While this is typically not a problem in recreational photography, processing of scientific data by collection devices prior to saving the information should always be a concern. Whenever possible, when working with images collected as scientific data, a thorough understanding of how the images are collected and processed by the system hardware is desirable. Unfortunately, this information is sometimes difficult to obtain from the manufacturer of the equipment or even worse, considered proprietary and so never revealed. We strongly feel that equipment and software manufacturers owe it to the scientific community to make critical information that can affect image fidelity readily available.

1.4.7 Your Image Is Your Data. Garbage in Will Result in Garbage Out

One should always be detail oriented in sample preparation, image collection, and in handling digital images. The factors listed in Table 1.1 and by Pawley (2000) that affect quantitative confocal microscopy imaging are equally important in the acquisition of images for qualitative studies in which "pretty" pictures to demonstrate a scientific point are required. Without heeding each of the factors it is unlikely that publication quality confocal images will be generated or that data collection from images will be maximized.

1.4.8 The Resolution and Bit Depth Present in a Digital Image are a One-Way Street

After image capture, resolution can only get worse through processing of the image. While it may be possible through gamma and other types of filters to improve the esthetic appearance of an image, as seen in Chaps. 6, 7, and 10, once an image is collected with hardware available on a system, any structures that can be resolved in the image will be present. Increasing the number of pixels in a digital image will not improve the resolution but only result in the creation of pixels by interpolation. These pixels are created by an algorithm such as averaging neighboring pixel values and appear as the computer "believes" they should look. One may also argue that image processing through deconvolution may improve the resolution of the data set, but the limits of resolution have already been determined by the hardware present on the microscope and the physical properties of the light used to collect it.

Deconvolution to remove out-of-focus light and enhancement of images following image collection may improve image quality and enable one to further define the data present, but the limits of resolution were set during collection of the image.

1.4.9 The Joint Photographers Experts Group Image File Format Is EVIL, But Useful

This statement applies to any file format that compresses the data and does not allow full recovery of all of the information present in the original file. The Joint Photographers Experts Group (JPEG) format is the one encountered most often in imaging and so the one we chose to single out. As noted above, resolution is a one-way street and the original data should be stored as collected. Chapter 6 shows that saving files in the JPEG format results in significant loss of information, and especially damaging to scientific images, this loss is greatest along the edges. All original data should be stored in a lossless format such as a tagged image file (TIF) or a proprietary version of a TIF format as provided by the instrument manufacturer. JPEG and other compression formats may be used in situations where images either need to be shared electronically or inserted into formats for lectures, seminars, and posters. In these situations, resolution may be sacrificed in favor of smaller file sizes to make handling of images more reasonable. However, these compressed images should never be used as the primary source of data. File format options will be discussed in detail in subsequent chapters.

1.4.10 Storage Media Is Essentially Free, and Infinite

Even though confocal data sets frequently approach a gigabyte or more in size it is essential that all original data be saved and archived and that all subsequent image processing be performed on a copy of the data. While this may consume large numbers of CDs, DVDs, or other storage media, the cost of data storage is minimal compared to generating new experiments if the data is questioned and the original files are no longer available. As noted in Commandment Six, an advantage of digital imaging is that multiple exact copies of data can be easily made. With the ready availability of high density inexpensive storage media archival copies of each step made in collection of the original image and the subsequent processing of the data should be stored.

1.5 Summary

These Ten Commandments for confocal imaging provide a set of principles to guide users in a confocal microscopy laboratory. Other commandments have occasionally been added to the list during our Workshops, but if close attention is paid

to each of the above, and a detailed understanding of the importance of each is developed, users will have a strong understanding of confocal technology for use in their research.

In Chaps. 2–7, we present information on the topics of fluorescence, specimen preparation, and digital imaging which are essential for understanding confocal imaging. In subsequent chapters, we present information on various types of confocal instruments, the proper setup of operating parameters for confocal imaging, and appropriate techniques for enhancing and analyzing confocal images. Topics pertinent to the various commandments as well as some frequently asked questions such as:

1. Are these fluorescent markers co-localized?
2. Can I quantify the amount of labeled material present based on the fluorescence intensity which is present?
3. Can I measure the size or area of these structures based on a confocal data set?
4. How deep can I image into my sample?

Will be addressed. Hopefully, by learning the basic principles of confocal imaging the quality of the confocal imaging experience of many beginning and intermediate users of the technology will be improved.

References

Berek, M. 1927. Grundlagen der tiefenwahrnehmung im mikroskop. Marburg Sitzungs Ber 62:189–223

Eggar, M.D. and Petráň, M. 1967. New reflected light microscope for viewing unstained brain and ganglion cells. Science 157(786):305–307

Inoué, S. 2006. Foundations of Confocal Scanned Imaging in Light Microscopy. In Handbook of Biological Confocal Microscopy, Third Edition. Pawley, JP (ed). Springer. 985pp

Minsky, M 1957. U.S. Patent #3013467. Microscopy Apparatus

Minsky, M. 1988. Memoir on inventing the confocal scanning microscope. Scanning 10:128–138

Nipkow, P. 1884. German Patent no. 30,105. Germany

North, AJ. 2006. Seeing is believing? A beginners' guide to practical pitfalls in image acquisition. J Cell Biol 172:9–18

Pawley, J. 2000. The 39 steps: A cautionary tale of quantitative 3-D fluorescence microscopy. Biotechniques 28:884–888

Petrán, M. Hadravsky, M., Egger, M.D., Galambos, R. 1968. Tandem-scanning reflected-light microscope. J. Opt.Soc. Am. 58: 661–664

White, JG, Amos, WB and Fordham, M. 1987. An evaluation of confocal versus conventional imaging of biological structures by fluorescence light microscopy. J Cell Biol 105:41–48

Chapter 2
The Theory of Fluorescence

W. Gray (Jay) Jerome

Keywords Fluorochrome • Green fluorescent protein • Photobleaching • Quantum yield • Stokes' shift

2.1 Introduction

Confocal microscopy can be performed in transmission or reflection mode for observing nonfluorescent material. However, for most biological work, the confocal microscope is used in conjunction with fluorescent samples. Fluorescence imaging provides a specific, high contrast signal that maximally exploits the ability of the confocal microscope to remove out-of-focus light. For this reason, it is imperative for confocal microscopists to have a basic knowledge of fluorescence theory and imaging. In this chapter, we review the fundamentals of fluorescence as applied to confocal imaging. In most cases, these basic principles are also applicable to widefield fluorescence microscopy.

2.2 General Principles

Fluorescence microscopy usually involves observing light within the visible range, although detection systems such as charge coupled device (CCD) cameras are available that will detect fluorescence in the ultraviolet (UV) and infrared (IR) range. Although UV and IR detectors have their uses, the current discussion will be limited to detecting visible light, since this is the range of wavelengths used most in biological confocal microscopy.

W.G. (Jay) Jerome (✉)
Department of Pathology, Vanderbilt University Medical Center,
U-2206 MCN, 1161 21st Ave, South Nashville, TN 37232-2561, USA
e-mail: jay.jerome@vanderbilt.edu

R.L. Price and W.G. (Jay) Jerome (eds.), *Basic Confocal Microscopy*,
DOI 10.1007/978-0-387-78175-4_2,

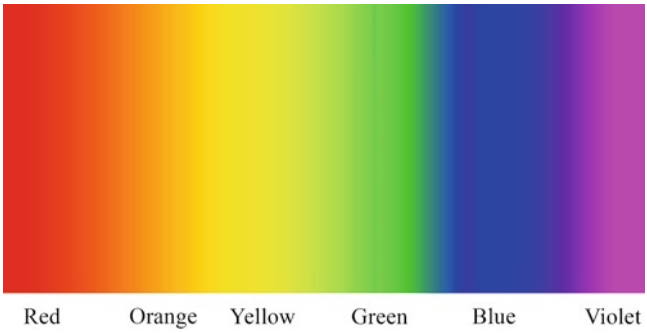

Fig. 2.1 The visible electromagnetic spectrum

Visible light is the portion of the electromagnetic spectrum that can be detected by the human eye. The color that the brain perceives is a function of the specific wavelength of the light; this encompasses electromagnetic wavelengths in the range from about 380 to 750 nm. Although the visible light spectrum is continuous, it can be somewhat arbitrarily divided into discrete colors (Fig. 2.1) according to wavelength. These divisions are violet (380–425 nm), indigo (425–450 nm), blue (450–495 nm), green (495–570 nm), yellow (570–590 nm), orange (590–620 nm), and red (620–750 nm). Indigo is not well differentiated from violet by human eyes, so wavelengths in the indigo range are often included in the violet category. Near-UV light (300–380 nm) is useful in fluorescence microscopy primarily as a source of excitation photons, and the near-infrared wavelengths (750–1,400 nm) are useful for multiphoton excitation (Chap. 8).

A fluorescent molecule (fluorochrome) is one that absorbs a photon of light of a particular wavelength and, after a brief interval, emits some of that energy in the form of a photon of a different wavelength. The delay in emission is called the fluorescence lifetime. Some of the absorbed energy is lost to nonradiation processes and so the emitted photon has less energy than the absorbed photon. Plank's law indicates that the radiation energy of a photon is inversely proportional to its wavelength. Since the emitted photon will have less energy, it will have a longer wavelength and thus a different color than that of the absorbed photon. The difference in wavelength between the absorbed and the emitted light is called the Stokes' shift. Although the shift will always be to a longer wavelength, the degree of shift is highly dependent upon the molecule being excited. Table 2.1 lists the excitation and emission maxima for some fluorochromes often used in confocal microscopy.

Energy absorption by the fluorochrome is the result of interactions between the oscillating electric field vector of the light wave and the electrons in the fluorochrome. For a given electron, a certain amount of energy is required for an electronic transition. Only energies close to this transition energy will be absorbed. Since energy and wavelength are related, this means that for each fluorochrome, there are only certain wavelengths capable of a productive interaction that generates fluorescence. This provides specificity to the fluorescence process.

Table 2.1 Excitation and emission wavelengths for some common fluorochromes

Dye	Excitation max (nm)	Emission max (nm)	Difference
Hoechst 33342	352	461	109
DAPI	358	461	103
Lucifer Yellow VS	430	535	105
FITC	490	523	33
Alexa Fluor® 488	495	519	24
Propidium iodide	536	617	81
Cy 3	548	562	14
DiI	549	565	16
TRITC	557	576	19
Lissamine rhodamine B	575	595	20
Texas Red	596	615	19
Cy 5	649	669	20
Alexa Fluor® 647	650	668	18

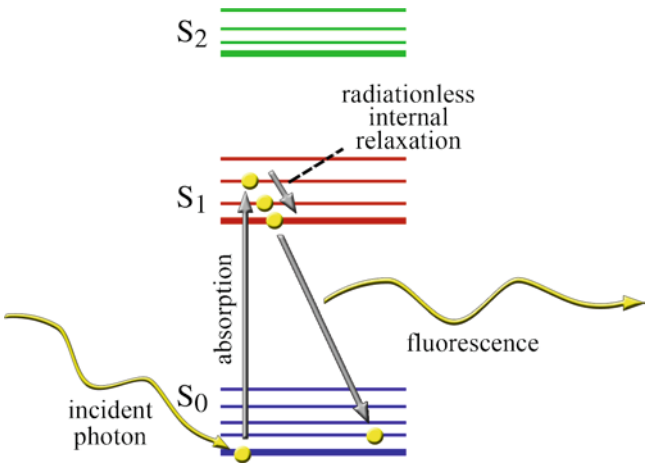

Fig. 2.2 Jablonksi diagram of excitation and fluorescence

The absorption and emission of photons by a fluorochrome are best illustrated using a Jablonski energy diagram (Fig. 2.2), named after Aleksander Jablonski, the Polish physicist who introduced the diagram in 1953. In this diagram, increasing energy is depicted along the vertical axis, from bottom to top and time is depicted along the X axis from left to right. At room temperature, most fluorochromes will only have enough energy to exist in the lowest energy (ground) state (S_0). However, the absorption of a photon by a fluorochrome transfers the photon's energy to the fluorochrome and raises the excitation state of the fluorochrome to a higher state, usually the S_1 state (first excited singlet state), although higher singlet states are also possible (e.g., S_2).

Absorption occurs within femtoseconds. Within each state (S_0, S_1, S_n), several vibrational sublevels exist and the transition can be to any of the possible sublevels, depending upon the energy absorbed. Soon after absorption (~ picoseconds),

the fluorochrome's energy relaxes to the lowest vibrational level within the energy state. This process is termed internal conversion and does not result in the generation of a photon. Rather, the energy is released in nonphoton-generating reactions. Most often, this loss is in the form of heat absorbed by the surrounding solvent. Eventually, the electron reaches the lowest S_1 sublevel (lowest excited singlet state). From the S_1 state, the fluorochrome's energy can undergo a slower (~nanoseconds) decay back to the S_0 state. The energy is lost in the form of a photon that has lower energy (longer wavelength) than the excitation photon. This is the observed fluorescence. For good fluorochromes, most of the return to the S_0 state involves this fluorescence pathway. Importantly, only the decay from S_1 to the ground state is capable of producing fluorescence. Thus, for any given fluorochrome, the emission spectrum will be predictable.

In addition to fluorescence, there are other competing methods by which the excited molecule can lose energy. The most common methods are heat generation and transfer of energy to a neighbor molecule. These alternative processes can reduce the fluorescence emitted by a population of fluorochromes.

Molecules can exist in more than one excited state. For organic fluorophores, the singlet state is the most common. In the singlet state, all electrons are spin paired. However, molecules can also exist in a triplet state, where one set of electron spins is unpaired. There is an increasing likelihood of a molecule undergoing an intersystem crossing from the singlet to the triplet state when the energy absorbed excites the molecule to states above the S_1 level. From the triplet state, the energy can be lost as internal conversion to heat, allowing decay back to the S_1 state, generating a photon (albeit with delayed timing). This is called phosphorescence. However, the excess energy can also promote chemical modifications of the molecule that render it no longer capable of fluorescence. This is called photobleaching. A major cause of photobleaching is the reaction of the excited molecule with oxygen. Thus, antioxidants are often used to help retard photobleaching of fluorochromes during microscopy.

For an individual molecule, absorption is an all-or-none phenomenon; it occurs only if the incident light has sufficient energy for an electronic transition of the fluorochrome to a higher energy state. These states are determined by the atomic organization of the molecule. The limitation on allowable wavelengths that will excite a fluorochrome is due to the fact that the transition from ground state to excited state happens so quickly that the molecules cannot move. Thus, the only transitions allowed are those in which the electron positions in the ground and excited state will overlap. This restricts the wavelengths (energies) that can produce a transition. This is a key property for the use of fluorochromes in microscopy because it allows the identification of specific fluorochromes in a sample based on their excitation and emission frequencies.

As a number of closely spaced energy sublevels exist within each excitation state of a molecule, there is not a single energy but a range of energies that can excite the fluorochrome. The emitted photons also have a distinct range of energies. For this reason, a population of a particular fluorochrome will have a range of excitation and emission energies with maxima at the most likely energies. For instance, Texas Red absorbs wavelengths in a range from about 470 to 630 nm, with a

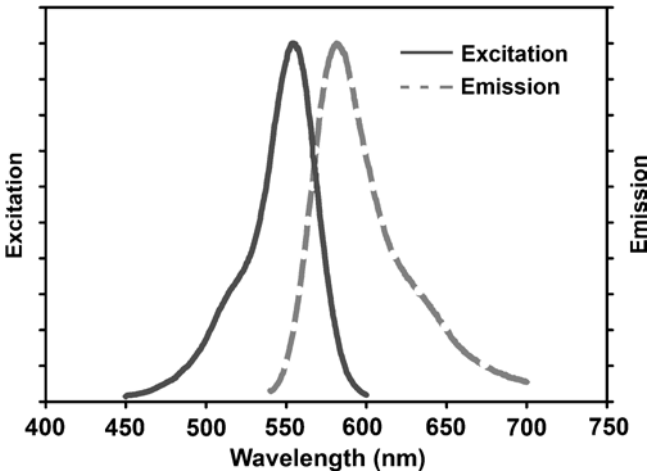

Fig. 2.3 Excitation and emission spectra for tetramethylrhodamine isothiocyanate (TRITC) in methanol

maximum at about 596 nm. In comparison, the absorption spectrum for Lissamine rhodamine B ranges from about 470 to 610 nm and has a maximum at 575 nm.

For most fluorochromes, the photon absorption and fluorochrome excitation spectra are matched; i.e., the molecule is maximally excited when photons are maximally absorbed. Since it is easier to measure the excitation of the molecule, this is the information that is usually provided. Figure 2.3 shows the excitation and emission spectra for tetramethylrhodamine isothiocyanate (TRITC) in methanol. Obviously, since more than one wavelength can excite a specific fluorochrome and result in the emission of photons with a range of wavelengths, when designing fluorescence experiments it is important to know the range of wavelengths applicable for a particular fluorochrome in addition to knowing the excitation and emission maxima.

Excitation and emission characteristics of fluorochromes are typically provided in the Material Safety Data Sheet (MSDS) supplied when a fluorochrome is purchased. If the spectral information for the fluorochrome is not readily available, it is usually possible to find it on websites such as that of the Invitrogen Spectra Viewer (http://www.invitrogen.com/site/us/en/home/support/Research-Tools/Fluorescence-SpectraViewer.html). Websites of this nature are also valuable when selecting multiple fluorochromes to ensure minimal overlap of excitation and emission spectra as discussed in Chap. 3.

The fact that the emitted wavelength is longer than the absorbed wavelength is the fundamental property that permits fluorescence microscopy because it allows for the excitation light to be filtered from the specific wavelengths emitted from the specimen. In this way, the final image contains only the information from the fluorescence emitted from the specimen. This provides a very high contrast image where only the emitted light is observed. The bright, high contrast image produced by fluorescence microscopy is ideally suited for confocal microscopy.

Table 2.2 Quantum yields

Fluorophore	Solution	QY
Bodipy® FL	Water	0.90[a]
Cy 5™	PBS	0.27[b]
Fluorescein	Aqueous 0.1 N NaOH	0.94[c]
JOE™	Water	0.60[a]
Oregon Green® 488	Water	0.90[a]
Rhodamine B	Water	0.31[d]
Tetramethyl rhodamine	Water	0.20[a]
Texas Red	Water	0.90[a]

[a] VL Singer, ID Johnson. http://www.promega.com/geneticidproc/ussymp8proc/21.html
[b] RB Mujumdar, LA Ernst, SR Mujumdar, CJ Lewis, AS Waggoner. Cyanine dye labeling reagents: sulfoindocyanine succinimidyl esters. Bioconj Chem, 1993, 4:105–111
[c] Douglas Magde, Roger Wong, Paul G Seybold. Fluorescence quantum yields and their relation to lifetime of rhodamine 6G and fluorescein in nine solvents: Improved absolute standards for quantum yields. Photochem Photobiol, 2002, 75:327–436
[d] DM Magde, GE Rojas, P Seybold. Solvent dependence of the fluorescence lifetimes of xanthene dyes. Photochem Photobiol, 1999, 70: 737–744

An additional important piece of information about a fluorochrome is its quantum yield. This is the ratio of the number of photons emitted to the number of photons absorbed (2.1) and is, therefore, a measure of the efficiency of fluorescence.

$$\mathrm{QY}(\Phi) = \frac{\text{photons emitted}}{\text{photons absorbed}} = \frac{k_{\mathrm{f}}}{(k_{\mathrm{f}} + k_{\mathrm{nr}})}, \tag{2.1}$$

where QY is the quantum yield, k_{f} is the rate constant for fluorescence decay, and k_{nr} is the sum of rate constants for nonradiative effects (e.g., internal conversion and quenching).

A perfect emitter would produce one photon of longer wavelength for every photon absorbed. However, in most situations, nonradiative phenomena such as heating and photobleaching reduce the energy, leading to quantum yields that are less than 1. Table 2.2 lists the quantum yields for several typical fluorochromes. Another important, and related, fluorescence parameter is the molar extinction coefficient. The extinction coefficient is the quantity of light absorbed as a function of the path length of the excitation light and the concentration of the fluorochrome. It is usually measured at a path length of 1 cm and at a one molar concentration. As a direct measure of the ability of a molecule to absorb light, it is obvious that the molecules with high molar extinction coefficients are more likely to exhibit fluorescence.

2.3 Factors Affecting Fluorescence Emission

While it may seem intuitive that fluorochromes with the highest quantum yield, such as fluorescein isothiocyanate (FITC) at 0.94, should be used for confocal microscopy, the probability of fluorescence emission is greatly dependent upon the surroundings

of the fluorochrome. Contact with any adjacent particle that has the ability to accept transferred energy from the fluorochrome can rob the fluorochrome of sufficient energy that is required for a fluorescence event to occur. For instance, binding of a fluorochrome to another molecule, such as an antibody, usually reduces the probability of fluorescence. The loss of energy due to transfer to surrounding molecules is known as vibrational relaxation. It is very common in fluids or gasses because in these situations, the solvent molecules are more likely to collide with the fluorochrome. The resulting vibrational relaxation produces a reduction in fluorescence intensity of a population of fluorochromes. It is important to remember that these interactions do not alter the shape of the emission spectrum; only the height of the curve (intensity) is reduced, indicating decreased emission of photons.

We described earlier the intersystem crossing to the triplet state. Transition back to the singlet state is not chemically favored and so when a molecule enters the triplet state, most of its energy is lost to nonfluorescent radiation such as photobleaching or phosphorescence. Photobleaching is a critical concept for successful fluorescence microscopy. Although most fluorochromes can go through multiple excitation/relaxation cycles, chemical reactions can eventually alter the molecule such that it no longer fluoresces. It is estimated that a single FITC molecule can undergo about 30,000 cycles before it can no longer absorb an incident photon. At this point, the FITC molecule is said to be "bleached." For confocal microscopy, the bleaching process for FITC occurs very rapidly, and even though fluorescein has a very high quantum yield, its bleaching characteristics when excited with a high-intensity laser often make it unsuitable for confocal microscopy.

2.4 Multiphoton Excitation

As described above, under most conditions, a fluorescence event involves absorption of a single photon of relative high energy resulting in the emission of a single photon of relatively lower energy. The single nature of the event is because absorption must occur very rapidly. However, if a large number of photons are packed into a very small space, the probability of two or more photons transferring their energy simultaneously, or nearly simultaneously, to a fluorochrome increases to the point that such an event might occur. This is known as multiphoton excitation. When the energy from multiple photons is absorbed, it is additive, resulting in the transfer of enough energy to a fluorochrome molecule to raise it from the resting S_0 state to the excited S_1 state (Fig. 2.4). In this multiphoton event, unlike single photon excitation, the emitted photon is of higher energy than the additive low energy excitation photons (although the emitted photon's energy is still lower than the sum of the excitation photons). Thus, if a fluorophore is normally excited by photons with a wavelength of 425 nm, it will also be excited if it absorbs two photons that are each of around 850-nm wavelength.

Since the probability of two photons colliding with a fluorochrome at precisely the same time decreases rapidly away from the focal point of a light beam (the point

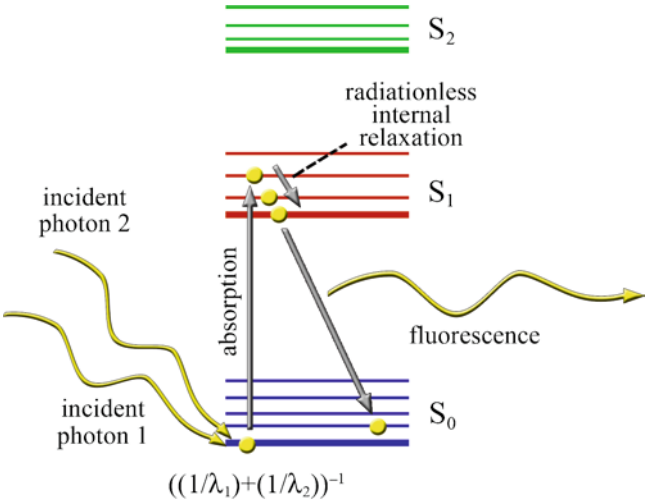

Fig. 2.4 Jablonski diagram for two-photon excitation and fluorescence

where large numbers of photons are packed into a small space), in multiphoton microscopy, the excited volume of a sample is confined to the area where the beam is focused. Fluorochrome molecules that are away from the focal point remain quiescent. The confinement of the excitation volume to the focal point and the fact that longer excitation wavelengths are employed provide advantages for fluorescence imaging of living material and increase the specimen depth from which useful information can be obtained. More details on the phenomenon and the use of multiphoton excitation in biological imaging are provided in Chap. 8.

2.5 Biological Specificity of Labeling

Fluorescence in subcellular imaging is most useful when there is specificity to what is fluorescently labeled. There are a number of mechanisms by which specificity can be assured. The most often employed method is to link the fluorochrome to an antibody molecule and use the specificity of the antibody binding to localize an antigen of interest. Details of this technique are provided in Chap. 5. However, this is not the only means of providing specificity. All types of ligand–receptor interactions can be exploited to bind a reporter molecule to a molecule of interest for microscopic localization. For instance, phalloidin has a high affinity for f-actin molecules. Fluorescent analogs of phalloidin can be used to label the actin cytoskeleton of cells. In a similar manner, the binding of fluorescently labeled cDNA sequences to complementary sequences on DNA or RNA can be used to localize these sequences in cells or on isolated chromosomes. A fluorochrome linked to a biologically active substance is called a fluorophore.

Another method of identifying specific molecules, particularly large complex molecules, involves providing a small fluorescent precursor and allowing the cell to assemble the more complex molecule within the cell. Since the molecule contains the fluorochrome, it can be visualized microscopically. In a similar manner, the gene for a fluorescent protein, such as the green fluorescent protein (GFP), can be linked to the gene for a known cellular molecule. Cells transfected with this construct will then synthesize a molecule of interest with its fluorescent reporter molecule already attached (for review, see Tsien 1998). The 2008 Nobel Prize in chemistry was awarded to Osamu Shimomura, Martin Chalfie, and Roger Tsien for the isolation of GFP and the development and modifications of this protein into useful cytological tools.

Localized environmental conditions within a cell can also be probed using fluorophores that fluoresce only in a specific environment. These fluorochromes change their fluorescence properties in conjunction with changes in their environment. Lysosensor Yellow/Blue DND-160™ (Invitrogen) is one such molecule. This dye fluoresces blue at a neutral pH, but emission is shifted to longer wavelengths as the pH becomes more acidic. Thus, this fluorochrome can be used to follow the acidification of organelles (Diwu et al. 1999). Similar dyes are used for imaging calcium fluxes (Fura) and other environmental physiological changes, and are also available for examining various cellular processes (O'Connor and Silver 1998).

Finally, cells contain naturally occurring fluorochromes that can be probed by fluorescence microscopy. The fluorescence properties of some of these are sensitive to their biochemical state. The reduced form of nicotinamide adenine dinucleotide (NADH) is fluorescent, while the oxidized form (NAD^+) is not. Because of this shift, one can use NAD's fluorescent properties to monitor the redox state of NAD (Williams et al. 1994; Piston and Knobel 1999).

2.6 Recently Developed Fluorescent Probes

The use of fluorescence microscopy has greatly expanded in the past 10 years, fueled in part by an increase in the number of fluorochromes available. Many of the newest generation of fluorochromes, such as the Cyanine and Alexa Fluor® family of dyes, have been specifically engineered to have greater quantum yield and narrower excitation and emission spectra that match the demands of confocal imaging.

Most of the newer probes rely on standard organic fluorochrome chemistry. However, some nontraditional approaches to fluorescence are now being developed. Among these are quantum dots. These are fluorescent semiconductor nanocrystals. Like organic fluorochromes, they emit light at a longer wavelength than that of the absorbed light. Several properties of quantum dots make them attractive for biological imaging; primary among these properties are their high quantum yields and extreme photostability. Quantum dots are very bright and exhibit very little photobleaching. Moreover, for a given composition of quantum dot, different sizes of the same crystal will emit at different wavelengths (Fig. 2.5). This means

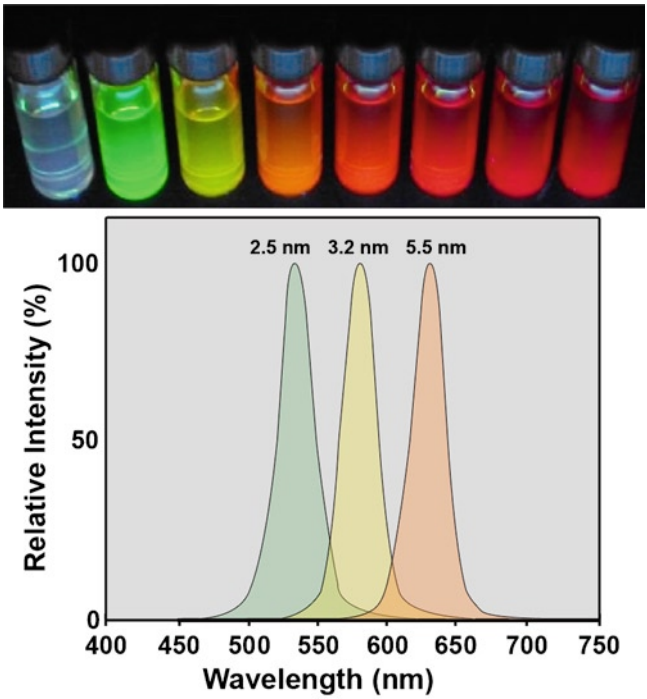

Fig. 2.5 Quantum dot fluorescence. The *top image* shows fluorescence obtained from solutions of CdSe nanocrystals (quantum dots) of diameters 2.0, 2.5, 3.0, 3.2, 3.9, 4.4, 5.5, and 7.3 nm, respectively. All vials are excited at 375 nm. The graphs below show the emission spectra for CdSe nanocrystals excited at 375 nm for sizes 3.2, 3.9, and 5.5 nm (image of quantum dot vials provided by Drs. James McBride and Sandra Rosenthal)

that a single type of material, for instance CdSe, can produce an array of colors with similar brightness and chemical properties, such as binding to ligands. In addition, quantum dots absorb a broad spectrum of wavelengths below their emission wavelengths; thus, a single wavelength can be used to excite multiple fluorophores. This is ideal for experiments in which two or more structures are analyzed using fluorochromes of different colors. Multicolor experiments are also simplified with quantum dots because the crystals emit within a very narrow spectrum (Fig. 2.5). This allows a large number of different color reporters to be separated visually.

Two key problems currently limit the usefulness of quantum dots for biological assays. These are the large size of quantum dots and their toxicity. Quantum dots are not water soluble; therefore, for biological use, they must have some type of coating to make them water soluble. This additional layer overlays the inorganic shell (such as ZnS) that is applied to the nanocrystal to reduce nonradiative transitions and boost the quantum yield. The need for multiple coatings produces complexes that are much larger (usually >10 nm) than reporters labeled with organic fluorochromes. Figure 2.6 compares the size of quantum dots with some other useful biological labels. In addition to size limitations, if quantum dots are to

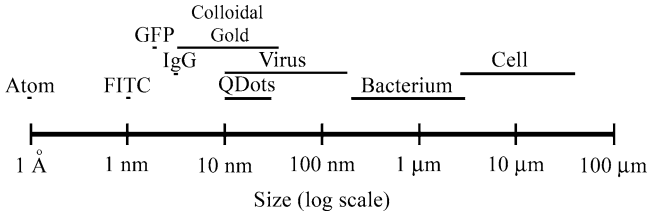

Fig. 2.6 Diameters of various labeling molecules

be used for imaging living material, care must be taken that the surface coat resists leakage. During irradiation, the excitation photons can dissolve the core particle releasing toxic materials such as Cd. Despite these drawbacks, the exceptional fluorescent properties of quantum dots have spurred research in overcoming these limitations, and progress has been made in making quantum dots more biologically friendly. In addition to quantum dots, other inorganic and organic–inorganic composites are being explored for fluorescence properties. For instance, other nanocrystals, such as gold and silver nanodots, are under development. Like quantum dots, they have tunable fluorescent properties. All these developments will expand the choices of molecules available for biological fluorescent labeling studies.

A key problem for all current fluorescent molecules used for subcellular imaging is the need to get the reporter molecule (and any attached binding molecules) to the site to be labeled. Even a relatively small complex such as an IgG Fab fragment attached to Alexa 488® (Invitrogen) is about 5 nm in diameter (Fig. 2.6). The size and hydrophilic nature of most reporter–ligand complexes make transport of these compounds across lipid bilayers into the cell difficult, and once inside the cell, their size can restrict their movement and limit their access to the site to be labeled. This is not a critical issue for staining of thin histological sections for confocal microscopy. However, where the interest is generally in whole cells or thick tissue samples, the penetration of probes becomes an important concern. A lot of effort is being put into making probes smaller and in providing coatings that will facilitate entry of the probes into the cell and subsequent trafficking. None of these have yet been totally successful, but progress is being made. Suffice it to say, however, that the diffusion property of a reporter molecule needs to be considered in any confocal experiment. It should not be assumed that the reporter molecule will have access to a ligand or that two different fluorophores will have equal access to their respective ligands. Lack of access may result in false-negative labeling experiments, and unequal access to ligands may result in incorrect interpretation of co-localization studies.

As described earlier, an alternate approach to the problem of label penetration into a sample has been provided by the elucidation of the gene for GFP. This breakthrough, when coupled with modern molecular biology techniques, has led to the development of a mechanism for the synthesis of a fluorophore inside the cell, instead of being provided exogenously. The coordinated cellular expression of the GFP protein covalently fused to another gene product of interest allows the synthesis of a fluorescently labeled molecule targeted to specific sites or with

specific fluorescent properties. This can simplify the labeling of a molecule and circumvents the need for the fluorophore to cross the plasma membrane to migrate into the cell.

Although the introduction of GFP technology, and the development of additional fluorescent proteins of differing colors expand the range of problems that can be attacked by confocal microscopy, there are several important constraints that must be considered when using the growing number of fluorescent proteins. Chief among them are the need for controlled but ectopic expression of the gene, the possibility that fusion of the two proteins may interfere with the function of the proteins, and the relatively large size of fluorescent proteins. Nonetheless, new and creative variations in the use of fluorescent proteins for biological labeling are being published at an accelerated rate, indicating that there will be continued improvements in this exciting technology. There is little doubt that additional and improved variants of fluorescent proteins will soon become available.

References

Diwu, Z., C. Chen, C. Zhang, D. Klaubert, and R. Haugland. 1999. A novel acidotropic pH indicator and its potential application in labeling acidic organelles of live cells. *Chem Biol.* **6**:411–418.

O'Connor, N., and R. Silver. 1998. Ratio imaging: practical consideration for measuring intracellular calcium and pH in living tissue. *Methods Cell Biol.* **81**:415–433.

Piston, D., and S. Knobel. 1999. Real-time analysis of glucose metabolism by microscopy. *Trends Endocrinol Metab.* **10**:413–417.

Tsien, R. 1998. The green fluorescent protein. *Annu Rev Biochem.* **67**:509–544.

Williams, R., D. Piston, and W. Webb. 1994. Two-photon molecular excitation provides intrinsic 3-dimensional resolution for laser-based microscopy and microphotochemistry. *FASEB J.* **8**:804–813.

Chapter 3
Fluorescence Microscopy

W. Gray (Jay) Jerome and Robert L. Price

Keywords Filters • Fluorochrome • Laser • Magnification • Objective lens • Refractive index • Refractive index mismatch

3.1 Introduction

To harness the power of fluorescence for biological microscopic imaging, a number of additional components must be introduced to the standard light microscope. The most important modifications are (1) a strong illumination system that provides suitable wavelengths for exciting a specific fluorochrome, (2) some mechanism to limit the illumination beam to specific wavelengths so that only the fluorochrome of choice is excited, and (3) a means to image only the light emitted from the fluorochrome so that the excitation light (and other stray wavelengths) does not degrade the image. In this chapter, we will discuss a basic set-up that meets these criteria. Subsequent chapters will expand on this theme and discuss additional modifications required for laser scanning and spinning-disk confocal fluorescence.

3.2 The Optical Path in a Fluorescence Microscope

In standard transmitted light microscopy, a beam of light is focused onto the specimen by a condenser located below the specimen (trans-illumination light path in Fig. 3.1). The light is altered as it traverses the specimen and this altered light is collected by the objective lens and transmitted ultimately to the imaging device (eye, camera, etc.). While this design can be used for fluorescence, there are significant

W.G. (Jay) Jerome (✉)
Department of Pathology, Vanderbilt University Medical Center, U-2206 MCN, 1161 21st Ave, South Nashville, TN 37232-2561, USA
e-mail: jay.jerome@vanderbilt.edu

R.L. Price and W.G. (Jay) Jerome (eds.), *Basic Confocal Microscopy*,
DOI 10.1007/978-0-387-78175-4_3,

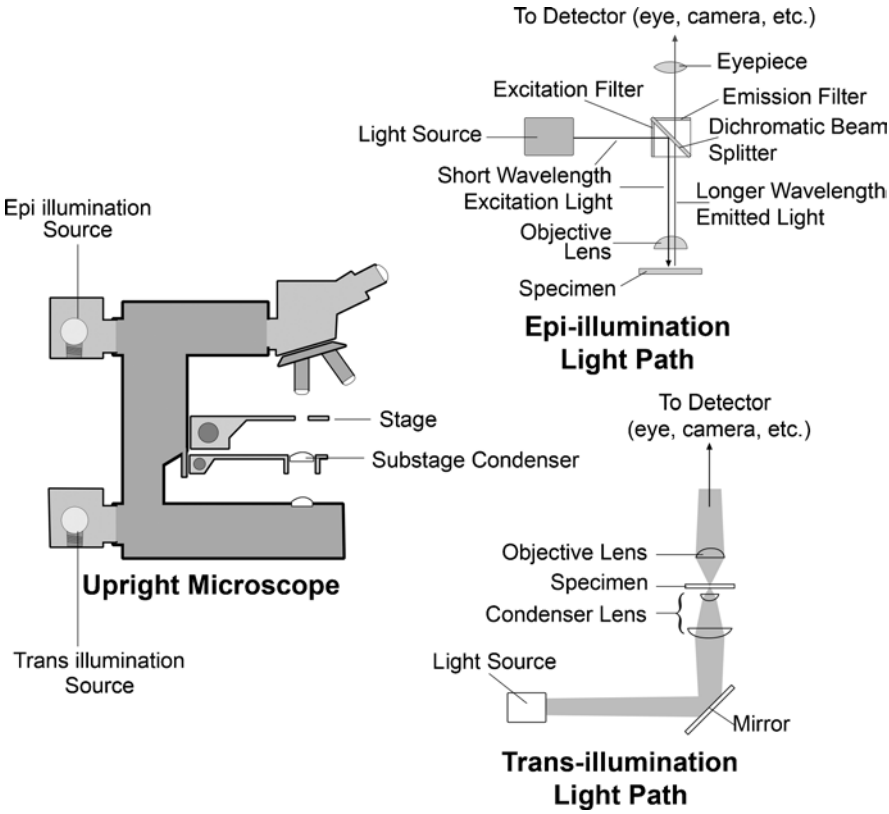

Fig. 3.1 Optical path in epi-illumination and trans-illumination microscope designs. Depicted here is the setup for an upright microscope. However, the trans- or epi-illumination design can be implemented just as easily with an inverted microscope

problems involved in separating the excitation light from the light emitted by the fluorophore. Obviously, it is critical to image only the emitted light, since all other wavelengths are false signals that degrade image quality and might be incorrectly interpreted.

The separation of emitted light from other wavelengths is much easier when the emitted light is traveling in the opposite direction to the excitation light. For this reason, most fluorescence is done using a type of illumination called epi-illumination (Fig. 3.1). In this design, the excitation illumination is focused onto the specimen by the objective lens rather than by a condenser lens (i.e., the objective lens acts as a high-quality condenser lens). The objective lens is also used to collect and focus the light emitted by the fluorophore, just as it would be in a trans-illuminated light set-up. By illuminating the specimen with incident light, the only excitation light in the imaging path is that which is emitted from the specimen or that reflected from glass surfaces. When effectively minimized, the reflected light has a very minor

intensity compared to that of the light emitted from the excited fluorochrome. Limiting reflection is a key component of successful epi-fluorescence microscopy. The incident light is further reduced by appropriate filters that block its transmission to the imaging device (see Sect. 3.5). This epifluorescence strategy is useful for both widefield and confocal fluorescence microscopy.

3.3 Light Sources

As indicated in Fig. 3.1, the light path for epi-illumination begins with the light source. A suitable light source must be able to provide a high photon flux at a wavelength that will excite the fluorochrome of interest. High levels of excitation are necessary because the fluorescence emission is usually low due to fluorochrome and specimen characteristics such as low quantum yield, limited labeling, and loss of light within the optical path of the microscope. These limitations are discussed later in this chapter and in the chapters on specimen preparation, immunolabeling, and system components. The bottom line is that it is usually necessary to maximally excite the fluorochrome in order to get a signal that is distinguishable from the general background noise level.

A second requirement of a fluorescence lamp is that the intensity of the illumination should be uniform at the back aperture of the objective lens. If not, uneven sample excitation and uneven brightness in the final image may result. This can also be a problem if the illuminating source is not properly aligned. Checking the source alignment on a regular basis should be a routine procedure.

Traditionally, two sources that meet the above criteria of uniformity, intensity, and specificity have been employed: mercury arc lamps and xenon arc lamps. Both lamps produce photons as the result of a voltaic arc running through an ionized gas. The mercury bulb produces photons with wavelengths that cover the full visible spectrum and the UV range, as well. For this reason, they are well suited for exciting fluorochromes with absorbance maxima below 380 nm and those with absorbance in the visible range. However, the intensity at different wavelengths is not uniform. Mercury arc lamps show peak intensities at 313, 334, 365, 406, 435, 546, and 578 nm (Fig. 3.2a). The intensities at other wavelengths are much lower. For this reason, when using a mercury lamp, it is best to carefully select fluorochromes that have good absorbance at, or close to, the peak wavelengths.

Like mercury lamps, xenon lamps are arc lamps using an ionized gas to generate light. Xenon lamps have a more uniform distribution of intensities across the visible range, but their intensities fall off rapidly at wavelengths below 400 nm, and so they are less suitable for exciting fluorochromes with UV absorption (Fig. 3.2b). The intensities at peak wavelengths are also not as high as those of the most intense wavelengths of mercury lamps. Another drawback of xenon lamps is that they give off significant radiation in the infrared range, which can produce excessive heat. This heat must be efficiently dissipated because excessive heat can damage specimens and affect the characteristics of environmentally sensitive fluorochromes.

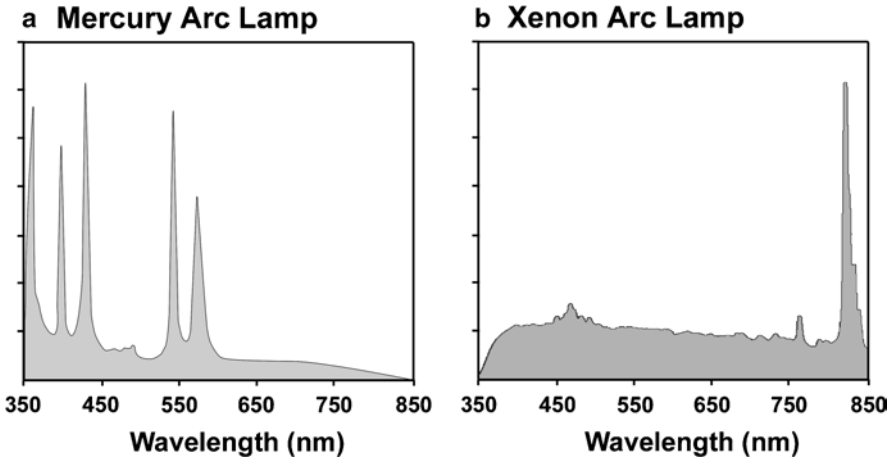

Fig. 3.2 Spectrum of light emitted from mercury arc (**a**) and xenon arc (**b**) lamps

With both xenon and mercury lamps, one must keep track of the number of hours the bulbs are used. Beyond the useful life of the bulb, the spectral emissions can change dramatically, altering the microscopy results. The increase in the use of fluorescence microscopy, however, has spurred innovative approaches to improve arc lamp design. A recent advance has been the introduction of mercury arc lamps, such as the X-Cite ® series of lamps from EXFO (EXFO Photonic Solutions Inc., Ontario, Canada). These lamps include a cleaning cycle technology that removes burned material that builds up on the walls of the arc lamps. This can greatly extend the useful life of the lamp by as much as tenfold.

Although arc lamps are very useful in fluorescence microscopy, they have their drawbacks. Chief among these are the relatively short lifespan, instability, and the need to filter out unwanted wavelengths. In addition, the heat from xenon lamps can be problematic for live cell imaging. In recent years, newer light sources have been introduced that overcome some of the issues with arc lamps. A particularly exciting change is the development of high-performance light-emitting diodes (LEDs). The newest breeds of LEDs have several advantages over mercury or xenon arc lamps in fluorescence microscopy. Like arc lamps, LEDs have a high and stable output. However, they have very low energy consumption and generate less heat. They are also relatively inexpensive and have a very long usable life span. The drawback is that their light output is less intense than the output from arc lamps, but this parameter is improving rapidly.

LEDs can produce light within narrow wavelengths, so filtering nonspecific wavelengths is simplified. An array of LEDs can be employed to cover the spectrum from near-UV to red; consequently, the choice of fluorochromes is not limited. Although these new, high-performance LEDs are a recent advancement, light sources based on LED technology are already becoming available for fluorescence microscopes.

Arc burners and LED arrays are often used in modern spinning-disk confocal microscopes. However, for single-point scanning confocal microscopes, a laser is usually the light source of choice. Laser is an acronym for *Light Amplification by Stimulated Emission of Radiation*. Chapter 2 discussed spontaneous emission of light. Laser light represents stimulated emission. This is a situation where an atom or molecule retains its excess energy until stimulated to emit the energy as light. Lasers both produce and amplify this stimulated form of light. Like spontaneous fluorescence, the emission is restricted to specific wavelengths that are dependent upon the light source. Thus, most lasers produce an intense, monochromatic beam that is coherent and highly collimated. The coherence of the beam introduces problems when used in standard widefield microscopy because scattering and interfering diffraction patterns are produced at all of the surfaces in the optical path, including any dirt in the system. However, this is much less of a problem when a tightly focused beam is rastered point by point across the specimen and the image information collected sequentially from each illuminated point. This is exactly the procedure utilized in single-point scanning confocal microscopy.

At its simplest, a laser consists of a gain medium contained in a reflective optical cavity with an energy supply (Fig. 3.3). Light is generated within the cavity and by placing mirrors within the cavity; the light is reflected back and forth within the gain medium. This leads to an amplification of the energy. The energy for amplification (pumping) is usually supplied as an electrical current or light of a different wavelength.

The gain medium is a material capable of stimulated emission. It can be a gas, liquid, plasma, or solid. The gain medium absorbs the pumped energy, resulting in electrons in the medium becoming excited. In spontaneous emission, this energy would be rapidly lost and the electrons would return to the ground state. In stimulated

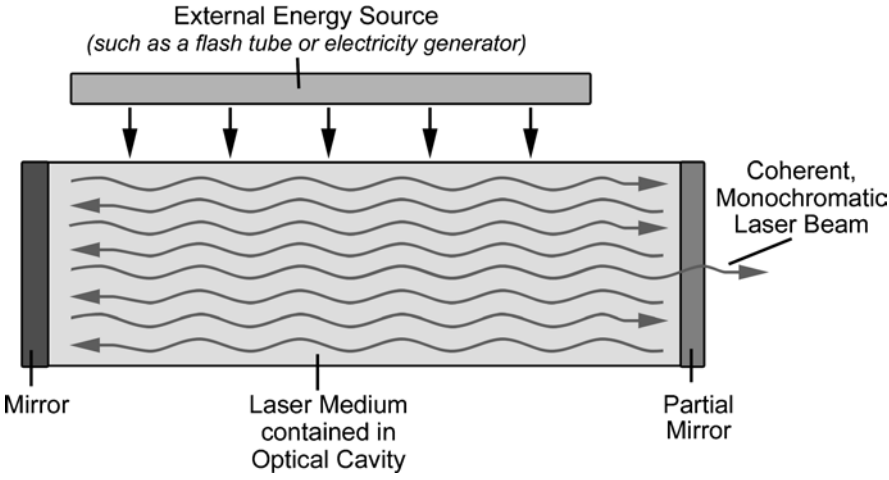

Fig. 3.3 Diagram of general laser principle

emission, the electrons maintain their higher energy state. When the number of excited state electrons exceeds those in a lower state, this is called population inversion, which is a requisite for laser emission. In this state, when a photon is absorbed, the energy released as the atom returns to the ground state will exceed the energy of the photons absorbed. Thus, the light is amplified. Because the injected light passes back and forth through the medium multiple times, the emission becomes greatly amplified.

Although there are a variety of materials that can be used as the gain medium in lasers, for general biological laser scanning confocal microscopy, gas lasers are predominantly used. The most popular, because of available wavelengths, cost, and ease of operation, have been argon–ion and helium–neon lasers. Recently, however, the technology involved in other forms of lasers has advanced sufficiently to make them useful for laser scanning microscopy. In particular, titanium-doped sapphire (Ti:sapphire) solid-state lasers have gained prominence for multiphoton excitation. For these lasers, sapphire is doped with titanium to provide the appropriate energy states for stimulated emission. Ti:sapphire lasers are tunable to a variety of wavelengths in the IR range and can be engineered to produce ultra-short pulses. These properties make them ideal for multiphoton excitation.

Another form of laser is the diode laser. Diode lasers are semiconductor devices where a crystal substrate is doped with two very thin layers of material that will form positive (P) and negative (N) diode junctions (diodes). The difference in chemical potential between the n- and p-type semiconductors produces a depletion region at the interface. An electrical bias causes charge carriers (holes and electrons) to be injected into the depletion region from the p-doped (holes) and n-doped (electrons) sides. The recombination of electrons and holes in the depletion region produces photons which are stimulated by incident photons. The stimulation leads to amplification. The first diode lasers that were developed emitted mostly in the IR region. However, advances have increased the power output of diode lasers and have led to the development of diodes that emit in the blue and red regions, making them useful for fluorescence microscopy. One should expect to see more and more diode lasers available for confocal microscopy in the near future.

One of the strengths of lasers is the monochromatic nature of the emitted photons. For microscopy, the fact that the excitation light exists essentially as a single wavelength simplifies filtering of nonspecific light. However, just like with LEDs, separate lasers are required for each excitation wavelength of interest. At best, a single laser may provide several suitable wavelengths. Unlike LEDs, though, practical considerations, such as cost, usually limit the number of lasers provided with laser scanning confocal microscope systems. This means that a particular instrument is usually not equipped to cover the full visible spectrum and so the choice of fluorochromes that can be employed is limited. Luckily, fluorochrome manufacturers have realized an opportunity, and a great deal of work has been done in the last two decades to develop fluorochromes with properties that match those of the standard laser lines available with most laser scanning confocal microscopes. Thus the presence of limited wavelengths is no longer as restrictive to biological experiments as it was previously.

3.4 Objective Lens Characteristics and Terminology

All components in the optical path are important in the collection of a high-quality confocal image. However, the objective lens may be the most critical element since the initial image is formed, the resolution determined, and most of the magnification of the final image obtained by the objective. Even with an optimum specimen and the operating parameters of the confocal system set up properly, if the objective lens is of poor quality, or an improper lens is used, the image will be inferior. While everyday users may not have control over the choice of available objectives on a core or established instrument, it is important to understand the optical characteristics of each available objective and how these characteristics may affect the collection and interpretation of the data. For example, if a limited number of objective lenses are available, it may be necessary to use a standard 40× oil immersion objective to collect data from both a cell culture sample and a 100-µm-thick section of tissue labeled with multiple fluorochromes. However, this objective is a poor choice for imaging thick specimens if optional 40× water immersion optics are available.

In this section, we give a number of examples demonstrating how the selection of an optimum objective lens can improve the acquisition, reconstruction, and interpretation of confocal data sets. However, before giving the examples, we will first provide several definitions and information about objectives that are essential in understanding why it is essential to have the correct optics on a confocal microscope for the acquisition of a given data set. Much of the discussion relates to a fundamental problem that we face when imaging; the optical components of our systems and the specimens we are trying to image have fundamentally different chemical structures. This results in refractive index mismatch as various wavelengths of light pass through each component (Table 3.1).

With regard to confocal microscopy, refractive index refers to a measurement of how the wavelength of photons is affected as they pass through a substrate. This is important for two reasons. First, light rays change direction when they cross the interface from the objective to air or the immersion fluid used for immersion and dipping lenses. Second, light reflects partially from surfaces that have a refractive index different from that of their surroundings. The refractive index of each

Table 3.1 Refractive index depends on concentration and molecular weight of proteins and nucleic acids (Voros 2004[1]; Samoc et al. 2007[2]). Mismatch of refractive indices of various components in optical path results in significant loss of signal in confocal imaging

Substrate	Refractive index
Air	1.0
Water	1.32–1.34
Immersion oil	1.515
Glycerol (75%)	1.44
Polyvinyl alcohol	1.52–1.55
Protein[1]	1.36–1.5
Nucleic acids[2]	1.5–1.6

component in the optical path, including the optics of the objective lens, the filters used to separate the various wavelengths of photons, the immersion fluid or air the lens is designed to image through, the coverglass, the mounting medium of the specimen, and the specimen itself, is specific and based on the molecular composition of the material. As photons, both excitatory and emitted, pass through each component, their path is affected. If the refractive indices of each component are not matched, refractive index mismatch occurs, resulting in image aberrations and loss of signal (Dunn and Wang 2000; Diaspro et al. 2002). Some common refractive indices for various materials are given in Table 3.1. Refractive index mismatch introduces a number of aberrations in an image and potentially results in loss of signal and/or improper interpretation of experimental results.

3.4.1 Objective Lens Inscriptions

Inscribed on all objectives is information concerning the objective specifications and information about the type of imaging for which they are optimized. Figure 3.4 shows several Zeiss and Nikon objectives. Inscribed on each is information concerning the type of lens, the magnification, the focal length, the numerical aperture (NA), if it is an immersion lens, whether it is corrected for use with water, oil, or glycerol, and the coverglass thickness for which the objective is corrected. Definitions and considerations important in lens selection for confocal imaging are presented below. Several images are also shown in the following sections which illustrate the importance of matching the correct objective with the goals of the experiment.

Plan objectives are flat-field objectives corrected to eliminate curvature of the lens, which may result in loss of focus in peripheral regions of image. Since the purpose of the confocal pinhole is to remove out-of-focus light, this may also result in loss of signal in peripheral regions of the image. If Plan lenses are not available, which may be the case for low-magnification objectives, the confocal software can be used to zoom the image and limit image acquisition to the central area of the objective.

Numerical aperture provides an indication of both the light-gathering capacity and resolution of a lens. A brief introduction to resolution with respect to NA is presented at this point to introduce the topic and provide the necessary information to understand the inscriptions on the microscope lenses. A more thorough theoretical discussion of resolution is presented in Sect. 7.2 which deals with the process of image capture. As NA increases, the number of photons that can be collected by the lens increases, and the resolution the lens is capable of producing is also improved. Key components in determining the numerical aperture, as shown in the equation:

$$\mathrm{NA} = n \sin\theta, Z$$

Fig. 3.4 Various types of objective lenses showing inscriptions on the barrel of the objective. (**a**) ×40 Plan Apo with correction collar for adjustment to correct for coverglass thickness and refractive index mismatch; (**b**) ×63 Plan Apo oil immersion; (**c**) ×20 Plan Achromat water immersion; (**d**) ×20 Plan Apo

are refractive index (n) of the medium (air, immersion oil, glycerol, or water) between the lens and the coverglass, and the half-angle (θ) of the cone of light that enters the objective. The significance of the refractive index and examples of refractive index mismatch between the components of the optical path will be discussed in detail in Sects. 3.4.2 and 3.4.3. As discussed in several sections, one of the limiting factors in confocal imaging is the acquisition of an adequate number of photons.

Thus, high NA lenses are essential for high-resolution confocal imaging as shown in the equation for resolution:

$$d = 0.61\lambda \mathrm{NA},$$

where d is the resolution and λ is the wavelength of the photons. As numerical aperture increases, resolution also improves.

Depth of field (Z) refers to the distance along the vertical or z-axis of the optical path that the specimen, or an object within the specimen, remains in focus. As shown by the equation below, similar to resolution, depth of field is highly dependent on the NA, wavelength of light (λ) used as the imaging source, and the medium between the lens and object (n):

$$Z = n\lambda \mathrm{NA}^2.$$

As the numerical aperture increases, which is desirable for high-resolution confocal images, the depth through which focused images can be obtained rapidly decreases. This is often a problem with confocal experiments, where it is desirable to collect high-resolution 3D z-stacks of images, but the required use of high-NA oil-immersion objectives limits the depth from which images can be collected.

Depth of focus refers to the thickness of the image plane, or depth of the area around an object in an image, that is in focus. Since this refers to an image plane, the position of the object in the specimen is not changed. If the confocal pinhole is set properly and image collected appropriately, the depth of focus in confocal imaging is not as critical as the depth of field.

Infinity-corrected optics are included on nearly all new optical microscopes (1980s and beyond). In infinity-corrected objectives, light leaves the back of the objective as parallel rays which do not come to a focal point to form an image until a tube lens (Telan lens) brings the light to a focal point. The advantage of infinity-corrected optics, especially in fluorescence microscopy, is that multiple components such as barrier filters and beam splitters can be placed in the optical path without affecting the parallel paths the light rays take out of the objective lens. After passing through the components of the optical path, the light is focused by the tube lens. In non-infinity-corrected optics, light is focused to an image after passing through the back focal plane of the objective. This then requires considerable correction to ensure that all components of the optical path are matched, thus preventing light diffraction as light rays pass through filter cubes, beam splitters, and other components of the optics. If all components are not optically matched, a number of image aberrations, as discussed below, can occur.

Immersion objectives are designed to minimize the refractive index mismatch between the components of the lens and other components within the optical path. For example, the optical components of oil-immersion objectives are closely matched with that of the coverglass used to mount specimens. This minimizes the refractive index mismatch as excitation photons pass through the objective and coverglass prior to exciting fluorochromes in the specimen. This is also advantageous

as emitted photons must also pass through the same glass components of the coverglass and objective lens. Typically, oil-immersion objectives have a very high numerical aperture (1.3–1.4), which also results in a high-resolution objective.

Other types of immersion objectives also exist. Water immersion objectives closely match the refractive index of the biological components (proteins, nucleic acids, and water) by using a drop of water between the objective and the coverglass, rather than using air or oil, as the intermediate medium. While water immersion objectives are excellent at minimizing refractive index mismatch and allowing deeper imaging into tissues, the numerical aperture of these lenses is not as high as those available for oil immersion optics. Objectives are also available for immersion in glycerol to match the mounting medium used for many biological specimens. In addition, some objectives are classified as multi-immersion objectives and these can be used for various mounting media or dipping lenses which can be placed directly into the buffer mounting media of the specimen without the use of a coverglass. Immersion and dipping objectives are typically expensive, and cost increases as the numerical aperture and versatility of the lens increase.

The *working distance* of a lens is the distance between the objective and the coverglass (or specimen if using a dipping lens) when the specimen is in focus. Low-magnification objective lenses and water immersion lenses typically have a long working distance, while oil immersion lenses have very short working distances. Care must be taken when focusing all objectives, but one must be diligent in making sure that short working distance oil-immersion objectives are not focused on the coverglass of the specimen, which may result in damage to the objective. A potential problem that exists with automated microscope systems is the use of samples of varying thicknesses with objectives of different working distances. One should always focus a new sample at low magnification (i.e., 10×) prior to using a short working distance lens. An example of a potential problem with the fully automated Zeiss microscope in our core facility is that a number of investigators utilize the 63× NA 1.4 oil lens to image co-localization in cells cultured on coverglasses. Other investigators may use the same objective to image the surface of sectioned samples that are several microns thick. Since the automated system brings the focal point back to the one previously used, it is essential that those using thick specimens first focus their sample at low magnification to avoid contact of the short working distance objective with the sample.

Wavelength-corrected objectives and chromatic and spherical aberrations: One of the most important characteristics of an objective used for acquisition of confocal images is the combination of wavelengths of light for which it is optimized to collect. Since wavelengths of photons emitted from different fluorochromes vary, the focal point of each after it passes through the objective lens will also differ. It is essential to use objectives corrected for the various fluorochromes being used so that all are focused in the same optical plane. If the fluorochromes are focused in different optical planes, chromatic and spherical aberrations are introduced into the image which can affect data interpretation, as discussed in Sects. 3.4.2 and 3.4.3.

Inscriptions on the barrel of the objective indicate the level of correction. Achromat lenses are designed to minimize chromatic aberrations in the blue and red wavelengths and spherical aberration in green wavelengths of light. Fluar objectives

are corrected not only for chromatic aberration in blue and red wavelengths but also for spherical aberration in these ranges. Apochromat objectives are corrected for chromatic aberration for red, green, blue, and possibly UV light, and spherical aberration for red and green light. In addition to these basic classifications, objectives such as the C-apochromats for up to six color corrections in water immersion lenses have been introduced for specific uses. However, even with advanced correction, it is essential that care be taken when interpreting multicolor data, as shown in the next several examples.

3.4.2 Effects of Chromatic Aberration

Use of lenses not specifically corrected for collection of multiple wavelengths of light may result in the introduction of chromatic aberration in the image. This can result in image artifacts and improper interpretation of data. Figure 3.5 diagrammatically illustrates the effects of chromatic aberration on the imaging of photons of different wavelengths. In objectives that have longitudinal (axial) chromatic aberration (Fig. 3.5a), photons of shorter emission wavelengths (blue) are focused closer to the objective than those of longer wavelengths (green or red). As shown in Fig. 3.5b, lateral chromatic aberration may result in a change in magnification, with

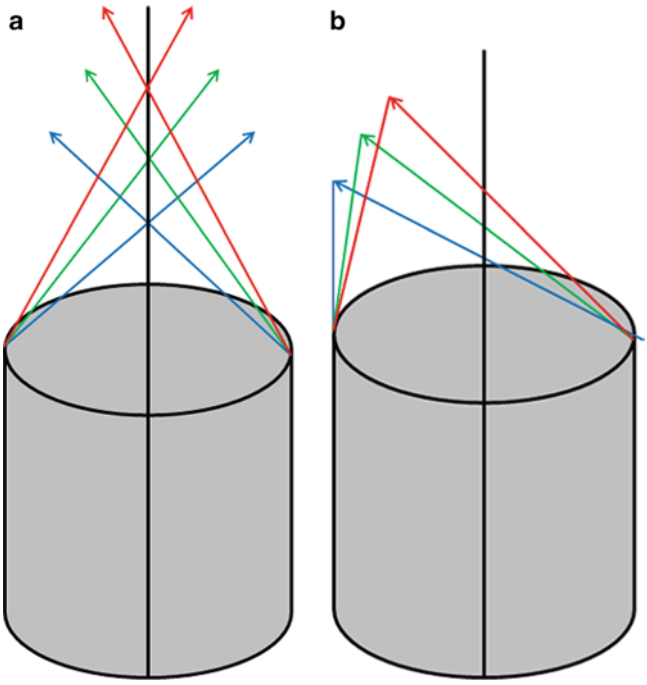

Fig. 3.5 Diagrams of the effects on focal plane and magnification of longitudinal (**a**) and lateral (**b**) chromatic aberrations

shorter wavelengths of light being magnified more than long wavelengths by 1–2%. The correction of chromatic aberration is typically accomplished in the design of the objective by inclusion of multiple lens elements with different optical characteristics. This results in different wavelengths of light being brought into focus in the same plane.

Chromatic aberrations may result in two types of defects in the image. First, since out-of-focus photons are removed from the image by a pinhole, the resulting signal may be significantly reduced in the wavelengths that are out of focus. The second artifact may result in a misinterpretation of co-localization data since photons of different wavelengths that are imaged from a single point in the specimen will be out of register in the *X*-, *Y*-, and *Z*-directions and observed as being in different points in the specimen. If working at low magnifications where *Z*-resolution is relatively poor, this may not be significant. This is why many low-magnification objectives are not highly corrected for chromatic aberrations. However, in high-resolution confocal imaging, it is essential that highly corrected objectives be used for collection of images from samples labeled with multiple fluorochromes.

The effects of chromatic aberration on the interpretation of co-localization of structures in a sample have been illustrated by Dunn and Wang (2000), and are shown in Fig. 3.6. In this set of experiments, they first imaged a mirror and fluorescent beads with 40× Fluor and 100× Plan Apo objectives at photon emission values of 520, 600, and 680 nm (Fig. 3.6a). With the Plan Fluor objective corrected for red and green emission, these two colors were co-localized while the emission at 680 nm was displaced by 1.2 μm in the *z*-axis. With the Plan Apo 100× objective, which was corrected for all three wavelengths of light, the signals coincided. To demonstrate this effect in a biological sample, they simultaneously labeled transferrin (Tf) molecules in cell endosomes with fluorescein, rhodamine, and Cy5. Since there is a very high expression of Tf sites available in these cells, a high probability for triple-label co-localization exists. In this case, true co-localization of the structures should be observed in the images if no longitudinal chromatic aberration is present. In Fig. 3.6b–d, the Plan Apo 100× objective was used to image fluorescein (520-nm emission) and Cy5 (680-nm emission). With this objective, images correctly show a high coincidence in signal localization and intensity, indicating that the fluorochromes are co-localized as indicated by yellow color in Fig. 3.6b and arrows in Fig. 3.6c, d.

The same sample was then imaged with the 40× Plan Fluor objective corrected for green (fluorescein) and red (rhodamine) emission. Figure 3.6e again shows the co-localization of these two signals collected with an objective corrected for these fluorochromes. However, when the 40× Plan Fluor objective was used to collect fluorescein and Cy5 signals and the images were overlaid, the Tf molecules no longer appeared co-localized. With this objective, the image had distinct red and green colors, indicating no co-localization (Fig. 3.6f). When a Z-series was collected (Fig. 3.6g) and projected, the signals again appeared co-localized, indicating a shift in the *Z*-positioning of the emitted photons. When the individual fluorescein images collected in Fig. 3.6f were shifted 1.2 μm in the *Z*-direction, the fluorescein and Cy5 signals correctly appear co-localized (Fig. 3.6h). Figure 3.6i, j show that if

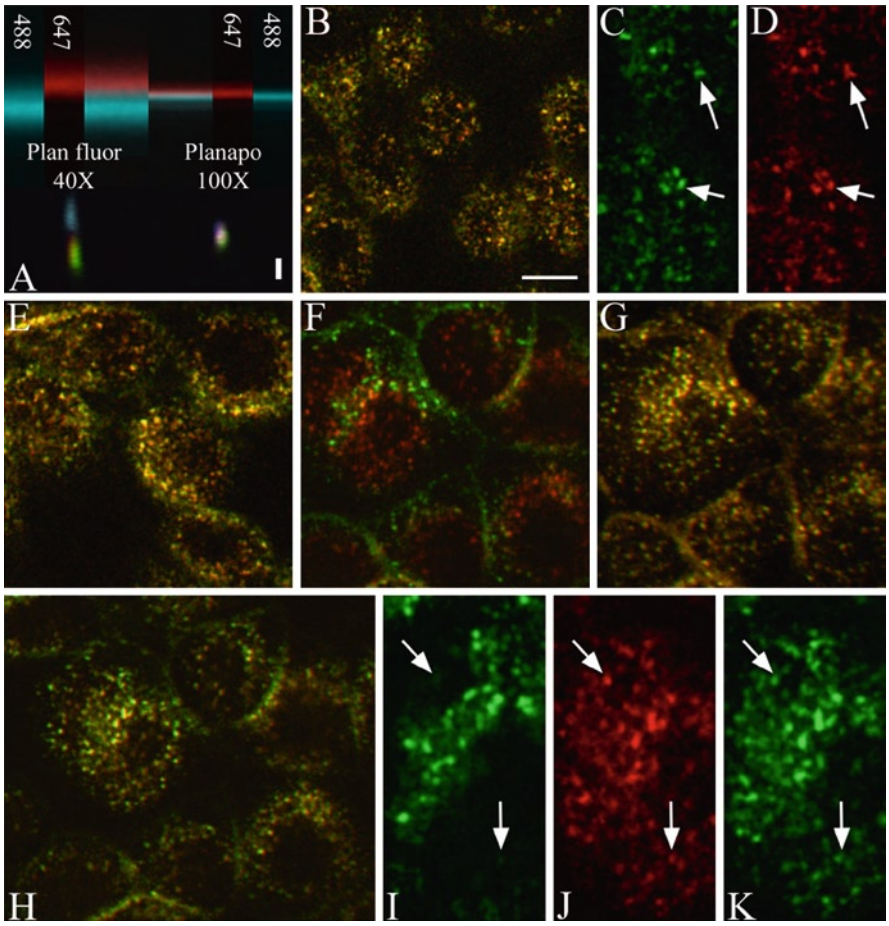

Fig. 3.6 Chromatic aberration in confocal microscopy. (**a**) XZ-sections of glass reflection (*top*) and microsphere fluorescent (*bottom*) images collected with a poorly color-corrected Plan Fluor ×40 objective (*left*) and a well-corrected Plan Apochromat ×100 objective (*right*). In the reflection images at the *top* of this *panel*, 647-nm light is shown in *red* and 488-nm light is shown in *blue*. In the fluorescence images of fluorescent beads, 520-nm emissions are shown in *green*, 600-nm emissions are shown in *red*, and 680-nm emissions are shown in *blue*. For all images, the focal axis is oriented vertically, with the sample bar indicating a distance of 1 μm. (**b**) An image of a field of cells labeled with both fluorescein-Tf and Cy5-Tf collected with the ×100 Plan Apochromat objective. Higher magnification images of the component green and far-red fluorescence are shown in panels (**c**) and (**d**), respectively. (**e**) An image of a field of cells labeled with F-R-Tf collected with a ×40 Plan Fluor objective. (**f**) An image of a field of cells labeled with both F-Tf and Cy5-Tf collected with the Plan Fluor objective. (**g**) The projection of the vertical series of images from which panel (**f**) was obtained. (**h**) The same field shown in (**f**), but combining green and far-red planes collected at 1.2 μm apart. Higher magnification images of the green and far-red fluorescence from the same focal plane are shown in panels (**i**) and (**j**), while panel (**k**) shows the green fluorescence from a focal plane 1.2 μm lower. *Scale bar* in (**b**) represents a 10-μm length for panels (**b**)–(**h**) and a 5-μm length for panels (**i**)–(**k**) (used with the permission of the authors and Biotechniques, 2008)

the same focal plane is collected in the fluorescein and Cy5 channels, poor image registration of the Tf labeling results, as shown side by side. However, if the fluorescein image is collected at a depth of 1.2 μm greater, there is perfect registration of the signal.

In the above set of experiments, a 100× Plan Apo objective corrected for common fluorochromes in the 500–680 nm emission range was used. With the development and addition of new lasers that have extended the range of fluorochromes that can be used in confocal microscopy, additional care must be taken when selecting fluorochromes for co-localization studies. In a set of experiments similar to those above, we have used a Zeiss Plan Apo 63× objective to image F-actin in cardiac myocytes labeled with 405- and 633-nm phalloidin. A similar assumption to the transferrin model above is made here in which both fluorochromes should be co-localized on the F-actin. As above, this apochromat objective is corrected for fluorochromes emitting in the 500–700 nm range; it is not well corrected for fluorochromes such as the 405-nm fluorochrome excited with the 405-nm diode laser which emits in the 475 nm range. As a result, the two signals are not co-localized in the image even though they label the same structures (Fig. 3.7). As near-UV lasers become more common on many confocal systems, care must be taken in selection of fluorochromes used in co-localization studies to ensure that they match the lasers and optics of the available confocal microscope.

These experiments clearly show the importance of knowing both the objective lens and fluorochrome characteristics when designing an experiment. When dealing with co-localization data, it is important to select fluorochromes for which objectives are available to correct adequately for focal shifts due to differing wavelengths

3.4.3 Refractive Index Mismatch and Spherical Aberrations

Refractive index mismatch is the primary cause of spherical aberration in microscope systems. This type of aberration results in peripheral rays of light that enter an objective being focused at a different point than the central rays of light that enter (Fig. 3.8). This may result in blurring of the image and significant loss of signal as the confocal pinhole effectively removes the out-of-focus light from the image. Much of the refractive index mismatch that occurs in a confocal system results from differences in the refractive indices of air or immersion oil and common specimen mounting media that are primarily water based, such as the 1:1 PBS:glycerol mix used in many laboratories.

To address problems with refractive index mismatch, immersion lenses may be used. By utilizing immersion fluids rather than air as the interface between the lens and the specimen, a closer match in the refractive indices in the optical path occurs. This can significantly improve resolution as in the case of high-NA oil immersion objectives, or depth of imaging in the case of water immersion optics. Similar to their experiments demonstrating the effects of chromatic aberrations,

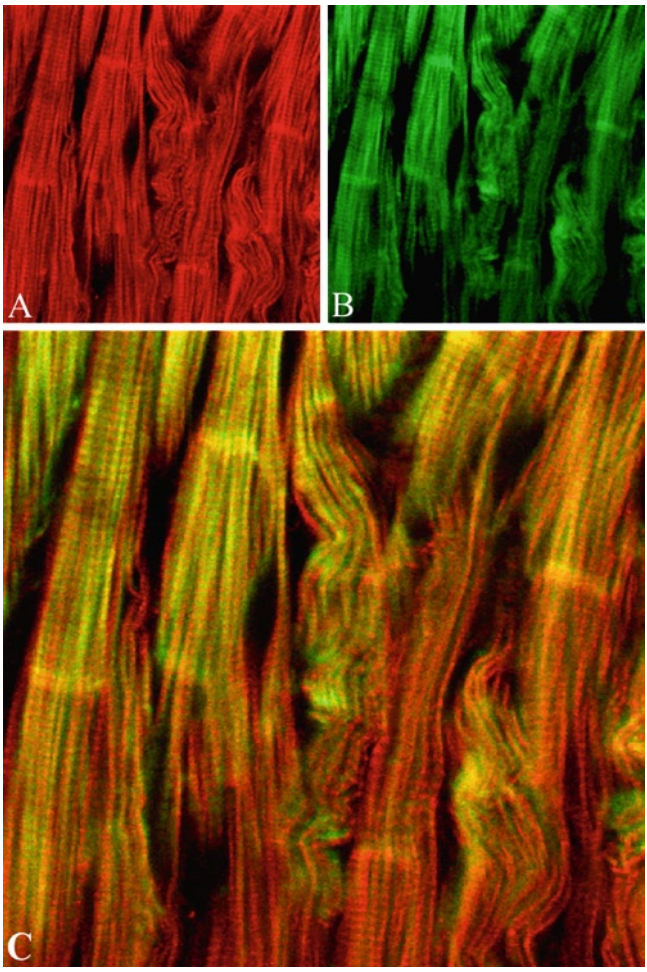

Fig. 3.7 A section of adult mouse heart labeled with 633 phalloidin (**a**) and 405 phalloidin (**b**). Both are labeling f-actin in the cardiac myocytes but due to chromatic aberrations in the system, the *red* and *green* signals do not show 100% overlap as shown in the merged image (**c**)

Dunn and Wang (2000) have also used fluorescein-Tf-labeled endosomes to demonstrate the effects of refractive index mismatch by imaging the same sample with a 100× Plan Apochromat oil immersion objective and a 60× Plan Apochromat water immersion objective (Fig. 3.9). When imaging near the surface with the 100× Plan Apochromat oil immersion objective, a strong signal can be obtained. However, due to refractive index mismatch between the immersion oil and the water-based mounting medium of the sample, signal is rapidly lost due to spherical aberration as imaging depth is increased (Fig. 3.9a, b). At a depth of only 35 μm, essentially no signal was available for imaging. When using the 60× Plan Apochromat water immersion lens, which minimizes refractive index mismatch

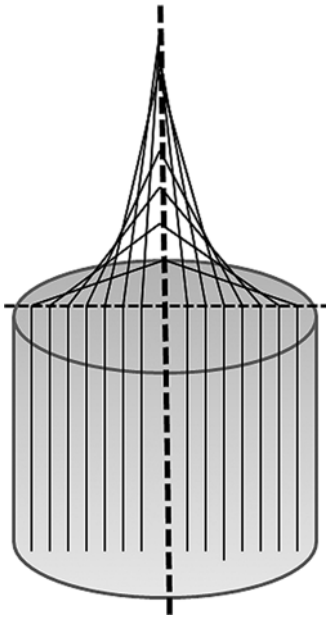

Fig. 3.8 Diagram showing the effects of spherical aberration resulting in peripheral rays of light being focused closer to the objective lens surface than rays of light coming through the central regions of the lens

between the immersion and mounting media, excellent images were obtained 66-μm deep in the specimen (Fig. 3.9c, d).

In addition to spherical aberrations associated with refractive index mismatch between the immersion and mounting media, depth of imaging, even with water immersion optics, can be dramatically affected by the specimen itself. One of the common questions asked by investigators beginning confocal imaging is how deep can I image into my specimen? As seen above, knowing the specifications of the objective being used is important in answering this question. Equally important is a basic knowledge of the characteristics of the specimen being imaged. Figures 3.10 and 3.11 illustrate the effects of specimen (protein?) density on the depth of imaging. In Fig. 3.10, Cy3–phalloidin was used to label the somites of a chicken embryo, which was then imaged with 20× NA 0.75 air and 20× NA 0.5 water immersion objectives. With the 20× air objective, signal was significantly decreased at a depth of 100 μm in the specimen. However, with the water immersion objective, a strong signal was still available at this depth and signal did not decrease until a depth of 150 μm was tested.

Using the same 20× optics and Cy2-phalloidin label, we also imaged adult mouse heart, which is a much denser sample than the embryonic tissue imaged above. With this sample, signal was lost at a depth of less than 25 μm with the 20× dry lens, but was still strong with the water immersion lens at this depth

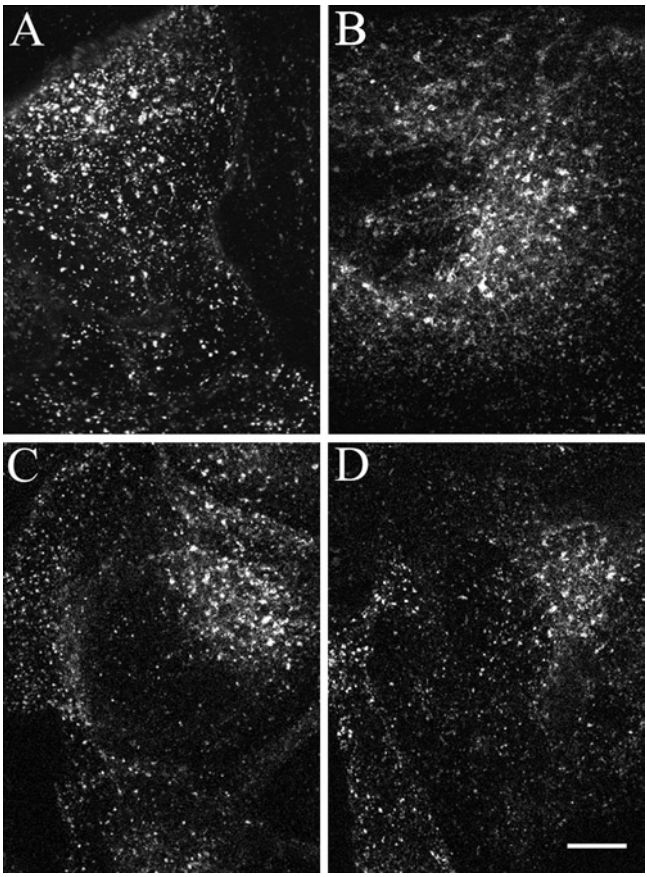

Fig. 3.9 Spherical aberration in confocal microscopy. Images of cells labeled with F-Tf and imaged with either the ×100 Plan Apochromat oil immersion objective (**a** and **b**) or the ×60 Plan Apochromat water immersion objective (**c** and **d**). Endosomes were imaged at the surface of the coverslip panels (**a**) and (**c**) or at a depth of 35 μm (panel **b**) or 66 μm (panel **d**) into the aqueous sample medium. *Scale bar* is 10 μm in length (used with the permission of the authors and Biotechniques, 2008)

(Fig. 3.11). Imaging depth of dense adult cardiac tissue was approximately 25% of that obtainable with embryonic tissue using the same preparation protocols and optics, illustrating the importance of knowing specimen characteristics in addition to optical specifications when determining imaging parameters.

An additional factor that affects spherical aberration is the thickness of the coverglass, since this affects the length of the optical path through the glass. While it may not be practical to measure the actual thickness of every coverglass used, one must be aware that minimal variations in the thickness of a coverglass can affect image quality and interpretation. Minimally, coverglasses that match the system objectives should be used. Manufacturers have addressed this problem, as well as the

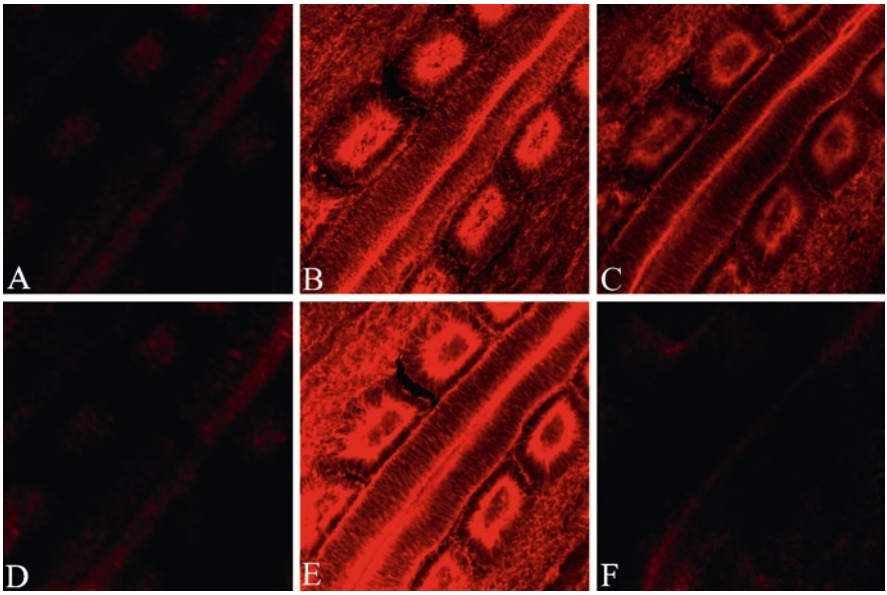

Fig. 3.10 Effects of refractive index mismatch on depth of imaging. A 200-μm thick section of mouse embryo was labeled with Alexa 543-phalloidin (*red* channel) and somites imaged with a ×20 NA 0.5 water immersion lens (**a**–**c**) and a ×20 NA 0.75 dry lens (**d**–**f**). A Z-series was collected with image acquisition optimized for collection at 50-μm deep in the sample. Images (**a**) and (**d**) were collected at the surface of the sample, images (**b**) and (**e**) 50-μm deep, and (**c**) and (**f**) 100-μm deep. With the ×20 dry objective, all signals were lost at 100 μm into the section, while a strong signal was still present at this depth with the ×20 water immersion objective. Signal was not lost with this objective until a depth of 150 μm was imaged

above factors affecting spherical aberrations, by providing objectives with correction collars. Correction collars can be adjusted to accommodate small variations in coverglass thickness and minimize image aberrations. While fairly expensive, these objectives are ideal for imaging deep into a specimen with minimal spherical and chromatic aberration, as shown by another set of experiments performed by Dunn and Wang (2000). Using a 60× water immersion objective with a correction collar and excitation wavelengths of 488 and 647 nm, they first collected images at the glass surface followed by a set of images at a depth of 63 μm in an aqueous medium (Fig. 3.12a). The signal from these two wavelengths differed by a depth of 0.6 μm in both cases, indicating that the shift in *Z*-direction was not due to imaging depth.

They then collected images from a triple-labeled bead with emissions at 520 nm (green), 600 nm (red), and 680 nm (blue). With the correction collar adjusted for a measured coverglass thickness of 174 μm, the green and red signals coincided while the blue signal was offset, as expected from the measurements made from glass. When the correction collar was purposefully misadjusted for a 150-μm coverglass to introduce spherical aberration, the red and green signals no longer

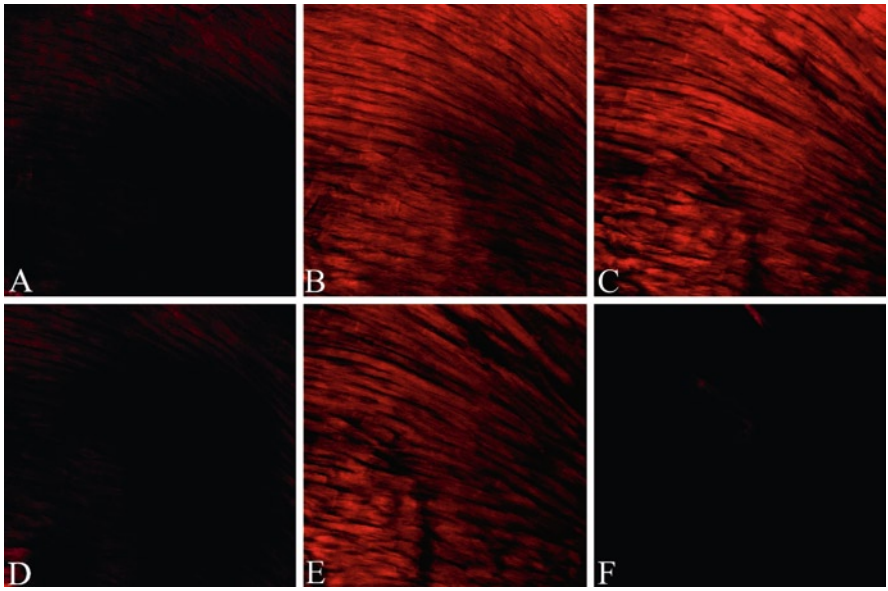

Fig. 3.11 Effects of refractive index mismatch and tissue density on depth of imaging. A 100-μm thick section of mouse heart was labeled with Alexa 543-phalloidin (*red* channel) and myocytes imaged with a ×20 NA 0.5 water immersion lens (**a**–**c**) and a ×20 NA 0.75 dry lens (**d**–**f**). A Z-series was collected with image acquisition optimized for collection at 15-μm deep in the sample. Images (**a**) and (**d**) were collected at the surface of the sample, images (**b**) and (**e**) 14 μm deep, and (**c**) and (**f**) 28 μm, deep. With the ×20 dry objective, all signals were lost at 28 μm into the section, while a signal was still present at this depth with the ×20 water immersion objective. Signal was not lost with this objective until a depth of 50 μm was imaged. Compare this to the results of imaging depth with embryonic tissue which could be imaged much deeper into the specimen

coincided and image intensity was significantly reduced. This type of error is often encountered since the thickness of coverglasses from a single batch may vary by up to 40 μm around the thickness value at which they are sold.

To further demonstrate how these optical effects might lead to misinterpretation of co-localization data, Dunn and Wang (2000) again collected a series of images from Tf-labeled endosomes. In this set of experiments, they utilized the 60× water immersion lens and imaged through aqueous media at a depth of 63 μm. As shown in Fig. 3.12b, a chromatic shift was present when imaging with fluorescein- and Cy5-labeled Tf. However, by projecting a Z-series of the images (Fig. 3.12c), the chromatic shift is no longer apparent and the Tf molecules properly appear co-localized.

Consistent with the data presented in Fig. 3.12a, when fluorescein- and rhodamine-labeled Tf molecules are imaged at the surface of the sample, they appear co-localized (Fig. 3.12d). However, even though imaging is at the surface of the sample, when fluorescein- and Cy5-labeled Tf molecules are imaged, there again is a chromatic shift indicating labeling of discrete populations of endosomes (Fig. 3.12e). If the fluorescein image is again collected 0.6 μm deeper, the co-localization is again apparent

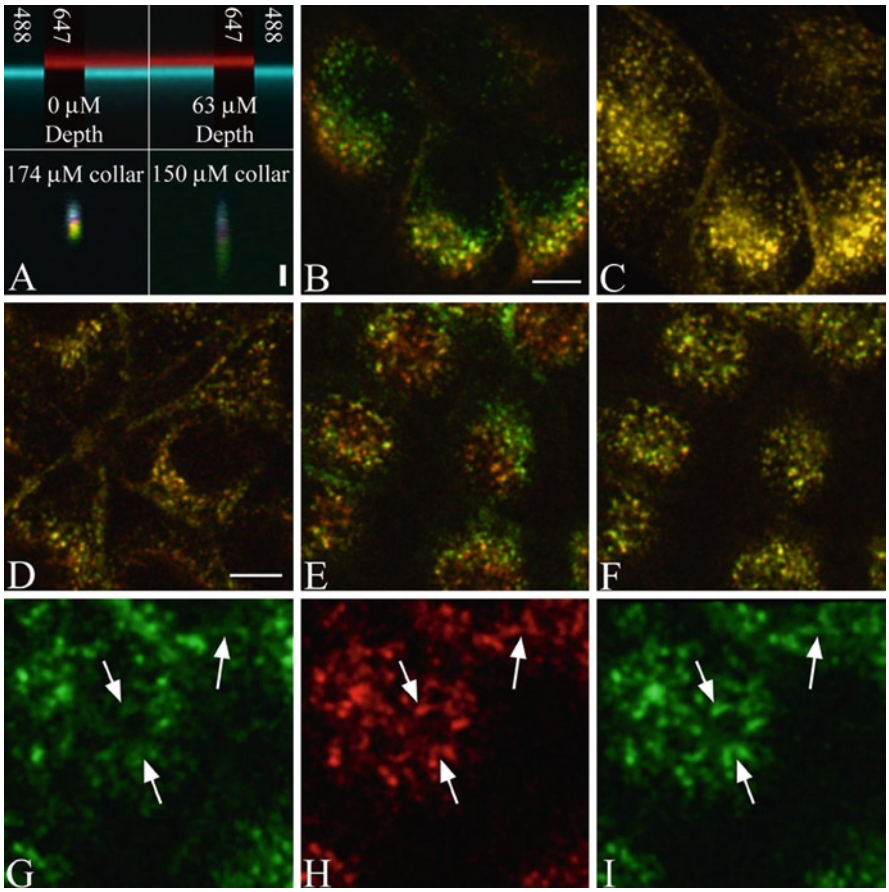

Fig. 3.12 Chromatic aberration in the ×60 Plan Apochromat water immersion objective. (**a**) XZ-sections of glass reflection (*top*) and microsphere fluorescence (*bottom*) images. Reflection images are shown for depths of either 0 or 63 µm into an aqueous medium, with 657-nm light shown in *red* and 488-nm light shown in *blue*. Fluorescence images of fluorescent beads are shown for an objective with correct (*left*) and incorrect (*right*) coverslip-thickness collar setting, with 520-nm emissions shown in *green*, 600-nm emissions shown in *red*, and 680-nm emissions shown in *blue*. For all images, the focal axis is oriented vertically, with the *scale bar* indicating a distance of 1 µm. (**b**) An image of a field of cells labeled with F-Tf and Cy5-Tf collected at a depth of 63 µm into an aqueous medium. (**c**) The projection of the vertical series of images from which panel (**b**) was obtained. (**d**) An image of a field of cells labeled with F-R-Tf collected at the coverslip surface. (**e**) An image of a field of cells labeled with both F-Tf and Cy5-Tf collected at the coverslip surface. (**f**) The same field shown in panel (**e**), but combining green and far-red planes collected 0.6 µm apart. Higher magnification images of the green and far-red fluorescence from the same focal plane are shown in panels (**g**) and (**h**), while panel (**i**) shows the green fluorescence from a focal plane 0.6 µm lower. *Scale bar* in panel (**b**) represents 10-µm length in panels (**b**) and (**c**). The *scale bar* in panel (**d**) represents 10-µm length in panels (**d**)–(**f**) and 5 µm in panels (**g**)–(**i**) (used with the permission of the authors and Biotechniques, 2008)

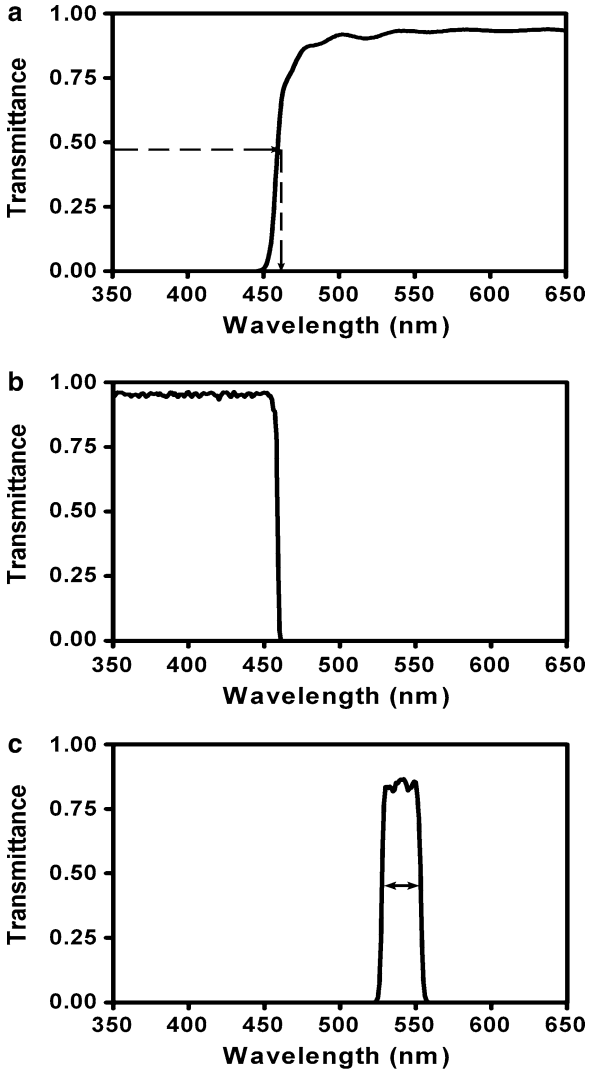

Fig. 3.13 Spectra for typical long-pass (**a**), short-pass (**b**), and band-pass (**c**) filters

(Fig. 3.12f). Figure 3.12g–i shows separate channels for fluorescein (Fig. 3.12g), Cy5 (Fig. 3.12h), and fluorescein collected 0.6 μm deeper (Fig. 3.12i) to further illustrate the misregistration of images due to spherical aberration.

The examples above demonstrate the critical importance of carefully selecting and knowing the specifications of the objective lenses used in confocal and fluorescence imaging. Co-localization studies are common in confocal microscope laboratories, and misinterpretation of co-localization data can easily occur if lenses are not corrected for the wavelengths of fluorochromes being used. Another common

application of confocal systems is three-dimensional reconstruction of data sets. To optimize these experiments, minimizing spherical aberration in the optical path is essential in maximizing the usefulness of the confocal system.

3.5 Filters

In fluorescence microscopy, filters are often necessary for ensuring that only light emitted by a fluorochrome in the sample is passed on to the detector and for blocking any stray light in the system. In addition, filters are needed to separate the various wavelengths of light emitted from different fluorochromes when using more than one color fluorochrome. Finally, in situations where non-monochromatic light is used for excitation, filters are necessary for restricting the excitation wavelengths to only those necessary for excitation of the fluorochrome and for restricting the wavelengths that might be mistaken for emitted photons.

Basic filters can be classified roughly as short-pass filters (also known as low-pass filters), long-pass filters (also called high-pass filters), and band-pass filters. A long-pass filter (Fig. 3.13a) blocks all light below a certain wavelength and transmits wavelengths longer than that cutoff. Conversely, short-pass filters (Fig. 3.13b) transmit wavelengths shorter than the cutoff and block longer wavelengths. Band-pass filters (Fig. 3.13c) pass light within a certain range of wavelengths and block all wavelengths above and below that range.

For a long-pass filter, the filter is named by the wavelength at which 50% of its peak transmittance is passed. Figure 3.13a shows the transmission curve for a 459-nm long-pass filter. The filter transmits only 1% of 450-nm light that reaches the filter. However, 92% of 500-nm light passes through the filter. This is the maximum transmittance for this filter. The half-maximum value is 46% and this value is attained with light having a 459-nm wavelength. The filter would thus be designated a 459-nm long-pass filter. Similarly, short-pass filters are named for the wavelength at which 50% of their peak transmittance is blocked.

Band-pass filters transmit a range of wavelengths. The range can be very narrow, as is the case for the filter depicted in Fig. 3.13c, or the spectrum can be broad. Band-pass filters are designated by their central wavelength and the range of wavelengths they transmit. The lower and upper boundaries of the range are determined as the wavelength at which the half-maximum values are achieved. This is often referred to as the full-width half-maximum (FWHM) value (double arrow in Fig. 3.13c). The central wavelength is the arithmetic mean of the upper and lower boundaries. For the filter depicted in Fig. 3.13c, the peak transmittance is 87%. Half of this value, 43.5%, is attained at 528 and 554 nm. The arithmetic mean of 528 and 554 is 541, and the range from 528 to 554 nm is 26 nm. The filter would thus be designated as a 541/26-nm band-pass filter.

Fluorescence microscopy also employs a specialized type of filter called a dichromatic beam splitter (also known as a dichroic mirror). Most filters are designed to have a zero angle of incidence. This is the angle between the optical

axis of the incident light and the angle normal to the filter surface. The dichromatic beam splitter is designed for high incidence angles, usually 45°. The beam splitter reflects light of short wavelengths and passes light of longer wavelengths, thus separating higher and lower wavelengths.

Figure 3.1 shows the filter arrangement in a standard epi-fluorescence microscope using an arc lamp source. An excitation filter (usually a band-pass or, sometimes, a short-pass filter) limits the wavelengths of light that illuminates the specimen. This helps to make sure that only the desired fluorophore is excited. A dichromatic beam splitter reflects this light to the back focal plane of the objective lens which focuses the excitation beam onto the specimen. In a well-designed microscope, very little of this excitation light is reflected back. In this way, only the light emitted from excited fluorophores is collected and focused by the objective lens. The emitted photons travel back to the dichromatic beam splitter. Since these have a longer wavelength than the excitation light, they are transmitted through the dichromatic beam splitter. A filter on the other side of the dichromatic beam splitter helps to limit the wavelengths that reach the detector. This emission filter (also called a barrier filter) is usually a long-pass or a band-pass filter.

3.6 Types of Filters

3.6.1 Glass Filters

A variety of devices are available that discriminate and separate different wavelengths. The most common are colored glass filters. These are inexpensive, have long useful lives, and are relatively insensitive to incidence angle. However, there are limitations to glass filters. Chief among them are low transmittance and high autofluorescence at longer wavelengths. Thin film interference coatings are an alternate method of making filters. These have high transmittance and can be designed to provide a wide variety of filtering parameters. The drawbacks of thin film coatings are that (1) their blocking performance holds for only specific wavelengths, so other blockers must often be added; (2) they are very sensitive to angle of incidence; and (3) coatings that work well for visible light are usually not ideal for UV and so UV performance is compromised. The monochromatic nature of laser emission means that barrier filters are not required to restrict the wavelengths of excitation light. However, lasers are high-intensity sources. While the high intensity of lasers can be an advantage in exciting fluorochromes and generating high signal levels, in many cases the intensity is so high that it is desirable to attenuate or decrease the intensity of light entering the optical path. Control of the intensity of light on the excitation side of the optical path is necessary to minimize photobleaching of the sample and to prevent cell death when imaging living samples. In early generation instruments, this was accomplished by placing a neutral density filter in front of the laser to decrease the amount of light entering the scan head. For instance, in the BioRad MRC 1024 line of instruments, neutral density filters that allowed 0.1, 0.3, 3, 10, 30, or 100% (no filter) of the laser light through were

options when imaging a sample. When samples were either very bright or susceptible to photobleaching or death, filters that allow small percentages of laser light through to the sample could be selected. When samples generated a relatively poor signal, neutral density filters that allow more excitation photons into the optical path could be used to improve the signal generated from the sample. However, this method of controlling the amount of excitation light contacting the specimen was limited in the selection of intensity level and also resulted in excitation of the entire sample area; no imaging could be done on smaller regions of interest (ROIs).

3.6.2 Acousto-Optical Tunable Filters

Many newer laser confocal systems utilize acousto-optical tunable filters (AOTF) to provide precise control of the laser intensity and the area of sample, or ROI, that is excited. AOTF assemblies consist of a quartz filter subjected to various levels of ultrasound. By adjusting the intensity of the ultrasonic wave, the intensity of the laser light passing through the quartz can be adjusted between 0 and 100% in 0.1% increments. This provides very precise control over the intensity of light entering the optical path. In addition, selection of single or multiple excitation wavelengths of light for excitation is much easier with an AOTF than with a filter wheel containing multiple excitation filters. This is an important advantage when imaging multiple fluorochromes either simultaneously or sequentially.

An additional advantage of AOTF systems is that specific ROIs can be selected for excitation, while the remaining areas of the sample are not exposed to excitation photons (Fig. 3.14). This is often important in samples that are sensitive to intense beams, such as living cells, since regions of the specimen outside the area of excitation are not illuminated and thus escape any damage. ROI imaging is also very useful for applications that involve rapid processes or restricted illumination of only small areas of the sample, such as Förster resonance energy transfer (FRET) or fluorescence recovery after photobleaching (FRAP).

3.6.3 Acousto-Optical Beam Splitters

There are several potential problems with the dichroic filters that are commonly used to sort the excitation and emission photons in widefield fluorescence and confocal microscopes. In many confocal studies, multiple fluorochromes are used and this requires the use of a series of filters in order to separate the excitation and emission wavelengths of the multiple fluorochromes adequately. Typically, the number of filters available in a system is limited and the ones available may not provide the optimal transmission of photons for the range of fluorochrome wavelengths being generated. Even if multiple dichroic filters are available on a system, it is necessary to shift between these beam splitters mechanically as different fluorochrome excitation and emission wavelengths are generated. Although the filter changes are software

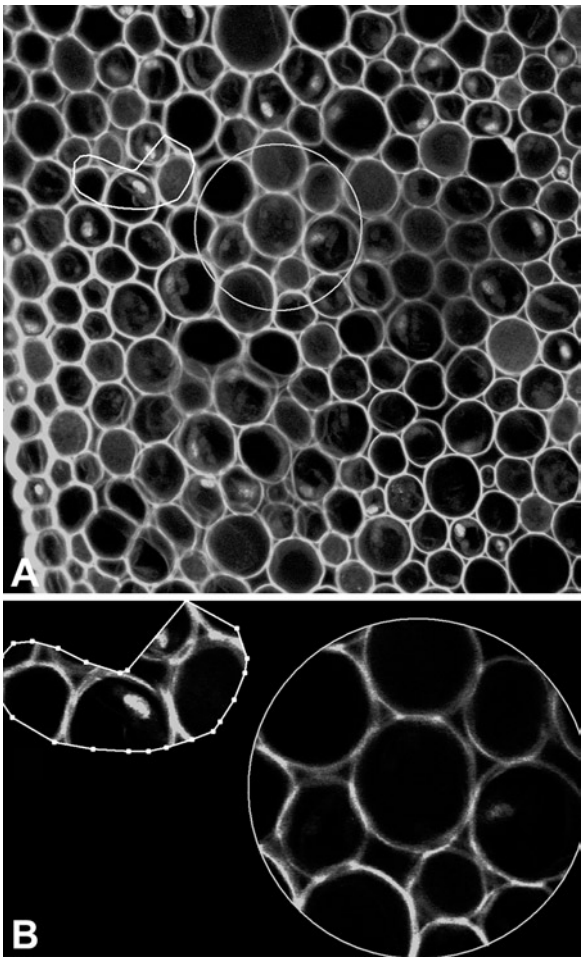

Fig. 3.14 Illustration of selection of ROI areas for scanning to increase the speed of scanning in select regions and to preserve the specimen in areas outside of the ROI. In (**a**), the entire specimen (Convallaria root tip) has been scanned and then a standard *circle* ROI and a hand-drawn ROI selected and scanned as shown in (**b**)

driven and relatively fast, they do slow acquisition times when imaging multiple channels. Moreover, the mechanical shifting of filters can introduce vibrations. Finally, glass filters are not absolutely efficient and so not all incident photons are passed through the filter. This decreases the signal and may adversely affect the signal-to-noise ratio in the final image.

In 2002, Leica introduced the acousto-optical beam splitters (AOBS) as an alternative to dichroic mirrors in their confocal systems (Borlinghaus et al. 2006). Similar to dichroics, the AOBS transmits short-excitation wavelengths of light to the specimen and also directs the transmission of longer wavelength photons emitted from the specimen to the detector. However, the AOBS utilizes an electronically

tunable acoustic crystal in place of the dichroic mirror and is a fixed device. The ability to tune the AOBS electronically eliminates the need for dichroic mirrors to be mechanically inserted or removed from the optical path. This allows for faster switching between laser excitation wavelengths (lines), the use of up to eight illumination lines simultaneously, and the selection of narrow bands of light (0.6–2.0 nm) for excitation of fluorochromes. All these are done without having to move the filters physically.

3.7 Determining an Optimum Filter Combination

Choosing the correct filter set for a given fluorophore is simply a matter of matching the characteristics of the fluorochrome with those of the filters. In Chap. 2, Fig. 2.3 depicts the excitation and emission curves for TRITC. This fluorochrome has a peak excitation at 555 nm and peak emission at 580 nm. The range of excitation wavelengths at FWHM is 533–571 nm. To optimize fluorescence, the microscopist would like an excitation beam that is within this range and as close to the excitation maximum as possible. However, overlap with the range of emission wavelengths should be avoided. For TRITC, the emission range at FWHM is 563–610 nm. Thus, there is an overlap of the excitation and emission FWHM values between 563 and 571 nm.

A 540/25-nm band-pass filter would limit the excitation light to below the TRITC emission range. The 543-nm wavelength of a helium–neon laser could also be used for excitation of TRITC. This wavelength is well out of the emission range of TRITC, but would promote sufficient absorption. A 565-nm dichromatic beam splitter would reflect the excitation light and pass most of the light emitted from TRITC. Finally, a 575-nm long-pass filter would ensure that most of the signal hitting the detector is specifically from the excited TRITC. This, of course, is not the only filter combination that could be used with TRITC. For instance, a 610/75-nm band-pass filter would also work as a TRITC emission filter, as would an optimally tuned AOBS.

For detecting fluorophores of a single wavelength (single color detection), the choice of the filters to use is relatively simple since you do not need to worry about specific excitation of or emission from competing fluorophores. This is not the case when you want to detect two or more fluorophores in a single sample. The presence of multiple fluorophores increases the probability of spectral overlaps. This is a problem because in fluorescence microscopy, the detectors most often used do not discriminate between wavelengths (i.e., they do not recognize color); they only record the presence or absence of photons (the standard detectors used in confocal microscopy are described further in Chap. 7). The color specificity assigned to photons is arbitrary but generally based on assumptions about the wavelengths that are transmitted to the detector by the filters that are placed in the light path. If the microscopist has selected these filters incorrectly, spurious interpretations can occur.

Two principal types of artifacts can occur with imperfect filtering when two or more colors of fluorescence are analyzed. The first artifact results when the emission from the first fluorochrome has the proper wavelength to excite the

second fluorochrome. This situation is depicted in Fig. 3.15. The emission peak of fluorochrome I falls within the excitation wavelengths of fluorochrome II. Without attention to proper filtration, this scenario could result in the fluorescence coming from both fluorochromes I and II being incorrectly interpreted as coming only from fluorochrome I based on the excitation wavelength employed. However, with a suitable emission band-pass filter, the emission from fluorochrome I can be discriminated from that arising from fluorochrome II as long as there is no substantial overlap of the two emission spectra. Figure 3.16 depicts two hypothetical emission peaks and indicates a band-pass filter which would allow detection of emission from only fluorochrome I. An alternative would be to choose different fluorophores where the emission spectrum of one does not overlap the excitation spectrum of the other. This is the safer alternative.

The second problem in assuring specificity of detection arises when two emission spectra have substantial overlap as shown in Fig. 3.17. If both signals are strong, as depicted in Fig. 3.17a, it would not appear that the fluorochrome I emission (stars) makes up a substantial component of the emission assigned to fluorochrome II (circles) using a band-pass filter designed for fluorochrome II (in this case, a 600/50-nm band-pass filter). However, if the signal from fluorochrome II is low compared to that of fluorochrome I, the emission assigned to fluorochrome II could be substantially overestimated. Moreover, even if fluorochrome II was not present, a signal would be detected and spuriously assigned to fluorochrome II. Thus this overlap of emissions (termed bleed-through) must be carefully guarded against and proper controls initiated to test for possible overlap. Of course, one could use narrower band-pass emission filters to collect only photons from the nonoverlapping regions, but, as in the example shown in Fig. 3.18, this may substantially reduce the number of photons collected. In fact, the signal could be reduced enough so that it is not distinguishable from noise, leading to spurious conclusions about the amount of fluorophore present. A better approach is to excite the two fluorochromes

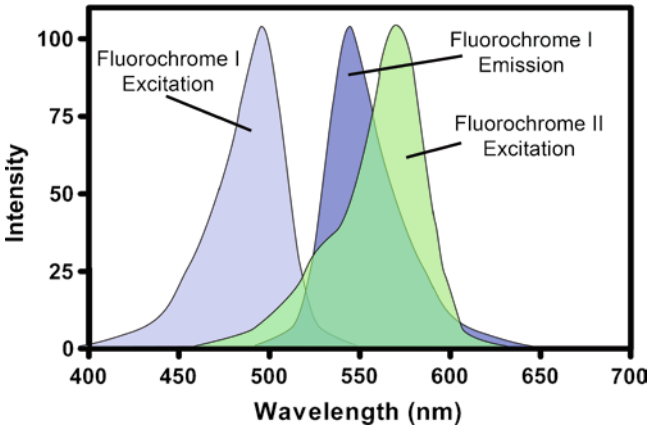

Fig. 3.15 Spectral overlap of emission from one fluorophore with excitation of a second fluorophore

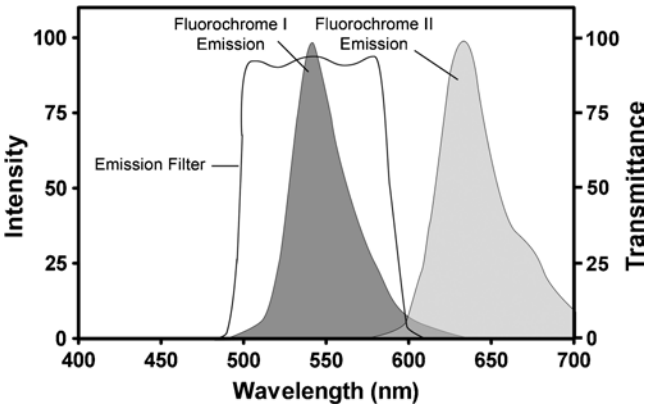

Fig. 3.16 Use of band-pass filter to separate emission of one fluorophore from emission of a second fluorophore when the two fluorochromes have similar excitation spectra

separately in a sequential fashion rather than attempting to collect the two signals simultaneously. Sequential collection removes the necessity to discriminate between two simultaneously excited fluorochromes. Advancements in automation of functions such as filter switching make sequential imaging of two or more fluorochromes much faster and easier. Most modern confocal microscopes are ideal instruments for such a sequential approach.

There are also mathematical techniques that attempt to determine the contribution of two or more overlapping fluorophores to a complex spectrum. These techniques, often referred to as spectral analysis or spectral unmixing, are discussed in Chap. 9 and are an advancement found in the latest generation of laser scanning confocal microscopes. They allow for specific detection of fluorochromes with overlapping spectra. However, by far, the best and easiest approach to separate fluorescent signals is to use fluorochromes with widely separated emission spectra, whenever possible.

In all cases, you need to confirm that your filter combinations are working as expected. This can be done by exciting one fluorochrome at a time while monitoring the emission being transmitted through all the other filter combinations. There should be no signal above background through any of the filter sets other than the one for the fluorochrome of interest.

3.8 Optimizing the Fluorescent Signal

Because of a number of factors, the amount of light reaching the detector in a fluorescence microscope is relatively low. Even with very sensitive detectors, one must still ensure that the signal strength is sufficiently high compared to background noise. Otherwise, you cannot be confident regarding the accuracy of what is detected. Throughout the remaining chapters of this book, we will discuss methods to

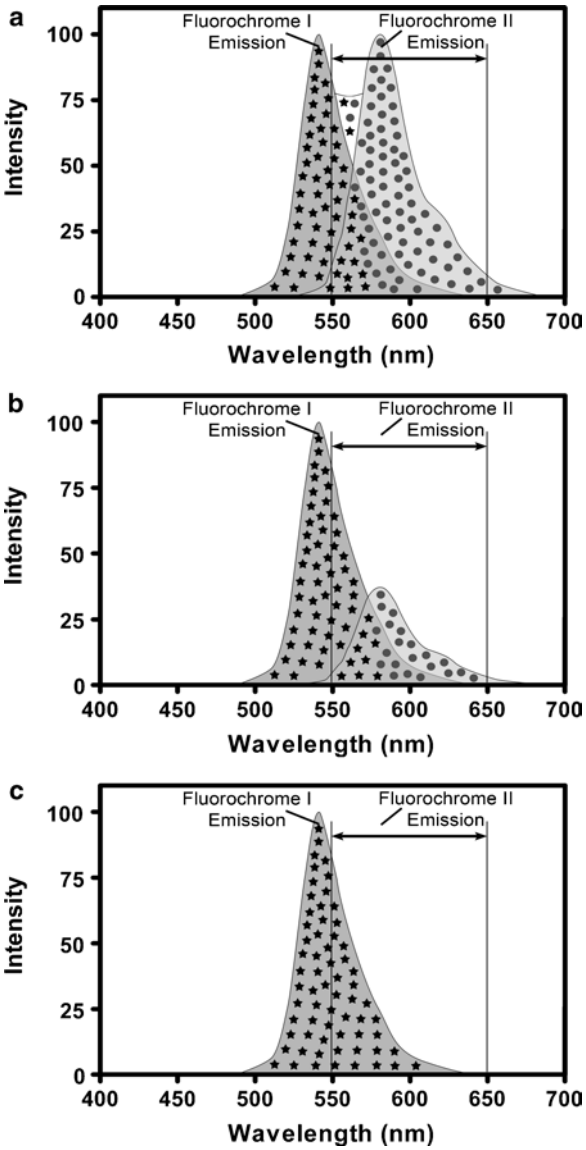

Fig. 3.17 Simultaneous two-color fluorochrome detection and the effect of bleed-through of signal assigned to the higher wavelength fluorochrome. (**a**) When the signal from fluorochrome II (*circles*) is strong, the bleed-through of fluorochrome I (*stars*) has a limited but still significant effect on the signal detected using a 600/50-nm band-pass filter. (**b**) When the signal strength of fluorochrome II is weak, the bleed-through of fluorochrome I becomes the dominant signal. (**c**) When fluorochrome II is not present, the bleed-through produces a signal that could be spuriously interpreted as the presence of fluorochrome II

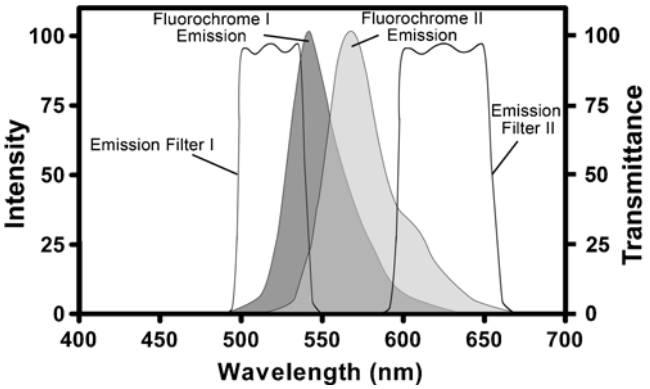

Fig. 3.18 Band-pass filters for separating nonoverlapping regions of two fluorophores with overlapping spectra

increase the number of photons detected. This aspect of confocal microscopy cannot be overemphasized. "Photons are your friends, don't abuse them!" should become your mantra. In order to maximize signal, it is imperative to review the excitation and emission spectra of your fluorophore(s) carefully and choose your filters based on these spectra. It is cheaper in the long run to buy additional filters, if needed, than to misinterpret critical data because of sloppy microscopy. Once the correct filters are in place, additional key elements for maximizing signal strength include (1) properly aligning all elements of the excitation and emission pathways, (2) removal of dirt and other obstacles that would impede the flow of photons to the detector, (3) matching, as close as possible, the refractive indices of all parts of the imaging path, including the specimen so that photons are not lost due to refractive index mismatch, (4) minimizing loss of energy to competing processes (e.g., photobleaching) which decreases the fluorescence signal, and (5) using a high-numerical aperture lens to collect as much of the emitted light as possible.

References

Borlinghaus R, Gugel H, Albertano P, Seyfried V (2006) Closing the spectral gap - the transition from fixed parameter fluorescence to tunable devices in confocal microscopy. Proc SPIE 6090: 60900T60901–60906.

Diaspro, A. Federici, F, and Robello, M. 2002. Influence of refractive-index mismatch in high-resolution three-dimensional confocal microscopy. Applied Optics 41(4):685–690.

Dunn, KW. And Wang, E. 2000. Optical aberrations and objective choice in multicolor confocal microscopy. Biotechniques 28(3): 542–550.

Samoc, A., Miniewicz, A., Samoc, M., and Grote, J.G. 2007. Refractive-index anisotropy and optical dispersion in films of deoxyribonucleic acid. J Applied Polymer Science 105:236–245.

Voros, J. 2004. The density and refractive index of adsorbing protein layers. Biophysical Journal 87:553–561.

Chapter 4
Specimen Preparation

W. Gray (Jay) Jerome, John Fuseler, and Robert L. Price

Keywords Objective lens • Paraformaldehyde/formaldehyde • Photobleaching • Refractive index • Refractive index mismatch • Signal-to-noise ratio • Working distance

4.1 Introduction

A key difference between confocal microscopy and widefield microscopy is that the aim of confocal is to explore the structure and structural relationships along the optical (*Z*) axis as well as in the *X*-*Y* plane. In other words, the investigation of spatial relationships is being evaluated in at least three dimensions. Often, this involves the collection of a series of planar images along the *Z* axis and the reconstruction of the data into an image that depicts all three dimensions. However, even when the interest is solely in a single *X*-*Y* plane, the goal is to separate as thin a plane of information as possible from the planes directly above and below. Obviously, in order to acquire and analyze three-dimensional (3D) structural information, the 3D structural relationships must be preserved during the preparation of the sample. In contrast, in standard widefield microscopy information along the *Z*-axis is merged into a single 2D image. Because of the added need to preserve the 3D structure for confocal images, methods suitable for preparing samples for widefield microscopy must often be altered to accommodate the additional demand of preserving relationships in the third dimension.

In confocal, as with any other microscopy technique, there is no single best method of preparing a sample that can accommodate all types of samples, all possible methods of staining specific structures, and all possible modes of imaging. Optimum biological sample preparation for confocal microscopy is very dependent upon the cell or tissue type, the labeling technique, and type of data to be collected.

W.G. (Jay) Jerome (✉)
Department of Pathology, Vanderbilt University Medical Center,
U-2206 MCN, 1161 21st Ave, South Nashville, TN 37232-2561, USA
e-mail: jay.jerome@vanderbilt.edu

R.L. Price and W.G. (Jay) Jerome (eds.), *Basic Confocal Microscopy*,
DOI 10.1007/978-0-387-78175-4_4,

In this chapter, however, we will review some basic concerns that need to be addressed for all types of samples and lay out some basic principles that help guide decisions about sample preparation.

4.2 Preserved Samples Versus Live Imaging

After defining the goals to be achieved for a particular confocal imaging application, the next decision is whether it is most appropriate to view living or preserved (fixed) samples. Key questions to guide this decision include the following: (1) Will rapidly changing events be analyzed? (2) Will native fluorescent molecules or exogenous fluorochromes be imaged? And (3) how bright is the fluorochrome? Live imaging is a powerful technique that allows the analysis of dynamic events and avoids some of the artifacts that can be introduced by specimen preservation and processing. Although it is possible to image thin tissue slices in organ culture, live imaging usually involves continuous viewing of cells in culture. Specimen preparation for live cell imaging is more straightforward than for imaging fixed material, but this often comes at a price. Since the specimen is not preserved, the microscopist must ensure that the act of viewing the sample does not introduce artifacts. Fairly elaborate systems for keeping the cells healthy during imaging are also required. In addition, the excitation (laser) energy must generally be kept at a low level to minimize photodamage and cell death. This reduces the signal that can be generated from fluorochromes and so increases the need to make sure that signal collection is maximal. If a fluorophore is already a weak emitter, it might be better to consider imaging it in a fixed material where higher intensity excitation energy can be used because cell death is not a consideration. There are also fewer fluorophores available for live cell imaging, although this is improving with the development of several varieties of fluorescent proteins such as green fluorescent protein (GFP), red fluorescent protein (RFP), and others that have been designed for live cell work.

Finally, one needs to consider the rate at which the event of interest occurs. The number of frame captures per second in laser scanning confocal can vary depending upon conditions, but will generally fall between 0.1 and 1 frame per second in most confocal microscopes. This is adequate for following some processes, but many reactions such as calcium fluxes in cells happen at a faster rate than this. If the event of interest occurs at a faster rate, one should consider faster imaging methods, such as spinning disk confocals, or abandon confocal altogether and use a widefield microscopy approach.

Working with fixed samples negates the ability to observe events in real time, although dynamic processes can sometimes be inferred from a series of static images. Fixed material, though, is easier and more forgiving to image. In fixed samples, one does not have to worry about keeping the cells or tissue alive, neither is specimen damage much of a concern, since fixed material will hold up to most confocal viewing modes. Fluorophore bleaching, though, remains a critical issue. Even though there is less concern about artifacts induced by the photon beam's

interaction with the specimen when viewing fixed material, one must be very concerned about the effects of fixation and subsequent specimen preparation on the sample architecture. The next few sections provide some details regarding specimen preparation and concerns for fixed material and live material imaging.

4.3 Working with Fixed Samples

In many ways, working with fixed material simplifies microscopy imaging. In particular, you do not have to worry about keeping the sample alive and healthy. Moreover, a fixed sample is generally more resistant to excitation beam-induced changes. The choice of available fluorophores and techniques to employ fluorophores is also much greater when working with fixed material. For this reason, the majority of confocal experiments use fixed samples. However, the trade-off for the simplification of microscopy is the fact that more processing of the sample is required prior to microscopy and one must make sure that this processing does not induce unrecognized artifacts. There are few absolutes regarding the best method of specimen preparation. However, if one understands the general principles and has clearly defined the experimental goals, a reasonable set of decisions can be made regarding the most appropriate procedure.

4.3.1 Fixation

The first parameter to consider when working with fixed samples is which fixative to use. A perfect fixative should maintain all cellular structures in their native state, eliminate destructive autolytic processes, and protect the material against damage during subsequent processing and microscopy. In addition, if the sample will be immunostained, the ideal fixative should also preserve the ability of subcellar molecules to bind their antibodies. As with most things in microscopy, a perfect fixative does not exist and so the microscopist must weigh the relative benefits and drawbacks of each fixative protocol relative to the experimental goals.

Fixatives can be divided into two general types: precipitating fixatives and those that cross-link proteins. Precipitating fixatives are generally organic solvents. The most common ones in use for microscopy are alcohols and acetone. Precipitating fixatives work by dehydrating and precipitating some components, usually proteins, within the cell or tissue. Because many of the changes brought about by these fixatives can be reversed by rehydration during staining, they are often employed in immunocytochemistry experiments because the reversal sometimes increases antibody binding to the antigen of interest. An additional advantage is that they remove the lipids and small soluble cellular molecules. This permeabilizes the membranes and enhances the access of antibodies to cellular antigens. However, they should not be the first choice for confocal experiments because cell shrinkage can be as high as 70%, particularly along the optical axis as cells are dehydrated and lose

their contents. Although this is useful in widefield fluorescent experiments because the inherent flattening of the sample lessens the amount of out-of-focus material that blurs the image, this shrinkage can severely alter the 3D relationship of intracellular structures. It is our experience that, often, structures not generally adjacent in real life become co-localized in space after ethanol fixation.

An alternative to precipitating fixatives is cross-linking fixatives. Aldehydes are the most often used cross-linking fixatives, with solutions of formaldehyde or glutaraldehyde being the most common. These work by forming intermolecular bridges between components of the cell. The fixation generally involves binding of the aldehydes to free amino groups to create a network linking the cellular constituents together and holding them in place. Cross-linkers do a better job of maintaining structural integrity than do fixatives that act by dehydration and precipitation. However, they often reduce the antigenicity of molecules more severely. In addition, because they do a better job of maintaining membrane structure, intracellular staining with antibodies generally requires sectioning, permeabilization, or both, to allow stains to access intracellular structures.

Glutaraldehyde in a concentration range of 2–5% in buffer does a better job of preserving fine structural detail than does formaldehyde. However, glutaraldehyde is highly autofluorescent, in part due to the presence of free amines after fixation. The autofluorescence can be partially quenched by incubation with 1% sodium borohydride but, in general, it is best to avoid glutaraldehyde for confocal microscopy experiments unless you are using a very bright fluorophore which can be easily detected above the autofluorescence. If it is essential that glutaraldehyde be used, it may be possible to avoid the typical green-yellow autofluorescence of aldehydes by selecting a fluorochrome which emits in the far-red range, allowing you to filter out the green-yellow aldehyde fluorescence.

Dilute solutions of formaldehyde (3–10%) in buffer are the most common fixatives used for confocal microscopy. However, formaldehyde in solution can quickly decompose to formic acid. This contaminant reduces the fixation efficiency of formaldehyde solutions. For this reason, working strength solutions of formaldehyde should be made fresh or diluted from higher strength solutions of formaldehyde that have been stored in an inert environment.

Sealed vials containing 10–25% formaldehyde in nitrogen gas can be purchased and used to make up working strength formaldehyde solutions. The lack of oxygen in the vial prevents the formation of contaminants. Alternatively, formaldehyde, which is a gas, can be liberated into solution by heating paraformaldehyde powder in an alkaline solution. Paraformaldehyde is a crystalline condensate of 8–100 formaldehyde molecules. Regardless of how the working strength formaldehyde solution is made, it should be refrigerated and used within a few days to avoid the formation of contaminants. The purity of the formaldehyde solution can be tested by comparing the absorbance of a 0.5% solution at 235 nm and 280 nm. If the ratio of these values is less than 2, it indicates minimal contamination and the solution can be used. Formaldehyde fixatives having a ratio of higher than 2 should not be used as a fixative for confocal microscopy. A standard protocol for making a formaldehyde solution from paraformaldehyde is provided in Fig. 4.1.

To make 100 mL of a 10% solutions of formaldehyde in 0.1M Cacodylate buffer (this is sometimes referred to as a 10% paraformaldehyde solution):

1. In a 250 mL flask, add 20 grams of paraformaldehyde to 80mL of distilled water
2. Heat gently but do not allow to boil
3. At 60 C, water will start to condense on the inside of the flask and the paraformaldehyde will begin to dissolve.
4. When the solution has reached 60 C, add two drops of 2N sodium hydroxide (approximately 1 ml).
5. Maintain the solution at ~ 60-65 C and do not allow to boil. The solutions should slowly begin to clear as the paraformaldehyde crystals dissolve and the released formaldehyde goes into solution.
6. If the solution does not clear within 10-15 minutes, add an addition 2-3 drops 2N NaOH.
7. Cool the solution and add distilled water to 100 mL. This replaces any water that evaporated).
8. Add 100 mL of 0.2M Cacodylate buffer.
9. Keep solution refrigerated and use within 3 days.

The working strength fixative solution is produced by diluting the 10% solution just prior to use. Some researchers include 1% calcium chloride to help preserve membrane structure.

Fig. 4.1 Protocol for preparing buffered formaldehyde from paraformaldehyde

Aldehyde fixation protocols vary depending upon the application and the method of staining. However, a few concerns are reasonably consistent across applications. Aldehyde fixatives should always be made fresh, kept cold, and be used within a few days. Although it is best to keep fixatives refrigerated until used, the actual fixation should take place at room temperature or warmer. Cold temperatures disrupt cytoskeletal elements and so can alter cellular size, shape, and the interrelationships of subcellular organelles. Both the sample and fixative should be at room temperature or warmer when fixation is initiated. After an hour of fixation, however, fixation can be continued in the cold. The length of time the sample is fixed and the concentration of fixative will vary depending upon the staining technique that will be employed. In general, however, a concentration of 4% formaldehyde for 1–2 h is generally suitable for samples that are thinner than 500 μm along at least one axis. An overnight fixation, at room temperature for the first hour and in the refrigerator for the remaining time, is a general fixation protocol that is often employed. Shorter periods or more dilute solutions may be required for some antibodies used as stains. Empirical testing is the only sure way to maximize fixation protocols for your unique needs.

It is always best to process, stain, and image samples immediately after fixation is complete. However, this is not always possible. Fixed samples can be kept refrigerated in fixative for weeks, but additional cross-linking may occur which can further alter epitopes leading to additional reduction in staining affinity. Glutaraldehyde-fixed samples are generally stable and can be rinsed and placed in a buffer solution after fixation for storage up to a few weeks. In contrast, the cross-links formed by formaldehyde are less stable. In some cases, prolonged time in buffer solutions (or water) can reverse the effects of fixation. This can prove advantageous in some instances, since antigenicity may be restored and staining improved. However, for most applications, prolonged storage of formaldehyde-fixed samples in buffer should be avoided. It may lead to a reversal of fixation,

increased autolysis, and loss of the 3D architecture. In extreme cases, loss of all sample structure may occur. If prolonged storage of formaldehyde-fixed samples is necessary, it may be advisable to store in buffer with 0.5–1% formaldehyde added. This solution should be changed weekly as formic acid and other contaminants may form in the stored sample.

4.3.2 Mounting Specimens

Immunostaining of fixed specimens is covered in Chap. 5. After staining, the prepared samples can be viewed with an inverted microscope without further processing. Culture chambers attached to thin cover glasses or tissue culture plates with part of the bottom of the plate replaced with a cover glass allow cells to be grown, processed, and observed directly with an inverted confocal microscope. These tissue culture/viewing chambers can be made in the laboratory or purchased from suppliers of microscope accessories. Figure 4.2 provides a few examples of the many alternatives that are commercially available. Chambers that are affixed to glass microscope slides or plastic dishes can also be used to view samples directly. However, using standard glass slides or plastic culture dishes results in part of the working distance of the objective lens being used to image within the glass, and this reduces how much of the specimen depth can be probed.

The more important reason, though, for avoiding imaging through thick glass slides or glass dishes is that their optical properties are not matched to modern

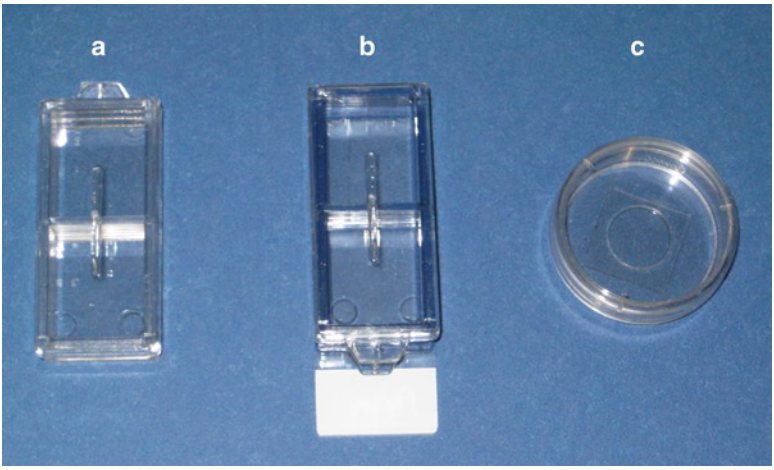

Fig. 4.2 Commercially available culture chambers adapted for microscopy include culture chambers on cover glasses such as the Labtek chamber cover glass (**a**) from Thermofisher Scientific (Rochester, NY), culture chambers on glass microscope slides such as the Labtek chamber slide (**b**) from Thermofisher Scientific, and plastic culture dishes with cover glass over a central viewing hole in the plastic such as the MatTek glass-bottom dish (**c**) from MatTek Corporation (Ashland, MA)

objective lens. Plastic dishes have the same limitation and their optical properties result in even further loss of photons and decreased signal-to-noise ratio. In contrast, cover glasses are thinner allowing more usable working distance within the specimen. Chambers mounted on thin cover glasses or plastic dishes with a thin cover glass window for use with inverted microscopes are readily available commercially.

Whether using an inverted or upright microscope design, it is critical to use a number 1½ cover glass with your samples unless the objective lens that is being used is designed to be used without a cover glass. Almost all high-resolution lenses are specifically designed to work with a number 1½ cover glass. This represents a thickness of about 170 μm. Since the refractive index of a 1½ cover glass is considered in the design of the lens, cover glasses of other thicknesses can produce a mismatch of refractive indices, leading to a loss of photons collected from the image. The deleterious effects of refractive index mismatch are discussed further in Chap. 3.

The closeness of the tolerance permitted in number 1½ cover glasses varies among suppliers, but no group of 1½ cover glasses will all be exactly 170-μm thick. Subtle differences in cover glass thickness will influence the image quality and this will be particularly apparent with high-numerical aperture lenses. For this reason, the best of these lenses are supplied with correction collars that allow the microscopist to adjust the tube length to compensate for the actual cover glass thickness as discussed in Chap. 3. Suffice it to say that using the proper cover glass thickness is important for achieving maximum image quality.

For widefield microscopy, one additional benefit of having a cover glass present is the fact that it flattens the viewed surface of the specimen. This minimizes variations in light scattering that can occur from a rough surface. With most samples, the cover glass flattens more than just the surface; it can greatly compress the entire thickness of the sample. In widefield microscopy, the decrease in specimen thickness decreases the amount of out-of-focus information from the sample and, thus, increases specimen contrast and improves visibility. Of course, this is at the expense of preserving the 3D architecture. For this reason, in confocal imaging where the goal is to analyze the 3D architecture, it is best to avoid this kind of artifactual flattening. The best way to do this is to provide some type of riser to maintain the cover glass at a suitable height above the specimen. However, the cover glass should not be placed too high above the specimen because this would result in too much of the working distance of the lens being used to image the fluid above the specimen, thus limiting the depth within the specimen that can be imaged.

Risers can be fashioned out of any material. Many microscopists place shards of broken cover glasses at the four corners of a cover glass to hold the cover glass at a height of 170 μm. Risers can also be fashioned out of VaLaP (Molé-Bajer 1968). This is a nontoxic mixture composed of equal parts (by weight) of *Va*seline petroleum jelly, *la*nolin, and low melting point (56°C) *p*araffin. All the components are available from most scientific supply houses, and Vaseline and lanolin are also available at most drug stores. VaLaP is a compressible solid at 37°C but melts to a liquid at low heat (45–50°C). This makes it easy to fashion VaLaP into desired shapes within a temperature range which will not damage cells.

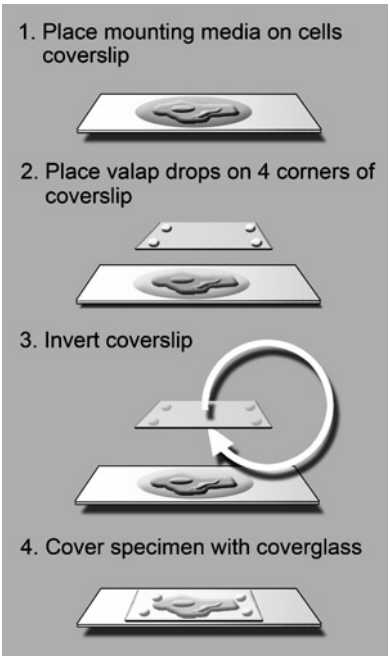

Fig. 4.3 The use of VaLaP to prevent cover glass from overly compressing mounted samples

VaLaP risers are made by applying a small drop of liquid VaLaP on each corner of a cover glass and letting it cool to hardness (Fig. 4.3). A wooden applicator stick or fine point watercolor brush are ideal for placing VaLaP drops on the cover glass. When the VaLaP has hardened, the cover glass is inverted and placed over the wet sample on a glass slide, extruding excess fluid but not allowing the coverslip to smash the sample. Gentle pressure will compress the VaLaP risers to the desired height and adhere the risers and cover glass to the underlying slide. Liquid VaLaP can then be painted around the edges of the mount. When hardened, this will form a watertight seal that will prevent the mounting fluid from evaporating and drying out the sample. Brief exposure of cells to the 45–50°C temperature of warm VaLaP is well tolerated by most cells.

An additional benefit to using VaLaP as a sealant is that if some of the VaLaP should accidentally be transferred to an objective lens by contact, it can be easily removed. This is not true for some of the commercially available sealants or the ubiquitously used finger nail polish. Many an expensive objective lens has been lost due to contact with not quite dry fingernail polish. The VaLaP seal, however, can breakdown over time and so is not suitable for long-term storage of slides. If long-term storage is required, after initial viewing, the VaLaP sealant (but not the risers) can be peeled away and replaced with a more permanent sealant. Just make sure that ample time is allowed for the sealant to dry completely before the preparation is viewed under the microscope. A wait of at least 2 days before viewing is a good rule of thumb.

Samples for confocal microscopy are usually wet when mounted. The use of a suitable mounting media is encouraged. Commercially available mounting media, such as 1,4-diazabicyclo[2,2,2]octane (DABCO; Sigma-Aldrich), are available for this use. They are applied to the sample just prior to coverslipping the sample. These mountants match the refractive index of most biological samples and contain antioxidants that can retard photobleaching. However, equally good mounting media can be formulated inexpensively in the laboratory. Figure 4.4 provides a recipe for a very useful "lab-made" mounting media.

Mounting media that are applied as liquid and then harden to a solid that encases the sample are wonderful for long-term preservation of fluorescent samples. ProLong® (Invitrogen, Carlsbad, CA) is an example of this type of mountant. Unfortunately, although these mounting media are excellent for preserving samples, they contain polyvinyl alcohols and so are generally not suitable for most confocal experiments. Polyvinyl alcohol can produce severe tissue shrinkage that will disrupt the 3D architecture of the sample. Polyvinyl alcohol is also a powerful lipid solvent, so it is unsuitable for experiments where lipids must be preserved.

Although most objective lenses are designed for use with cover glasses, one class of lenses, known as dipping lenses, is made to be used without a cover glass (Fig. 4.5). These lenses are waterproof and can be lowered directly into a fluid

Phosphate buffered saline……100 ml
Glycerol……..……35 g
Para-phenylenediamine……0.25 g

Mix the ingredients and aliquot into 1ml units. Wrap in foil to protect from light. Store at -80 C.

This solution will keep for several years at -80 C.

Before use, the solution can be diluted with PBS to match even closer the refractive index of the specimen.

Para-phenylenediamine is an antioxidant which reduces photobleaching. It is light sensitive so avoid prolonged exposure to light.

Fig. 4.4 Recipe for a mounting media with suitable refractive index and anti-fade properties

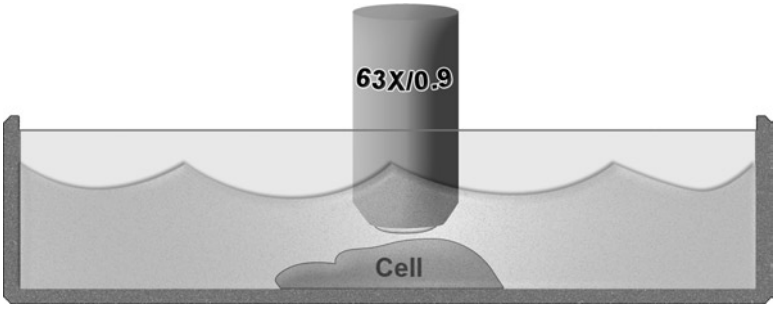

Fig. 4.5 Use of a dipping lens for viewing cells or tissue without a cover glass

environment, such as tissue culture medium, in order to image a specimen directly. A cover glass or mounting medium is not required with these lenses. This lessens the number of refractive indices that need to be matched. Dipping lenses generally also have longer working distances (up to about 2.5 mm). However, they have slightly lower numerical apertures (about 1–1.1) compared to similar water immersion lenses that are designed for use with cover glasses (usually NA of 1.3). They do, however, allow direct viewing of samples using upright microscopes without the worries of correctly coverslipping the sample. Further information on the use of various dipping and immersion lenses is presented in Chap. 3.

4.3.3 Working with Very Thick Samples

Even if the optical elements in the light path are optimized, only a few hundred micrometers of tissue can be imaged reliably. The effective depth of viewing is dependant on the content of the sample. Beyond this depth, photon scattering and absorption degrade the signal to undetectable levels. To image deeper regions of a sample, one can cut the tissue into sections to expose deeper areas. In most cases, this is done by mechanically slicing the sample into segments with the aid of specialized microtomes. If the sample is to be stained with exogenously applied fluorochromes, the slicing is usually done prior to staining because sectioning the tissue facilitates penetration of the stains.

The most common microtomes for slicing in conjunction with fluorescence staining are tissue slicers and vibrating blade microtomes. Tissue slicers consist of a blade attached to an arm which is mechanically raised and lowered while the underlying sample is shifted slightly after each stroke to slice the sample like a loaf of bread. In contrast, a vibrating microtome, such as a Vibratome (Vibratome Inc, St. Louis, MO), shaves sections off the top surface of a specimen using a rapidly vibrating blade. The material is kept cool in a fluid bath (generally water for fixed tissue or buffer for live material). The cool temperature makes the tissue more rigid to enhance slicing, the buffer helps maintain tissue viability, and the presence of a fluid helps lubricate the cutting operation. Sections are then retrieved from the bath onto a glass slide or other substrate for staining.

Some fixed tissues, such as liver, may be sufficiently rigid to allow sectioning without further stabilization. In most cases, though, it is preferable to add additional support to the sample before sectioning. This can be done by encasing the sample in a material that can be liquefied at low temperature for application, but which at room temperature or when slightly cooled (but not frozen) becomes rigid and provides support to protect the tissue from being distorted during slicing. A particularly useful material for encapsulating the sample is a 3–5% solution of agarose or a mixture of agarose (1%) and acrylamide (3%) (Germroth et al. 2005). Compared to paraffin wax embedment or other methods of embedding samples for microtomy, agarose encasement is simple, minimizes specimen manipulation that can produce artifacts, and does not require harsh solvents such

1. Melt Sigma type IA low gelling agarose in phosphate buffered saline in tube in a 55 C water bath to make a 5% agarose solution
2. Wash fixed tissue in same buffer as used for fixation.
3. Pour agarose solution into a small plastic weigh-boat. Immediately submerge tissue in agarose. Work quickly; the agarose will begin to set in about 5 minutes as it cools.
4. Chill sample in refrigerator to solidify agarose.
5. Remove the block from the weigh-boat.
6. Trim the block so that only a small amount of agarose surrounds the sample.
7. Blot the base of the block to remove excess fluid.
8. Superglue the agarose block to a Vibratome planchette or tissue slicer platform.
9. Use Vibratome or tissue slicer to slice into 50 μm thick sections following manufacturer's directions for the equipment.

Fig. 4.6 Protocol for preparing tissue for slicing prior to staining

as xylene or toluene, or the use of high heat. Figure 4.6 describes a standard procedure for preparing a sample for slicing.

4.4 Working with Live Cells or Live Tissue

Although tissue slices or thin organs (such as isolated blood vessels) can be imaged, the bulk of live imaging involves viewing cells. The principal benefit of live imaging is the ability to observe events in cells or tissue as they happen. However, to image samples in the live state requires that the cells or tissue remain viable and without artifactual structural changes. There are real challenges to accomplishing this goal and insufficient space in this text to address all of the concerns. However, a few guiding principles are worth mentioning. For a more complete discussion on the topic of live imaging, the reader is referred to a recent review by Waters (2007).

4.4.1 Live Cell Imaging Instrument Configuration

With respect to instrumentation, live imaging can be carried out with standard laser scanning confocal microscopes. However, for most applications, spinning disk confocals or multiphoton excitation imaging (Chap. 8) on an inverted microscope platform provides better alternatives because their imaging methodologies are not as likely to generate some of the negative influences on cell viability discussed below. In addition to the confocal capabilities, the microscope should ideally be equipped with phase contrast or differential interference contrast, and polarized light objectives. These modes of optics for live cell imaging are most useful in studies involving events associated with cell migration, motility, and cell division (karyokinesis and cytokinesis).

The primary concern associated with imaging of live cells and their responses to experimental conditions is being able to maintain the cells alive and under the stressful conditions of imaging. A key to cell viability is keeping the cellular environment in the necessary range with respect to temperature, CO_2 concentration, and humidity. In addition, these parameters need to be stable throughout the analysis period, which can be minutes to days or even weeks. For short-term experiments, some simple solutions can be devised, but longer experiments require special systems to maintain a suitable and stable environment. Most biological properties of living mammalian cells must be recorded at 37°C. This requires that heat be applied to the system to maintain the cells. Numerous solutions have been applied in trying to resolve this problem. One early approach was to heat the entire microscope by putting the instrument into a warm room with atmospheric control. This was impractical because the microscope could not be used for anything else, and water contamination was a severe problem leading to degradation of the microscope and optics.

Several commercially available stage heaters have been developed which heat the stage and optics Additionally, and various size chambers which may enclose the entire microscope or only a small platform on which the cells are grown have been devised. An innovative approach has been to construct a miniature version of an environmental control chamber (tissue culture chamber) which is mounted directly on a heated microscope stage. Various types of culture chambers can be used, including both closed and open systems. The simplest and least expensive of these culture systems are specialized tissues culture dishes (MatTek) which have a cover slip over an opening in the bottom of the dish on which the cells are grown. Cells grown in MatTek culture plates maintained in an environmental chamber have been continuously imaged for up to 72 h. These dishes are an open system that has the advantages of being inexpensive and easy to use. The main disadvantages of these culture dishes are that media exchange is difficult when performing wash-in/wash-out and laminar flow experiments.

For live cell imaging, plastic tissue culture plate dishes are usually unsuitable for several reasons. The thickness of the plastic culture dish is usually >2 mm, which is much greater than the depth of focus of both medium (20×) and high (40–100×) NA objectives, meaning that the specimen cannot be brought into focus. Additionally, the plastic dish is not optically flat or homogeneous over the surface in which the cells are grown. This results in degradation of the image of the specimen using any objective. In addition, the plastic used in the dish may be fluorescent, which can add high background fluorescence. Most plastics used in the culture dishes are also birefringent and cannot be used with differential interference contrast (DIC) or polarized light optics.

4.4.2 Live Cell Imaging Modes

Once the problem of keeping cells viable is solved, the next problem is deciding which imaging mode to use. Many biological and cellular processes have been studied in living unlabeled cells using specialized optical methods. The processes studied

cover both intracellular events (chromosome movements, vacuole formation kinetics, etc.) and cellular events (cellular migration and motility, cilia movements, cell division, etc.). The most commonly used optical system for imaging live cells involves phase contrast optics (for review, see Slayer 1976). However, with phase contrast, no optical sectioning is possible since phase contrast imaging is accomplished in the aperture plane of the microscope objective. Phase contrast imaging has limited use when combined with fluorescence imaging, but the fidelity of the fluorescent image or phase contrast-fluorescence overlay is dependent on absorptive characteristics of the phase plate and annulus which may adversely affect the fluorescent signal.

DIC provides a number of advantages for live cell imaging. Like phase contrast, DIC produces an image in which differences in the optical path through the specimen are made to appear as differences in intensities. However, with DIC the in focus region of the DIC image is remarkably shallow. Moreover, the DIC image is also free of specimen edge halos and disturbances from out-of-focus objects that reduces the utility of phase optics. This property makes the DIC image neatly sliced and isolated from out of focus information above and below the focal plane. Since DIC image formation is accomplished in the image plane of the objective lens, optical sectioning of the specimen becomes possible, albeit the optical sections are not as thin as those of an optimum confocal slice. Additionally, DIC images are completely compatible with fluorescence signals from the same specimen, making overlays of confocal fluorescence and DIC images useful.

4.4.3 Selection of Fluorescence Imaging Mode

It is possible to image endogenous molecules, such as NADPH (Piston and Knobel 1999; Williams et al. 1994), but more often the fluorophore is delivered exogenously. There are far fewer possible fluorophores that can be adapted to live imaging compared to those available for labeling fixed material. However, as discussed in Chap. 2, the advent of genetically encoded fluorescent molecules such as GFP, RFP and others has expanded the repertoire of possible live imaging probes. Application of these selective fluorescent probes offers several distinct advantages for live cell imaging. Included in these advantages are a high degree of sensitivity as, in many cases, the fluorescence signal allows visualization of single molecules. These can have a high degree of selectivity for detecting and visualizing precise locations of molecules to very specific regions or moieties of the molecules of interest. Under appropriate imaging conditions, the intensity of the fluorescence can also be used to quantify the number of molecules or binding sites of interest since, under normal conditions, fluorescence emission is linear with respect to the number of probe molecules bound to the molecule or site of interest.

There are several strategies available for loading living cells with an exogenously-delivered fluorescent probe. The easiest and most straight forward are the probes that are readily taken up by cells and include vital dyes and the AM-ester compounds. Vital dyes (acridine orange, for example) are minimally toxic or nontoxic at low

concentration and readily penetrate cell membranes and associate with the appropriate intracellular organelles. In general, vital dyes change emission spectra and/or intensity of emission when the intracellular environment is altered. For example, the AM-ester compounds are cell permeant as a result of the presence of the AM-ester moiety. Once the AM-ester compound enters the cell, the AM-ester moiety is removed by nonspecific cytoplasmic esterases, rendering it incapable of leaking through the membrane and back out of the cell. This approach allows for a precise amount of the fluorescence probe compound to be introduced into the cell and the emission quantified. These compounds are typified by the AM-ester probes used for the determination of intracellular calcium concentrations.

Fluorescent probes can also be taken up by cells by making use of the natural processes of pinocytosis or phagocytosis. In general, fluorescent molecules can be attached to substrates such as dextran, which the cell perceives as a usable sugar molecule. Dextran is not degraded by intracellular enzymes, and the dextran: probe conjugate is stable in the intracellular environment. This process can be enhanced by using additional agents to induce elevated rates of pinocytosis to increase the influx of the fluorescent reagent into the cell.

Introducing other types of probes, such as labeled ligands or antibodies, into cells and assuring that they reach their proper destination and do not perturb cell viability or structural integrity remains problematic and there is no single solution to this quandary. Gentle and transient permeabilization of cell membranes, microinjection of probes, and crafting probes that are freely permeable to membranes are just some of the approaches that have been used. Other more complicated approaches for introducing probes into cells, including physical microinjection and electroporation, have also been used with varying degrees of success (Beckerle 1984; Berglund and Starkey 1991).

4.4.4 Selection of a Fluorescent Probe

An efficient fluorescent probe for live cell imaging should have a high absorbance, a high quantum yield, a large Stokes shift, and a narrow emission spectrum. Additionally, the probe should have high specificity for the target molecule, since nonspecific binding of the probe will increase background fluorescence and result in degraded contrast of the image. In designing experiments, it is advisable to select fluorescent probes which use excitation/emission wavelengths close to those of filter sets that are most commonly available. The most commonly used filter sets for single and multiple labeling include DAPI (360/460), Cy2, FITC (490/515), Cy3, TRITC (555/570), and Cy5 (635/670).

4.4.5 Imaging the Living Cells

In collecting live cell images, the interaction of the excitation beam with the specimen is an important consideration. Major adverse conditions may arise as light interacts

with the probe, causing the generation of toxic compounds (phototoxicity) or photobleaching. Phototoxicity may also be induced in bright field imaging, but it is more commonly associated with fluorescence imaging. In experiments where time-lapse image collection of a fluorescent probe is extended for several hours and, in particular, when image collection is carried out over several days, phototoxicity becomes a real issue. Excitation of fluorescence molecules in the presence of oxygen leads to fluorochrome bleaching and generation of free radicals. These free radicals are predominantly derived from oxygen and induce potent and toxic hydroxyl radicals, singlet oxygen, and superoxide radicals, which react with water leading to the production of hydrogen peroxide. These free radicals and hydrogen peroxide can rapidly kill the cells.

Additionally, the interaction of bright field or fluorescent light with cells leads to the production of heat. Elevation of heat within the cell rapidly alters cellular function and results in cell death. To maintain the cells under normal homeostatic conditions, steps must be taken to limit the effects of chemical and heat phototoxicity. The time that the cells are exposed to the incident illumination must be carefully limited. This can be accomplished by limiting the exposure of the cells to periods of light only during image collection. Under these conditions, the cells are exposed to light for the optimal exposure time as determined by the experimental setup and camera used for image collection. Maximization of light collection, which results in shorter exposure times, can be accomplished by the use of high-NA immersion objectives. In general, the choice of optics and objectives will depend on the time duration of the experiment and how frequently images must be acquired to generate the data set.

Another problem frequently encountered in real-time or time-lapse imaging of cells is loss of image quality due to image and/or focus drift. In severe cases, the image of the specimen may be completely lost during short time periods of time-lapse image collection. There are two principal causes of image drift: mechanical and thermal. The major component of mechanical drift occurs as the microscope stage is moved to focus the specimen. For live cell time-lapse imaging, it is best to use a fixed-stage microscope, where focusing of the specimen is carried out by movement of the objectives. Loss of image quality can also be induced by focus drift of the objectives. Most live cell imaging systems have motorized focusing in the *Z*-axis to focus the objectives. The most common system in microscopes to move the objectives is a friction drive to control the level of fine focus of the specimen. The use of friction drives to control the fine focus is thus indirect and subject to slippage and focus drift. Drift is always a problem in these microscopes. Ideal control of the focal plane of the specimen is best acquired by the use of stepper motors directly mounted to gears controlling the fine focus. The use of gears and stepper motors constitutes a direct drive system with no possibility for focus drift.

Loss of specimen image quality due to thermal drift is the result of expansion and contraction of elements of the microscope. Since most biological properties of mammalian cells must be recorded at 37°C, this temperature must be maintained for the live cell specimen and elements of the microscope directly involved in viewing the specimen. Maintenance of constant temperature serves to minimize the effects of thermal expansion and contraction on focus. In all microscopes, inverted

or upright, the stage and especially the objectives act as heat sinks and are the main source of thermal induced focus shifts. The easiest solution to minimize thermal drift is to heat just the stage and the cells or specimen. This can be accomplished by the application of an environmental chamber to enclose the stage, cells, and objective being used. This type of system requires heat, CO_2, and humidity controllers and is relatively expensive, but easy to control and use. An alternative to these elaborate systems is a simple warm box mounted on the stage which encloses the specimen and objective being used. This simple arrangement has a significant drawback in that it is difficult to control the CO_2 and humidity accurately, but has the advantage of being inexpensive and easy to use.

4.4.6 Summary of Live Cell Imaging

As can be seen from the above discussion, imaging of living cells and tissues is not a trivial issue. It is imperative to limit specimen exposure. This involves working with low levels of excitation light, limiting the area probed, restricting the time the excitation beam dwells on a single microvolume, and scanning an area as few times as possible. However, all of these factors can lead to minimal interaction of the excitation photons with the sample and result in greatly reduced signal-to-noise ratios. It is always a good idea to optimize the system to collect as much fluorescence signal as possible from your sample, and in live cell imaging, this is imperative. To accomplish this, the refractive indices along the optical path must be accounted for and accommodated to make sure as much of the signal as possible remains focused on the confocal pinhole and thus reaches the detector. In some cases, it might be necessary to increase the size of the pinhole. This reduces the resolution along the optical axis (*Z*-axis) but allows more light to the detector. The use of high-NA lenses and high quantum efficiency detectors is also an important factor in the collection of sufficient signal. Finally, the use of scrupulously clean optical elements is important because even a small amount of dirt on a lens surface can deflect sufficient photons to degrade the image noticeably.

References

Beckerle, M. 1984. Microinjected fluorescent polystyrene beads exhibit saltatory motion in tissue culture cells. *J Cell Biol.* 98:2126–2132.

Berglund, D., and J. Starkey. 1991. Introduction of antibody into viable cells using electroporation. *Cytometry.* 12:64–67.

Germroth, P.G., R.G. Gourdie and R.P. Thompson. 2005. Confocal microscopy of thick sections from acrylamide gel embedded embryos. *Microscopy Res Tech*. 30(6):513–520.

Molé-Bajer, 1968 Studies of selected endosperm cells with the light and electron microscope. The technique. *Cellule*. 67, 257–265.

Piston, D., and S. Knobel. 1999. Real-time analysis of glucose metabolism by microscopy. *Trends Endocrinol Metab.* 10:413–417.

Slayer, E.M. 1976 Optical Methods in Biology/Robert Krieger Publishing Co. Huntington, NY. pp288–302.

Waters, J. 2007. Live-cell fluorescence imaging. *Methods Cell Biol.* 81:115–140.

Williams, R., D. Piston, and W. Webb. 1994. Two-photon molecular excitation provides intrinsic 3-dimensional resolution for laser-based microscopy and microphotochemistry. *FASEB J.* 8:804–813.

Chapter 5
Labeling Considerations for Confocal Microscopy

Ralph M. Albrecht and Julie A. Oliver

Keywords Affinity • Antibodies • Avidity • Cross-reactivity • Epitopes • Emission • Excitation • Fluorochrome • Quantum efficiency

5.1 Introduction

Some components of biological systems can be readily identified solely by their unique structure or other intrinsic physical properties which are evident when visualized in brightfield or various types of interference-based light microscopy (LM). However, for the unambiguous identification and localization of most biological molecular or macromolecular elements within a structural framework, some type of staining/labeling must be employed. This is important for a variety of applications including identification of particular tissues, identification of cells and subcellular components/structures, tracking of cells or subcellular components, and co-localization of cells and cellular components on or within tissues or cells. Labeling is also used to provide quantitative comparisons of epitope density, cell numbers, organelle numbers or volume, and a variety of other types of quantitative data. However, considerable caution must be taken when attempting quantitative or even semi-quantitative analyses. Efficiencies of labeling for different epitopes and antibodies or antibody mixtures vary. The exact relationship of color density, particle numbers, or fluorescence intensity (which can fade during observation), to the actual numbers of labeled sites is critical and often not known. These factors often make quantitative estimations or comparisons very risky.

R.M. Albrecht (✉)
Department of Animal Sciences; Pediatrics; and Pharmaceutical Sciences, University of Wisconsin – Madison, 1046 Animal Science Bldg., 1675 Observatory Drive, Madison, WI 53706, USA
e-mail: albrecht@ansci.wisc.edu

R.L. Price and W.G. (Jay) Jerome (eds.), *Basic Confocal Microscopy*,
DOI 10.1007/978-0-387-78175-4_5,

5.2 Types of Labels

A number of opaque, chromatic, and fluorescent-based labels have been developed for staining/labeling purposes. A wide variety of histo(cyto)logical stains, such as the well-known Wright's stain or H&E stain, and many others are commonly used. More recently, the conjugation of antibody to various metal nanoparticles including gold, silver, palladium, iron, and others has facilitated direct observation by interference LM methodology. The particles can be metal enhanced following labeling to render them visible in brightfield or white light confocal LM.

Histo(cyto)chemical staining techniques also make substantial use of chromatic and opaque methodologies. Various opaque or colored precipitates and dyes are available. This includes stains for enzymes such as peroxidase, phosphatase, or esterase. Certain enzymes can be conjugated to antibody labels, and the specific cytochemical reaction is subsequently used to localize the antibody. A typical example is the peroxidase stain where a precipitate forms at the site of the enzyme–antibody complex. This is identified in LM by its dark brownish color and can be stained with osmium. The resulting black precipitate can be visualized in LM. It is also electron dense and visible in the electron microscope. The fluorescence-based labels also have broad-based applications, particularly in the research arena. The advent of various nanoparticle-based labeling technologies has been particularly valuable for correlative light, electron, and force-based microscopies. While certain nanoparticles are fluorescent, others rely on their chromatic or opaque nature for identification. Currently, confocal microscopy is predominantly used in the area of fluorescence-based imaging; however, it should be noted that white light confocal microscopy or simultaneous confocal and wide-field imaging can be used to image and reconstruct images enhanced by chromatic or opaque labeling techniques. The development of high-sensitivity electron multiplying charge-coupled device (EMCCD) cameras used in conjunction with spinning disk confocal systems has facilitated the use of chromatic and opaque labeling along with the more common fluorescent labeling technology.

The use of small organic dyes or quantum particles that can be excited at one wavelength of light and then emit light at a different wavelength provides an extremely versatile labeling technology. The fluorescent dyes or particles can be conjugated directly to specific molecules of interest or to highly specific "identifier" species such as antibodies or ligands which bind selectively to the species of interest. When illuminated by the appropriate excitation wavelength, the resulting emission can be viewed. This provides an accurate localization for the dye molecule or particle and hence the conjugate as well. Fluorescent species having different, nonoverlapping, excitation and/or emission properties can be employed simultaneously to facilitate comparisons of the location of different molecular species and to examine co-localization of the different species.

Unfortunately, other than in multiphoton systems, any fluorescent molecules in the pathway of the illuminating excitation beam, whether in the front or at the back of the plane of focus, will also be excited and fluoresce. Due to the minimal

depth of focus in photon-based imaging, this results in the generation of substantial out-of-focus fluorescent light. The confocal microscope provides a mechanism of illumination in which out-of-focus information is minimized, providing a clear view of fluorescence from a single in-focus plane. Individual planes can be stored and subsequently combined to reconstruct a totally in-focus 3D image of the label localization. Such images can be superimposed on wide-field or interference-based images in order to put the labeled species more in the context of the biological structure.

5.3 Practical Considerations in Labeling

There are a number of practical considerations that have to be addressed relative to the particular question the investigator wishes to address. Suitable dyes have to be selected and matched with excitation sources of appropriate strength and wavelength. Historically, fluorescent dyes were developed which matched the emission peaks of mercury vapor lamps. Xenon lamps with a more broad emission peak permitted the use of dyes with excitation peaks not covered by mercury. A number of laser-scanning types of confocal light microscopes have been developed to provide appropriate illumination for confocal fluorescent labeling. This has resulted in the development of newer fluorescent dyes whose excitation wavelengths match the available, reasonably priced, laser excitation wavelengths. The spinning disc type of confocal microscopes, in addition to providing real-time imaging, can use either the traditional vapor lamp source of photons or laser sources in addition to newer diode illumination. This generally provides a wider range of excitation wavelengths.

The actual labeling process is not necessarily complex, but considerable attention to detail is required. Perhaps the first question that needs to be addressed relates to the information that the investigator wishes to obtain. This volume deals primarily with confocal microscopy and, while confocal microscopy is an extremely useful tool, it is wise to consider alternative methodologies relative to the particular question at hand. Wide-field imaging, often in conjunction with image deconvolution methodology, will often be the method of choice for thin specimens, particularly if living material is being observed. Images of live or otherwise dynamic specimens can be readily obtained. Substantially less light is required. Lasers are unnecessary. As with spinning disc confocal imaging, a wide variety of excitation/emission combinations is available and imaging is in real time. Rapid and direct comparisons of fluorescence images with brightfield or various interference-based imaging modes can be made. Simultaneous interference-based imaging with wavelengths of light in, for example, the IR or far-red region can be used to follow living material without damage, while simultaneous fluorescent imaging or fluorescence ratio imaging can be performed. A variety of fluorescent and nonfluorescent, opaque and chromatic, labels can be used simultaneously.

Identification of structures or areas of interest is absolutely dependent upon distinguishing those areas from the surrounding tissue. This requires a specific label. A wide variety of labeling methods can be employed, but almost all methods rely on creating a visual difference between the area of interest and the surrounding tissue.

5.4 Fluorescence

As discussed in Chap. 2, a fluorochrome absorbs a single photon at one wavelength, enters an excited molecular state, and then emits a photon at a longer, less energetic wavelength when the fluorochrome returns to its resting state. Distinguishing this emitted light from the incident light is the basis of image formation in fluorescence microscopy (Chap. 3).

Fluorescent markers are especially well suited for confocal microscopy. They can provide high quantum yield, and under optimized labeling and specimen preparation conditions, they provide excellent signal-to-noise ratio.

5.4.1 Photobleaching

A significant disadvantage of fluorescence detection methods is the occurrence of photobleaching or fading. Bombarding fluorochrome molecules with high-energy illumination at their optimal excitation wavelength (i.e., maximum energy absorbance) can damage their chemical structure. In addition, fluorochromes are highly reactive in their excited state, and can form covalent associations with other molecules, decreasing their fluorescence capacity. Fading is a particular obstacle when imaging weakly labeled specimens, as the extended illumination times required to obtain a detectable signal can lead to extensive photobleaching. In addition, in single-photon confocal microscopy, the entire specimen is illuminated throughout the scanning period, even though signal is collected from only one focal plane at a time. Fluorochromes that are highly susceptible to photobleaching, such as fluorescein, can have a significant proportion of the available molecules bleached by the time the last step of the Z-series is imaged.

A number of approaches can be employed to address photobleaching. First, fluorochromes are differentially susceptible to fading. Replacing the susceptible molecule with a comparatively resistant fluorochrome possessing a similar excitation and emission profile leads to improved imaging. For example, substituting fluorescein (excitation peak at 494 nm and emission peak at 521 nm) with the more photostable Alexa Fluor 488 (excitation peak at 495 nm and emission peak at 519 nm) allows for higher intensity illumination and higher signal yield, or prolonged signal at a lower illumination intensity.

A second approach to diminish photobleaching is to use anti-fade reagents during imaging. Most photodamage occurs when excited fluorochromes interact with

molecular oxygen to produce singlet oxygen, a reactive oxygen species. Depleting oxygen in the specimen environment can attenuate photodamage; of course, this is not practical in many live samples. Including reagents that scavenge reactive species and free radicals can markedly prolong the photostability of the fluorochrome. Examples of common anti-fade reagents are *p*-phenylenediamine (PPD), *n*-propyl gallate (NPG), and 1,4-diazobicyclo[2.2.2]octane (DABCO). A number of commercially available anti-fade mounting media are also available (Vector Labs, Molecular Probes). It is important to note that not every anti-fade reagent is compatible with every fluorochrome, and incompatibility can result in nearly complete quenching of the fluorescent signal.

Finally, particles such as quantum dots or other doped metal oxide particles such as europium-doped YVO particles can be conjugated to antibodies or antibody fragments. Fluorescent yields are good and there is little to no fading with the particles.

5.4.2 Autofluorescence

The fluorescent signal in samples arises from a number of sources. Endogenous compounds, such as flavins and nicotinamide adenine dinucleotide (NAD/NADH) that function in metabolic oxidation–reduction reactions, absorb and emit light at wavelengths very similar to those used for imaging, producing what is known as autofluorescence. Lipofuscins, collagen, and elastin are also autofluorescent compounds. In plants, chlorophyll, carotene, and xanthophyll all absorb and emit light resulting in autofluorescence. Pollen grains produce such a strong autofluorescent signal that they are often used as demonstration samples for traditional fluorescent and confocal microscopes.

In addition to naturally occurring fluorescence, aldehyde fixatives also produce autofluorescent signal. Formaldehyde gives moderate fluorescence, but glutaraldehyde gives strong fluorescence. Free aldehyde groups are thought to be responsible for the signal detected with these fixatives; however, it has been proposed that some signal results from the interaction of the aldehydes with amines. Paraformaldehyde solutions, which contain formaldehyde monomers freshly released from the solid paraformaldehyde polymer, give the lowest autofluorescence levels among the aldehyde fixatives.

5.4.3 Sources of Fluorescence

The source of fluorescence most commonly used for imaging is organic dyes. Fluorescein and rhodamine, which give green and red emission spectra, respectively, are probably the most broadly used fluorochromes. Most dyes in current use were developed because they have absorption spectra that roughly match the spectral lines, or output peaks, produced by high illumination intensity mercury

vapor lamps. High-intensity xenon vapor lamps give more uniform signal output across the visible spectrum than do mercury sources, and work well with the same dyes developed for mercury lamps. In confocal microscopy, intense monochromatic laser light sources are usually employed, and the fluorochromes used have at least one absorption peak that matches the laser emission. Many of the dyes most frequently used for confocal microscopy and flow cytometry are excited with a 488-nm blue argon laser. Examples include fluorescein, Alexa Fluor 488, PerCP, R-phycoerythrin, and R-phycoerythrin coupled to cy5, cy5.5, cy7, or Texas Red.

R-phycoerythrin and PerCP (peridinin–chlorophyll protein) are naturally occurring fluorochromes that are derived from red algae and photosynthetic dinoflagellates, respectively, and function to transfer energy to chlorophyll for food production. Another naturally occurring fluorochrome is green fluorescent protein (GFP), which was originally isolated from the bioluminescent jellyfish *Aequorea victoria*. GFP is a small (27 kD) protein that has been adapted for use as a fluorescent reporter of protein expression (Chalfie et al. 1994).

Mutations that have been introduced include a single-point mutation that shifted the absorption maximum to 488 nm (Heim et al. 1995). Additional modifications have resulted in yellow (YFP), cyan (CFP), and blue (BFP) fluorescent reporters (Heim and Tsien 1996). BFP can be used as the donor in fluorescence resonance energy transfer (FRET) studies, with GFP serving as the fluorescence acceptor (Heim and Tsien 1996). However, optimal results are obtained using GFP or CYP as the donor, with YFP as the fluorescence acceptor, as it allows for excitation at a visible wavelength rather than in the UV range. GFP and its variants provide excellent photostability. In addition, when employed as recombinant fusion proteins, they provide unequivocal detection of the recombinant protein, in that every molecule expressed carries the marker. Depending on the number of GFP gene copies per cell and the strength of the promoter driving its expression, GFP reporters can provide extremely high signal.

5.5 Desirable Features of Molecules Used as Markers

As discussed above, localizing a fluorochrome marker to a molecule or structure of interest is the primary challenge of labeling. In the absence of genetically engineered fluorescent fusion proteins or autofluorescence, an exogenously applied fluorescent identifier is required to label cells and tissues for confocal microscopy. A variety of molecule types can be used in identifiers, but good markers must all have a number of features in common.

5.5.1 Affinity

First, they must bind to the labeling target with high affinity. Once bound to the target, a high affinity label will remain in place, even through multiple wash steps in

which the concentration of the label in the surrounding medium becomes essentially zero. For live labeling studies, the affinity should be so high (K_d values in the low nanomolar, or even picomolar, range) that it is irreversible for practical purposes. If the label is to be fixed in place, a lower affinity can be tolerated, but perhaps at the risk of causing higher background staining as a result of less vigorous washing.

Binding of antibodies to their antigenic targets is among the highest affinity interactions employed in labeling protocols. Antibody affinities can range from micromolar on the weak end of the spectrum, to high picomolar at the strong end. Most monoclonal antibodies available for investigational use are at the mid-to-high end of the range. An even higher affinity interaction is seen between the small vitamin biotin and the large tetrameric protein avidin. The avidin–biotin interaction has the highest affinity described, with a K_d in the femtomolar range (Green 1963). Together with the amplification made possible through the four biotin-binding sites found in avidin, this interaction has been put to very successful use in labeling protocols.

5.5.2 Avidity

Second, avidity also influences labeling efficiency. Avidity is the number of binding sites for the target molecule that a label possesses. A label with moderate affinity but high avidity can give labeling efficiency equivalent or superior to a high affinity label with lower avidity.

5.5.3 Cross-Reactivity

A third feature of a good marker is low nonspecific binding capacity. If the label can bind to the cell or tissue through cross-reactivity (binding to molecules similar to, but distinct from, the target) or undesirable, albeit specific binding, its usefulness may be limited. When using antibodies for labeling, a serious concern is whether the antibody has cross-reactivity with antigens other than the target. Generally, this is a bigger problem with polyclonal antibodies than with monoclonals (see Sect. 5.6 below) because the source animal serum will contain at least some antibodies to all the antigens to which the animal has ever been exposed, intentionally or not. Polyclonal reagents can be affinity purified on immobilized antigen, thus removing reactivity to all but the target antigen. While monoclonal antibodies are less likely to have cross-reactivity than polyclonals, some closely related proteins have highly conserved sequences that can lead to significant cross-reactive staining. However, the incidence of antibody cross-reactivity in intact cells or tissues is relatively infrequent. This is because intact epitopes are three dimensional. They rarely involve contiguous amino acid sequences and are heavily

influenced by the environment provided by the neighboring amino acid sequence, also in three dimensions (Horsfall et al. 1991). Antibodies that recognize linear sequences, such as those that can be used for Western blotting, often show significant cross-reactivity in confocal labeling protocols.

Antibody epitopes are also influenced by posttranslational modifications, such as phosphorylation, acetylation, sulfation, or amidation. This has the potential to be problematic if one requires a reagent that labels a target under all circumstances. However, a level of antibody specificity that distinguishes modified and unmodified molecules can make a very powerful research tool. For example, antibodies that recognize only the phosphorylated version of signal transduction molecules have been the cornerstone of cell signaling studies. On the contrary, laboratory manipulations can destroy the ability of an antibody to recognize its antigen. For example, fixation, especially with cross-linking aldehydes, destroys many monoclonal antibody-binding sites, and a significant portion of polyclonal sites as well. The best retention of antigenicity is obtained with live or frozen specimens.

5.5.4 Stability

Stability is also an important feature of a good marker. The molecule and its interaction with the target need to hold up through the entire specimen preparation and imaging procedures. Likewise, stability of the target is an important consideration. If the marker recognizes the target after specimen fixation, the high quality of the target preservation can result in optimal imaging. For any labeling application, good access of the marker to the target is critical. If the markers are small and flexible, binding will be maximized, even if the target is partially obscured. Target access can be increased by permeabilization (mild detergent), proteolysis (enzymatic digestion), or unmasking (heating at low or high pH, or with chelators) techniques.

5.5.5 Identification

Finally, identification of the marker in the microscope is crucial to its function. Multiple techniques can be used to identify the marker. It may have some inherent characteristic, such as a readily identifiable shape. Alternatively, it may have some characteristic, such as antigenicity, that makes it identifiable with a secondary marker, such as a fluorescent- or particle-conjugated “second” antibody. It may also be directly tagged with a fluorochrome or an enzyme that identifies the location of the marker with higher resolution than is generally achieved with a secondary marker.

A number of types of molecules can be used as identifiable markers for labeling the feature of interest in specimens. Most common is the use of antibodies, glycoproteins produced in an animal as a specific, defensive response to a challenge with a foreign protein. However, ligands that bind specifically to cellular receptors can

also be used as markers. These can be the natural ligand that binds as part of a normal physiological function, or it can be a molecule that serves as an agonist or antagonist at the receptor. Likewise, molecules that bind to some particular component of a cell organelle can be used as an identifying marker. For example, fluorescent dyes that interact with nucleic acids can be used to stain nuclei (DAPI and propidium iodide) or even mitochondrial DNA (ethidium bromide). Reagents that sequester preferentially in one type of organelle by virtue of charge or pH (e.g., LysoTracker), or become trapped in a cellular compartment following an enzymatic cleavage (e.g., acetoxymethyl esters of fluorochromes) or an oxidation reaction (e.g., MitoTracker) are routinely used for identifying structures in specimens.

Another approach that can be exploited in the identification of structural elements is the binding of toxins to their cellular target. An excellent example of this method is labeling with fluorochrome-conjugated phalloidin, a toxin isolated from the poisonous mushroom *Amanita phalloides*. Phalloidin binds selectively to filamentous actin and stabilizes the filaments, helping to preserve their structure throughout the specimen preparation procedure.

Yet another labeling approach is the use of lectin conjugates. Intracellular structures enriched in particular carbohydrate moieties can be identified through the selective binding of lectins to the sugar or glycoprotein. For example, the interaction of wheat germ agglutinin (WGA) with *N*-acetylglucosamine and *N*-acetyl-neuraminic acid (sialic acid) residues concentrates WGA binding within the Golgi apparatus. The interaction of concanavalin A with alpha-mannopyranosyl and alpha-glucopyranosyl residues can be used to identify smooth endoplasmic reticulum. The use of lectins as markers varies according to whether the carbohydrate to which the molecule binds is broadly distributed through cells or tissues. Affinity of the lectin–carbohydrate interaction is also a significant factor (Cummings and Etzler 2009). Some interactions are of such low affinity that washing after the lectin incubation is sometimes eliminated from the labeling protocol in order to better preserve labeling.

5.6 Antibody Generation

Antibodies are immunoglobulins that recognize foreign proteins, known as antigens, at specific regions, known as epitopes. Generation of antibodies is part of the normal adaptive immune response of vertebrates, and provides for an especially diverse immune response in mammals, where the theoretic capacity to generate 10^{10} distinct antigen recognition sequences is obtained via an elegant genetic recombination mechanism (French et al. 1989). Antibodies are produced by B lymphocytes in response to an antigen binding a B-cell receptor that specifically recognizes it. B-cell proliferation and maturation occur upon cross-linking of B-cell receptors, together with a second signal provided by antigen-specific T helper lymphocytes in secondary lymphoid tissues (e.g., lymph nodes, spleen, and tonsils), or cross-linking by a T-independent antigen. A B lymphocyte that is terminally differentiated to secrete large amounts of antibody is known as a plasma cell.

Antibodies can be described as polyclonal or monoclonal depending on the number of epitopes of the immunizing antigen they recognize. Polyclonal antibodies are made by immunizing animals and bleeding them to obtain antiserum. The serum can be used directly, or the immunoglobulin fraction can be purified from it. Polyclonal reagents contain a collection of antibodies produced by multiple clones of antibody-secreting plasma cells. These cells are located in lymphoid tissues such as lymph nodes or spleen. Each individual clone produces antibody of only one specific type and epitope specificity. The different species of antibody in a polyclonal will include high and low affinities, specificities toward linear and nonlinear epitopes and multiple immunoglobulin classes (see below). Polyclonal antibodies are thought of as "hearty" because they contain multiple antibodies each specific for a different epitope in a single antigen. If target antigenicity is compromised during specimen preparation due to inactivation of some, but not all, epitope types, it is likely that there will be one or more species within the polyclonal antibody that will be specific for those epitopes that retain antigenicity. However, the more generalized binding characteristics associated with polyclonals may lead to undesirable cross-reactive binding (see below).

Monoclonal antibodies are of a single binding specificity. The first step in generating monoclonals is also immunizing an animal (usually a mouse), followed by fusing B cells from secondary lymphoid tissue such as the spleen with an immortal myeloma cell line. The resulting hybridoma cells are cloned by limiting dilution so that each colony that grows originates from a single fused cell, i.e., the cells are monoclonal. The antibodies secreted by the hybridoma cells selected through screening will be of a single antigen specificity that is the same as that of the B cell from which it arose. Antibodies of relatively high affinity are usually selected for further study during the screening process, although antibodies with lower affinities will be selected if a clone with a very useful or rare specificity is found. Because the antibodies are of a single specificity, cross-reactivity is seen less often with monoclonal than with polyclonal reagents.

5.7 Immunoglobulin Classes and Structure

The immunoglobulin found to be in the highest concentration in mammalian plasma is immunoglobulin class G (IgG), but IgM is also present at significant levels. IgA is present in plasma at lower concentrations than IgG and IgM, but is the immunoglobulin at the highest concentration in secretions such as mucus, saliva, and tears. The structure of IgG, IgM, and IgA is shown in Fig. 5.1. Free IgD and IgE are found only at low levels in plasma because these molecules are generally sequestered on cell surfaces. Most monoclonal antibodies used in labeling applications are IgGs; some IgMs with unique epitope recognition are also commonly used. IgMs are much larger than IgGs, and are generally of lower affinity, making them less desirable than IgGs for many labeling procedures. IgGs and the functional fragments made from them have predictable sizes and structures that give consistent labeling efficiencies that vary only according to the

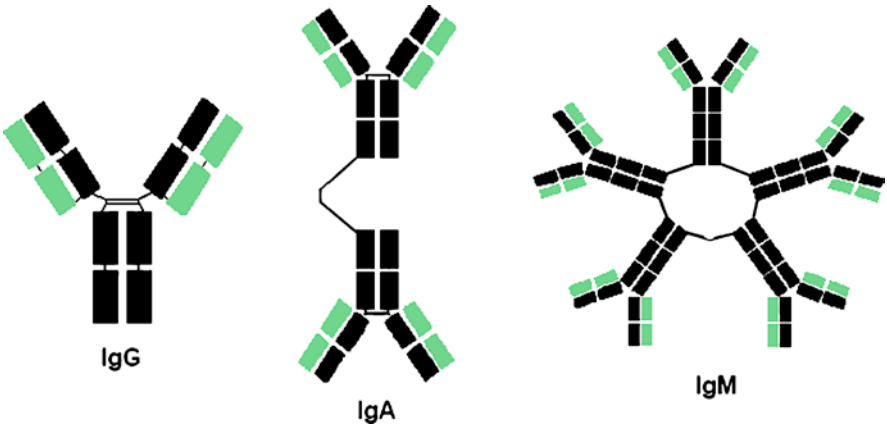

Fig. 5.1 Basic organization of the major antibody classes. IgG is the dominant species in the blood. It is monomeric and divalent. IgM exists as a pentomere with ten antigen-binding sites. IgA is generally present in dimeric form and is found primarily in secretions

individual antibody affinity and target antigen accessibility. The average diameter of a correctly folded IgG is 12.9 nm, $F(ab')_2$ fragments (see below) of IgG have an average diameter of 9.8 nm, and Fab fragments have an average diameter of 5.3 nm.

IgG is a large glycoprotein of 150,000 kD that is made up of four subunits – two 50,000-kD heavy chains and two 25-kD light chains (Fig. 5.2). The heavy chain distinguishes the Ig classes from one another: IgG has a heavy chain of isotype gamma (γ), IgM has isotype mu (μ), IgA has isotype alpha (α), IgD has isotype delta (δ), and IgE has isotype epsilon (ε). In birds, reptiles, and amphibians, the dominant circulating immunoglobulin is IgY, named because it has a heavy chain isotype found on antibodies that can be isolated from egg yolk. Immunoglobulins found in bony fish include IgM, IgD, and IgT. IgT carries a unique tau (τ) heavy chain restricted to teleost, or bony, fish (Hansen et al. 2005).

Immunoglobulin light chains in mammals are of two types: kappa (κ) and lambda (λ). Birds lack kappa light chains. A sigma (σ) light chain was first found in *Xenopus* and has since been described in all cold-blooded vertebrates, including teleost fish. Another primordial light chain that originated before bony fish diverged from cartilaginous fish (σ-cart) has been described (Criscitiello and Flajnik 2007), and is restricted to elasmobranchs. Antibodies of mammalian and avian (specifically chicken) origin are routinely used in labeling applications.

5.7.1 Immunoglobulin Subclasses

There are four well-described subclasses of IgG in both humans and mice, each carrying a subclass of the γ heavy chain. In humans, the subclasses are IgG1, IgG2, IgG3, and IgG4; in mice, they are IgG1, IgG2a, IgG2b, and IgG3 (Fig. 5.3). The molecular

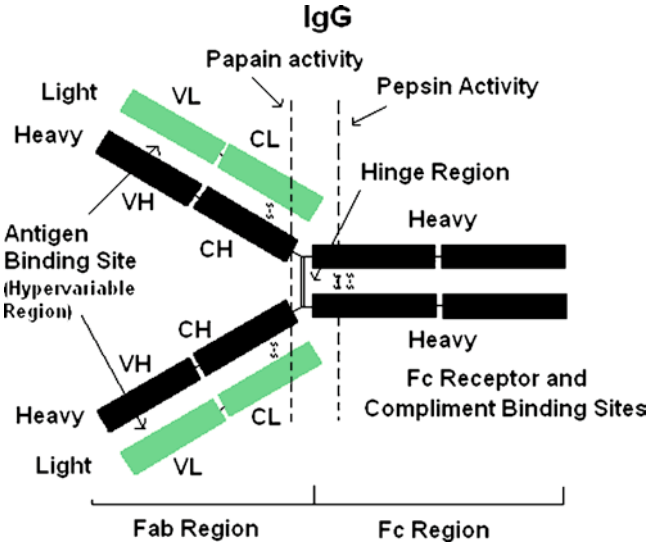

Fig. 5.2 A typical IgG antibody. The molecule is composed of two heavy and two light chains (either kappa or lambda) which are connected by disulfide bridges. The tail or Fc region is composed of heavy chain constant regions. The Fc portion of the molecule contains Fc receptor-binding sites and complement-binding sites. The Fab portion of the molecule is comprised of constant, "C_H" and "C_L," and variable, "V_H" and "V_L," regions of the heavy and light chains, respectively. A hypervariable region within the variable region is the site of epitope binding. The IgG molecule can be enzymatically cleaved at various places, resulting in specific antibody fragments. Pepsin cleavage results in the separation of the two Fab fragments from the Fc portion. The Fab fragments remain connected resulting in an $F(ab')_2$ fragment and an Fc fragment. Cleavage by papain results in two separate Fab fragments and an Fc fragment. Separation of the active antigen-binding site from the remainder of the antibody molecule produces a single-chain variable fragment (scFv; Fig. 5.5). The fragments from the light and heavy chains must be reconnected via a short peptide bridge. scFv can be genetically engineered via phage display technology and produced in bacteria

formulas of the different mammalian immunoglobulin classes differ. As mentioned above, IgG consists of two heavy (γ) chains and two light chains (κ or λ), giving formulas of $\gamma 1_2\kappa_2$ or $\gamma 2b_2\lambda_2$, for example. By contrast, circulating IgM is pentameric, with a molecular formula of $(\mu_2\kappa_2)_5$ or $(\mu_2\lambda_2)_5$. In addition, IgM contains an 18-kD joining, or J, chain (Fig. 5.4a). IgA consists of two subclasses and is generally dimeric, giving molecular formulas such as $(\alpha 1_2\kappa_2)_2$ or $(\alpha 2_2\lambda_2)_2$, for example. However, IgA can also be tetrameric. Like IgM, IgA contains a J chain that holds the immunoglobulin monomers together (Fig. 5.4b). Additionally, secretory IgA is associated with an aptly named secretory component. This is a remnant of a poly-Ig receptor responsible for the uptake of IgA on the basolateral side of mucosal epithelial cells and its incorporation into endocytic vesicles. The vesicles are transported to the luminal surface of the epithelial cells, where enzymatic cleavage of the receptor allows subsequent release of IgA and the remaining associated receptor fragment into the lumen (Kindt et al. 2007). IgD and IgE are monomers.

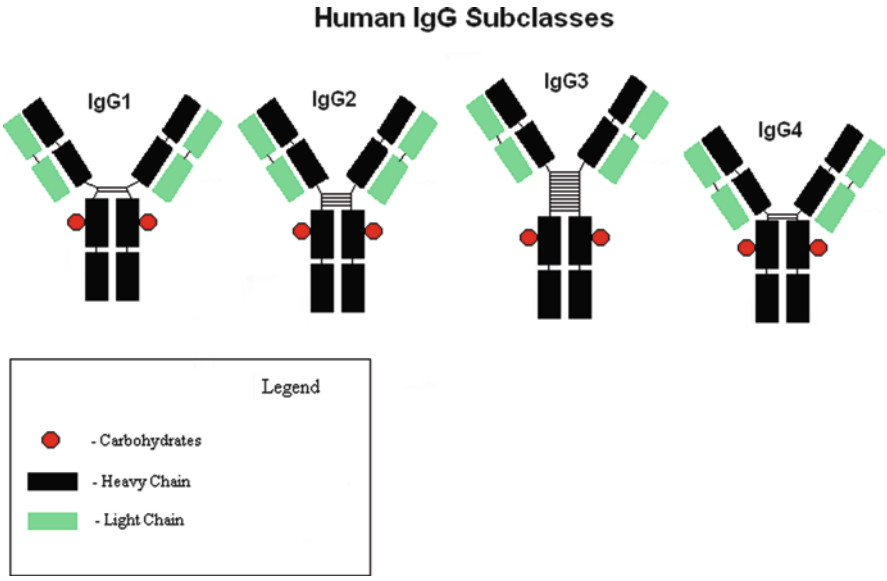

Fig. 5.3 Examples of human IgG subclasses. Variation is seen in the hinge regions of the different subclassses

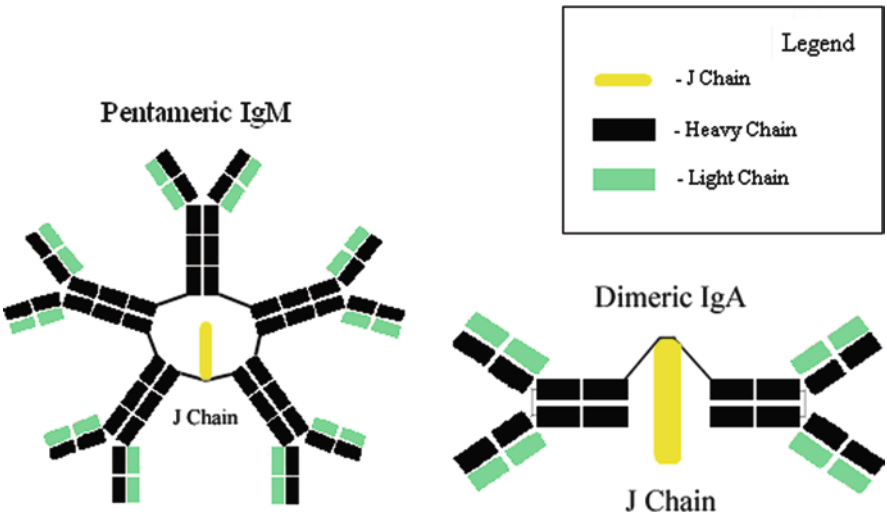

Fig. 5.4 Structure of an IgM molecule and an IgA molecule. The IgM is comprised of five individual immunoglobulin molecules that are cross-linked to each other by disulfide bonds as well as connected via a joining or "J" chain. The IgA is usually in a dimeric form also connected by a joining chain

5.7.2 Antibody Structure and Fragments

The shape of antibody molecules is similar to the letter "Y." If portions of the molecule are described in terms of function, the "arms" of the "Y" are called the variable, or antigen-binding, regions and the base of the "Y" is called the constant region. The variable, or Fab, region is responsible for antigen recognition. The constant, or Fc, region is responsible for biological effector functions of antibodies, such as binding complement to induce lysis of antibody-coated cells such as invading bacteria, or binding antibody-coated bacteria to specific Fc receptors on phagocytic cells that are capable of engulfing and killing pathogens (Fig. 5.2).

Disulfide bonding is critical to the structure of antibodies. Interchain disulfide bonds create the Ig loops that characterize members of the immunoglobulin superfamily, which contains a wide variety of proteins of diverse functions. Some members of the Ig superfamily have roles in normal immune function, but many do not. IgG, IgD, and IgA have four Ig loops in their heavy chains, while IgM and IgE each have five Ig loops in their heavy chains. Light chains have two Ig loops. Each of the loops is named according to whether it is on the heavy or light chain, and whether it is in the variable or constant region of the molecule. Beginning at the variable portion of an IgG (the "arm" of the "Y"), the structure of the heavy chain is V_H, C_H1, C_H2, and C_H3. The light chain is made up of V_L and C_L (Fig. 5.2).

Interchain disulfide bonds are responsible for the association of the two heavy chains with one another, and for the association of a light chain with each of the heavy chains. In IgG, two or more disulfide bonds between heavy chains at the "neck" of the "Y" are found in the hinge region. This is a flexible area of the antibody structure that allows for the arms to move relatively freely with respect to one another during antigen binding. The heavy–light interchain disulfide bonds are found near the hinge region, slightly closer to the variable region (Fig. 5.2).

Functional antibody fragments can be generated by enzymatic digestion of whole antibody molecules. Digestion with pepsin cleaves the heavy chains just below the interchain disulfide bonds. The result is a bivalent product capable of cross-linking antigen through its two antigen-binding sites, but missing its Fc portion. These fragments are called $F(ab')_2$ (Fig. 5.5), and they are very useful in labeling applications where Fc-mediated antibody binding gives high background staining. Digestion of whole IgG with papain cleaves the molecule at a site between the heavy-heavy chain disulfide bonds, and the heavy-light chain disulfide bonds. The product is two monovalent fragments with antigen binding capacity, and one Fc fragment. The antibody-binding portions are called Fab fragments (Fig. 5.5), and they are useful in labeling applications where both Fc binding and antigen cross-linking are undesirable. Both $F(ab')_2$ and Fab fragments are smaller than whole IgG molecules (110 and 50 kD, respectively, compared to the 150 kD whole molecule), and can therefore provide better specimen penetration and potentially more accurate localization of antigens. The increased penetration is particularly important in the case of confocal microscopy where imaging can extend tens of microns and well into the specimen.

5.7.3 *Variable Antibody Domains*

The smallest functional antibody fragment is a combination of the V_H and V_L domains. These fragments can be generated through protein engineering rather than by enzymatic digestion of whole molecules. The product is a called a single-chain variable fragment, or scFv (Fig. 5.5) (Huston et al. 1988). The variable regions of the heavy and light chains do not have a naturally occurring connection such as an interchain disulfide bond, so a bridge between the two sequences is engineered into the construct used to produce the single-chain product. This bridge generally spans 3.5–4.0 nm. It has been reported that introducing disulfides to stabilize the structure without altering the antigen-binding sequence can increase affinity and half-life of the molecules (Reiter et al. 1994). Affinity purification methods can be used with scFv, similar to those used with whole molecule antibodies. However, the bacterial proteins A and G (originally derived from *Staphylococcus aureus* or group G *Streptococci*, respectively), which bind to the Fc fragment for purifying whole antibodies, will not work with fragments. Instead, immobilized bacterial protein L (originally derived from *Peptostreptococcus magnus*) that binds to $V_L\kappa$ can be used to purify Fab and scFv (Nilson et al. 1993). This method will not work for antibody

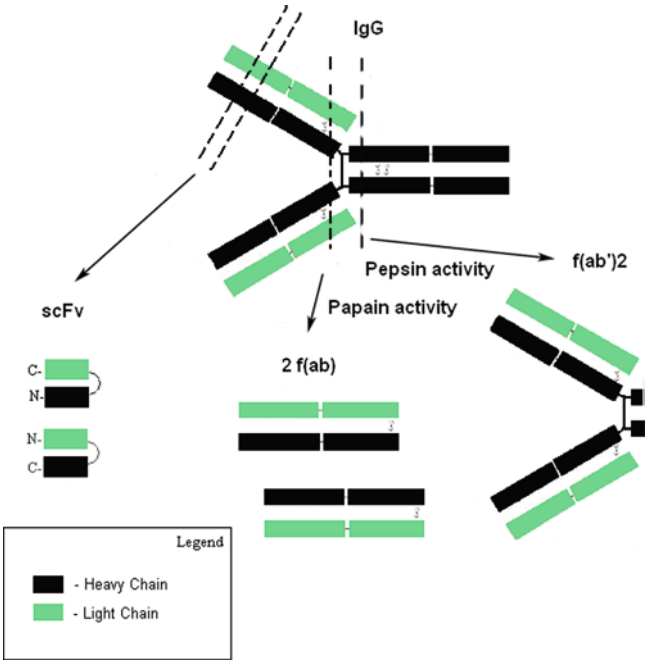

Fig. 5.5 Active antibody fragments, $F(ab')_2$, Fab, and scFv in order of decreasing size, that can be used to reduce overall label size and eliminate Fc receptor or complement binding. The $F(ab')_2$ is divalent, while the Fab and scFv are monovalent with respect to the number of specific antibody-binding sites

fragments with λ light chains, but 60% of human and 95% of mouse antibodies have κ light chains (Kindt et al. 2007).

Because the structures of scFv are relatively simple and do not require posttranslational modifications, they can be produced in *Escherichia coli*. The DNA sequence of the variable region can be cloned from cDNA of hybridoma cells producing monoclonal antibodies of known antigenic specificity and affinity. Producing the recombinant protein in bacteria allows for high volume production more quickly and affordably than can generally be achieved with whole antibodies grown from hybridoma cells in mouse ascites fluid or in mammalian cell culture.

Within the variable regions of antibodies, there are specific amino acid positions that vary more than the others; these variations account for a great deal of antigen specificity. Clusters of these hypervariable amino acids found in V_H and V_L are referred to as the complementarity-determining regions (CDRs). The CDRs are found on the outside of fully folded immunoglobulin molecules, where they have maximal access to antigenic epitopes. In the construction of scFv molecules, screening antibody phage display libraries for antigen binding can identify CDR DNA sequences that will produce the desired specificity (McCafferty et al. 1990). CDR sequence modules can be introduced into scFv constructs for high-throughput generation of panels of recombinant antibody fragments.

Another, even smaller variation of antigen-binding regions is seen with nanobodies. These can be derived from antibodies made in camelids – dromedary camels, Bactrian camels, llamas, alpacas, guanacos, and vicuñas, and in some shark species. Animals from this family produce antibodies consisting of two heavy chains and no light chains (Fig. 5.6), in addition to the more typical two heavy

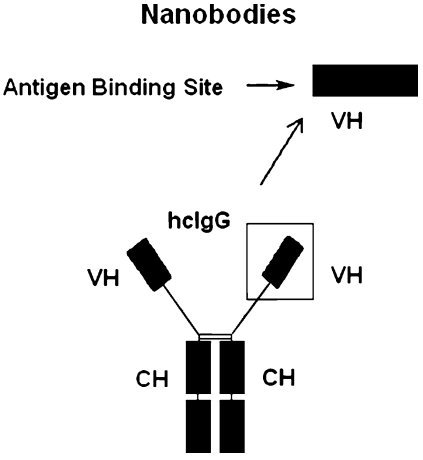

Fig. 5.6 Nanobodies are heavy chain variable fragments from *Camelidae* sp., which exhibit specific binding without the need for a variable light chain and are robust with respect to variation in temperature, pH, and resistance to enzymatic degradation. The variable heavy chain region, "V_H," is isolated from the heavy chain immunoglobulin molecule, "hcIgG"

chain + two light chain molecules (Hamers-Casterman et al. 1993). Naturally occurring antibodies devoid of light chains are unusual for two reasons. First, the antigen recognition site has contributions from both V_H and V_L, and both are expected to be necessary to achieve a complete antigen-binding repertoire. However, the heavy chain-only antibodies found in camelids have broad antigen-binding capacity. Second, heavy chains are dependent on light chains for good solubility. Heavy chains isolated from other mammals tend to agglutinate, but non-aggregated camelid forms are readily found in circulation. These characteristics allow for the production, through protein engineering, of fully functional V_H segments that are one-tenth the size of whole IgGs. The smaller size gives nanobodies greater access to antigens than larger antibodies or fragments have. Nanobody conjugates or fusion proteins used for detection in labeling protocols will also be significantly smaller than the corresponding whole molecule or fragment, providing more accurate localization of target molecules or structures. The camelid-derived nanobodies are significantly more resistant to heat, pH, and enzymatic digestion than other antibodies or fragments from other species. This provides flexibility in labeling protocols that could potentially extend to the oral administration of labels to live animals.

5.8 Labeling Considerations

5.8.1 Review the Literature

There are literally thousands of protocols developed for a wide variety of labeling applications. Perhaps the best rule of thumb is to define clearly what information is needed and then proceed with a thorough review of the literature looking for previous studies designed to obtain similar information. This often avoids a substantial amount of trial and error. Sources of antibody as well as types or subtypes, specific fluorescent dyes, use of chemical or physical fixation, even buffers, and conditions of labeling can all be reasonably estimated from prior labeling protocols used by others. Obviously, modifications may have to be made and in some instances, totally new protocols will have to be developed. Once the information required is defined, it is also advisable to attempt the least complex protocols first. There are no extra points for overly complex protocols when the desired information can be reliably obtained by a relatively simple direct approach. Try to avoid “overkill” which may be impressive technologically and which may be able to provide additional information. However, if the additional information is irrelevant to the study at hand, much additional time and expense may be saved by a less impressive but more direct methodology.

5.8.2 Use a Hierarchy of Applications

There is often a hierarchy of technologies, with each designed to better maintain epitope antigenicity. This often involves starting with a classical buffered aldehyde fixation. The aldehydes interact chemically with a number of functional groups in biological specimens. Formaldehyde is thought to cause less cross-linking and hence preserve antigenicity better than the dialdehyde, glutaraldehyde; however, this may not always be the case. Mixtures of formaldehyde and glutaraldehyde may be preferable to preserve structure for interference-based LM structural studies or correlative EM studies. If a classic fixation adversely affects antigenicity of one or more of the epitopes of interest, a brief fixation in dilute, 0.5%, or less formaldehyde, followed by labeling and then a more concentrated, structure maintaining, fixative may be used. For preservation of even less robust epitopes, fixation in the cold may be sufficient to inhibit epitope inactivation. More complicated procedures such as fixation in the cold followed by freezing and labeling of frozen sections, or freeze-substitution procedures with fixation may be needed. Finally, a physical fixation approach may be required. This can involve ultra-rapid freezing followed by labeling of cryosections without any fixation. As a last resort, it may be necessary to label living specimens and follow labeling with fixation or freezing steps. However, labeling parameters for living cells must be designed to account for the effects of the formation of antibody–antigen or ligand–receptor complexes in or on living cells and any subsequent changes in cell structure, cell activity, or movement of the antigen–antibody complexes.

5.8.3 Know the Antibody

With regard to the antibody or antibody fragments used in the labeling process, the primary antibody should be well characterized as to species, type, and subtype if possible. It is important to know if a polyclonal (cross-absorbed) or monoclonal antibody is being employed. It is also important to know if whole antibody or active antibody fragments are being used. The affinity and avidity of the antibodies are also useful information. This is particularly the case with monoclonal antibodies where specificity may be high but the affinity may be lower. Monoclonal antibodies may be extremely specific, with minimal cross -reactivity, but they react with only one epitope. This may present difficulty if the preparation of the sample masks or alters the single epitope. Polyclonal antibody may have the advantage in such cases because it often contains higher avidity antibody, and antibodies specific to several or all of the epitopes. Thus inactivation or blocking of one epitope will not necessarily compromise identification of the entire molecule.

However, as noted above, this may also lead to higher levels of cross-reactivity. Cross-reactivity may be substantially reduced by cross-absorption, while antibody species with high affinity can be selected by specific absorption against the antigen or even the specific epitope of interest.

Other considerations in the labeling process include the isoelectric point of the antibody. Antibodies are proteins and behave as such. Labeling at pH values substantially divergent from the isoelectric point may compromise affinity and/or avidity. This is not usually a problem with whole antibody, where the isoelectric point will be in the range of commonly used physiologically relevant buffers. However, active antibody fragments, described above, may have a wider range of isoelectric points, necessitating modification of labeling buffer pH. The use of particular ions to maintain epitope structure may also affect antibody affinity and avidity.

5.8.4 Antibody Concentration

Antibody concentration is also of obvious importance. A reasonable estimate of the concentration is essential. Often, antibodies are supplied or purified to be in the range of 1 mg/ml or roughly $1 \times 10^{15–16}$ antibody molecules/ml. Standard instructions often recommend dilutions of 1:10, 1:100, or even 1:1,000 prior to use in labeling protocols.

When concentrations reach the 1×10^{12} range, 1 μg/ml or below, particular attention needs to be paid to the time of labeling since 100% epitope coverage can be attained in several minutes at 1×10^{13}, while it may take hours to days at 1×10^{11}. The former may be useful for live cell labeling in cases where maximal labeling needs to be accomplished rapidly. The lower concentrations may be useful to minimize background, where labeling is performed overnight in the cold. The antibody concentration in commercial antibody preparations often depends on whether the antibody is polyclonal or monoclonal.

Another factor affecting antibody concentration is related to freezing and thawing. On thawing, a precipitate may form in frozen antibody preparations. The usual procedure is to centrifuge or filter the sample in order to remove the precipitate. However, it must be kept in mind that the precipitate generally contains a portion of the antibody, and the concentration of soluble antibody may be significantly reduced in the remaining soluble fraction. Antibody should always be divided into aliquots and frozen. Aliquots are thawed as needed, so the antibody is frozen and thawed only once. Multiple freezing and thawing will promote precipitate formation and a substantial reduction in antibody concentration or even the total elimination of antibody.

5.8.5 Antibody Conjugation and Level of Fluorescence

The level of fluorescence is determined not only by the number of antibody molecules or number of active antibody fragments but also by the number of fluorescent molecules per antibody molecule. In general, each antibody molecule can be conjugated with four to five fluorescent molecules, with little effect on the parameters

of binding. As noted previously, other factors specific to the dye also play a role. These include wavelength of excitation and emission, quantum efficiency, extinction coefficient, and quenching rate.

Direct conjugation of the primary antibody to fluorescent or other markers has several advantages (Fig. 5.7a). There is less chance of cross-reactivity when the specimen is incubated with only one antibody. Cross-reactivity and nonspecific binding of the second antibody are eliminated. Considerations relative to the binding avidity and affinity of the second antibody to the primary antibody are also eliminated. Finally, spatial resolution is maximized and measurements of semiquantitative aspects are more reliable.

However, primary antibody is often available in small quantities and, if purchased commercially, is generally expensive. Fluorochrome-conjugated primary antibody is often not available commercially. In-house conjugation may require testing and the availability of relatively larger amounts of specific antibody. In order to avoid conjugation of primary antibody to a fluorescent dye and the potential loss of antibody and/or activity, a second antibody–fluorescent dye conjugate is generally used. The second antibody reacts specifically with the primary antibody and can be more general in nature (Fig. 5.7b). Second antibodies can be conjugated to a variety of fluorescent dyes so that there are a number of possible excitation/emission combinations available.

If the primary antibody is obtained from mouse, then antibody from any of several other species such as rabbit, chicken, goat, and so forth can serve as the second antibody. Generally, multiple second antibody molecules will bind to each primary antibody molecule. Each of the second antibody molecules will be conjugated to four or five fluorescent molecules and hence the signal will be substantially enhanced. The source of the fluorescence will come from a slightly larger area around the specific labeled epitope, but at LM levels of resolution, this is not a problem. With molecular resolution LM or high-resolution EM studies, the closer the indicator is to the actual location of the epitope of interest, the better.

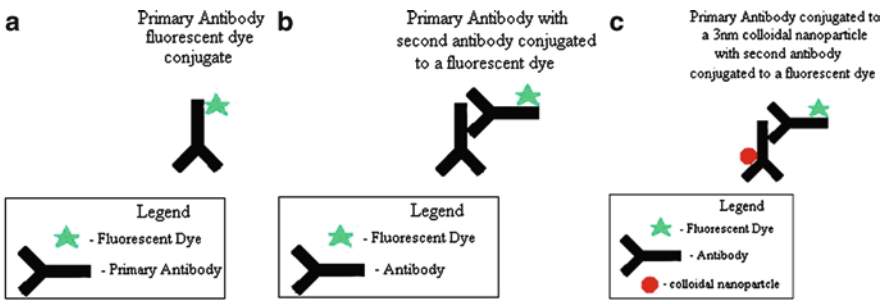

Fig. 5.7 (**a**) Primary antibody–fluorescent dye conjugate. Generally, three or four individual dye molecules are linked to each IgG molecule. (**b**) Primary antibody with second antibody conjugated to a fluorescent dye. (**c**) Primary antibody conjugated to a 3-nm colloidal nanoparticle with second antibody conjugated to a fluorescent dye

Small nanoparticles conjugated to the primary antibody to provide maximal spatial resolution for EM in combination with fluorochrome-conjugated second antibody for LM and confocal imaging can be employed in these cases (Fig. 5.7c) (Kandela et al. 2007, 2008; Albrecht and Meyer 2008). This also avoids quenching of fluorescent dye, which occurs when it is conjugated directly to the same antibody molecule as the colloidal metal particle (Kandela and Albrecht 2007). It is also important to realize that primary conjugates used for cell sorting purposes may not be applicable to microscopic imaging with standard CCD cameras. This is due to differences in the quantum efficiency of sorting, as opposed to imaging instrumentation. High-sensitivity EMCCD cameras may be more useful in the detection of lower signal levels from primary conjugates.

5.8.6 Use of Second and Third Antibodies

All the considerations relative to the primary antibody must also be observed in the case of the second (or third) antibody. If an antibody fragment is used as the primary antibody to facilitate penetration throughout the sample or for facilitating semiquantitation of epitopes, it is important to also use an active antibody fragment for the second antibody. Whole second antibody will defeat the purpose of the small primary probe. The concentration, affinity, and avidity of the second antibody should be known. Second antibodies are often better characterized than primary antibodies because of their general use. The cost also tends to be substantially less. The use of a second antibody that is more specific for the primary antibody is preferred. This facilitates labeling of more specific determinants rather than the more general shared determinants. For example, if the primary antibody is a mouse IgG2b, it is preferable to use an anti-mouse IgG2b rather than simply using a polyclonal antibody which labels mouse whole (H+L chains) antibodies. This reduces nonspecificity and can enable simultaneous multiple labeling for other mouse primary antibodies such as an IgG2a.

5.9 Antibody Sources

There are a variety of sources for polyclonal and monoclonal antibodies. Offerings from commercial sources fill volumes and can be searched on the Internet. A useful source of information on antibodies and related products is Linscotts Directory of Immunological and Biological Reagents which currently has over 480,000 different listings in their antibody section (Linscotts Directory of Immunological and Biological Reagents 2010). While an antibody may have specificity for an antigen or epitope of interest, it is important to know the context of that binding. Antibody may be used for labeling of in vivo or in vitro systems; in ELISAs, Western blots, and cell sorting applications; in various binding assays; or in functional inhibition

tests. A specific antibody may be effective in a variety of these labeling applications or restricted to several or even one application. Binding to an antigen in one context does not guarantee binding in another.

5.9.1 Polyclonal Whole Molecule

Various levels of purity for polyclonal preparations are available. Whole serum from immunized animals; purified immunoglobulin fractions; fractions of particular immunoglobulin subtypes such as IgG, IgM, IgE, or IgA; highly cross-absorbed antibodies; and affinity-purified antibodies are all available. The cost is generally directly proportional to the level of purification and absorption. Some more commonly used primary antibodies can be purchased as fluorescent conjugates, but generally this is not the case. Primary antibody, as above, may be directly conjugated in-house to an appropriate fluorescent dye or, more commonly, they are used with a fluorochrome-conjugated second antibody. The commercially available antibody preparations are generally well characterized. Antibody preparation, concentration, known cross-reactivity, preservatives, and preservative concentrations, as well as references to papers describing the initial preparation and subsequent uses are generally included or available online from the supplier.

Antibodies may sometimes be obtained directly from other investigators who have generated the antibody and have sufficient amounts to share, either as gifts or at relatively low cost. This may be the case where one group has developed an antibody with a specific activity and the antibody is not yet available commercially. Gift antibodies are often less well defined than those available from commercial sources, but they have generally been tested and work well for the specific needs of their laboratory of origin. They may be in various stages of purification, from whole serum to affinity-absorbed specific antibody, depending on the needs of the original investigator. When obtaining such antibodies, it is important that there be a clear understanding of how these antibodies will be used; author requirements for publications, patents, and other public disclosures; and limitations with respect to the use of antibodies by individuals other than the specific investigator receiving the gift.

If no other sources exist, antibodies can be prepared in-house. Often, there are biotechnology facilities that will guarantee specific antibody to a particular antigen which you supply in a pure (as is reasonably possible) state and at a concentration required by the antibody production facility. For in-house preparation, there are requirements for animals and animal care, antigen preparation and purification, adjuvant selection, and an immunization protocol, which are many depending on the animal, the antigen, and the type of antibody required. Most antibodies must be separated from blood serum, although IgY from chickens is purified from egg yolks. Antibody is then purified and absorbed to increase specificity and reduce cross-reactivity. The entire process is involved and may be costly, but necessary, if you are working with a unique antigen or epitope. It also facilitates studies where large amounts of antibody are required, or where direct conjugation of primary

antibody to a fluorescent dye or other indicators is desirable. There are also a number of commercial concerns that will work with the investigator to provide specialty antibodies. Cost varies but may be an issue if funds are limited.

5.9.2 Monoclonal Whole Antibody

Commercial concerns are the primary source for monoclonal antibodies. Literally thousands of monoclonal antibodies are available commercially. The antibody is generally well characterized as to antibody type and subtype. The concentration is usually provided, but affinity and avidity are often listed as "high" or "low." While specificity of monoclonal antibodies may be high, it may take a certain amount of good fortune to find a monoclonal antibody with exceptionally high affinity, so care must be exercised in establishing the affinity and avidity of any monoclonal antibody.

It is helpful if the specific epitope on the antigen recognized by the antibody is also known, but this may not be available. Often references are provided which discuss the original preparation and use of the particular antibody. This may provide more information on subtypes, epitope specificity, cross-reactivity, and avidity/affinity. Most commercially available monoclonal antibodies are sold in small volumes and are relatively expensive.

Monoclonal antibodies may also be obtained as gifts. As is the case with polyclonal antibodies, monoclonal antibodies obtained directly from colleagues or other investigators can be the only source when antibodies to specific epitopes are otherwise unavailable and the laboratory originally producing the antibody has sufficient stocks to provide antibody to other investigators. Monoclonal antibodies obtained as gifts may come well characterized and with publications describing their preparation and use; however, information provided is often less than that provided with commercial preparations. One major advantage is direct advice that may be provided via the Principal Investigator or other investigators in the laboratory producing the particular monoclonal antibody. Also, the investigators may have produced several clones with antibody specific to epitopes on your antigen of interest. It is sometimes helpful to test antibodies from multiple clones to find the antibody best suited to provide the information you require. In some instances, investigators will provide cells from the specific hybridoma clone. These antibody-producing cells can be propagated in vivo or in vitro, thus ensuring a substantial supply of antibody. Agreements for the use of monoclonal antibodies or for cell clones producing monoclonal antibodies have to be carefully prepared to avoid any subsequent issues related to commercialization or patents.

Monoclonal antibody can also be produced in-house. The process is involved and costly. Many investigators have access to a biotechnology laboratory that will produce a guaranteed number of hybridoma clones, each of which produces antibody specific for the antigen you provide. The affinity of the monoclonal antibody from the clones is often a problem. However, if monoclonal antibodies that are

specific for a unique antigen or epitope of interest do not exist elsewhere, this is the only option. If studies require large amounts of antibody, having a hybridoma clone which produces a functional monoclonal antibody ensures a sufficient supply of antibody. This is important when primary antibody is directly conjugated to fluorescent dyes or colloidal nanoparticle markers, since a substantial amount of antibody may be used in refining the conjugation process. It is also important when active antibody fragments are prepared by fractionation of whole antibody molecules.

5.9.3 Antibody Fragments

Active fragments such as Fab, Fab'_2, or scFv for some antibodies are available from commercial sources. However, the demand for fragments from specific antibodies is generally such that it is not profitable to produce fragments which are held in stock. Often, commercial or in-house biotechnology services can prepare various fragments on a fee-for-service basis. Kits are also available from various manufacturers which can be used to prepare Fab or Fab'_2 fragments from whole antibody preparations, or cloned in bacteria. For in-lab or service facility preparation, sufficient antibody must be available as loss of antibody during the fragment preparation is inevitable. The scFv is a fusion protein of the heavy and light chain variable regions. The label can be made by converting monoclonal antibody into the scFv form. Another methodology includes the use of a phage display and the expression of the scFv in one of several bacterial systems.

5.9.4 Second Antibody

Second antibodies are generally available commercially. The expense is usually less than that of primary antibody since substantial amounts of the same second antibody are used to identify a variety of primary antibodies from a specific animal source. For example, goat anti-mouse antibodies can be used to label a wide variety of primary mouse antibodies. Second antibodies are generally well characterized and used routinely. They can be produced from a number of sources, including chicken (egg yolk),or serum from rabbits, goats, donkeys, mice, and other species. Various preparations are available commercially, which include a hierarchy of specificities ranging from specificity for any immunoglobulin from a given species, through individual immunoglobulin subtypes from a given species, to antibody fragments from a given species, and so on.

Second antibody can be obtained as a gift through colleagues and it can be generated in-house using the primary antibody or antibody fragment as antigen and highly cross-absorbing the specific antibody. It can be affinity-purified if necessary.

5.9.5 Control Antibody

Control antibodies can be obtained commercially, as gifts, or generated in-house. They are often less costly than primary specific polyclonal or monoclonal antibodies. There are several levels of sophistication. The use of pre-immune serum as a control simply provides a mixture of blood proteins and antibody, none of which, unless there is cross-reactivity, binds to the specific epitope. Pre-immune serum permits the delineation of general nonspecific binding.

The use of purified immunoglobulin fractions as a control narrows the specificity to nonspecific binding of immunoglobulins, while the use of a purified immunoglobulin subtype identical to the primary antibody provides an even more precise control.

Perhaps the most specific control involves the use of an antibody that is specific for the inappropriate haplotype of the antigen. These controls can be identical in every respect to the primary antibody, with the exception that they bind to an alternative antigenic haplotype. Since they are generally monoclonals to an inappropriate haplotype, there is no cost saving when compared to the primary antibody which does bind to the appropriate haplotype.

5.10 Conditions of Labeling

It is not the intent here to review any of the thousands of labeling protocols or even to try to provide a "one size fits all" generic protocol. Hopefully, the discussion here simply serves as a reminder that there are some basic conditions which must be met for labeling to be successful.

5.10.1 Maintain Antigenicity

First, the conditions prior to and during labeling must maintain antigenicity of the antigen or epitope. With polyclonal antibody, this means that at least one and preferably as many multiple epitopes as possible on a given antigen need to remain recognizable by a specific antibody. For monoclonal antibody, the specific epitope recognized by the antibody has to retain antigenicity. As noted previously, there is often a hierarchy of technical approaches that can be employed to protect the antigenicity of epitopes. Generally a standard chemical, often aldehyde, fixation is tried first. Ultimately it may be found that physical fixation, i.e. frozen without chemical fixation is required to maintain epitope antigenicity. In some cases even that may compromise antigenicity and labeling of living material may be necessary to prevent epitope inactivation and insure recognition by specific antibody. Other factors important in retaining antigenicity include ions and ion concentration, pH, buffer type, temperature and time of fixation and labeling, and the use of agents, such as the detergent Triton X-100, to increase permeability and penetration.

5.10.2 Maintain Optimal Affinity and Avidity

Similarly, the affinity and avidity of the labeling molecule, whether antibody or ligand, must also be optimized. This requires close attention to buffer composition, osmolarity, and temperature. Often, 0.1 molar phosphate buffer at pH 7.2, or 0.15 molar phosphate-buffered saline with up to 1.0% bovine serum albumin is used in washes and in the specific labeling step. However, particularly for active antibody fragments, ligands or ligand fragment, or scFv constructs, the buffer type and pH may vary.

5.10.3 Minimize Nonspecific Binding

It is also critical to minimize nonspecific binding. Blocking agents such as albumin, pre-immune serum, skim milk, or fish gelatin can be used to mask "sticky sites" where proteins bind nonspecifically. Blocking agents vary in their ability to mask nonspecific labeling in a particular labeling situation. If one type of blocking agent does not provide the level of activity needed, then it is important to try others either individually or in combination. Specific anti-Fc receptor antibodies, aggregated IgG, or Fc fragments can be used to block Fc receptor binding if pre-immune serum proves unsatisfactory. Salt solutions such as sodium chloride or various surfactants such as Tween 20 can be used to minimize surface charge and limit electrostatic charge–charge interactions. The use of free aldehyde-blocking agents such as 0.5–1.0% sodium borohydride or 0.01–0.04 M glycine can be used to eliminate any free aldehyde groups generated during the fixation process. Such groups can nonspecifically cross-link proteins, including antibodies, to the specimen.

5.10.4 Preserve the Specimen Morphology

Generally, there is also need to preserve morphology at some level of resolution such that the labeling can be viewed in the context of biological structure. Again, there is a hierarchy of methodology. Structural preservation for imaging with photon-based methodology may not be as stringent as for electron- or force-based imaging. Preservation of structure is compatible with a number of labeling protocols, although modifications may be necessary, particularly where high-resolution structural information is required.

5.11 Considerations in Labeling with Ligands

Ligands, particularly those with small dissociation constants, can be useful to label specific receptors or binding sites (Fig. 5.8). They can often be used to determine if binding sites are in their active state. A specific antibody may label epitopes

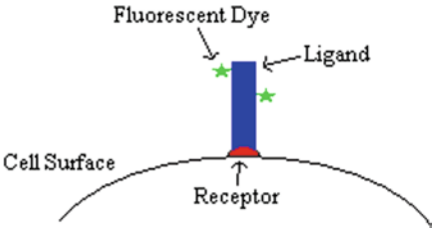

Fig. 5.8 Ligand conjugated to a fluorescent dye. Ligand conjugates can be effective for labeling active receptor sites, particularly for live cell applications

within components of receptor sites without regard to the activity of the receptor. Specific ligands bind only to the active receptor site. Thus, antibody labeling can be used to determine the location and density of receptor molecules, while ligand labeling will identify only the active receptor sites. As with specific antigens or epitopes for antibody binding, fixation can often alter receptor structure and reduce or eliminate ligand binding.

There are a number of options for ligand labeling. Natural ligand can be directly fluorochrome conjugated or conjugated to fluorescent, chromatic, or opaque nanoparticles. Ligand can also be identified with a second, fluorescent- or particle-labeled, anti-ligand antibody. For some receptors, a number of pseudo-ligands, some of which are drugs, may exist. Attachment of ligands to receptors or binding sites can proceed by various mechanisms. Bond types and strengths vary; both non-covalent or semi-covalent binding can occur depending on the particular ligand–receptor combination. Noncompetitive agonists or antagonists are preferred because of their strong irreversible binding; however, competitive agonists or antagonists and even partial agonists can be used and concentrations adjusted to provide a high efficiency of labeling.

As with antibodies, active fragments of a ligand can be derived from a whole ligand or synthesized directly to provide smaller labels to promote penetration or to better provide semiquantitative information with respect to receptor or binding site density (Fig. 5.9).

Ligand labeling is particularly effective in living cell systems where tracking of ligand–receptor complexes is desirable, or the effects of ligand–receptor interaction on subsequent cell activity and structure are needed. Just as for whole IgG antibody molecules, some ligands are divalent and can link two or more receptors on cell surfaces, leading to various types of receptor ligand-induced activity. Ligands can be obtained from a variety of sources including commercial concerns, as gifts, or purified/synthesized in-house. Few commercial preparations of fluorochrome-conjugated ligands, pseudo-ligands, or active ligand fragments are available commercially.

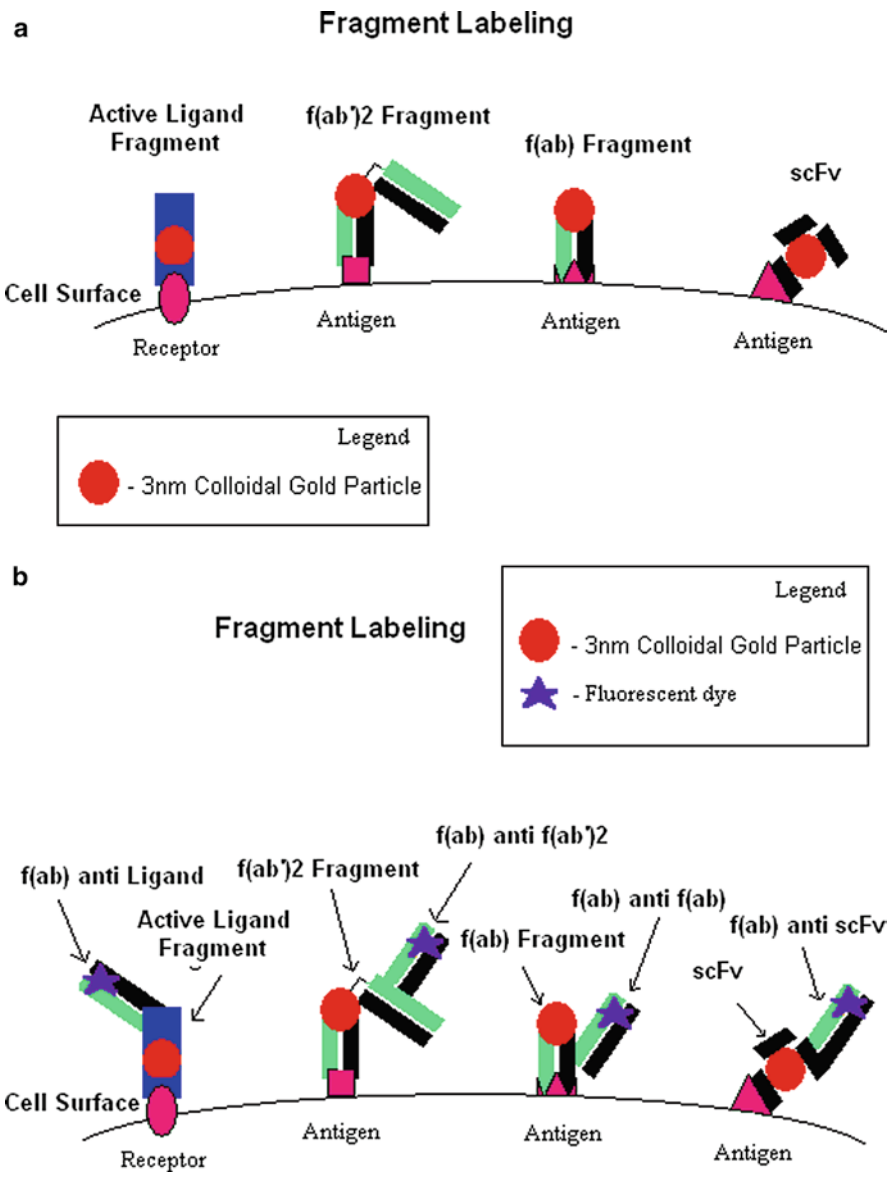

Fig. 5.9 (**a**) Labeling receptor sites or antigenic sites with ligand or antibody fragments with particles. Colloidal metal conjugates can be used for EM applications and can be further enhanced for LM as well. Conjugation of fluorescent dye to fragments may also provide LM signal if sufficient dye and conjugates are present and/or if a highly sensitive CCD camera is employed. (**b**) The primary fragments can also be identified using fluoresceinated anti-ligand antibody or fluoresceinated anti-fragment second antibody. If penetration is a problem due to the nature or thickness of the specimen, the fluoresceinated second antibody may also have to be an antibody fragment as shown. Whole antibody, with more dye molecules, is preferred if signal strength is a limiting factor. The use of a fluorescent third, anti-second, antibody may also be considered to further increase fluorescence levels

5.12 Live Cell Labeling

Live cell labeling may be employed where any type of chemical or physical fixation alters the antigenicity of epitopes or modifies ligand–receptor interactions. Live cell labeling may also be important to follow the movement or endocytosis of antibody-labeled and cross-linked antigens on or in cells, or to follow the movement of receptor–ligand complexes. When cross-linking is not desirable, monovalent Fab or scFv labels can be used as can active ligand fragments. Cells may be cooled prior to labeling, provided the cooling process does not compromise the presence or availability of the epitopes of interest. Where possible, labeling should be performed on washed cells in simple buffer or in cell culture media with no or minimal levels of added serum protein. In some instances, low levels, 2% or less, of serum may be required in the washing and/or labeling buffer to block nonspecific sites and to reduce Fc binding, if this is an issue. However, it should be kept in mind that serum contains a mixture of proteins some of which may also bind to the living cells and influence cell structure or function. After labeling, the cells can be returned to standard culture media if necessary.

High concentrations of antibody or ligand should be employed to facilitate rapid binding of available antigenic sites and a high efficiency of labeling. It is often necessary that a primary antibody be directly conjugated to fluorescent dyes or particles. There may be insufficient time to employ a second antibody to label a primary antibody or a specific ligand. A second antibody may also produce extensive cross-linking of the primary antibody–antigen complexes.

Penetration of antibody, ligand, or active fragments of antibodies or ligands can be problematic. Various permeabilization techniques can be used. These range from the use of electric currents as in electroporation, ballistic penetration, use of specific endocytosis activators, or detergents which produce a reversible temporary increase in cell permeability.

5.13 Labeling with Particles

Colloidal nanoparticles have been used for a number of years as labels in electron microscopy and for correlative LM/EM as well as in force-based labeling (Albrecht and Meyer 2008; Eppell et al. 1995). Conjugation of particles to primary or secondary antibody provides markers visible in TEM and SEM. Bulk concentrations of particles provide an opaque image in LM. In the case of gold this can be black or a red to orange color. Individual particles as small as 10 nm can be identified and tracked by their inflated diffraction image in interference-based LM imaging.

For correlative confocal LM/EM imaging, particles as small as 3 nm can be conjugated to the primary antibody or antibody fragment. This provides spatial resolution for epitope identification and localization in the sub-molecular range

for EM. A fluorochrome-conjugated second antibody can be used for LM/confocal localization. While the fluorescent signal comes from a larger area around the epitope, it is still well within the resolution range of the LM. Having a fluorescent dye on the second antibody also substantially reduces fluorescent quenching, which is often greater than 99% when metal particles and fluorescent dyes are on the same antibody molecule. Recently, colloidal particles of uniform small to 3 nm size but having different elemental composition such as gold, palladium, platinum, silver, and others have been conjugated to different antibody labels so that simultaneous multiple labeling at EM levels of resolution can be performed. This is analogous to the use of multiple fluorescent dyes on different antibodies to provide simultaneous labeling of antigens at the LM levels of resolution. Particles can be differentiated by EDX or EELS in an aberration corrected STEM/TEM, or by ESI/EELS imaging in an EFTEM, although EELS identification requires particularly thin specimens. Core-shell configurations further expand the number of labels that can be differentiated and hence used simultaneously. Particles of similar size but having different shapes have also been developed. For particles of different composition or of different shapes, the correlative confocal LM proceeds as above. Each particle–antibody combination is labeled with a second antibody with a particular fluorescent dye of unique excitation/emission properties. This allows multiple antigens or epitopes to be differentiated in LM, confocal and/or wide field, and subsequently at much higher resolution in EM (Kandela et al. 2007).

Other approaches to correlative fluorescent LM/EM have employed quantum dot particles. The quantum cores of these particles consist of cadmium-selenium or tellurium (Bruchez et al. 1998; Chan and Nie 1998). The cores fluoresce when they are illuminated with light of sufficient energy. The wavelength of illumination is not critical. The size of the quantum core determines the emission wavelength. They also exhibit minimal photobleaching. This makes them particularly desirable for confocal imaging over long time periods. The core is generally surrounded by a shell of zinc sulfide. The particle is further stabilized by an amphiphilic polymer with a functionalized, often PEG, surface. The final size is substantially greater than the 5–10 nm quantum core and can be as large as 20–30 nm for the particle without conjugated antibody. This can reduce their effectiveness for high-resolution EM labeling. The density of the quantum core is also not great, and identification by EM is possible but somewhat more difficult than the identification of heavy metal nanoparticles. Ultraviolet light can destroy the cores and release toxic cadmium, but the stabilized particles appear to be generally stable in the visible spectrum.

Correlative confocal labeling with other fluorescent nanoparticles that are stable and nontoxic is under development. Oxides, such as yttrium vanadium oxide, doped with rare earth elements, for example, europium, fluoresce at specific wavelengths and can be identified in EM, but additional studies are necessary to determine the ultimate utility of these particles for confocal labeling or in correlative confocal LM/EM studies.

5.14 Sequential Versus Simultaneous Labeling

For simultaneous labeling of multiple antigens/epitopes or receptors/binding sites, the question of sequential vs. simultaneous labeling must be considered. For live cell imaging, usually simultaneous labeling with high concentrations of each label is necessary as sequential labeling may require too much time. The order of labeling may also affect cellular responses, particularly if antibody or ligand cross-linking is involved. For fixed material, if there is minimal cross-reactivity and a blocking regime that reduces nonspecific binding for all the antibodies can be employed, simultaneous binding can be used. However, concentrations of each label may have to be adjusted relative to the specific antigen–antibody interactions.

The affinities of the different labels may vary and the overall conditions should allow for the maximal efficiency of labeling to be attained for each label, whether a ligand or an antibody. In some cases, a sequential approach may be desirable, particularly where optimal labeling for each antibody requires significantly different pH or specific ion concentrations. Brief fixation steps may be required between application of each label, but care must be exercised not to reduce or eliminate antigenicity of unlabeled epitopes prior to their labeling. Sequential labeling can involve labeling of a living system followed by fixation and subsequent labeling of additional epitopes depending on the information required.

5.15 Troubleshooting

There are three basic areas where problems arise.

5.15.1 "Operator Error"

The first, and most common, is the "operator error" category. Often, the symptom is no labeling or substantially reduced labeling. This may involve improper storage or too lengthy storage of fixatives, which can result in polymerization and inactivation of fixative.

One of the more common operator errors involves composition and dilution of reagents. This may result in buffers or fixatives lacking critical components or concentrations of components that can be an order or more in magnitude too weak or too strong. Primary, second, and third antibody are all generally diluted in buffer prior to use. Any error in antibody concentration or in the composition of the dilution buffer can reduce the efficiency of labeling. Higher than required antibody concentration can result in an increase in nonspecific background labeling.

Errors in buffer composition can lead to labeling at inappropriate pH or osmolarity, which can eliminate or substantially reduce labeling. Length of time of labeling relative to antibody concentrations is also important as is temperature of incubation. Even differences in prevailing "room temperature" may alter labeling. A shortened or lengthened time of incubation with primary or secondary antibody or with blocking reagent can also adversely affect the efficiency of labeling.

The labeling process is multistep and each step must be carried out carefully. In instances where a particular protocol is unfamiliar to the investigator, it is not uncommon that certain steps may be accidentally or purposely omitted. Generally, each step is important to the final result and missing or skipping steps can have unintended results. All labeling, washing, and blocking steps need to be completed. Once good labeling is obtained via an existing protocol, the investigator can modify the protocol to eliminate possible unnecessary steps or streamline the process.

Care must be taken not to freeze and thaw antibody repeatedly as this can result in aggregation and/or denaturation of antibody. Long-term storage at temperatures just above freezing will often lead to a gradual loss of antibody activity. Each antibody preparation behaves somewhat differently. Some antibodies stored in the refrigerator may maintain their activity over several months or longer, while others show marked deterioration in days or weeks.

5.15.2 Background Labeling

High levels of background labeling is the commonly encountered second problem. This often results in substantial levels of labeling throughout the sample and/or significant amounts of labeling seen in controls. This can result from several sources. Fc receptors on cells in the sample may bind to Fc portions of the whole antibody molecule. This can occur with primary or second antibody, or both. There is substantial cross-species Fc–Fc receptor binding. For example, murine Fc, particularly IgG2a and IgG3, will bind strongly to human Fc receptors, while other murine antibody subtypes bind but at somewhat lower affinity (Lubeck et al. 1985). Use of Fab or Fab'_2 antibody fragments that lack the Fc is one approach to eliminate Fc binding. Blocking of Fc receptors via the use of pre-immune serum can also be used.

Non-epitope-specific binding of antibody via complement components can also produce background which can be eliminated via the use of Fab or Fab'_2, which also lacks the complement-binding sites. Specific blocking of complement is also possible.

Nonspecific binding of antibody by hydrophobic bonding or by charge–charge bonding is also a possibility. At its isoelectric point, an antibody molecule is maximally hydrophobic and can bind to hydrophobic regions on other molecules. In addition, the antibody molecules, even at their isoelectric point, may have charged regions within the molecule, facilitating charge–charge interactions with oppositely

charged regions in other protein molecules. Usually, these nonspecific antibody–protein interactions can be reduced or eliminated with an increase in blocking agent concentration or via the application of additional blocking agents.

High background may also be a result of excessive concentrations of primary or second antibody. This may be remedied by simply decreasing antibody concentrations. If some or all of the specific antigen are diffusible, the antigen or even antigen–antibody complexes may redistribute throughout the sample. This may also result in diffuse labeling which appears nonspecific. This type of artifact can be reduced through the use of more aggressive fixation or a more thorough washing.

Autofluorescence or aldehyde autofluorescence can also produce a diffuse background or a specific pattern of nonspecific labeling. Autofluroescence is difficult to eliminate and may require the use of fluorescent labels with excitation/emission wavelengths that will not be confused with autofluorescence. Aldehyde or aldehyde-induced fluorescence can be eliminated by labeling specimens prior to fixation or after a very light fixation with formaldehyde. The cryo-preparative methodology which does not use chemical fixatives may also be employed. Coagulating fixatives such as ethanol may prove useful to eliminate fixative fluorescence, but the alcohols tend to extract or dissolve specimens. However, for some antigens, alcohol fixation is required. The use of counterstains to mask background is also possible. Stains such as toluidine blue or pontamine sky blue have been recommended as potential counterstains to mask nonspecific background due to autofluorescence or aldehyde fixatives.

Some non-diffuse but nonspecific labeling can result from several sources. Fixation may produce or expose normally hidden cross-reactive antigenic sites, resulting in labeling which may appear specific. The use of monoclonal primary antibody against selective epitopes may be used to reduce this type of nonspecificity. As above, labeling prior to fixation, labeling after a very light formaldehyde fixation, or cryo-preparative methodology which does not employ fixatives may reduce aldehyde-induced cross-reactive antigens.

Sequestered or trapped antibody may also appear similar to specific labeling. Antibodies may diffuse into specimens but subsequently have difficulty diffusing out of specific locations. Additional washing and attention to the specific location relative to cell and tissue structure may help to avoid misinterpretation of these labeling patterns. Phagocytosed antigen may appear in phagosomes or phagolysosomes of phagocytic cells if at least some of the antigen epitopes are resistant to degradation in the phagolysome or if labeling is sufficiently soon after antigen ingestion so as to avoid significant destruction of antigen epitopes.

5.15.3 Specificity and Affinity

A third significant problem relates to levels of specificity and affinity. The intensity of labeling may appear substantially lower than expected based on other

measurements of antibody–antigen binding. This unexpectedly reduced binding may occur as a result of several factors. Antibody avidity and specificity can be checked via Western blots, ELISAs, or both. Variations between techniques can be due to technique-dependent structural variation in the antigen or the antibody. Epitopes available when an antigen is in a gel or in solution may not be available in vivo. Thus antigens in ELISA or Western blots may label extremely well, but labeling in vivo is still substantially less than expected.

Specific epitopes may be masked or unavailable in the context of cells or tissues. This is more of a problem with monoclonal species since only one epitope is labeled. If that particular epitope is partially masked or unavailable in vivo, labeling can be reduced or absent and conclusions relative to the presence or absence of a particular molecular species may be in error. Where molecules expected to be present are not labeled by a specific monoclonal antibody, it is useful to employ a polyclonal antibody as a check. In this case, multiple epitopes on the molecule can be recognized by the polyclonal antibody. Since there is less of a chance that all epitopes within the molecule of interest are masked in vivo, there is a much greater probability that labeling will occur. However, as discussed previously, there is more chance of cross-reactivity and nonspecific labeling with the polyclonal antibody preparation. Absorbing polyclonal antibody against the antigen and eluting the specifically reactive antibodies will eliminate antibody molecules that are not specific for the antigen of interest. This may reduce nonspecific binding and also increase overall specific binding, with a concomitant increase in signal. Specificity can be checked prior to labeling using a Western blot with the specific antigen and with closely related antigens.

Finally, for post-embedding labeling of sectioned samples, masking by the embedding media material is a consideration. With the exception of dried, unembedded frozen sections or sections where the embedding media is dissolved away, antibody access to epitopes is limited to the surface of the section. This severely restricts the number of exposed epitopes that can be labeled. Furthermore, specific antigens or epitopes may interact with the embedding media such that they are masked. This further restricts labeling. Solutions include the use of different embedding polymers with different properties, or the use of etching agents to dissolve a very thin layer of polymer on the surface of the section. This latter approach increases the amount of embedded material on the surface and hence additional epitopes, if they resist the etching process, are available to the antibody labels. There are also a variety of antigen "retrieval" protocols which can be used to restore antigenicity of a fixed and processed antigen. These protocols are designed to restore epitope antigenicity presumably by reversing fixative induced crosslinks. Antigen retrieval techniques employ low pH washes, high pH washes, various heating protocols, detergents, and proteolytic enzymes separately or in various combinations.

It has been suggested that the generation of antibodies against fixed epitopes may be helpful for the labeling of specific epitopes in fixed specimens. Unfortunately, fixatives generate a number of fixation-specific epitopes that are the same in all fixed tissues, resulting in substantial cross-reactivity. Possibly, preparation of monoclonal antibodies for specific fixed epitopes may be useful; however, to date, this has not been the case.

Acknowledgement The authors wish to thank Mr. Andrew Zuehlke for assistance in preparing the figures.

References

Albrecht, R.M., and Meyer, D.A. 2008. Molecular labeling for correlative microscopy: LM, LVSEM, TEM, EF-TEM, and HVEM. Ch 6, Low Voltage Scanning Electron Microscopy. H. Schatten and J. Pawley (eds) Springer Science, New York, 171–196.

Bruchez, Jr., M., Moronne, M., Gin, P., Weiss, S., Alivisatos, A.P. 1998. Semiconductor nanocrystals as fluorescent biological labels. Science 281:2013–2016.

Chalfie, M., tyu, Y., Euskirchen, G., Ward, W.W., Prasher, D.C. 1994. Green fluorescent protein as a marker for gene expression. Science 263:802–805.

Chan, W.C.W., Nie, S. 1998. Quantum dot bioconjugates for ultrasensitive nonisotopic detection. Science 281:2016–2018.

Criscitiello, M.F. and Flajnik, MF. 2007. Four primordial immunoglobulin light chain isotypes, including lambda and kappa, identified in the most primitive living jawed vertebrates. Eur J Immunol. 37(10):2683–2694.

Cummings, R.D., Etzler, M.E. 2009. Antibodies and lectins in glycan analysis. Ch. 45, Essentials of Glycobiology, Second Edition. A. Varki, R.D. Cummings, J.D. Esko, H.H. Freeze, P. Stanley, C.R Bertozzi, G.W. Hart, M.E. Etzler (eds.), Cold Spring Harbor Laboratory Press, Cold Spring Harbor, New York, pp. 633–648.

Eppell, S.J., Simmons, S.R., Albrecht, R.M., and Marchant, R.E. 1995. Cell surface receptors and proteins on platelet membranes imaged by scanning force microscopy using immunogold contrast enhancement. Biophysical J. 68:671–680.

French, D.L., Laskov, R., Scharff, M.D. 1989. The role of somatic hypermutation in the generation of antibody diversity. Science 244:1152–1157.

Green, N.M. 1963. Avidin 1. The use of [^{14}C]biotin for kinetic studies and for assay. Biochem J, 89:585–591.

Hamers-Casterman, C., Atarhouch, T., Muyldermans, S., Robinson, G., Hamers,C., Bajyana Songa, E., Bendahman, N. and Hamers, R. 1993. Naturally occurring antibodies devoid of light chains. Nature 363:446–448.

Hansen, J.D., Landis, E.E. and Phillips, R.B. 2005. Discovery of a unique Ig heavy-chain isotype (IgT) in rainbow trout: Implications for a distinctive B cell developmental pathway in teleost fish. Proc Natl Acad Sci U S A. 102(19): 6919–6924.

Heim, R., Cubitt, A., and Tsien, R. 1995. Improved green fluorescence. Nature 373 (6516): 663–664.

Heim, R., and Tsien, R.Y. 1996. Engineering green fluorescent protein for improved brightness, longer wavelengths and fluorescence resonance energy transfer. Curr Biol 6:178–182.

Horsfall, A.C., Hay, F.C., Soltys, A.J., Jones, M.G. 1991. Epitope mapping. Immunol Today 12:211–213.

Huston, J.S., Levinson, D., Mudgett-Hunter, M., Tai, M-S., Novotny, J., Maroglies, M.N., Ridge, R.J., bruccoleri, R.E., Haber, E., Crea, R., Oppermann, H. 1988. Protein engineering of anitbody binding sites: Recovery of specific activity in an anti-digoxin single-chain Fv analogue produced in *Escherichia coli*. Proc Natl Acad Sci U S A. 85:5879–5883.

Kandela, I.K., Bleher, R., and Albrecht, R.M. 2007. Multiple correlative immunolabeling for light and electron microscopy using fluorophores and colloidal metal particles. J Histochem Cytochem 55(10):983–990.

Kandela, I.K., and Albrecht, R.M. 2007. Fluorescence quenching by colloidal heavy metal nanoparticles: Implications for correlative fluorescence and electron microscopic studies. Scanning 29:152–161.

Kandela, I.K., Bleher, R., and Albrecht, R.M. 2008. Correlative light and electron microscopy imunolabeling on ultrathin cryosections of skeletal muscle tissue. Microsc Microanal 14:159–165.

Kindt, T.J., Goldsby, R.A., and Osborn, B.A. eds., 2007. Kuby Immunology, 6th edition, WH Freeman and Company, New York, 2007.

Linscotts Directory of Immunological and Biological Reagents. 2010 Linscotts USA. https://www.linscottsdirectory.com.

Lubeck, M.D., Steplewski, Z., Baglia, F., Klein, M.H., Dorrington, K.J., and Koprowski, H. 1985. The interaction of murine IgG subclass proteins with human monocyte Fc receptors. J. Immunol 135:1299–1304.

McCafferty, J., Griffiths, A.D., Winter, G., Chiswell, D.J. 1990. Phage antibodies: filamentous phage displaying antibody variable domains, Nature 348:552–554.

Nilson, B.H.K., Lögdberg, L., Kastern, W., Björck, L., Åkerström, B. 1993. Purification of antibodies using protein L-binding framework structures in the light chain variable domain, J Immunol Methods, 164:33–40.

Reiter, Y., Brinkmann, U., Jung, S-H., Lee, B., Kasprysyk, P.G., King, C.R., and Pastan, I. 1994. Improved binding and antitumor activity of a recombinant anti-erbB2 immunotoxin by disulfide stabilization of the Fv fragment. J Biol Chem 269:18327–18331.

Chapter 6
Introduction to Digital Imaging for Confocal Microscopy

W. Gray (Jay) Jerome

Keywords Histogram • Histogram stretch • Image formats • Gamma • Look-up-table • Pixel • Resolution • Voxel

6.1 Introduction

Image rendering in confocal microscopy is a digital technique. To optimize confocal image acquisition, the operator needs to have a basic understanding of what constitutes a digital image and how it can be employed effectively to help visualize specific details. In this chapter, we will introduce the topic of digital images, discuss the basic components of the digital image, and provide some basics on how to optimize collection of these components with regard to confocal microscopy.

6.2 Analog Versus Digital Information

An analog signal is a continuous one. Its possible values can be $-\infty$ to $+\infty$ in infinitely small increments. This means that values such as 1, 2, 2.02, and 3.0000023 are all possible. In fact, the set of possible values includes all real numbers. In comparison, a digital signal is composed of discrete elements that have values of one unit or some whole multiple of one unit. Thus, you cannot have a value that is a fraction of one unit, such as 0.33, or a fraction of a whole multiple, such as 2.57. Of course, at this point we have not defined the basis of our unit. In fact it could be a micrometer, a yard, or 2.65 ft. However, once the unit is defined, then all elements

W.G. (Jay) Jerome (✉)
Department of Pathology, Vanderbilt University Medical Center, U-2206 MCN, 1161 21st Avenue, South Nashville, TN 37232-2561, USA
e-mail: jay.jerome@vanderbilt.edu

R.L. Price and W.G. (Jay) Jerome (eds.), *Basic Confocal Microscopy*,
DOI 10.1007/978-0-387-78175-4_6,

of the set must be in whole multiples of that unit and no element can be less than one unit in size. Thus, the value of 1 unit (1 quantum of information) defines the lower limit of resolution.

Analog to digital conversion consists of converting the set of analog values to a set of digital values. Two steps are involved in this conversion. The first is determining the value of one unit. We will discuss the physical constraints on the size of a microscope image quantum in Chap. 7. The second step involves deciding the means by which the analog values are assigned to one of the discrete digital values. This process is depicted in Fig. 6.1 for analog values varying with respect to an *X* and a *Y* parameter. The value of 1 quantum in the *X* and *Y* directions is indicated by the width of tick marks. The converted digital *Y* values, which are based on discrete multiples of 1 quantum, are depicted by the heights of the gray bars. These are determined by the average of the analog *Y* values (rounded to the nearest quantum unit) occurring within each *X* quanta range. In the low resolution conversion, a relatively high value has been chosen for 1 quantum of *X* and *Y*. In the high resolution conversion

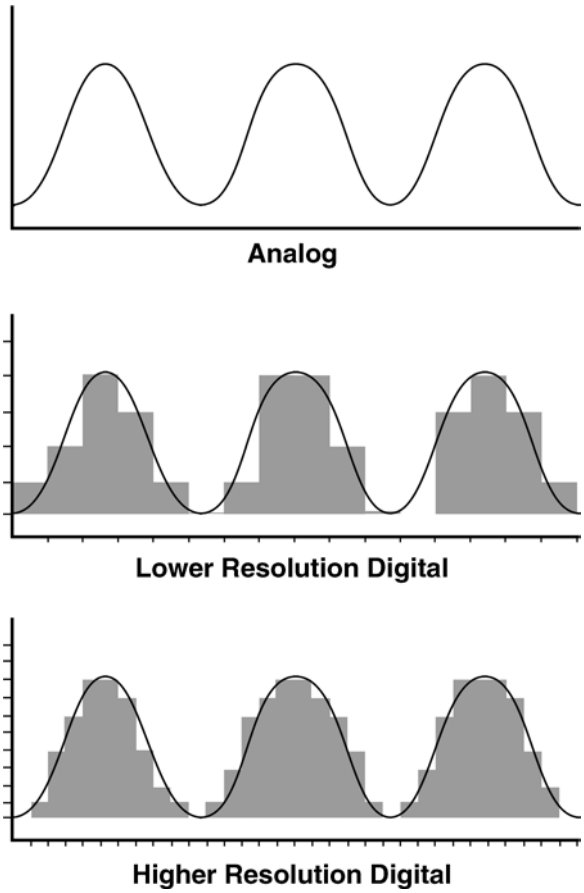

Fig. 6.1 Analog to digital conversion of a linear signal

a smaller value has been chosen. Of course, this smaller value results in a closer approximation of the digital graph to the original analog information. Similarly, selecting a high resolution value in the confocal software will result in a better approximation of the analog information viewed through the microscope with our eyes. However, as discussed below and in other chapters of this book, there are guidelines in selecting the appropriate resolution values available in the software. It is not always the best practice to select the highest digital resolution available.

6.3 Pixels

In the case of a two-dimensional micrograph, the spatial information in the image is divided up into a series of discrete two-dimensional picture elements (pixels). A pixel is one unit wide by one unit high. A pixel does not have to be square, in other words one quantum in width does not, necessarily, have to be the same as 1 quantum in height. However, in microscopy, square pixels are usually employed and we will confine our discussion for the rest of this chapter to square pixels.

A two-dimensional digital image is made up of a mosaic of pixels. To convert the analog information in the original sample to a digital representation, all of the values within a pixel area are averaged to a single value as depicted in Fig. 6.2. For a gray

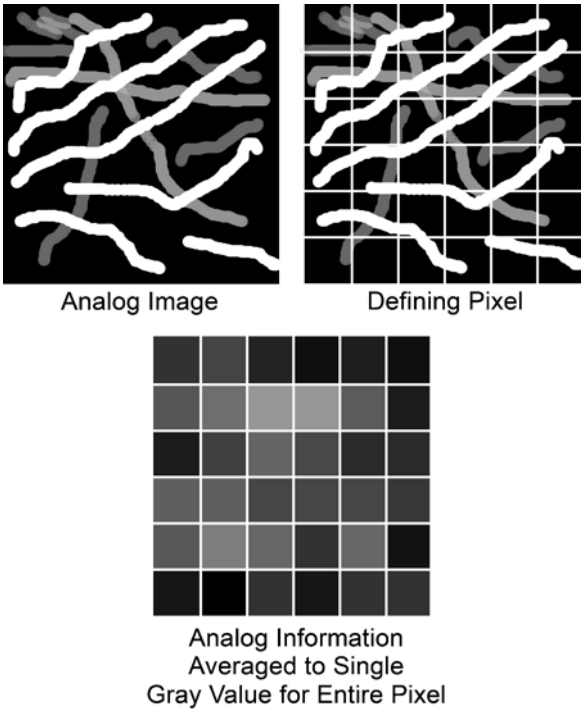

Fig. 6.2 Digital imaging analog to digital conversion

scale image, the value would be some gray value between black and white. In the simplest and most often employed conversions, this involves using the average of all the gray values in the pixel. For example, a pixel that contained 50% black and 50% white would be averaged to a gray value at the middle of the scale. Because all of the details within a pixel have been averaged to a single value, the smallest detail that can be represented in the digital image is no smaller than a pixel.[1]

It follows, then, that the smaller the pixel size, the more faithfully will be the digital representation of the original analog information. Figure 6.3 shows the results of different pixel sizes on an image. The pixels in Fig. 6.3a are 0.05 mm in height by 0.05 mm in width. The pixels in Fig. 6.3b are 0.11 mm high×0.11 mm wide.

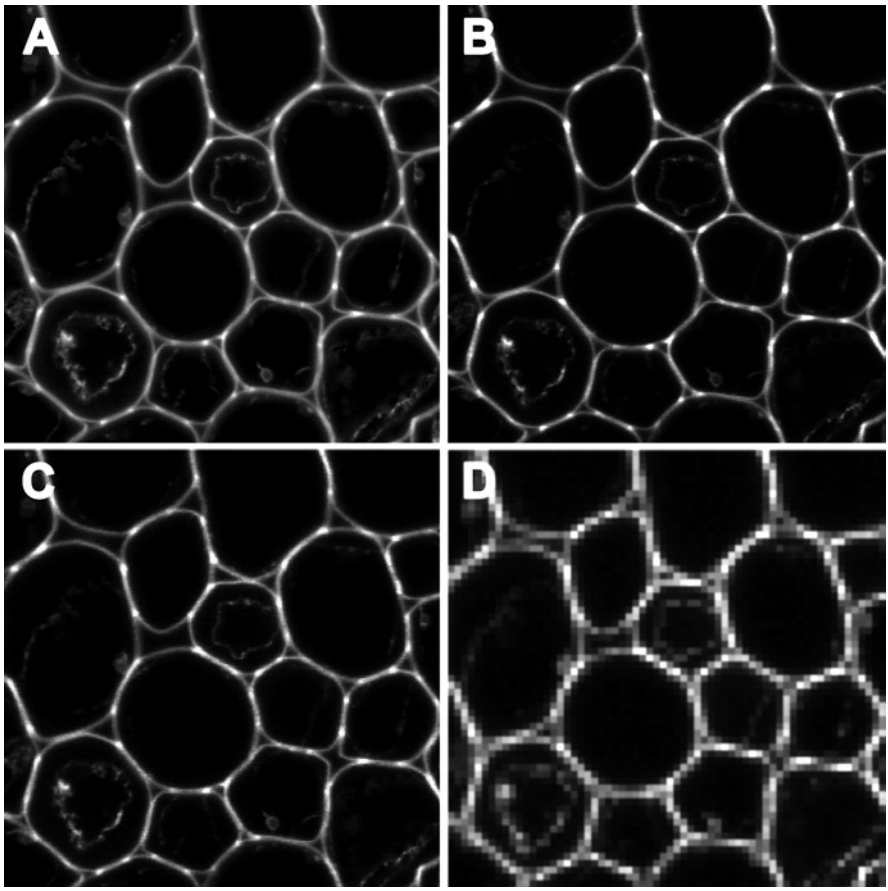

Fig. 6.3 Effects of different pixel sizes on image resolution

[1] In microscopy, the Nyquist–Shannon sampling theorem (Shannon 1998) tells us that we cannot accurately detect microscopic information smaller than 2 detector pixels by 2 detector pixels. This is related to the variability in signal collection and not specifically digital imaging, so we will ignore this signal processing issue until the discussion of detectors in Chap. 7.

With the larger pixel size in Fig. 6.3b some of the fine detail of the image is lost. This is even clearer in Fig. 6.3c where the pixels are 0.22 mm×0.22 mm. Finally, in Fig. 6.3d, the pixels are large enough (0.9 mm×0.9 mm) to be visible. Notice that each pixel in Fig. 6.3d contains a single uniform gray tone.

The number of pixels per inch (PPI) (or per mm) is a useful value for comparing the amount of information contained in two images. However, in microscopy this term is deceptive. It is only an accurate comparison if the two images are magnified to the same extent. In Fig. 6.4, both a and b have 400 PPI. However, if we magnify Fig. 6.4b to the equivalent size as Fig. 6.4a (Fig. 6.4c) the final rendering only has 67 PPI. Fine details present in Fig. 6.4a are not present in either Fig. 6.4b or c. Since, in microscopy, we are always dealing with magnification of images, PPI is only a useful comparator of the amount of information contained in two images when the magnification of the final, rendered images are equivalent.

More small structures than large structures can be placed in a defined area (i.e., they can occur with more frequency). For this reason, we refer to fine detail as high

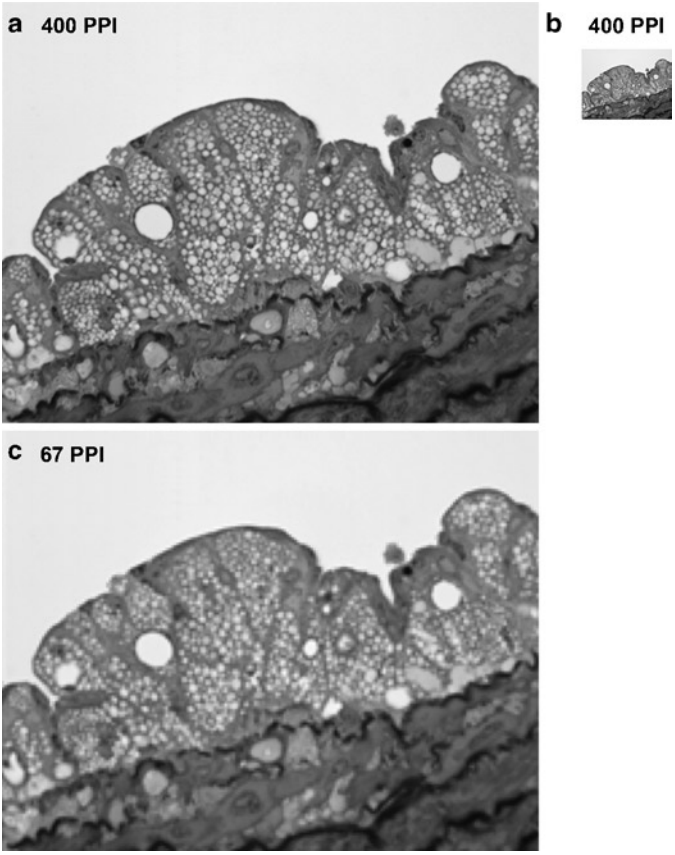

Fig. 6.4 Pixels per inch and image magnification

frequency information and grosser detail as low frequency information when describing the object being imaged. Under this definition, there is more high frequency information contained in Fig. 6.4a than in b or c.

At first blush, it would seem that you would want to use as small a pixel as possible for imaging. However, the smaller the pixel size, the more pixels are contained in the image. This requires more computer memory for storage and more bandwidth for transferring the image information to the rendering hardware (printer, monitor). In addition, it requires more time to capture the information during the microscope session. All of these need to be considered when determining the optimum pixel size for an application. It is inefficient to store an image at a resolution greater than the capability of the image capture method. The excess empty resolution costs both time and memory. For most applications, you should always attempt to match the resolution requirements with the final use of the image.

We will deal with the capture of images in Chap. 7. Here, we will consider practical considerations in determining image storage and rendering. In the last 5 years, computer memory has become extremely cheap so this is rarely a consideration any longer. However, bandwidth still remains a concern. Thus, it is useful to match the digital resolution to the output requirements. Most modern computer monitors have a resolution in the range of 60–130 PPI (most being between 90 and 100 PPI), although recently some monitors with >300 PPI resolution have come on the market. Thus, if you are only going to display an image on a monitor and the monitor being used is only capable of 100 PPI resolution, it is wasteful to store images at greater than this resolution. The pixels per inch displayed by computer projectors currently use very similar standards to computer monitors and so the same principals apply. In microscopy, however, monitor display is usually not the only or most important endpoint for our images. We usually will also print our images and often may wish to collect quantitative information from our captured images. Both of these require much higher resolution images than simply displaying on a monitor.

Printers are calibrated in dots per inch (DPI). This is not the same as pixels per inch and the two systems should not be confused. However, for digital printing, a stored image with a resolution of between 300 and 600 PPI is preferred. At this resolution, the human eye will generally not resolve the individual pixels in the print when the print is viewed at a normal viewing distance. Of course, if one gets very close to the image the individual pixels can begin to be apparent. It is estimated that the human sight can resolve about 1,200 PPI at a very close viewing distance. For normal viewing distances, though, a good rule of thumb is to prepare images at 600 PPI for printing. This is also true of images for submission to journals unless specifically instructed otherwise by the journal's editorial policy.

A computer, of course, does not have the same resolution constraints as the human eye. It sees the image as a series of numbers and so can discriminate differences as small as one unit. So, if the final use of the image will be to have the computer quantify physical characteristics, such as size, area, volume, or co-localization statistics, then one should store images at the maximum resolution feasible taking

into consideration only the sensitivity of the image capture device. Resolution limits imparted by the microscope and image collection methods are discussed in Chaps. 7, 8 and 9.

6.4 Pixel Density

For the analog to digital (A to D) conversion in Fig. 6.2, each pixel was filled with the average of the gray value contained within the pixel area. However, we did not define the range of gray levels that were possible. In computerized digital imaging, the range of possible values (gray levels) is based on binary mathematics, since computers are binary instruments. In binary space, the only values are 0 and 1. In other words, a one-digit number in binary space can have a value of 0 or 1. This means that we can only depict two gray levels. If we want to depict a range from black to white, then that means only black or white is possible. By convention, black is usually designated as 0 and white as 1. This situation is depicted in Fig. 6.5a. If, however, we use a two-digit binary number, we have four possibilities; 00, 01, 10, or 11. Each digit is called a bit, so Fig. 6.5b depicts the possibilities for a 2-bit image. Increasing to two bits expands our range of possibilities so that we can now depict black, dark gray, light gray, and white. Three digits expand the range (bit depth) even further so we can now represent even more gray levels (Fig. 6.5c). The range increases by 2 to the power of the number of bits. Thus:

1 digit = 2^1 = 2 (1 bit of information)
2 digits = 2^2 = 4 (2 bits of information)
3 digits = 2^3 = 8 (3 bits of information)
4 digits = 2^4 = 16 (4 bits of information)

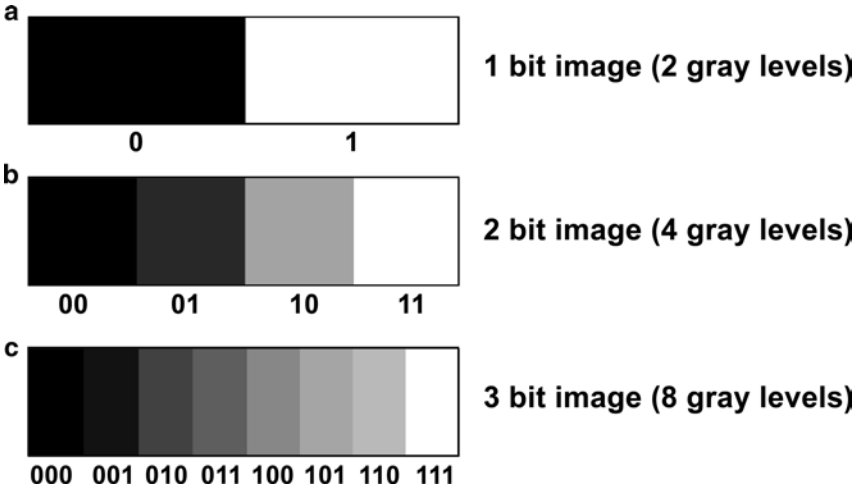

Fig. 6.5 Gray scale values for various digital dynamic ranges

As the number of possible values available to define the range from black to white increases, the range encompassed by each quantum decreases. In fluorescence microscopy, smaller gray scale quanta allow for the depiction of subtler differences in fluorescence intensity. An 8-bit image allows the depiction of 256 (2^8) gray levels. Based on the ability of the human eye to discriminate differences in contrast, this is considered the minimum required to accurately depict visual information. Of course, machines can discriminate more accurately so, for quantitative work, even more gray levels are preferable. Many confocal systems are capable of collecting 12 bit images (2^{12} or 4,096 gray tones). The advantages of 12 bit images will be discussed in subsequent chapters.

Most microscopists are not facile at working with binary numbers. For this reason, the binary representation of a pixel value is usually converted to a base ten number (Fig. 6.6a). In the case of a 2-bit image (4 gray levels) 0 is used to indicate black and 3 indicates white. The values of 1 and 2 indicate gray levels based on dividing the range from black to white into four representative gray levels.

In modern computing, eight bits is termed 1 byte. Thus, each pixel in an 8-bit image contains 1 byte of information. If you have an 8 in. by 10 in. gray tone image stored at 600 PPI, the image size would be 28,800,000 pixels. This is because you will have 4,800 pixels × 6,000 pixels which is equal to 28,800,000 pixels (28.8 megapixels). Since each pixel contains 1 byte of information it takes 28,800,000 bytes (28.8 mb) to store gray scale information for the picture.

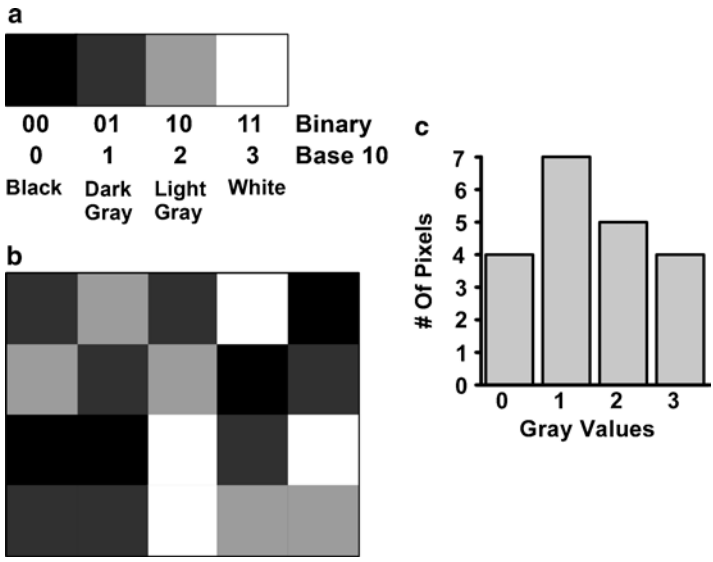

Fig. 6.6 Digital image histograms

6.5 Pixel Histogram Analysis

A useful way to analyze the gray levels in an image is by plotting a histogram of the number of pixels that have a specific gray level (Fig. 6.6b, c). Figure 6.6b shows a two-dimensional array of pixels from a 2-bit image (four possible gray values). Figure 6.6c shows a histogram indicating the number of pixels in Fig. 6.6b which have values of 0, 1, 2, or 3. Note that the histogram does not provide any spatial information. We do not know the location of the four black pixels indicated by the bar height for the *X* value of 0 (black); we have only recorded that there are four black pixels somewhere in the image. Figure 6.7a shows an 8-bit (256 gray levels)

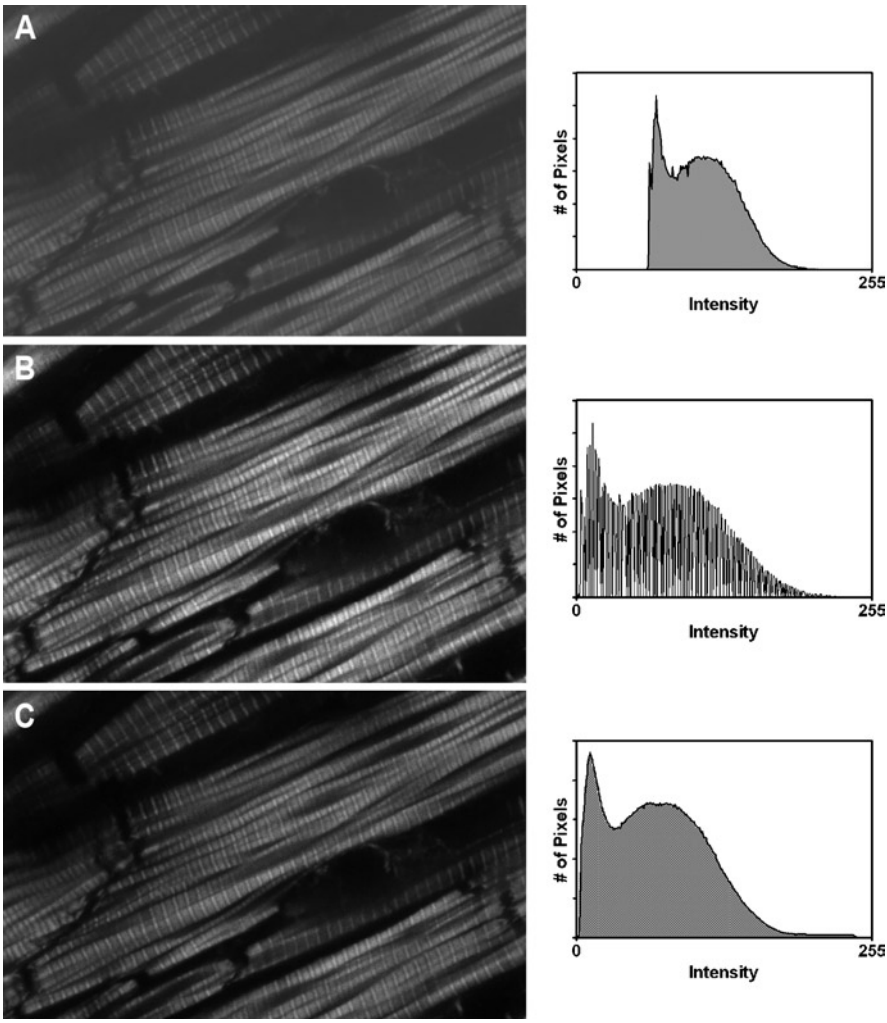

Fig. 6.7 Histogram stretch

image and the histogram from that image. The image has limited contrast with all of the gray level values bunched around the center (medium gray) values. Increasing the difference in density between two adjacent pixels (contrast) can be useful for increasing the visibility of structures. This can be done, based on the gray level (intensity) histogram, by stretching out the values to cover the full dynamic range of 256 gray levels (0–255). The process of stretching out the available pixel values to cover the entire 0–255 range available is called Histogram Stretch. Figure 6.7b illustrates the increased image contrast that results from spreading the gray values out to use the full dynamic range.

Most imaging software has at least one routine for reassigning pixel values to stretch or compress the gray level histogram. An important point about histogram stretching for scientific imaging is that histogram stretch does not alter the linear relationship of one pixel value to another; it only increases the difference in gray tone (contrast). Thus, for simply discriminating the location of some structure or examining fine detail, the data contained in the image has not been altered in any significant way; individual structures have simply been made more visible. However, if you are using the absolute pixel gray value as some measure of concentration of an analyte compared to another, you have altered this data by performing a histogram stretch or any other method of reassigning pixel values. Thus, even though procedures such as histogram stretch are relatively benign, they still need to be done with full knowledge of what you are changing. In looking at the histogram of the stretched image in Fig. 6.7b, you will note that there are now gaps in the histogram. So, although structural information stored in the image file have been made more visible, there are structural details that were not captured. This information cannot be regained. Thus, it is preferable to capture the original image using the full available range of gray values rather than having to extensively stretch the image after collection. Figure 6.7c shows the additional detail that is present when the image is correctly captured. Chapter 9 discusses how to insure that the full possible dynamic range is used for confocal image

6.6 Digital Image Gamma

Gamma is another useful, and relatively benign, parameter for increasing the visibility of specific parts of an image. Gamma is the relationship between the detected gray level (input value) and the gray level that is rendered in the final image (output value) as displayed on the computer screen or in a digital print (Fig. 6.8). Gamma is a power function. In an 8-bit image, gamma determines the output (rendered value) based on the equation:

$$y = 255\left(\frac{x}{255}\right)^{\gamma}, \tag{6.1}$$

where : y = output value
x = input value
γ = gamma

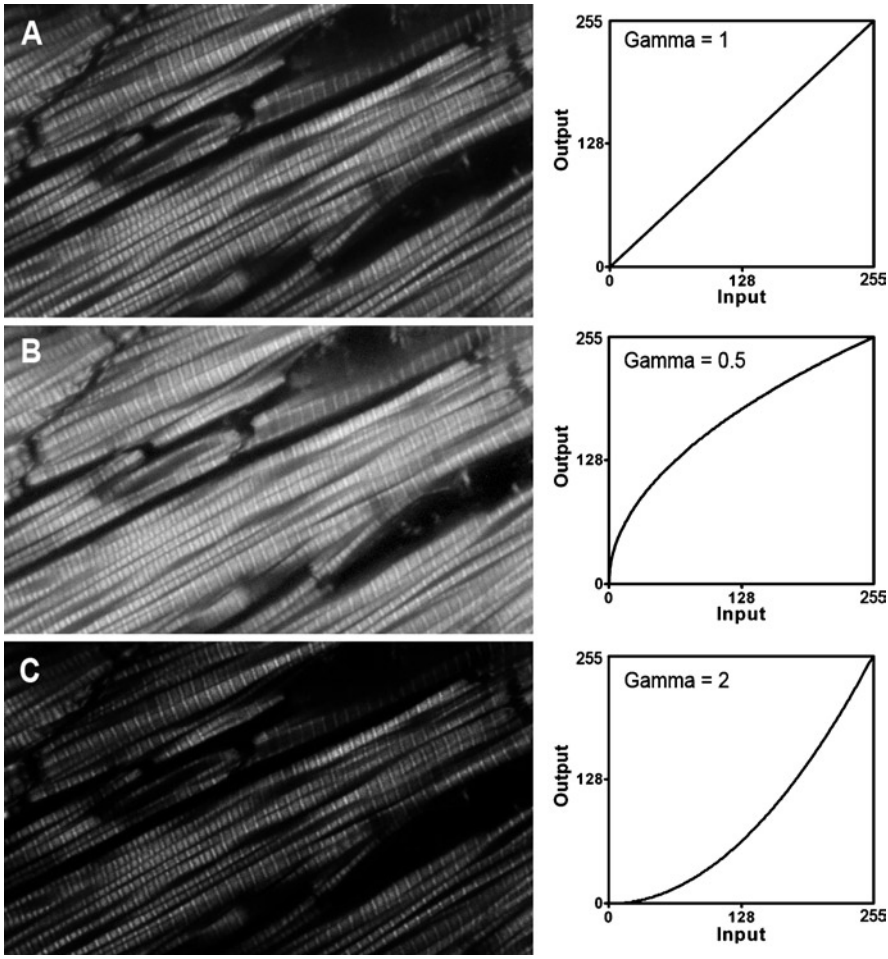

Fig. 6.8 Alteration of image gamma

With a gamma of 1, there is a one to one relationship of detected level and rendered level (Fig. 6.8a). An input gray value of 50 would be displayed as 50 and a gray value of 215 would be displayed as 215. In contrast, with a gamma of 0.5 (Fig. 6.8b) an input value of 50 would be displayed as 113 and 215 would be displayed as 234. A gamma less than one helps spread out the information in the darker regions to make it more visible but reduces the difference in intensity between values in the lighter regions. Conversely, a gamma greater than one (Fig. 6.8c) spreads out values in the lighter regions and compresses the darker values. As with histogram stretching, a change in gamma does not change the relative relationship of the original data. Moreover, with gamma, the original image can be regained by doing the inverse operation. The inverse is called a gamma

correction. Gamma correction routines in some software packages are also called Gamma, so do not be perplexed by this confusing usage. Importantly, changes in gamma do not affect the lowest and highest values. A value of 0 remains 0 and a value of 255 remains 255. Thus, changing the gamma does not alter the dynamic range of the image. This is not true for most functions that allow you to adjust contrast and brightness. These can significantly compress the dynamic range and we suggest you avoid these contrast and brightness functions. Instead, it is best to use the histogram stretch and gamma controls when it is necessary to enhance the visibility of objects in your image. These provide finer control on the image appearance. When necessary, histogram stretch should be done before changing the gamma.

6.7 Use of Histogram Stretch and Gamma Changes in Confocal Imaging

Histogram stretch and alterations in gamma are useful tools for making subtle details in your image more visible to a human observer. Gamma changes are particularly useful. The human eye does not have a linear response to light. Our eyes are more sensitive to variations in dark gray levels than equivalent differences in the brighter registers. The eye responds with a gamma of about 2.2. Scientific digital cameras are generally linear capture devices. This is critical for quantitative work but not necessarily for presenting your images to an audience. The makers of computer monitors, printers, and other digital hardware recognize this and often add a gamma function which converts the linear captured information into a presentation that more closely matches what your eye saw through the microscope. This is a useful tool but you need to be aware of the degree to which a correction is employed if you are using your image information to make quantitative or semi quantitative assessments. The gamma correction employed by a piece of software or hardware is information that is generally not made readily available to the end user. For recreational imaging it is probably not very important. However, for scientific evaluations, it is always worth digging into the product literature or contacting the manufacturer to determine what corrections your software program, monitor, or printer are imparting to your image data and to turn those features off, if necessary.

In practice, histogram stretch and gamma functions should be used to enhance the scientific usefulness of an image by bringing out additional detail. However, any quantitative analysis or comparison of pixel brightness must be done prior to applying any histogram stretch or gamma functions. Moreover, these and all other image processing steps should be done on noncompressed copies of the original image. The original image should always be stored, unaltered, on archival quality media such as a “write once” CD or DVD. The image should be stored in a lossless image format such as Tagged Image File Format (TIFF). Image formats are discussed later in Sect. 6.10.

6.8 Image Voxels

A major strength of confocal microscopy is the ability to image defined planes within the sample. Although the planes are thinner than those of a widefield imaging system, they do have a finite height. Thus, confocal images produce three-dimensional data. The depth of the image (not to be confused with pixel gray scale depth) combined with the *X* and *Y* dimensions define a digital volume element (Voxel) rather than a pixel. A voxel is the three-dimensional analog of the two-dimensional pixel (Fig. 6.9). In the same way that a pixel represents the average luminance within an area, a voxel's density will be the average of the luminance values within a defined volume. As such, a voxel represents the smallest unit of volume information that can be depicted in digital reconstruction of an analog object. Also, like pixels, the dimensions of voxels are defined in whole multiples of a unit value (quanta). However, again like pixels, the *X*, *Y*, and *Z* quanta defining the voxel do not have to be the same. In most cases, we want to use the same value for *X* and *Y*. However, as discussed in Chaps. 8 and 9, in microscopy, the *Z* quanta is usually restricted to a larger value by the physics of microscopy imaging.

Since voxels have three dimensions, voxel information can be used to reconstruct a single plane of the sample; if sequential planes are collected they can also be stacked on top of each other to produce a three-dimensional map of the entire specimen volume. Moreover, the digitized value for a voxel can be transformed in the same way pixel values can be transformed and the voxel histogram and gamma can be manipulated using the same techniques used for pixels. The methods by which the confocal microscope collects voxel information are discussed in Chap. 9. The constraints on voxel size imposed by the physics of microscope imaging are described in Chap. 8 and the methods of working with voxels to produce digital reconstructions are covered in Chap. 10.

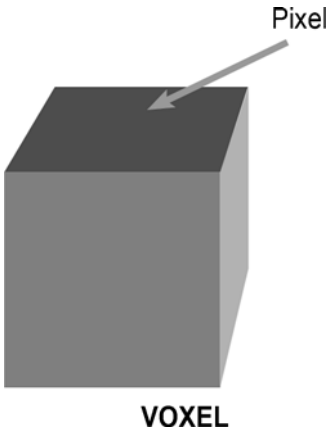

Fig. 6.9 Voxel and pixel relationship

6.9 Color Images

So far we have dealt only with gray scale images; those that are composed of pixels or voxels with various shades of gray. Digital color images are produced by combining color information encoded as multiple gray scale images.

In order to reasonably accurately depict the colors of the object under investigation, the microscopist needs to understand a few additional concepts about color rendition and color management. These concepts include Hue, Saturation, Brightness, and Luminance.

Hue defines the color. All blues have the same hue.

Saturation determines how intense the color appears. A fully saturated color is deep and brilliant. Less saturated colors appear faded compared to the fully saturated color.

Brightness is a measure of how light or dark the color appears. A brightness value of 0 indicates black.

Luminance describes the perceived brightness. The difference between luminance and brightness is that luminance takes into consideration the color sensitivity of the human eye. For instance, the human eye is much more sensitive to light in the yellow-green range than it is to blue.

The two most important color rendering methods (color spaces) for microscopists are the Red, Green, and Blue system (RGB color space) and Cyan, Magenta, Yellow, and Key (black) system (CMYK color space). RGB is the mechanism used for computer screens and the one closest to human and microscopic visualization. It is the method implemented on most commercial confocal microscopes. In contrast, CMYK is the system used by most printers.

The RGB system is an additive color system. Black is the absence of any color information while adding equal contributions of red, green, and blue produces white. Having only red information, and no green or blue, produces red. Likewise, having only green or only blue produces green or blue, respectively. However, by adding certain proportions of red, green, and blue we can produce a variety of colors. This is equivalent to combining three beams of different colored light. In practice, three gray scale images representing red, green, and blue respectively are combined. The hue and brightness of each resulting color pixel is the result of the addition of the information contained in each of the three overlain pixels. Thus, for a gray scale of 0–255, an RGB image will have 3 bytes of information for each pixel; 1 byte for red, one for green and one for blue. As discussed in Chaps. 7 and 9, in confocal microscopy we assign the gray scale density value based on the number of photons collected by the detector and the hue is assigned arbitrarily but usually based on the specific color filters used to collect the signal.

The CMYK system is a subtractive process. It is equivalent to mixing paint. Conceptually, the process begins with a blank white sheet on which the image will be produced. In the case of a digital image, this means the starting pixel is white. To this white pixel, a certain amount of cyan, magenta, and yellow color is added.

An equal contribution of each produces black. Since it mimics the printing process of applying ink to paper, the CMYK system is used by printers. In most printing processes, black ink is substituted for equal amounts of cyan, magenta, and yellow. This saves money on ink and produces deeper dark tones.

Microscopy uses additive light and so is best done in the RGB color space. However, some journals require CMYK images for publication because this system matches the printing process. Although there are similarities between the RGB and CMYK systems, they are not identical. When you convert between the two systems, such as when preparing micrographs for publication, you should check the results of the conversion carefully to make sure the converted image retains accurate color information. Your printer also converts the RGB information in your stored image to CMYK when printing. This sometimes requires some readjustment of the images on your part to make sure the printed image is faithful to what was viewed in the microscope or on the computer screen.

A 24-bit RGB color image (8 bits of red information, 8 bits of green information, and 8 bits of blue information) is capable of coding for approximately 16.7 million different colors. Unfortunately, limitations of the capture and rendering devices (cameras, scanners, printers, monitors, etc.) generally are not capable of accurately capturing or depicting 16.7 million different values. Since the deficiencies are not consistent across capture and rendering platforms, this further complicates the accurate reproduction of color information. For most scientific imaging, however, it is sufficient to realize that accurate color transfer is not achievable without a great deal of effort but that this level of accuracy is generally not necessary for confocal studies, especially since confocal imaging usually collects each set of color information separately. This is explained further in Chaps. 7–9.

Of course, any color in our image has been artificially added. The high resolution detectors used in modern confocal microscopy detect only the presence of photons. They do not measure the wavelength of those photons and so cannot assign color to the photon. The color component is added in software based on parameters the microscopist has defined. If a red filter is in place it is useful, but not obligatory, to display the value for the photons collected in the red channel as the red information in an RGB image. Typically color is assigned to images by assigning a specific color to the numerical value associated with each pixel or voxel. The association of each color with a specific numerical value is included in software programs called Look-up-Tables (LUTs). The procedure for assigning color to confocal images by the use of LUTs is discussed in Chap. 9.

6.10 File Formats

The file format is the set of instructions for storing and retrieving the image information. Formats can be broadly categorized into generic and proprietary formats. Proprietary formats are those that are system or software-dependent. The Adobe

PSD format is an example of a proprietary format. Many of the confocal microscope manufacturer's software also include proprietary formats. The Zeiss LSM and Leica LEI formats are examples. These machine-specific formats allow the software to acquire and store additional information about the image as part of the stored image. In the case of confocal microscopes, this often includes a wealth of information about the microscope settings used to collect the image. Having information about the pinhole diameter, magnification, laser settings, filters, etc. used during image collection is extremely useful. However, the down side of proprietary formats is that you have to have the proprietary software to decode the stored image. This makes it difficult to share the images with others or to import the images into other software programs. Luckily, most confocal software allows you to also save a copy in a generic format. Most confocal microscope manufacturers are now also making available a free browser that will recognize their proprietary formats. Although these free browsers have limited capabilities, they do at least allow you to share your images with others.

The alternative to proprietary image formats is generic formats. These are formats that are independent of machine, operating system, file system, compiler, or processor. Moreover, images stored in generic formats can be outputted to any hardware (printers, monitors, etc.) that recognize the format. Most modern image formats also maintain backward compatibility as the format evolves. A word of caution is that converting an image saved in one of the proprietary programs typically results in loss of the important operating parameters listed above from the file. It is very important when converting to generic formats that the original proprietary formatted image also be kept and archived.

There are numerous generic formats but the two most important for scientific imaging are the TIFF and Joint Photographic Experts Group (JPEG) formats. These formats are recognized by almost all imaging programs and most proprietary software allows the option of saving in these formats. For scientific imaging, the key difference between the two is that, in the TIFF format, the image information is not changed when the stored image is created. In contrast, the JPEG image format compresses the image so that less computer memory is required to store the image. When computer memory was expensive, compression was very useful. JPEG allows compression of the image at ratios >1:200. This compression, though, comes at the expense of image information. The goal of JPEG storage is not to store every bit of information in the digital image. Its goal is merely to store and reproduce the format in a "photorealistic" form. This means that the JPEG image, when rendered from storage, will "look" almost identical to the original. However, since your image is your data, just having an image look like the original is usually not sufficient. Figure 6.10a shows a TIFF image and Fig. 6.10b shows that same image after conversion to JPEG format. Figure 6.10c shows the subtraction of the two images from each other. All the nonblack pixels in Fig. 6.10c indicate pixels that were altered by the JPEG compression. It should be clear from Fig. 6.10c that scientific imaging should primarily employ lossless storage techniques, such as TIFF. We suggest TIFF because it is the most serviceable and widely accepted format for scientific image storage and use.

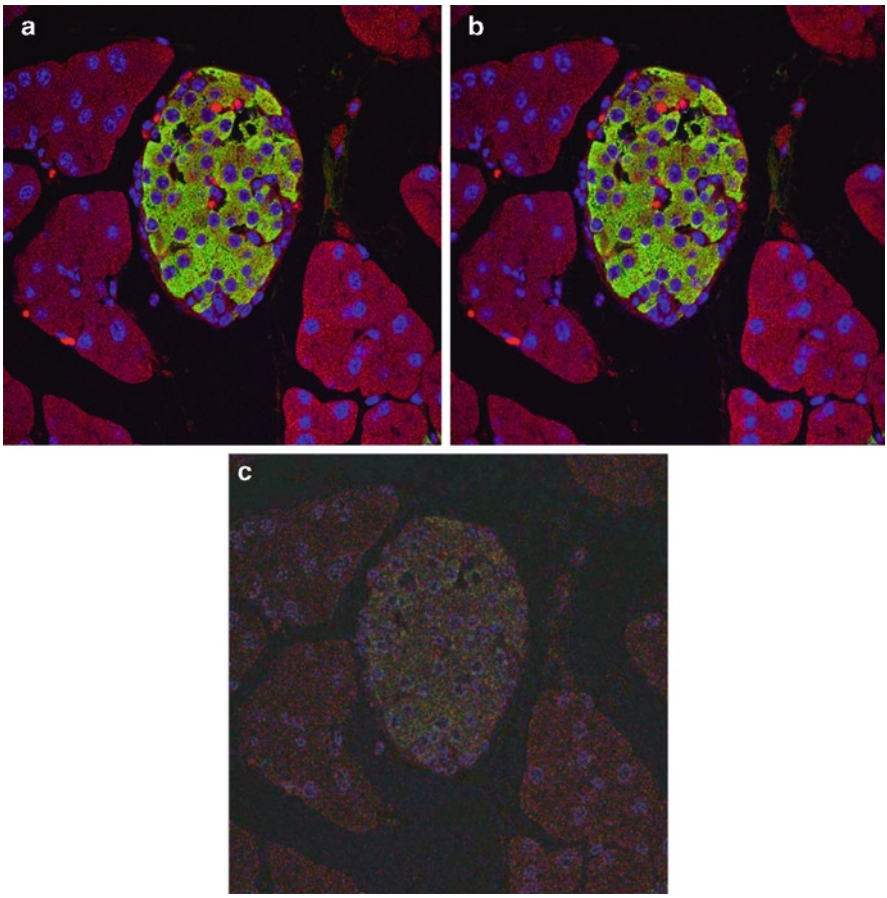

Fig. 6.10 TIFF and JPEG image storage. (**a**) Tiff image of fluorescently labeled pancreas. (**b**) Same image as (**a**) stored as JPEG image. (**c**) Subtraction of image (**b**) from image (**a**) showing pixels altered by JPEG compression

Because it degrades image information, the JPEG format should be avoided for most scientific imaging applications. Although the JPEG format allows one to choose the degree of compression (the higher the compression ratio, the more information that is discarded when storing the image), there is no option in the JPEG format for a lossless saving of the image data. It is also important to note that each time you save a JPEG image the program runs the compression algorithm. Thus repeated saving of an image in JPEG format leads to additive degradation of the image information. The image information loss is the reason why the Ninth Commandment of the Confocal Ten Commandments described in Chap. 1 is "The JPEG image format is Evil." However, sometimes you need to dance with the devil. This is admissible as long as you recognize the consequences and confirm that the changes occurring would not affect the conclusions drawn from the image.

For instance, emailing a 10-mb image to a colleague for review is usually not accommodated by most email systems. In this situation, JPEG compression to a 50 Kb image would be extremely useful. However, quantitative analysis of image information should never be done on a JPEG image. Moreover, as discussed above, it is a good rule of thumb never to resave a JPEG image. When you need to revisit the image, always go back and make a copy of the original TIFF image for doing any postcollection analysis.

It is worth reiterating here that "your image is your data!" Most modifications done to your image, including JPEG conversion, are irreversible. For this reason, it is critical that you maintain the originally collected image on archival media and only work from copies of the original for any image analysis or conversion routines that alter, in any way, the image information.

Reference

Shannon, C. 1998. Communication in the presence of noise. *Proc IEEE.* 86:447–457.

Chapter 7
Digital Image Capture for Confocal Microscopy

W. Gray (Jay) Jerome

Keywords Airy disk • Airy unit • Charge-coupled device • Dynamic range • Numerical aperture • Nyquist • Resolution • Signal-to-noise ratio • Point spread function

7.1 Introduction

Good microscopy includes optimizing the information obtainable from your confocal image with the minimum amount of effort and time. A key to achieving this goal is to match, as closely as possible, the parameters of all hardware and software in the image collection train. For reasons outlined later in this chapter, it is particularly important to match the resolution of your digital image to the output resolution from the microscope. In Chap. 6, we discussed the resolution parameters of the digital image. In this chapter, we cover the optical resolution obtainable from fluorescence confocal light microscopes, we review the important parameters of the image acquisition hardware that influence image information, and we illustrate how to match these two parameters to optimize confocal image acquisition.

For images, two related types of resolution are important; spatial resolution and contrast resolution. Spatial resolution defines the size (or fineness of detail) of objects that can be reliably detected. In addition to spatial resolution, to "see" an individual feature there must be a sufficient contrast difference between the feature and its surroundings. Blue writing on blue paper will not be visible, even if the letters are quite large, because there is no suitable difference in contrast. The contrast difference can be a difference in color or in brightness. Thus, bright yellow letters on a bright blue background will be easily distinguishable as will light gray letters on a dark gray background. Since an RGB color image is really three

W.G. (Jay) Jerome (✉)
Department of Pathology, Vanderbilt University Medical Center, U-2206 MCN,
1161 21st Ave, South Nashville, TN 37232-2561, USA
e-mail: jay.jerome@vanderbilt.edu

R.L. Price and W.G. (Jay) Jerome (eds.), *Basic Confocal Microscopy*,
DOI 10.1007/978-0-387-78175-4_7,

gray-scale images combined (see Chap. 6 for details), we will limit our contrast discussion to gray scale values (densities) but it should be remembered that in color images, differences in color are just as valid as differences in brightness. Chapter 6 discussed the dynamic range of a digital image. A larger dynamic range allows for smaller shading gradations and thus higher digital contrast resolution. Of course, our eye cannot distinguish the small differences between two adjacent gray values in the 4,096 value dynamic range of a 12-bit image. However, the computer can and so postimage processing can be used to selectively highlight specific values as long as the values were accurately captured during initial image acquisition.

The contrast resolution of a digital image collected with a fluorescent or confocal microscope is dependent upon multiple factors: (1) the inherent contrast differences in areas of the specimen, (2) the ability of the microscope and the camera to capture those inherent differences, and (3) the image storage and display system's ability to accurately render those differences. In other words, even if a specimen generates a bright fluorescent signal that is easily distinguished from the background noise, that information will not be resolved in the final image if our camera system cannot detect the signal differences or if the analog to digital conversion is not capable of converting and storing these differences as discretely different values. This is true even if the structures are well resolved spatially. A strength of the confocal microscope is that, by reducing or eliminating fluorescence signal from out-of-focus planes, the contrast difference between in-focus fluorescent objects and the background is increased.

7.2 Basics of Optical Microscopy Resolution

A highly magnified image is not very useful if it is not sharp. A fuzzy image lacks fine (high frequency) detail. Once lost, this detail cannot be regained no matter how high the image is magnified ("Resolution is a One Way Street!"). Increased magnification will only make the fuzziness more apparent. This excess magnification is referred to as "empty magnification" because it achieves no gain in image information. Since you cannot gain back information, it is imperative during image capture to obtain as much information as possible, or at least as much as is necessary for your experimental purpose. We can define the maximum image information obtainable under specific conditions as the highest resolution. If we could obtain infinitely fine resolution we could produce an infinitely sharp image of infinitely small objects. Unfortunately, the physical properties of light constrain the size of objects that can be sharply imaged using photons with wavelengths within the visible spectrum; objects smaller than this limit will be fuzzy. Cameras and the analog to digital conversion process introduce additional constraints that potentially can reduce the resolution of our final image. For this reason, the good microscopist must understand how the microscope hardware, the digital capture device, and the image storage method contribute to the loss of image information.

7.2.1 Lateral Spatial Resolution

The limitation in sharpness of a 2-D micrograph is termed the lateral (or angular) spatial resolution. The lateral resolution is usually defined in terms of how close two objects can be and still be recognized as two distinct objects. As the objects get closer together, it becomes harder to see the space between the spots. At some point, the space is no longer visible and the two spots appear to merge into a single object. At this distance, the space is no longer resolved. The corollary is that structures with dimensions smaller than this distance will also not be resolved because these fine details will blur together.

This definition works very well for a brightfield image where multiple points are illuminated at once and the light from adjacent objects can interfere. However, in fluorescence confocal microscopy, we generally project a focused point (or series of discrete points in the case of multipoint scanning instruments) into a sample and then image only that small illuminated area. Thus, each point in our final image is independently collected. For this type of imaging scheme, the important questions are (1) what is the smallest excitation spot size (probe diameter) that can be produced by focusing a beam of photons, (2) how does the imaging system affect the information arising from that illuminated volume as it is projected to the detector, and (3) how faithfully does the analog to digital conversion system (camera) collect the information projected by the microscope? This section deals with the first two of these questions.

Confocal microscopes illuminate a 3-D volume in the specimen but, since the constraints on the size of that volume are slightly different in the lateral (X, Y direction) and the axial (Z) direction, we will deal with the lateral and axial dimensions separately.

The key reason for the lateral image blurring in a microscope is diffraction of light waves. If the photons from a small point are focused through a lens (including the lens of our eyes), the 2-D image of the original point will not appear as a point in the lateral plane but rather will be seen as an Airy pattern (Fig. 7.1a). This pattern is named for the astronomer George Airy, who first described the phenomenon. The Airy pattern has a central bright circle (Airy disk) surrounded by a series of halos (maxima). The halos are separated from the central disk by dark rings (minima). As shown in Fig. 7.1b, which plots the intensity of light along the line x traversing the Airy pattern, most of the light from a point is focused into the Airy disk (about 97% of the light). The first maxima (first halo) contains most of the remaining light (about 1.7%). Each successive maxima after the first has progressively less light. In most situations, we can ignore the first maxima but you should always remember it is there. In some, low light situations it can contribute to the image.

It is obvious then that the Airy disk places a finite limit on how small an area we can illuminate in our specimen. This phenomenon also limits the size of the image of the illuminated area sent to a detector since this path also involves passage of light waves through a lens. The brightness at any particular point away from the center of the Airy pattern is dependent upon the strength of the light waves as they merge and the mixture of phases of all the merged wave fronts. The graph in

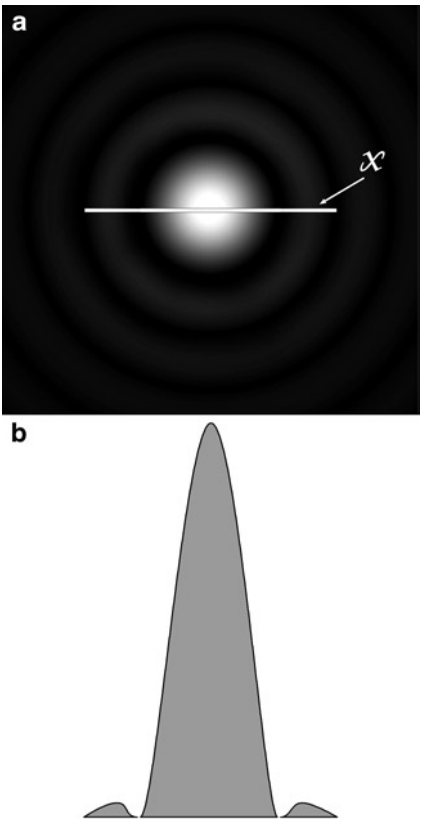

Fig. 7.1 (**a**) Image of an Airy pattern. The central bright spot is the Airy disk. (**b**) Plot of intensity along line *X* in (**a**)

Fig. 7.1b illustrates that there is no sharp demarcation between very bright and very dark regions of the Airy pattern but rather a continuous change in intensity from the very brightest point of the Airy disk to the very darkest region of the first minimum.

Although it is not critical to understand all the details of why the Airy pattern is formed, it is worth a brief discussion of the general theory behind the effect. An Airy pattern results from the diffraction of light. When electromagnetic waves, such as light, meet a solid edge the waves bend around the edge to form a new wave front. According to Huygen's Principle, each point on the wave front emits vibrations in multiple directions (Huygen wavelets). This concept is illustrated in Fig. 7.2a. At the point of focus of a lens, depicted by A in Fig. 7.2b, these wavelets arrive in phase and so their amplitudes are additive (Fig. 7.2c). However, wavelets also arrive at other points in the same image plane (S_i) away from the focus point A. In regions where wavelets arrive exactly out of phase, such as point B in Fig. 7.2b, their amplitudes will cancel each other out as illustrated in Fig. 7.2c.

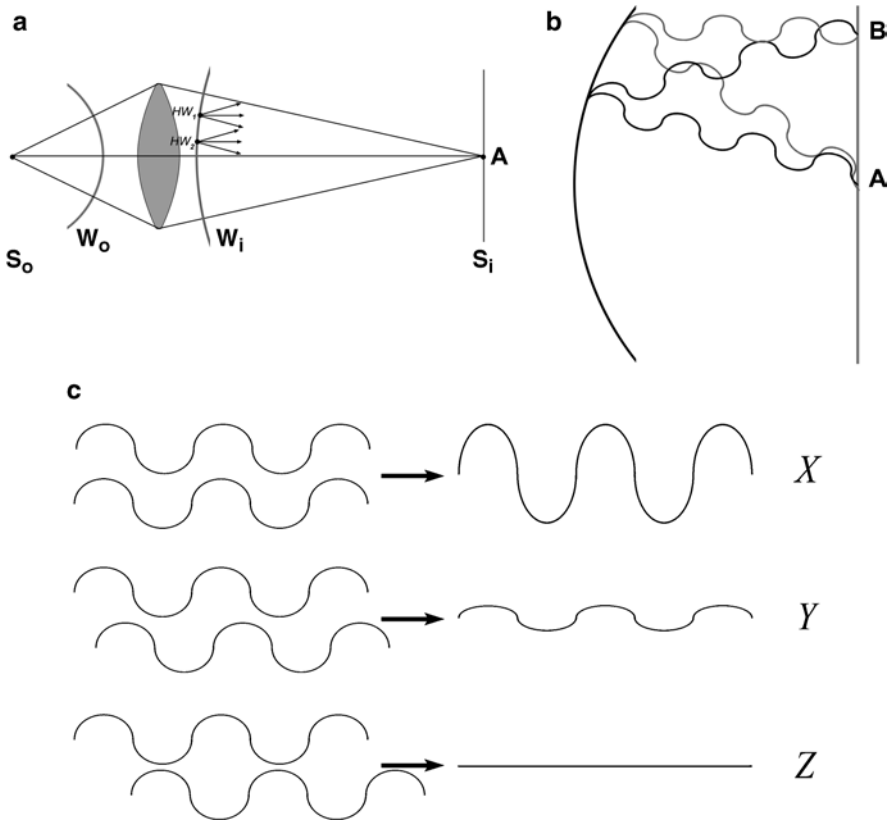

Fig. 7.2 Theory of Airy pattern formation. (**a**) Huygen wavelets (HW1 and HW2) are formed all along the wave front (W1). (**b**) At the focal point of the lens (point A), the Huygen wavelets arrive in phase and so are added together. At other points in the same plane (such as point B), the wavelets arrive out of phase and so are subtractive. (**c**) Waves that are exactly in phase (example *X*) will add together and the resulting amplitude will be the sum of the individual amplitudes, waves that are exactly out of phase (example *Z*) will cancel each other out and the resulting amplitude will be zero, waves that are not totally in or out of phase (example *Y*) will produce a signal with an amplitude in between that of *X* and *Z*

This subtraction will form the first dark ring (minima). Waves converging even further from the focal point will again arrive in phase and form the first halo (maxima). Most of the light will fall within the central (Airy) disk and this will be the brightest point. By comparison, the first maxima will be considerably dimmer than the Airy disk.

The size of the Airy disk and spacing of the halos are dependent upon the wavelength of the light and the proportion of the total light coming from the specimen that is collected by the lens (measured as the collecting angle). The radius of the disk (r) can be defined by the equation (7.1) given below.

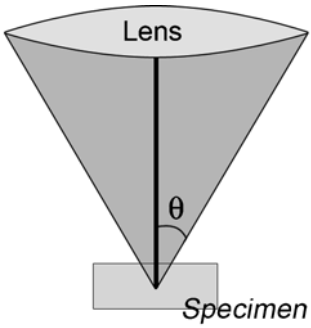

Fig. 7.3 Diagram of the cone of light collected by a lens. θ represents one half of the collecting angle of the lens

$$r = \frac{0.61\lambda}{\sin\theta}, \tag{7.1}$$

where: λ = wavelength

θ = half the collecting angle of the lens

The equation tells us that the radius of the Airy disk is equal to a constant times the wavelength of the illumination divided by the sine of half the collecting angle. Half the collecting angle of the lens is the angle between the optical axis and the edge of the lens (Fig. 7.3).

This equation defines an absolute value for the area of the specimen illuminated by visible photons. However, since we illuminate discrete volumes separately, in confocal microscopy we have the potential to localize the presence of individual small molecules that are smaller than the diameter of an Airy disk. In this scenario, though, because we have illuminated an area larger than the molecule, we cannot pinpoint the precise location. We can only determine that the emitter was contained within the area illuminated. Likewise, when the object we are viewing is smaller than an Airy disk, we have no information about its size and shape. In order to get this information, the object must be larger than an Airy disk. So the Airy disk provides practical limits to the fineness of the detail we can obtain from the optical images of an object.

7.2.2 Lateral Contrast Resolution

As discussed earlier, our ability to "see" two points as separate and distinct is dependent upon both the lateral spatial and contrast resolution. So, the observed resolution greatly depends on the detection method. In the early days of microscopy, the eye was the detection method and so early definitions of resolution were based on the ability of our eyes to discriminate contrast differences. In the nineteenth century, John William Strutt (Lord Rayleigh) examined the resolution problem

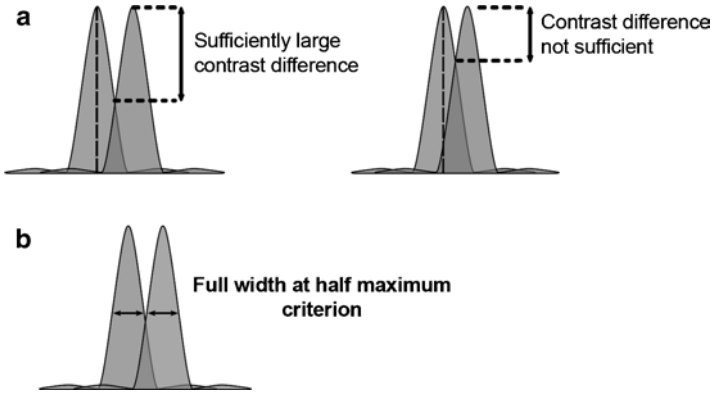

Fig. 7.4 (**a**) The Rayleigh criterion for contrast resolution. Two objects can be resolved only if the contrast difference is sufficiently large enough. (**b**) Illustration of full width at half max value for the Airy disks of two adjacent objects

and came up with a method of approximating the resolution limit in standard fluorescence microscopy. He proposed that there would be sufficient contrast between the centers of the Airy disks of two objects if the center of one Airy disk lies at or further away than the first minimum of the other (Fig. 7.4a). In other words, we can determine the resolution limit with the Airy disk equation (7.1) above. This is true in air or in a vacuum. However, in a material with a higher refractive index, the velocity of light slows down. Thus, when using immersion oil or water we need to account for this change in velocity because wavelength is related to velocity. Equation (7.2) shows this relationship.

$$\lambda = \frac{v}{f}, \tag{7.2}$$

$$\text{where : } \lambda = \text{wavelength}$$

$$v = \text{velocity}$$

$$f = \text{frequency}$$

The frequency of light waves does not change. So, as velocity decreases so does wavelength. We can account for this in equation 7.1 by adding a refractive index term to the equation. The refractive index of a medium is the ratio of the velocity of light in a vacuum compared to the velocity of light in the medium of interest.

$$n = \frac{v_v}{v_m}, \tag{7.3}$$

$$\text{where: } n = \text{refractive index}$$

$$v_v = \text{velocity of light in a vacuum}$$

$$v_m = \text{velocity of light in the vacum}$$

We can define a further term, the numerical aperture (NA) of a lens, as the sine of ½ the collecting angle times the refractive index of the medium used with the lens. This value is provided for all good quality lenses and is usually designated as the NA. Taking into consideration NA, we can formalize the Rayleigh criterion as the following:

$$r = \frac{0.61\lambda}{(\sin\theta)(n)} = \frac{0.61\lambda}{\mathrm{NA}}, \tag{7.4}$$

where: r = minimum resolved distance

λ = wavelength

θ = half of the collecting angle of the lens

n = refractive index

NA = numerical aperture

Some typical values for microscopy imaging would be 450 nm wavelength of light, sin θ=0.92 (for θ=67°), n=1.515. The NA would be 1.515×0.92 which equals 1.4. Given this, equation 7.4 allows us to determine that r (minimum resolved distance) would be 196 nm.

The Rayleigh criterion is a relative one and based on the ability of our eye to discriminate contrast. If we have a detector that exceeds our eyes' capacity, the value for r can be decreased further. A related criterion partially takes detector efficiency into consideration. In this criterion, usually referred to as "full width at half max" it is assumed that objects can be discriminated if they are at least as far apart as the full width of their image at the half-maximal brightness value (Fig. 7.4b). The double arrows in Fig. 7.4b indicate the full width of each curve at half the maximal intensity value (FWHM). For the eye, the FWHM distance will be only a little less than that determined by the Raleigh criterion. It is important to remember that neither the Rayleigh criterion nor FWHM represent absolutes. Rather, they are general rules of thumb. Methods that can increase contrast further or detectors that can discriminate smaller levels of contrast can resolve even smaller distances. One strength of the confocal microscope is the increase in image contrast. Based, at least partly, on this the confocal provides a gain in lateral resolution. This improvement in lateral resolution is defined in (7.5)

$$r(\text{confocal}) = \frac{0.4\lambda}{\mathrm{NA}}, \tag{7.5}$$

where: r = minimum resolved distance

NA = numerical aperture

λ = wavelength

In recent years, some newer, specialized imaging techniques have been developed that use multiple lenses or multiple illuminations to independently collect data below the diffraction limited level (Hell 2009; Lippincott-Schwartz and Manley 2009). These, super resolution fluorescence techniques present very exciting extensions of

our imaging capabilities for very specialized situations. The reader is urged to find out more about them and explore their usefulness. However, for most standard confocal fluorescence studies, $0.4\,\lambda$/NA best defines the optimum lateral resolution value in confocal microscopy. For this reason, we will utilize this criterion throughout the remainder of the chapter.

The equation for the Airy disk describes the minimum area that can be illuminated by an electromagnetic wave such as light. Since the image of that illuminated area is also the product of electromagnetic waves traversing a lens, the equation for the Airy disk also describes how the microscope affects the image of that illuminated volume. As the prominent early microscopist Ernst Abbe pointed out, we can think of a large object as a series of points that either emit or diffract light. Thus, the Rayleigh criterion defines the level of fine detail we can discern within a larger object. Resolution is, thus, the key determinant of how sharp detail will appear in our image. Just as we describe the pixel as the smallest resolvable unit of a digital image, we can define a resolved element (resel) as the smallest resolvable unit of a micrograph. Of course, there is also a role for magnification, the other major component of a microscope. For instance, our eye cannot discriminate distances much smaller than about 0.2 mm. Thus, we need to magnify the resel in order to see it. We will have more to say on this later.

It is worth reiterating that all criteria for resolution are intimately dependent upon the Airy disk size. We can circumvent some of its limitations but if we use a lens for imaging, we cannot completely get rid of the consequences of the diffraction of light.

7.2.3 Lateral Contrast Transfer Function

Just as a point of light is altered as it traverses the optical path, the contrast inherent in an object is also altered by the microscope and other components of the imaging system. The effect of the imaging system on contrast can be described by the contrast transfer function (CTF). Since resolution is intimately dependent on contrast, the CTF is just as critical as the point spread function (PSF) for understanding how an optical system affects resolution. Figure 7.5 depicts a theoretical CTF for a microscope. A full discussion of the CTF is more appropriate for an advanced optics book. However, a few key points can be easily seen from the graph. First, there is always a loss of contrast during the imaging process. Thus, the microscope does not faithfully reproduce an object down to the Abbe-defined defraction limit and then the image rapidly degrades; there is degradation in contrast at all levels. Second, the CTF is inversely related to feature size, e.g., small features will be reduced more in contrast than larger features. Throughout this chapter, we have reiterated the critical interdependence of spatial and contrast resolution in determining our ability to “see” an object. In fact, the Rayleigh criterion sets the resolution limit at that point where the image contrast is reduced to 25% (dotted line on graph in Fig. 7.5).

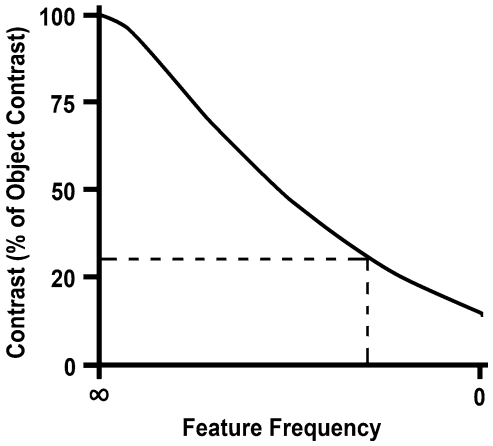

Fig. 7.5 Typical contrast transfer function (CTF) for a lens. The *dotted line* represents the Rayleigh criterion cut off point for contrast resolution

Figure 7.5 only depicts the CTF of a theoretical optical system. However, all aspects of the imaging train can also have an effect on the CTF. Thus, we also must concern ourselves with the ability of our eye or camera to detect contrast differences. In other words, we need to know something about the CTF of each of these components. Since confocal detectors are generally gray scale instruments, the contrast resolution of a detector is related to how many separate gray tones between black and white can be discriminated. For a digital image, this is the bit depth discussed in Chap. 6. A minimum requirement for most microscopy is 8 bits (256 gray levels) but, as discussed later in this chapter, higher bit depth (12 bit) detectors provide some significant advantages, particularly for quantization.

7.3 Image Production and Resolution in a Scanning Confocal Microscope

As explained further in Chaps. 8 and 9, the confocal microscope sequentially scans a focused point of light through the specimen and measures the fluorescence generated at each point. An image of the specimen's fluorescent intensity at each spot is then sequentially determined and stored as pixel information. The brightness of individual pixels in the resulting image is a representation of the fluorescence intensity at the corresponding spot in the specimen. The laser scanning microscope usually does this with a single point of light while the spinning disk uses multiple, but still independent, points at once.

To convert the signal from an excited area in the specimen into a pixel gray value in the image requires the collection and measurement of the photons generated

from the excited area by a detector. The resulting image pixel, representing a defined spot in the specimen, will have three critical values; the *X* and *Y* position of the pixel, the *X* and *Y* dimensions of the pixel (pixel size), and the gray value assigned to the pixel. Since the digital image of the scanned area is formed by summing all of the photons coming from the area illuminated into a single value that becomes the brightness value (gray scale value) for that pixel, it is clear that the resolution of an image cannot be any smaller than the size of the illumination spot projected into the specimen or onto the detector. Since, except for specialized situations, the radius of the illumination spot cannot be any smaller than the radius of the Airy disk, the Airy disk defines the smallest area we can illuminate. For other than very specialized situations, this places a theoretical limit on the lateral (*X*–*Y*) resolution that can be detected. However, we must have a detector that is capable of separating out these closely spaced signals. This means that the detector's spatial resolution must match or exceed the spatial resolution of the microscope image. In addition, the detector must be sensitive enough to discriminate the signal differences (e.g., have sufficient contrast resolution). Detectors for light signals run the gamut from film to diode arrays. However, most commercial confocal microscopes utilize one of two types of detectors. Photomultiplier tubes (PMTs) are generally employed in laser point scanning confocal microscopes while spinning-disk confocal microscopes usually have cooled charge coupled devices (cooled CCDs) as their detector.

Throughout this chapter, the term spinning disk will refer to disks containing an array of pinholes. However, for completeness, it should be pointed out that another variety of spinning-disk microscope (often referred to as a slit-scan confocal) uses a disk with a series of narrow slits rather than pinholes. As the disk spins, the slits scan the illuminate over the surface of the specimen and also restrict the light returning to the detector from out-of-focus planes. These instruments increase the light transmittance onto the specimen but at the cost of a decrease in the axial spatial resolution. Types of confocal instruments are discussed more thoroughly in Chap. 8.

7.3.1 Image Production in Single Point Scanning Confocal Microscope

Sensitivity is a key to determining the appropriate detection device for a microscopy setup. Fluorescence emission occurs over all angles, not just in the direction of the collecting (objective) lens. Thus, only a small percentage of the emitted photons enter the optical path of the microscope. Higher NA lenses will collect from a wider angle and so will gather more of the photons but even high NA lenses collect only about 30% of the emitted light. Loss of photons within the optical train due to absorption, reflection, and deflection lowers the number of photons that reach the detector even further. In a well-maintained system with high quality optics, it is still doubtful that more than about 20–25% of emitted photons will reach the detector.

Thus, highly efficient detectors are necessary to avoid attenuating the signal any further. Besides sensitivity, a detector needs to have low noise to maintain a high signal-to-noise (S/N) ratio (good contrast) even when the signal strength is low. A good detector also should be equally sensitive to all wavelengths and should have a linear response and broad dynamic range to accommodate both faint and bright signals.

Single point scanning confocal microscopes, such as laser scanning confocals, usually use a PMT as the detection device. With a PMT, incoming photons strike a photocathode. This liberates electrons that are then accelerated through a series of curved plates (dynodes) that amplify the electron signal. The strength of the output signal is proportional to the input signal and is translated into a gray scale value for each individual pixel of the digital image.

PMTs have very high sensitivity, good linearity, and very fast response rates. Their S/N ratio is excellent. On the downside, PMTs are relatively expensive and they only have a quantum efficiency of about 40%. However, the key limitation for PMTs in most imaging situations is that they do not collect spatial information. All photons absorbed by the photocathode are recorded regardless of their source of origin. However, in single point scanning microscopes spatial discrimination by the camera is not critical. This is because only a single area is excited at a given time. Thus, the source location is already known. The location of the pixel can be assigned from information about the location of the excitation beam at the time of collection. The size of the pixel is assumed to be equivalent in size to the excitation area in the specimen. The gray scale value of the pixel is assigned based on the signal strength, which is a function of the number of photons absorbed by the photocathode. Thus, the conversion of the analog information into a digital signal is relatively direct and straightforward in the single point scanning instrument.

7.3.2 Image Production in Multipoint Scanning Confocal Microscope

In contrast to single point scanners, detectors for multipoint scanners such as spinning-disk confocals, must be able to collect spatial information. Although these microscopes do excite individual points, multiple points are excited at once and it is critical to discriminate photons coming from one point in the image from those photons generated in a different location. For this reason cooled CCDs are the usual detection system for spinning-disk confocal microscopes.

CCDs consist of a matrix of photodiodes capable of sensing photons. The charge sensing region of the photodiode is coupled to a charge storage region. A schematic of a typical CCD array is depicted in Fig. 7.6. Each gray square represents an individual sensor. The light falling on each sensor creates an electric charge proportional to the light intensity at that location. After image collection, the stored charge from each row of diodes is transferred sequentially into a serial registry where the charge is read and converted into a voltage. The sequential collection is

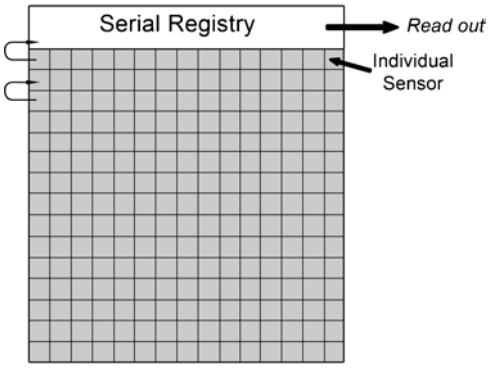

Fig. 7.6 Schematic of a charge coupled device (CCD)

accomplished by transferring the charge from each row of diodes to the neighboring diodes in the next row (arrows in Fig. 7.6) until the stored charge from all of the diodes have been emptied. In this way, row by row, the individual sensor information is collected, converted to a series of voltages, and transferred to image storage for conversion from an analog signal (voltage) to a digital gray scale value for the image pixel. The pixel size is, of course, the dimension of the sensor.

7.3.3 Matching Microscope Image Lateral Resolution to CCD Diode Size

CCDs have a high quantum efficiency and their dynamic range and linearity are excellent. However, their sensitivity is not as good as PMTs and the time to collect an image and transfer it to computer memory is slower than that of PMTs. Despite this, because multiple photodiodes are arrayed together in a single CCD camera, the overall frame capture rate can be faster than PMTs. The most important feature of CCDs that must be considered in microscopy is that, unlike PMTs, CCD photodiodes do have a physical size. This must be taken into account in order to optimize image resolution.

In addition to considering the size of the photodiode of your CCD, matching the microscope image resolution to the CCD also involves a knowledge of the resolving power of your lens. The CCD sensor size should be available from the camera manufacturer. A sensor size of 6.45 μm^2 is a popular size for high resolution microscope cameras. This turns out to be a very convenient size for microscopy.

From equation 7.5 we can determine that the resel obtained from an emitted beam of 550 nm focused with a lens having a NA of 1.3 (a pretty standard NA for the type of high resolution water immersion lens often used in confocal microscopy) will be a little less than 0.2 μm in diameter. We will round this number to 0.2 μm for the purposes of this discussion. If the lens had a magnifying power of 63 times, the smallest resolved objects (0.2 μm) would be projected onto the chip at a size of

12.6 μm (Table 7.1), this is roughly twice the size of the sensor. A 40× dry lens with NA = 0.93 will resolve structures of approximately 0.3 μm which would then be magnified onto the chip at a size of 12.0 μm. Again, roughly twice the size of single sensor.

The projection to twice the size of the sensor is important because of a key concept in sampling statistics called the Nyquist–Shannon theorem (Nyquist theorem, Nyquist criterion). This theorem is a fundamental principle in sampling theory. Obviously, the fidelity of the analog to digital conversion of signals, such as the irregular analog signal depicted in Fig. 7.7a is dependent upon how small we set

Table 7.1 Magnification of Airy disk radius by lenses with different NA and magnifications

Lens	NA	Airy disk diameter (μm)	Magnified diameter (μm)
×40 Dry	0.93	0.3	12.0
×63 Water	1.3	0.2	12.6
×100 Water	1.3	0.2	20

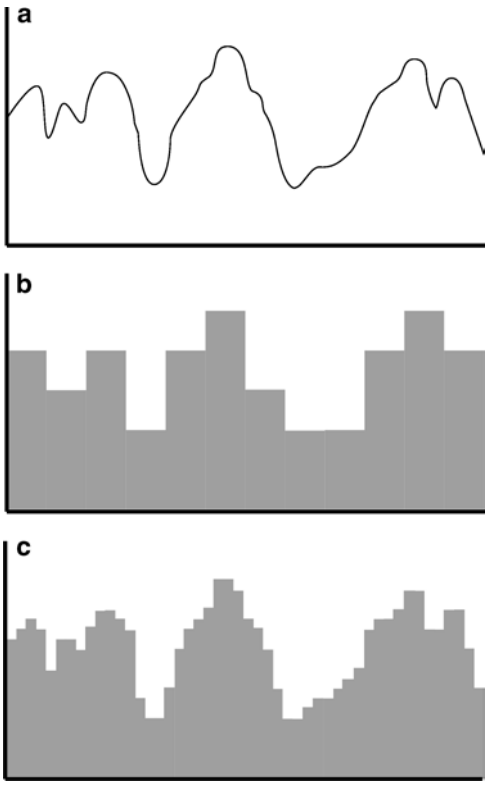

Fig. 7.7 Effect of digital sampling interval on signal reproduction

our sampling interval. In the case of analog to digital conversion, the sampling interval sets the quanta size. Figure 7.7c has a smaller sampling interval (digital quanta) than Fig. 7.7b and, thus, produces a better reproduction of the original analog signal. The Nyquist–Shannon theorem shows that an analog signal can be perfectly reproduced if the smallest element (frequency) of the signal is sampled at least twice. Alternatively, the theorem says that we can only reproduce with certainty portions of the signals that have been sampled twice. In the case of a digital image reconstruction, Nyquist–Shannon tells us that our sampling probe must have a diameter of half the size of the object in both the *X* and *Y* directions. Thus, a sensor of 6.45 μm is very close to the Nyquist criterion of 6.3 μm to sample a resel of 12.6 μm. In practice, the sampling interval is often set to sample the smallest detail 2.3 times to be sure of capturing adequate information.

Table 7.1 also describes the magnified resel for a 100×, NA 1.3 water lens. You can see that a 6.45-μm sensor far exceeds the Nyquist criterion. We can take advantage of this fact and combine, or bin, the information from four adjacent sensors to make a sensor with a size of 12.9 × 12.9 μm. This is again close to the Nyquist criterion (10 μm), although it slightly under samples the resel. Binning has the advantage that the image acquisition time can be enhanced and the S/N ratio decreased since we are collecting four times the signal with relatively little decrease in image resolution (there would be no decrease in image resolution if we exactly matched the Nyquist criterion). Of course, all of these calculations do not take into consideration that in confocal microscopy we are generally imaging a thick specimen. Interactions of both excitation and emitted photons with the specimen can reduce the resolution from that which is theoretically calculated. Moreover, there are other factors at play which can distort the PSF (see Sect. 7.5 for more information on the PSF). Despite these practical issues, it is always better to match as close as possible those parameters you can determine than to ignore physics and hope for the best.

7.3.4 Effect of Missampling

Incorrect sampling frequency can have significant affects on image quality. These are best illustrated by imaging a periodic test specimen, such as a grating with uniform spacing. Comparing the original grating to the image produced as depicted in Fig. 7.8, it is clear that sampling at the Nyquist frequency produces an accurate representation of the original. Oversampling adds no additional spatial information to the final image but does increase the exposure of the sample to a potentially harmful beam. This can exacerbate photobleaching and damage to the sample. In contrast, under sampling significantly alters the representation such that the original pattern is obscured in the image. If this were a real biological sample, then this obscuring would blur the detail of structures smaller than twice the sampling frequency. A potentially more problematic effect of incorrect sampling frequency, however, is spatial aliasing. Spatial aliasing is the occurrence in an image of structural information that was not in the original object. This occurs when periodic

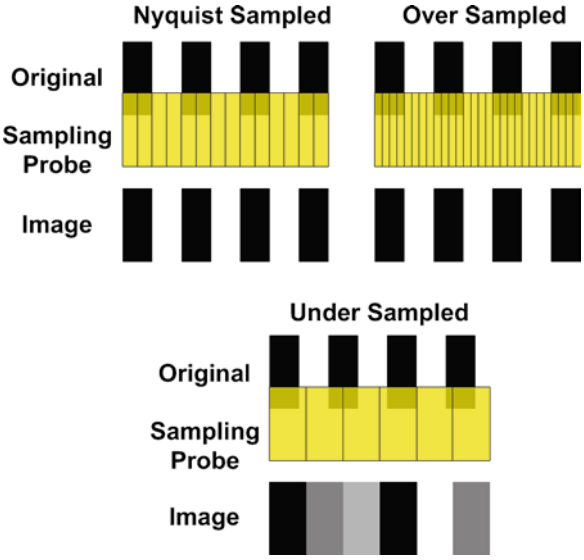

Fig. 7.8 Effect of under and oversampling a specific frequency

structures are under sampled at a frequency that leads to misinterpretation of the structural periodicity. Moiré patterns (Fig. 7.9b) are an example of spatial aliasing. Figure 7.9b shows a Moiré pattern formed when an image of a brick wall is collected at a too low sampling frequency. In contrast, no pattern is seen when the scene is correctly sampled (Fig. 7.9a). It is easy to spot such artifacts when viewing a known structure such as a brick wall. However, when these patterns arise in a biological sample of unknown structure they can be misinterpreted as specimen fine detail. Spuriously jagged outlines are another example of spatial aliasing.

7.4 CDD Dynamic Range and Array Size

It should be clear by now that the diode size and correct sampling are very important in determining the resolution and quality of the final digital image produced by a CCD camera connected to a confocal microscope. However, image contrast is just as important in the ability to recognize and record information from closely spaced objects. Thus, the dynamic range of the camera (number of gray values between black and white that the camera can accurately detect) is also critical. The dynamic range is affected primarily by the inherent noise level and the full well capacity of the sensor.

When photons hit the photodiode sensors of the CCD chip, electrons are generated. The well capacity, or well depth, is the number of electrons that can be generated before the capacity of the sensor is exceeded. Obviously, large capacities are desired. However, the smaller the sensor size the smaller will be the capacity.

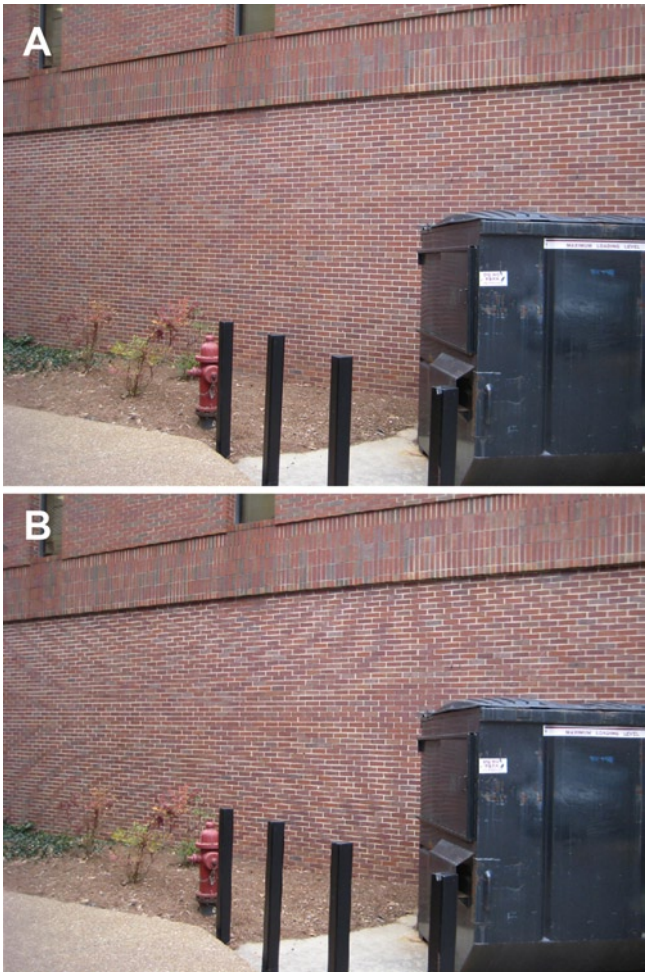

Fig. 7.9 Aliasing artifact caused by under sampling

The other major influence on dynamic range is readout noise. Most scientific grade CCD cameras are now cooled and this, coupled with electronic advances and reproducibility of signal readout, bring the noise in these cameras to very low levels of <10 electrons per sensor at reasonable readout rates.

The dynamic range of a CCD camera can be determined as the full well capacity divided by the noise (S/N ratio). A photodiode with a full well capacity of 41,000 electrons and a noise level per well of ten electrons would be able to detect 4,100 different gray values. In other words, it could produce a 12-bit image ($2^{12}=4{,}096$ gray levels).

$$\text{Dynamic range} = \frac{41{,}000}{10} = 4{,}100 \text{ gray values.}$$

Thus, even if the A to D conversion produced a 16-bit gray value (16 binary digits long) 4 of those digits would be spurious information because the sensor was only capable of an accuracy of 12 bits.

There is, however, a way of actually increasing the dynamic range of a CCD array. This is by binning several sensors together into a single virtual sensor. Since read out noise is not additive, binning of sensors produces huge increases in dynamic range. For instance, binning 4 pixels (two sensors along the *X* direction and two along the *Y* direction) for the sensors in the example above makes the camera capable of detecting 16,400 gray levels.

$$\text{Dynamic range} = \frac{41{,}000 \times 2 \times 2}{10} = 16{,}400 \text{ gray values.}$$

The array size (number of pixels in the *X* and *Y* direction) determines the size of the image that can be collected and thus the area of sample (field size) from which information can be collected for each image. Currently available CCD cameras for scientific use have array sizes in the range of about 1,000×1,000 pixels to upward of 5,000×5,000 pixels and larger. A 1,000×1,000 array of sensors with an individual sensor size of 6.45 μm would produce a camera that can capture an area of 6,450 μm×6,450 μm. With a 63× lens in place this means the confocal image would contain information from 102 μm×102 μm (10,404 μm^2) of sample area. Larger cameras collect more sample information but at the expense of slower readout rates.

7.5 Image Capture in 3-D

The most important aspect of the confocal microscope for most biological studies is the ability to acquire high resolution information about the 3-D architecture of the specimen. As discussed throughout this book, confocal microscopy isolates a defined planer thickness of the sample. In the case of a single slice, the third dimension is the thickness of the optical slice. In cases where a larger volume is built up by adding together multiple slices, the thickness of an individual slice remains a critical component of the 3-D data set. With this in mind, we need to consider the characteristics of all three dimensions of a point source projected into a sample. Just as the lateral dimensions of the image of a point source are blurred to form an Airy pattern, the axial dimension of the image is also blurred. The degree of blurring is referred to as the axial PSF. The PSF describes how the optical system affects the image of a point source along the *X*, *Y*, and *Z* axis. The Airy disk is the lateral component of the PSF. In this section, we consider the remaining axis; the optical axis.

Confocal microscopy of fluorescent objects is an incoherent imaging system. This means that each point of information is collected independently and, if the system is designed and aligned well, there should be no interference between the light waves coming from one point and those from a different point. In other words,

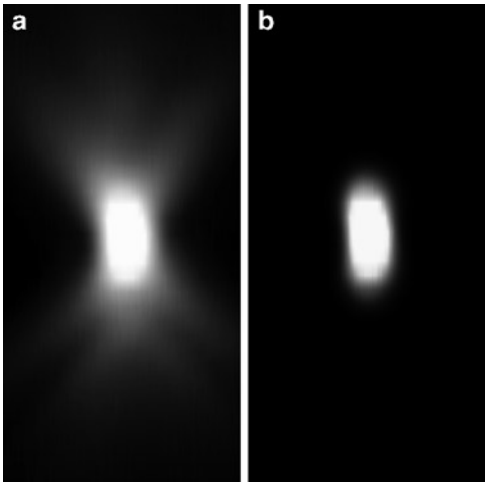

Fig. 7.10 Point spread function of a 0.15-μm bead imaged in the *X*–*Z* (axial) plane from a microscope without a pinhole (**a**) and one with the pinhole set to 1 Airy unit (**b**)

the light waves are independent. In the single point scanning confocal, incoherence is assured because each point is temporally separated. In a multipoint scanning system, each point collected at a single time point is sufficiently spaced as to be optically spatially separate.

The image of a point source along the axial plane will be an hourglass shape with the smallest point being at the focal point of the lens (Fig. 7.10a). By removing out-of-focus light, the confocal microscope converts the hourglass to an oblate spheroid (ellipsoid), as shown in Fig. 7.10b. Note that this means the PSF is not a sphere; the axial dimension is larger than the lateral dimension. Thus, the limit of resolution in the axial (*Z*) direction will not be as good as that in the lateral (*X*–*Y*) plane.

Like the Airy disk, the radius of the PSF along the optical axis is dependent on the illumination wavelength and the NA of the lens. Several equations have been generated to define confocal PSF resolution. Equation (7.6) describes the most often used equation and highlights the relationship between wavelength and NA when the pinhole aperture is set to exactly capture the full diameter of the Airy disk focused onto the aperture.

$$d_{\text{axial}} = \frac{1.4(\lambda \times n)}{\text{NA}^2}, \tag{7.6}$$

where: λ = wavelength

n = refractive index

NA = numerical aperture

Just as the Airy disk determines the lateral resolution, the PSF defines the volume resolution (3-D resel) and, therefore, determines the minimum digital voxel size

Table 7.2 Calculated *X*, *Y*, and *Z* dimensions for PSF at different wavelengths of an optical system with refractive index 1.515 and NA 1.4

Color	Wavelength (nm)	*X* and *Y* (μm)	*Z* (μm)
Blue	442	0.129	0.478
Green	541	0.158	0.585
Red	690	0.202	0.747

that can be accurately represented in a 3-D digital image collected by a confocal microscope. Table 7.2 presents some practical dimensions for the lateral and axial radii of the PSF for a lens with NA 1.4 in a system using immersion oil with refractive index 1.515. It is worth producing similar tables for the lenses and wavelengths you most often use for confocal microscopy and having them close by the microscope for quick reference. Of course, the resel dimensions listed are the minimum dimensions obtainable. Unlike the lateral resolution, reducing the pinhole below 1 Airy unit produces little gain in axial resolution but does significantly decrease the number of photons passing through the aperture. In contrast, if one opens the pinhole of the microscope greater than 1 Airy unit then more photons pass to the detector. This is because the photons passing are from the out-of-focus regions. This will blur the edges of objects and so will degrade both the lateral and axial resolution. However, opening the pinhole is useful when the signal is too low for efficient detection.

Since the PSF determines the volume being illuminated and imaged, an understanding of the PSF is important for determining how to correctly sample an object along the *Z* axis. The *Z* axis sampling rate is set by instructing the microscope how far to move the focal point along the *Z* axis between the collection of each image plane (slice thickness). Taking into consideration the Nyquist criterion, in the optical system defined in Table 7.2 using light of wavelength 510 nm the slice thickness should be set to 0.276 nm in order to correctly collect the details of the smallest resolvable structures in the sample volume. Luckily, the software that is provided with most modern confocal microscopes can automatically determine the volume being excited and detected based on the lens NA and the pinhole setting.

Often constraints such as acquisition time, fluorophore bleaching, and specimen beam sensitivity preclude one from sampling an object at the theoretical resolution limit. For instance, it would take about 72 scans to collect the full volume of a 20-μm thick specimen at a rate of 0.276 μm per slice (the frequency required for Nyquist sampling the smallest resolvable structures). This could well be impractical, particularly if your fluorophore was prone to photobleaching. It is perfectly permissible to use a different sampling frequency but the pinhole diameter should be adjusted accordingly. The ease of changing the pinhole diameter to match the situation is an advantage of laser scanning microscopes not shared by multipoint scanners.

There are multiple reasons why it is important to match the optical slice thickness to that which is actually being collected by the instrument during image formation. The first, and most obvious, is that if you image two very thin planes that are

widely spaced apart, the resultant 3-D image will either be flatter than the specimen (thus distorting 3-D relationships) or the computer will have to fill in the empty space with interpolated information. A second reason to match the optical slice thickness to the collection frequency is that it avoids the possibility of aliasing artifacts. Since detail smaller than the optical slice thickness will not be resolved, very little axial resolution is gained by maintaining a smaller pinhole (although an improvement in lateral resolution is gained by increased contrast). Finally, by opening up the pinhole, you collect a larger signal which can dramatically improve the S/N ratio of the image. All of the compromises made when selecting the pinhole size are addressed further in Chap. 9.

The discussion above outlined the factors determining the theoretic minimum PSF. However, alignment errors, lens aberrations, refractive index mismatches or discrepancies, and contamination can increase the PSF or introduce asymmetries in the PSF. The true PSF will also include the interaction of the light waves with the sample. However, the effect of interaction with the biological sample is very difficult to predict. This is because the specimen content is rarely homogenous and the composition is usually changing with time. The specimen interaction generally causes further blurring of the image and this effect becomes more pronounced as thickness of the specimen increases. Luckily, for quick calculations of optimal sampling frequency we can normally ignore the effect of the sample and use the theoretical calculations based mostly on what we know about the objective lens. Our lack of knowledge about the true PSF does, however, indicate that we must be aware that our image may contain artifactual information.

7.6 A Word About Color Image Capture – Don't!

The cameras for confocal microscopy are almost universally black and white cameras. These convert signal strength to a gray scale value within the dynamic range of the instrument. The image does not contain color information. Color information is provided separately by the use of specific Look Up Tables (LUTs) selected by the user. The color assignment is usually based on knowledge of the filters used to restrict the wavelengths reaching the detector. However, other colors could also be assigned. The green fluorescent protein signal could just as easily be displayed as yellow or red. Specifics of how this is done are provided in Chap. 9.

PMTs are inherently gray scaled and so color must always be assigned. On the other hand, color CCD cameras are available. At present, though, it is generally best to avoid these for high resolution work. The reason for this is that current color cameras acquire color information at the expense of image lateral resolution, image dynamic range (because of degradation of the S/N ratio), or by greatly lengthening exposure time. As discussed earlier, any increase in the exposure of the sample to the beam increases the potential for specimen degradation.

To understand why current color CCD cameras are problematic for high resolution work, we need to discuss the various ways by which CCD cameras can

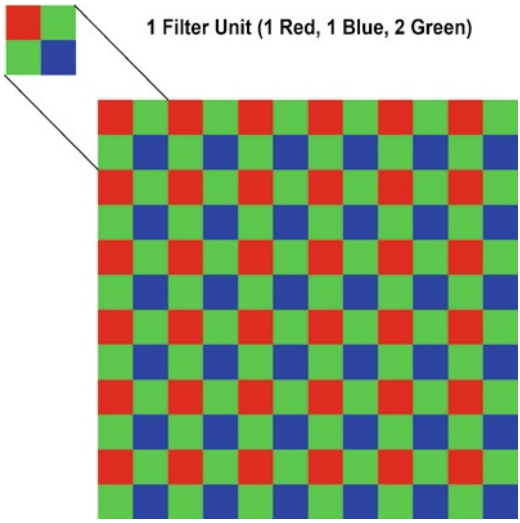

Fig. 7.11 Diagram of typical Bayer filter pattern present on a color CCD

capture color information. The most common type of color CCD array places an array of color filters in front of the photodiodes of the CCD. In this way, only narrow wavelengths of light get through to be detected by the photodiode. The most common type of color filter array is the Bayer Filter. This places a red, green, or blue color filter in a specific pattern (Fig. 7.11) in front of each individual sensor. Each unit cell of the filter encompasses four sensors: two collecting green light and one each for red and blue. The color assigned to each pixel in the image is a mixture of red, green, and blue based on the levels of red, green, and blue detected by the sensors. Depending upon the algorithm used for interpolation and anti-aliasing, this binning of pixels reduces the lateral resolution by a factor of two to four. It should be noted that the hue and brightness value assigned to each pixel is a blend of the information collected for that photodiode blended with the information collected for surrounding pixels.

A new development in color sensing arrays has been designed by Foveon (Foveon Inc, Santa Clara, CA). Their design uses three arrays stacked sequentially on top of each other with filters in between each array. Since red light penetrates deeper into silicon than blue light, the first layer captures the blue information. A filter prevents the blue light from traversing through to lower layers. In the same manner, the second array captures the green information and the bottom layer captures the red information. This scheme allows the full spatial resolution of the chip and avoids problems of postcollection alignment of the red, green, and blue images. However, so far this scheme has only been implemented on complementary metal oxide semiconductor (CMOS) arrays and is not commercially available for confocal microscopes. However, the technology shows promise if it can be adapted to CCD arrays.

For the reasons above, the best approach for color confocal microscopy using cooled CCD arrays remains sequentially placing filters in front of the CCD array. This allows the sequential collection of the red, then green, and then blue information separately. The three images can then be combined. This approach uses the full spatial resolution of the camera. It is not without drawbacks, however. One must remember that full color information requires at least three separate exposures of the specimen and, thus, increases the possibility of photodamage. The exposure time for image collection could be reduced to reduce damage but this increases the noise in the image. Sequential imaging also introduces issues of correct alignment of the three images that can reduce image resolution. Despite these drawbacks, the sequential approach remains the most useful color approach that retains full spatial resolution. Of course, collecting a gray scale image and assigning the color based on knowledge of the emission wavelengths detected remains the strongest approach for the use of CCDs in confocal microscopy.

7.7 Conclusions

It should be clear, now, that there are numerous user selectable options that allow optimization of the final confocal image. This is extremely useful but it does require diligence on the part of the user to assure image quality and fidelity. Optimization of the information in your image requires maximizing the spatial and contrast resolution in your image. Both the optical and digital restrictions on resolution must be considered as part of the optimization process. Failure to recognize the constraints and adapt the imaging procedure to these constraints at the least can result in loss of image information. Even more problematic, however, is that failure to recognize the constraints and adapt accordingly can lead to the inadvertent presentation of artifactual information as structural detail. Experimental and sample limitations may dictate that the theoretical optimal resolution is not feasible and that compromises must be made. It is imperative that any compromises are made rationally and with full knowledge of the consequences. For instance, it makes no sense to collect optical slices (movement of the focal plane between collecting individual image planes) at 1 μm intervals but have the pinhole set to resolve 0.5 μm slices. Rather, the pinhole should be set to a resolution along the Z axis which assures that the sampling frequency along the Z axis meets the Nyquist criterion. Without proper consideration of the various resolution constraints imposed by the sample, microscope, and detector the data contained in your image could be incorrectly interpreted.

References

Hell S (2009) Microscopy and its focal switch. Nature Methods 6: 24–32

Lippincott-Schwartz J, Manley S (2009) Putting super-resolution fluorescence microscopy to work. Nature Methods 6: 21–23

Chapter 8
Types of Confocal Instruments: Basic Principles and Advantages and Disadvantages

John Fuseler, W. Gray (Jay) Jerome, and Robert L. Price

Keywords Aperture • Fluorochrome • Nipkow disk • Numerical aperture • Pinhole • Resolution • Signal-to-noise ratio • Spinning disk confocal

8.1 Introduction

As noted in Sect. 1.2 of Chap. 1, several types of confocal microscopes have been introduced over the years. These can be broken down into three basic categories: Single-photon point-scanning confocal systems, multiphoton (nonlinear) point-scanning confocal systems, and spinning-disk confocal systems. New developments are continually being added to the hardware and software of these microscopes to improve their performance, but the majority of confocal systems will fall into one of these groups.

8.2 Single-Photon Point-Scanning Confocal Microscopes

These instruments, by far, represent the majority of confocal microscopes in today's laboratories and include basic instruments with only one laser, more advanced instruments with two or three (or more) lasers, all the way up to very advanced spectral imaging microscopes such as the Zeiss LSM 510 META and 700 lines of instruments, the LEICA SPE line of instruments, the Nikon Eclipse CSI, and the Olympus FV1000 equipped with a spectral imaging scan head. Point-scanning systems also include the recently introduced systems with resonant

R.L. Price (✉)
Department of Cell and Developmental Biology, School of Medicine, University of South Carolina, 6439 Garner's Ferry Road, Columbia, SC 29208, USA
e-mail: Bob.Price@uscmed.sc.edu

R.L. Price and W.G. (Jay) Jerome (eds.), *Basic Confocal Microscopy*,
DOI 10.1007/978-0-387-78175-4_8, © Springer Science+Business Media, LLC 2011

scanners and swept-field confocal scanning units that are designed to increase the rate of scanning of live cell imaging. These instruments address many of the problems associated with the initial design of confocal microscopes, the spinning-disk confocal systems discussed below.

Figure 8.1 illustrates a simplified diagram of the path that photons take prior to and after interaction with the specimen in a single-photon CSLM. After exiting the laser, photons pass through a neutral density filter or an AOTF that allows control of the laser intensity that contacts the specimen. The laser beam then passes through a dichroic filter present in most confocal systems, or an AOBS in microscopes such as the Leica TSP5 AOBS system. This filtering mechanism separates the higher energy short-wavelength excitation photons from the lower energy long-wavelength photons emitted from the specimen. The laser beam then passes through the scan head and objective lens before interacting with the specimen. As the laser is scanned across the specimen, fluorophores are excited resulting in the emission of photons from the specimen.

Photons emitted from the specimen take the reverse path of the excitation photons and first pass through the objective and then through the dichroic filter or AOBS. In the example shown in Fig. 8.1, blue, green, and red laser lines are used to excite the specimen. Emitted photons are then sorted by placing a dichroic mirror and long-pass filter in front of the first detector so that only red light passes through to the detector. Shorter wavelengths are redirected. In laser scanning confocal systems,

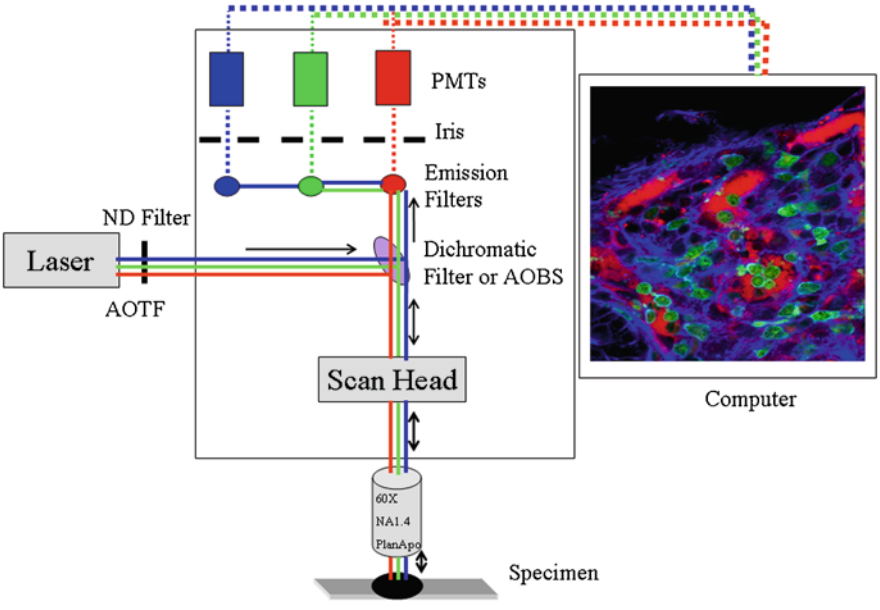

Fig. 8.1 Generalized diagram of the mechanism for sequentially exciting and collecting signal from a sample labeled with three fluorochromes

the detector is usually a photomultiplier tube (PMT). Many laser scanning systems, such as the one depicted in Fig. 8.1, have multiple detectors. PMTs do not recognize color; they collect and record photons of all wavelengths. It is the combination of filters between the specimen and detector that allows us to assign specific colors (wavelengths) to the detected photons. In the case of a three-detector system, when the long (red) wavelengths are passed on to a PMT, the remaining shorter wavelengths (green and blue) are redirected by the dichroic to other detectors. A second dichroic directs the green wavelengths through a band pass filter to a second detector, while shorter (blue) wavelengths are redirected to a third detector and long (any remaining red) wavelengths are blocked and do not progress further. The third PMT receives only the short wavelength (blue) light left in the emitted light. Combinations of filters and detectors can be used in this manner to sort multiple wavelengths of light. An exciting recent evolution in laser scanning confocal microscopy is the development of spectral detectors. These separate the light into its component wavelengths and have the ability to detect very narrow ranges of wavelengths, allowing the microscopist to analyze the spectrum of wavelengths emitted from a specimen more precisely. When planning an experiment, it is very important to know the filters that will be available before selecting a combination of fluorochromes to use for multiple labeling experiments. Improper selection of fluorochromes and filters may result in problems such as bleed-through and poor signal levels, as discussed in Chap. 3.

Prior to reaching the detector, a pinhole (may also be called an aperture or an iris) is placed in the light path at the light beam's focal point. This is a very critical component of a confocal microscope because this is the point where out-of-focus light is separated from light coming from the focal plane. In some systems, a pinhole is placed in front of each PMT, while in others, a single pinhole is used to remove out-of-focus light prior to the sorting and passage of photons to the various PMTs. Proper use of the pinhole is essential in achieving the essential feature of confocal microscopy so that only light from the focal point of the objective is used in image formation. Thus, *the focused point of the specimen and detection of the signal are in conjugate focus (confocal)*, resulting in the improved resolution, contrast, and S/N ratio characteristics of confocal images. Once the emission photons are sorted, the information is converted to a digital image as discussed in Chaps. 6 and 7.

The ability to remove out-of-focus light from the image and the use of high-resolution detection devices, along with microscope stages that can be tightly controlled in movement in the *Z*-direction, provide the capability to collect a series (Z-series) of in-focus images throughout the depth of a specimen. This feature allows high-resolution scanning in the *X*, *Y*, and *Z* axes for the collection and reconstruction of true three-dimensional (3D) data sets, which is a major advantage of CSLM systems when compared to widefield fluorescence systems (Fig. 1.4).

Choices made by the operator at each point along the optical path affect both the amount of specimen damage that may occur and image quality. Factors that increase the intensity of the laser contacting the specimen or the length of time the laser remains in contact with a point in the specimen will increase the number of

photons (signal) available for the formation of the image, but will result in increased specimen damage in the form of quenching of fluorescent reagents and/or cell death if imaging live cells. Other factors such as increasing the diameter of the pinhole will alter image parameters such as S/N ratio and resolution, but will not directly affect specimen damage since interaction of the laser with the specimen has been completed. Understanding the multiple compromises made in collection of the image is essential since nearly every change made in operating parameters will affect specimen damage, image quality, or both. Table 8.1 lists many of the compromises that must be made. Chapter 9 provides details on how the microscope should be set up to maximize specimen preservation and image quality.

Table 8.1 Comparison of several characteristics of single-photon CSLM, multiphoton CSLM, and spinning-disk confocal systems

Characteristics	Single-photon CSLM	Multiphoton CSLM	Spinning disk
Photon source	High-intensity short-wavelength lasers	Adjustable lasers capable of long wavelengths (IR)	Lasers, mercury, xenon, or metal halide lamps
Acquisition speed	At full resolution and frame size, scan speeds can be several seconds per frame. Fast scans of regions of interest at reduced resolution available on some systems	Similar limitations as those of single photon	Rapid – high frame rates of 20+ frames per second
X-Y resolution	Up to 4,096×4,096 on some systems	Up to 4,096×4,096 on some systems	Depends on CCD elements and binning
Z-Resolution	~0.6 μm optimum based on ×63 NA 1.4 oil objective with pinhole at 1 airy unit		Typically fixed (micro-lenses)
Detectors	Photomultiplier tubes (PMTs)	Photomultiplier tubes (PMTs)	Charge coupled device (CCD)
Multichannel imaging	Simultaneous or Sequential	Simultaneous or sequential	Sequential
Photobleaching and phototoxicity	May be problematic	Typically not a problem	Reduced based on fast imaging parameters
Region-specific bleaching	Possible on instruments that allow region of interest control of excitation areas	Possible on instruments that allow region of interest control of excitation areas	Requires additional hardware available for some systems
Depth of imaging	Limited based on optics and wavelength of laser	Greatly improved over single photon based on long-wavelength excitation	Limited

8.2.1 Limitations of Single-Photon Confocal Systems

An obvious limitation in the use of confocal microscopy is the cost of acquisition and maintenance. Depending on the configuration, commercially available basic instruments often approach $300–400K, and most laboratories require service contracts that are in the neighborhood of $20–25K per year depending on laser configurations and software packages. For this reason, most systems are placed in core facilities or within groups of well-funded investigators.

Confocals are also relatively difficult to operate requiring, at a minimum, a part-time operator for routine maintenance and training of new users. The importance of a skilled operator for training cannot be underestimated as the operating parameters of a confocal system can easily be set up incorrectly, resulting in the collection of data that does not accurately represent the sample. This can lead to artifacts with regard to the size of structures, 3D reconstructions, and interpretation of fluorochrome co-localization, as discussed in subsequent chapters. Helping the microscopists identify these critical parameters and understand how to set them properly is a key goal of this book.

Another disadvantage of single-photon CSLM systems is that, as with the case with epifluorescent microscopes, the entire volume of the specimen is exposed to the high-intensity laser. This means that as the focal plane of the specimen is being scanned, the optical planes above and below the focal plane are also exposed to the high-intensity photons of the laser (Fig. 8.2). This may result in specimen damage throughout the specimen such as photobleaching in fixed specimens and cell damage in live samples. In addition, photons emitted from the out-of-focus planes can

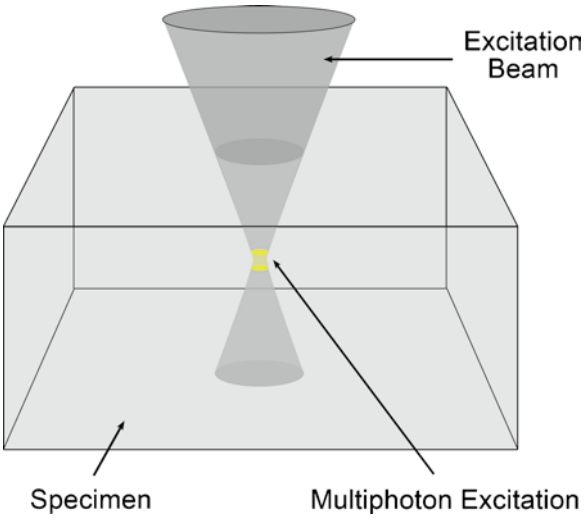

Fig. 8.2 The photon density is only high enough at the focal point of the excitation beam for two-photon absorption to occur. Fluorophores above and below the plane of focus remain unexcited

potentially contribute to the final image resulting in decreased resolution and image quality. As described in Sect. 8.3, multiphoton excitation can help minimize the beam interaction with fluorophores in the out-of-focus planes.

Another distinct disadvantage of the point-scanning systems is that image acquisition is a relatively slow process. In these systems, the lasers are scanned across the specimen by galvanometer mirrors in the scan head. The speed of the mirrors is limited, which in turn limits the rate the laser can be rastered across the surface of the sample. As a result, it often takes 2–3 s to collect a single frame. If the goal of the experiment is to image rapidly occurring events such as a calcium flux, imaging must be completed in milliseconds rather than seconds.

Spinning-disk confocal systems (discussed below) and modifications of point-scanning systems have been introduced to address the problem of slow image acquisition. Slit-scanning systems, rather than point-scanning systems, use slit apertures rather than pinhole apertures so that a wedge of light is used to excite the sample. These systems are capable of rapid imaging, but resolution is reduced due to degradation of the point-spread function (PSF) of the emitted light. The Nikon swept-field system is a combination of point and slit scanning so that the option of high-resolution or high-speed imaging can be selected based on the goal of the experiment.

High-speed resonant scanners are also being developed to address the problem of speed. Resonant scanners have been introduced on several instruments including the Nikon A1R and Leica TCS SP5 instruments. Resonant scanning systems use a galvanometer which vibrates at a fixed frequency, resulting in line scans which take approximately 125 μs. At this speed, resonant scanners are capable of collecting up to 30 frames per second (fps), which is fast enough to record most events in live cell imaging. The speed of acquisition also reduces many of the phototoxicity problems associated with using high-intensity lasers, since exposure is for a very short period of time.

Associated with the problem of speed in image acquisition in single-photon point-scanning systems is the problem of phototoxicity if imaging live cells. As noted above, the high-intensity lasers of single-photon systems may result in considerable photodamage, resulting in photobleaching of fluorescent dyes and the death of cells if imaging live samples. Both multiphoton and spinning-disk systems discussed below minimize these types of damage.

Resolution has been discussed extensively in Sect. 7.2 and the equation for calculation of resolution is given in (7.1). The resolution obtained with a confocal microscope is typically compared to that of an epifluorescent system and is, therefore, generally not considered to be a potential problem. However, even with confocal systems, the imaging source is light that has a long wavelength (λ) compared to that of electrons.

This limits the optimum resolution that can be obtained with confocal microscopy based on the physics of light wavelengths. In comparison, the resolution available with an electron microscope is orders of magnitude higher. As shown in Table 8.2 the wavelengths of visible light are significantly longer than those of electrons with the shortest wavelength of light typically used in confocal imaging being ~400nm. When operated at an accelerating voltage of 60 kV, which is relatively low for transmission

Table 8.2 Comparison of the wavelengths of visible light available for confocal imaging and electrons when an electron microscope is operated at 60 kV

Color/source	Wavelength in nm
Electrons	0.005
Violet	380–450
Blue	450–490
Green	490–560
Yellow	560–590
Orange	590–630
Red	630–760

electron microscopy, the wavelength of electrons is 0.005 nm. When these wavelength values are inserted into the equation for resolution (7.1) where 0.162 is a constant, λ is the wavelength of the illuminating source, RI is the refractive index value of 1.5 characteristic of many biological samples imaged by confocal microscopy, and NA is the numerical aperture of the lens (0.9 in this case), the optimal resolution of the confocal is 172 nm or approximately the 0.2-μm value associated with light microscopy. In contrast, theoretical resolution of a transmission electron microscope (TEM) operated at 60kV is 0.005 nm; although in practice due to astigmatism and spherical and chromatic aberrations, the actual resolution is closer to 0.1 nm. Figure 8.3 illustrates the difference in available resolution when imaging cardiac myocytes labeled with fluorochromes by CSLM and with colloidal gold particles by TEM. While specimen preparation for immunocytochemistry at the TEM level of resolution is much more difficult than that for confocal microscopy, TEM does provide an essential correlative technology to confocal imaging for high-resolution labeling. Additional details and examples of probes that can be used for both CSLM and electron microscopy for correlative studies are presented in Chap. 5.

8.3 Multiphoton Point-Scanning Confocal Systems

As described in Chap. 2, in addition to excitation by a single photon, fluorochromes can be excited if more than one photon is absorbed simultaneously. Although the potential for multiple absorptions of photons with different energies exists, in practice it is usually absorption of two photons of similar energies that is most often exploited. Thus, for the remainder of this section, we will focus on two-photon excitation microscopy. The quantum possibility of two-photon absorption was first proposed by Maria Göppert-Mayer in 1931. However, technical limitations delayed a practical test of the theory. As will become clear later in this section, the invention of lasers provided the needed excitation source for two-photon excitation, and the development of laser microcopy systems led to the development of two-photon microscopy based on the pioneering work of Winfried Denk and others in Watt Webb's laboratory at Cornell University (Denk et al. 1990).

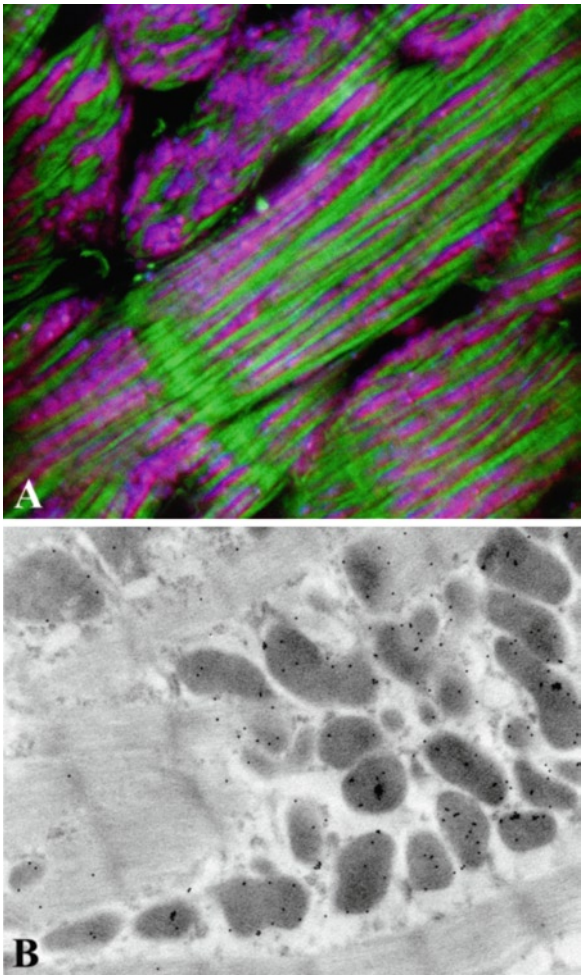

Fig. 8.3 Comparison of resolution levels of confocal microscopy (**a**) and transmission electron microscopy (**b**). In (**a**), cardiac myocytes are labeled with phalloidin for f-actin (*green*), mitotracker red, and cytochrome C (*blue*). Cytochrome C is primarily localized to the mitochondria, creating the purple color. In (**b**), even with minimal fixation for subsequent immunocytochemistry, actin fibers and 10-nm colloidal gold particles labeling cytochrome C in the mitochondria can be resolved

The general theory of two-photon excitation is relatively simple. The excitation of a fluorochrome requires the absorption of energy from an impinging photon. Once energy is absorbed, the fluorochrome is refractory to additional energy absorption for a finite amount of time. However, if two photons arrive within the absorption cross section of the fluorochrome simultaneously, the energies of both can be absorbed as long as their combined energies match the energy needed to excite the fluorochrome. In this respect, simultaneously means within about 10^{-18} s.

Thus, the absorption of two photons of lower energy is roughly equivalent to the absorption of a single photon of higher energy. Since the energy of a photon is inversely proportional to its wavelength, the two lower energy photons should be about twice the wavelength of the corresponding single higher energy photon. For example, a fluorophore that normally absorbs at 400 nm can also be excited by two photons of wavelength about 800 nm. Of course, neither of the 800-nm photons alone will have sufficient energy to excite the fluorochrome, so unless both photons arrive essentially simultaneously, the fluorochrome will not be excited.

Because the two-photon excitation requires simultaneous absorption, the generation of fluorescence emission depends on the square of the excitation intensity. In practice, the probability of two photons falling within the excitation cross section of a fluorophore is very small, except at the focal point of the excitation beam. At this point, the photons are sufficiently crowded together so that a significant number of two-photon excitations occur. This results in localized excitation within a narrow region around the focal point of the excitation beam, as depicted in Fig. 2.4. The fact that a highly focused beam of light greatly increases the probability of two-photon excitation means that the scanning confocal microscope would be an ideal tool for two-photon imaging.

The probability that two photons will hit a fluorochrome simultaneously and be absorbed is dependent upon the localized photon density. The density required for two-photon absorption is estimated to be about a million times greater than the density required for single-photon absorption. Thus, two-photon excitation requires very high photon densities. Unlike arc lamps, high-power lasers can provide sufficient photons for two-photon excitation. However, as discussed throughout this book, overly high excitation fluxes can damage both specimen and fluorophore. To overcome this, the laser excitation for two-photon excitation is pulsed. In this way, very high photon densities are delivered during the pulse, but the average laser energy over time is low (Denk et al. 1995). Pulse durations are ultrashort ranging from around 100 fs to 1 ps, with duty cycles (pulse duration divided by time between pulses) of about 10^{-5}. This is accomplished using mode-locked lasers. Although short, the pulses are still longer than the time scale of absorption events ($\sim 10^{-18}$ s) and so two-photon excitation is facilitated.

Several distinct advantages accrue from two-photon excitation. Since a signal is generated only at the focal point, there is no fluorescence from the out-of-focus planes. This means that the pinhole can be dispensed with in cases where there is a need to maximize signal. However, better resolution is still obtained by using a confocal pinhole (Gauderon et al. 1999) and so, in practice, it is useful to use an optimized pinhole unless emission intensity is limiting.

An additional advantage of two-photon excitation related to the localized excitation is that by limiting excitation to the focal plane, two-photon excitation can decrease excitation-induced specimen damage. With single-photon excitation, the entire beam path within the specimen is subject to potential specimen damage and photobleaching (discussed in detail in Chap. 9). In contrast, with two-photon excitation, only the small focal volume is excited. Damage and photobleaching are limited to this small excitation region (Fig. 8.2). This is of limited utility if only a

single plane is being imaged, but it is a tremendous advantage when collecting a stack of focal planes for 3D reconstructions. With single-photon excitation, fluorochromes above and below the focal plane are also excited. Thus, with multiple passes, each fluorochrome is excited multiple times and the probability of specimen damage or photobleaching is increased. However, with multiphoton excitation, each fluorochrome is excited only once. Moreover, since there is no out-of-focus absorption, more of the excitation beam reaches the plane of focus and is available to excite fluorophores. This can lead to a two- to threefold increase in the depth of tissue that can be successfully imaged (Centonze and White 1998). Finally, the two-photon excitation wavelengths used are, by necessity, longer wavelengths, usually in the red to far-red range. These wavelengths of light have the ability to penetrate deeper into wet tissue and produce less tissue damage than shorter wavelengths. Added together, these benefits mean that two-photon excitation provides a very distinct advantage for imaging thick living tissue (Piston 1999).

Of course, all of the advantages of multiphoton excitation are negated if the specimen is prepared incorrectly or the microscope is not set up to exploit the multiphoton capabilities maximally. Chapters 4, 5, and 9 discuss proper specimen preparation and optimization of microscope parameters. Here, we will only point out two important considerations that are sometimes overlooked during two-photon imaging of live material. The first is matching refractive indices. Using the PSF of a fluorescent bead to measure effective beam penetration, Gerritsen and deGrauw (1999) showed that two-photon excitation allowed imaging at much greater depths compared to single-photon laser scanning confocal systems, but this advantage was greatly reduced when oil immersion optics were employed. The degradation of the image was due to chromatic aberration introduced because of refractive index mismatches between oil and the essentially water environment of the specimen. In contrast, the advantages of two-photon excitation were exploited maximally when water-immersion optics were used.

The second mistake that one should be diligent to avoid is using the wrong optics. Since two-photon excitation involves long-wavelength photons, the objective lens (when using an epifluorescence set-up) must be suited to using far-red and infrared light. Ideally, the lens should have high transmittance in these wavelengths, provide minimal pulse broadening, be corrected for infrared wavelengths, and have a suitably long working distance for imaging thick samples. Luckily, many of the confocal microscope manufacturers are now making very good lenses that are suitable for two-photon microscopy; therefore, finding suitable lenses is not as difficult as it was in the past.

8.4 Spinning-Disk Systems

Unlike laser scanning systems, where the image is formed by moving a diffraction-limited spot of laser light across the object plane of the specimen in a raster pattern, in spinning-disk systems, the image is generated by the simultaneous illumination

of multiple spots in the object plane. Each spot is generated by a series of micro-lens or pinhole apertures in a rapidly spinning disk (Fig. 1.2).

8.4.1 The Nipkow Disk

In 1884, two seminal events in the progress of the development of light microscopy occurred. At about the same time as Abbe (1884) published his milestone work which provided the basic foundation for modern light microscopy, a young student in Germany, Paul Nipkow (1884), discovered how to encode a two-dimensional optical image into an electrical signal that could be transmitted as a one-dimensional or serial, time-dependent signal, similar to that of Morse code. This signal could then be transmitted over a single cable. Prior attempts at accomplishing this feat had resulted in the development of a highly complicated apparatus requiring multiple detectors and cables which gave very limited results. Nipkow's genius in solving this problem was to dissect the image by scanning it in a raster pattern using a spinning disk. The disk was opaque to light except where perforated with a series of rectangular holes spaced under specific geometrical conditions. The holes in the disk were placed at a constant angle relative to the center of the disk and at a constant, progressively decreasing radius to generate the raster pattern. Such a geometrical arrangement of apertures in the disk constitutes an Archimedes spiral (Fig. 8.4a). When such a disk is rotated at a constant velocity, the brightness of each image element passing through the apertures in the disk produces an image in a raster pattern. The brightness or intensity of each image element is essentially constant along the radii from the center to the margin of the disk. In addition, the arrangement of the pinholes describes the image as parallel concentric raster arcs. The arc of the pinholes also progressively traces out the image as adjacent parallel straight lines along the radii at any given *x*-*y* position over the specimen. The image output resulting from the raster pattern is captured by an appropriate device such as a CCD camera.

The arrangement of the pinholes defined by the Archimedes spiral results in a pattern which expresses equal peripheral pitch along the spiral pattern of the pinholes. In addition, the pattern produces equal radial pitch which results in equal illumination and scanning independent of the radius and rotation speed of the disk. Thus, there is minimal to no distortion of the image when it is obtained by the Archimedes spiral arrangement of pinholes in the Nipkow disk.

Alternate patterns of pinholes in the spinning disk are unsatisfactory for confocal image acquisition. When the pinholes are arranged in an equal fixed angular spiral or circular pattern, the light intensity at the outer margin of the disk is less than that in the inner regions of the disk. This unequal distribution of light intensity across the disk is the result of the pitch between the pinholes becoming wider toward the outer margin of the disk. Increased pitch results in an increasing distance between the pinholes at the periphery of the disk. Thus, in a given unit of time, fewer pinholes collect light information at the outer margin of the disk, resulting in

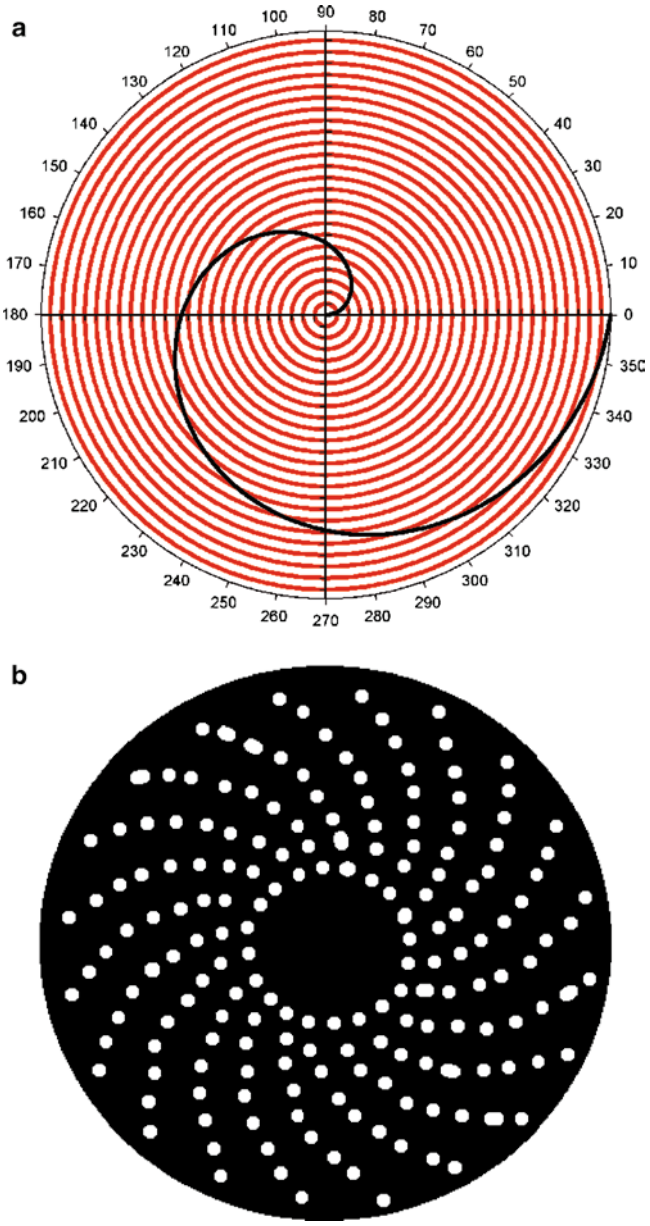

Fig. 8.4 The Archimedes spiral. (**a**) The Archimedes spiral plotted in polar coordinates (*black line*). When pinholes are placed on the Archimedes spiral at the intersections of the *black* and *red lines* and the Archimedes spiral is rotated, the pinholes sweep out concentric parallel raster lines (*red lines*). When multiple Archimedes spirals are present, the entire image field is continuously scanned without the presence of intervening scan lines. (**b**) A modern Nipkow disk, which is a blackened glass disk with pinholes arranged in Archimedes spirals

progressive degradation of the image in this region. If the pinholes are arranged in an equally spaced tetragonal pattern, there is no loss of light intensity across the disk. Since the pinholes are equally spaced, there is no imbalance of light intensity between the inner and outer periphery of the disk. However, when the disk is rotated, the scanning pitch of the pinholes is not equal, which results in the generation of light and dark stripes across the image (Tanaami et al. 2002).

The modern Nipkow disk (Fig. 8.4b) consists essentially of two major components. The core of the disk is an optically flat glass disk that is rigid enough to withstand rotation speeds of up to 2,000 rpm. On this glass disk, the Nipkow arrangement of pinholes is produced by photolithographic methods. This surface consists of a reflecting black chrome layer (<1.0 μm thick) with a reflectivity of only a few percent laid down on a glass disk. The most important criteria in the design of the Nipkow disk for confocal microscopy are the size and spacing of the pinholes.

8.4.2 Nipkow Disk Pinhole Size

In spinning-disk systems, collimated light impinges on the disk and the effective aperture of the light rays entering the microscope objective lens is determined by diffraction at the disk pinhole. The magnitude of diffraction by the pinhole is a function of the light wavelength and pinhole size (*R*-radius). Calculations have demonstrated that resolution in the *Z*-direction (d_z) is directly proportional to the square of the radius (*R*) of the pinhole (Kino 1995). If the pinholes in the disk are too small, loss of illumination intensity due to light rays being diffracted outside of the objective lens aperture occurs, and image information from emitted photons is lost as these photons are not able to enter the pinhole (Fig. 8.5a).

When the pinholes are too large (Fig. 8.5b), resolution of the image in the *X*-*Y* and *Z*-directions is significantly reduced. In this case, the collimated light rays that enter the pinhole aperture are diffracted into a relatively narrow beam which does not completely fill the aperture of the objective lens. This causes the objective lens to function at a lower NA than that designed for and results in loss of image resolution. In addition, light emitted from the specimen may not enter the appropriate pinhole. This results in further loss of resolution in the *X*-*Y* and *Z*-directions (Fig. 8.5b). In a pinhole of correct size (radius), the diffracted light from the pinhole fills the objective aperture and the refracted light from the specimen is maximally collected by the pinhole (Fig. 8.5c).

An equation which estimates the optimal pinhole radius was derived from the Fraunhofer diffraction theory for a circular aperture in the focal plane of the objective (see Goodman 1968; Kino and Xiao 1990 for details on the equations and assumptions used). The optimal pinhole radius is determined by the following equation:

$$R_{\mathrm{O}} = 0.25\lambda M/\mathrm{NA},$$

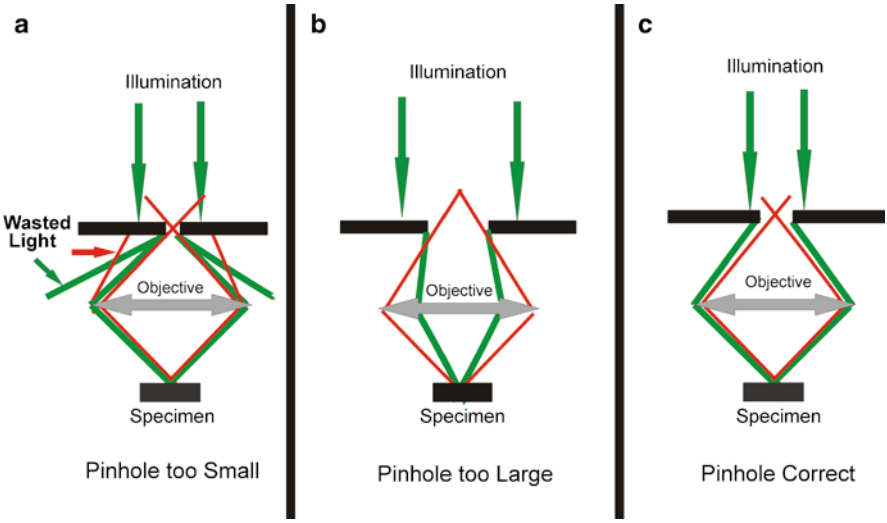

Fig. 8.5 Effect of Nipkow disk pinhole size (diameter) in Nipkow disk on image quality. In (**a**), the pinhole in the Nipkow disk is too small. Image quality is degraded by loss of higher order diffracted light rays not collected by the pinhole. In (**b**), the pinhole in the Nipkow disk is too large. Image quality (resolution) is lost because the light rays are insufficiently diffracted and do not completely fill the aperture of the objective. In (**c**), the pinhole in the Nipkow is of the proper radius. Under these conditions, diffracted light from the pinhole fills the aperture of the objective, and the refracted light or light emitted by the specimen is maximally collected by the pinhole

where λ is the wavelength of the light used, M is the magnification, and NA is the numerical aperture of the objective. This equation is applicable to microscopes with fixed tube length and infinity-corrected optics. The R_o value for a 100×, 1.4 NA oil immersion objective with light at a λ of 546 nm is 9.75 μm, and for a 10× (0.5 NA) objective under the same conditions, the R_o is 2.73 μm. This indicates that the ideal situation would require an individual disk with the appropriate sized pinholes to match each objective on the microscope. Since pinholes of these ideal sizes would result in a significant loss of illumination (1% transmitted light or less) and require multiple disks in a system, alternate approaches have been employed.

In general, a single disk is used with the optimal R_o value chosen to match the objective lens with the highest magnification and NA. The pinhole size used in early experimental designs of spinning-disk microscopes was usually 10 μm. Under this design criterion, the pinhole diameter is larger than optimal for the objectives, with lower magnification and NAs resulting in proportional loss of resolution at these magnifications. However, this loss of resolution for the lower magnification objectives may be acceptable if specimen resolution is less critical in this range of magnification. If R_o becomes very large, out-of-focus information in the Z-plane contributes to the image, and the system is no longer confocal and becomes a standard fluorescence microscope. Most modern commercially available Nipkow

confocal systems (Yokogawa systems) use a pinhole with a R_o of 20–25 μm to ensure the collection of sufficient light intensity for observation and image collection. This sacrifices some high-end resolution with high NA objectives and there is a similar loss of resolution at low magnification. Loss of signal and resolution is often a disadvantage of spinning-disk confocals, but these compromises are balanced by the speed of imaging for live cell applications.

8.4.3 Nipkow Disk Pinhole Spacing

The Archimedes spiral of a spinning disk is governed by the simple polar equation:

$$r = a + b\theta.$$

The parameter a refers to the turn of the spiral and b is the distance between successive turnings. In the Archimedes spiral, the successive turns have a constant separation distance which is equal to $2\pi b$ when θ is measured in radians. Applying this to the Nipkow disk for confocal microscopy, identical pinholes are laid out circumferentially on the rotational arm of an Archimedes spiral at a constant angle (θ) and at constantly increasing distances (r) from the center of the disk. Multiple Archimedes spiral arms are present on the Nipkow disk, resulting in 20,000–200,000 pinholes depending on the size and manufacturer of the disk.

As the spacing between adjacent pinholes in the disk is decreased, the pinholes become too close together and the aggregate area of the pinholes approaches the total area illuminated. Under these conditions, the signal intensity emitted from the specimen no longer decreases sharply with the defocus distance characteristic of the objective lens. Instead, a portion of the out-of-focus light emitted by the specimen can return to the detector through alternate adjacent pinholes, leading to loss of intensity and image resolution. An additional problem also arises when spacing between the pinholes is too small. Here, the closeness of the pinholes, equal to or less than 5 pinhole radii apart, can result in interference between images, thereby resulting in a speckle effect. This is especially true when a monochromatic laser or narrow band pass filter is used as the excitation source. This phenomenon can be minimized by placing a diffuser or a phase randomizer in front of the illumination source.

Spacing of the pinholes too far apart results in uniform loss of excitation light intensity to the specimen and emitted light from the specimen. Both result in deterioration of overall image quality.

The ideal spacing of the pinhole along the arch of the Archimedes spiral is a function of the magnification, NA, and the Z defocus distance characteristic of the objective lens. Here, as with the size of the pinhole, compromises have been made in pinhole spacing to reduce the complexity of the mechanism and to moderate the cost of the instrument. A current typical Nipkow disk has a pinhole spacing of

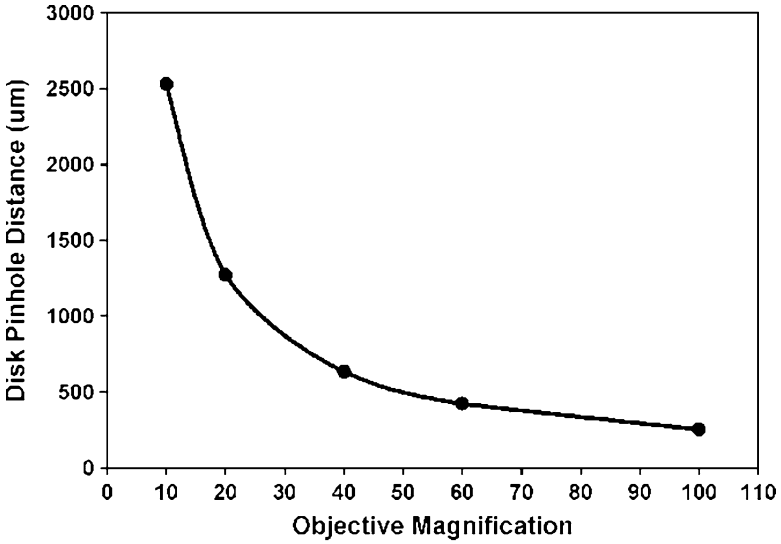

Fig. 8.6 Relationship between ideal pinhole spacing and magnification power of the microscope objectives

253 μm based on high-magnification (100×), high-resolution (NA = 1.4) immersion objectives. With objectives of lower magnification and NA, the ideal pinhole spacing increases in distance (Fig. 8.6). This adjustment of the pinhole spacing does not produce a significant loss of image resolution, provided the emitted light rays from the specimen are focused on the pinhole. However, there is loss of both excitation and emission light intensity with low magnification and NA objectives and short pinhole spacing.

8.4.4 The Petrán Microscope

The initial application of the Nipkow disk to optical microscopy led to the development of the tandem-scanning reflected-light microscope (TSRLM) by Petrán et al. (1968, 1985). Here, the disk is perforated with many holes along the path generated by a multiple set of interweaving Archimedes spirals. The pinholes are separated by a distance large enough so that there is no interaction between the images formed by the individual pinholes. The complete image is formed by moving the pinholes (spinning the disk) so as to fill the space between them. Although TSRLM had the advantages of real-time imaging and good cross-sectioning ability, it possessed numerous disadvantages which limited its usefulness. The most serious problems were a poor light budget with only about 1% of the light being useful, complicated mechanical components which were required to reduce internal

reflection from the disk, and considerable difficulty in maintaining the alignment of the large number of optical components required for operation of the system.

8.4.5 The Xiao and Kino Microscope

The next advancement in spinning disk-based confocal microscopy was the development of the real-time scanning optical microscope (RSOM) which can detect light from the same pinhole from which a given area of the specimen is illuminated (Xiao and Kino 1987; Xiao et al. 1988). This is accomplished by constructing a disk of highly reflective black chrome. The surface of the disk produces a reflected beam which is easily eliminated by an optical stop. The disk is tilted and the optical stop placed in a position where the light reflected from the disk is focused (Xiao et al. 1990). Tilting of the disk can distort the image due to defocusing of the pinholes near the edge of the field of view. Typically, for a few degrees of tilt, the distortion is minimal. However, when imaging requires high resolution or extremely accurate metrology, tilting of the disk is inappropriate and other systems must be used.

Additionally, to further reduce interference by reflected light, the light from the source is polarized and the light reaching the eyepiece is observed through an analyzer with its plane of polarization rotated 90° to the polarized source. A one-fourth wave plate is placed in front of the objective lens such that light reflected from the plane of polarization is rotated 90° so it can be observed through the eyepiece (Fig. 8.7). This set-up and orientation of optical components enhance the S/N ratio of the image. However, because fluorescent light emitted from a fluorescently labeled specimen is randomly polarized, a small fraction of the desired signal is also eliminated from the image. This loss of fluorescent signal can be minimized by setting the polarizer and analyzer in a parallel orientation. Additionally, for fluorescence, the reflected light from the disk can be removed by a dichroic beam splitter and a barrier filter.

In real time, illumination of the specimen is accomplished by using a relatively broadband light. This results in low temporal coherence and minimal speckle effects that arise from interference between neighboring layers within the specimen, or between reflections from the specimen and reflecting components within the microscope. Because of the low transmittance of light through the disk, light sources of high intensity such as mercury or Xenon arc sources, or more recently metal halide lamps, are used. Metal halide lamps are particularly useful in this application since they emit at an essentially constant illumination power across the objective field.

Application of Kohler illumination to the spinning-disk configuration also improves the image quality. Each point on the source is focused to a point in the back focal plane of the objective lens when the disk is not present. When the disk is introduced into the optical path, Kohler illumination ensures that the central axis of the diffracted beams passing through the individual pinholes all pass through the center of the back focal plane of the objective. This configuration gives uniformity to the illumination and optimizes resolution over the field of view.

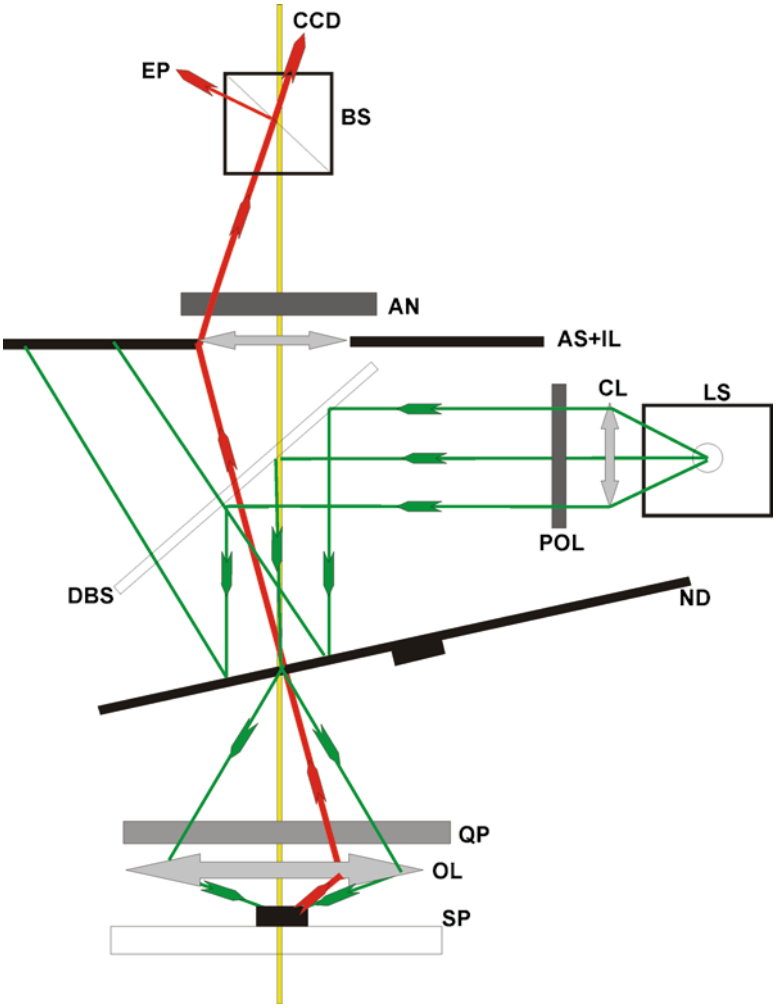

Fig. 8.7 The tilted Nipkow disk confocal microscope. The design of Xiao and Kino. In this design, the Nipkow disk is tilted to eliminate reflected incident light from the disk from interfering with light emitted by the specimen. Diagram traces the ray path for incident and emitted light interacting with one pinhole. *Green lines* – incident light from light source (LS); *red line* – emitted light by the specimen (SP); *yellow line* – optic axis of the microscope. Components: *LS* light source; *CL* collecting lens; *POL* polarizer; *DSB* dichroic beam splitter; *ND* Nipkow disk with pinholes; *QP* quarter-wave plate; *OL* objective lens; *SP* specimen; *AS + IL* aperture stop and intermediary lens; *BS* bean splitter; *EP* eyepiece; *CCD* CCD camera

8.4.6 The Corle Microscope

The design of the spinning-disk confocal microscope by Corle et al. (1991) further improved image quality by eliminating the tilt of the Nipkow disk and improving

the overall optical path of the excitation and emission photons. The initial improvement was achieved by selectively isolating the most stable portion of the mercury or xenon arc light source. These light sources exhibit an inherent instability across the arc, especially at the margins. The most stable portion of the arc is the central region directly between the electrodes. In this microscope design, the spot of maximal intensity of the arc near the cathode is isolated by imaging it on to a pinhole aperture using the condenser lens. This concentrates the maximal intensity of the light source into a bright point source of illumination. This makes the illumination as uniform as possible across the field of view. The illumination in the plane of the Nipkow disk is collimated by the addition of a collecting lens behind the pinhole aperture. Before reaching the Nipkow disk, the collimated rays of light are further refined by the addition of a field stop to remove aberrations from the outer edge of the illumination and to define the size of the field to be illuminated.

A polarizer is then placed in the collimated beam to eliminate spurious reflected light in the system. The polarizer and analyzer in the Corle system are analogous to those used in the RSOM described above. Light exiting from the polarizer is focused onto a 90° beam splitter and the Nipkow disk as a collimated beam of light by a secondary objective lens. The diffracted light from the pinholes of the Nipkow disk is passed through a field lens situated just below the disk. This lens serves to minimize vignetting which produces darkening of the edges of the image field as a result of light falling outside of the aperture of the lower objective lens. This field lens focuses the central rays of the diffracted beam to the center of a tube lens, which collimates the beam to the aperture of the lower objective. This in turn focuses the light onto the specimen (Fig. 8.8). The light emitted by the specimen passes back through this lens system and the pinhole of the Nipkow disk, where it is focused by the secondary objective as a collimated beam. This collimated light then passes directly through the dichroic beam splitter, a field stop, and the analyzer, and is focused by a tube lens to the eyepiece for direct viewing or to an appropriate camera for image collection.

8.4.7 The Yokogawa Spinning-Disk Confocal Microscope

Although spinning-disk confocals can obtain images at a very rapid rate, the need for a nonoverlapping spacing (described above) means that a large area of the disk lacks openings. Thus, only a small portion of the available light is used to illuminate the specimen. A significant improvement was made on the spinning-disk confocal microscope by the addition of a second spinning disk containing an array of micro-lenses (Ichihara et al. 1996; Nakano 2002; Genka 1999) which collect and focus more of the available light into the pinholes. This design forms the basis of the compact confocal scan head developed by Yokogawa (Yokogawa Electric Corp). Yokogawa confocal heads are currently used by several confocal manufacturers, including Perkin-Elmer and VisiTech.

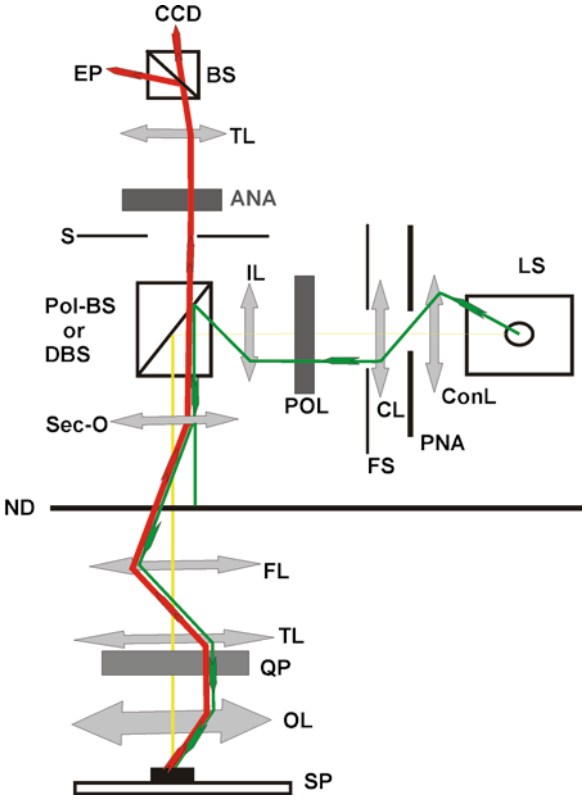

Fig. 8.8 Nipkow spinning disk microscope: Corle design. The diagram traces the ray path for incident and emitted light interacting with one pinhole. *Green lines* –incident light from light source (LS); *red line* – emitted light by the specimen (SP); *yellow line* – optic axis of the microscope. Components: *LS* light source; *Cond L* condenser lens; *PHA* pinhole aperture; *Col L* collimating lens; *FS* field stop; *POL* polarizer; *IL* intermediary lens; *Pol-DSB* polarized or dichroic beam splitter; *SO* secondary objective; *ND* Nipkow disk with pinholes; *FL* field lens; *TL* tube lens 1; *QP* quarter-wave plate; *OL* objective lens; *SP* specimen; *AS* aperture stop; *Ana* analyzer; *TL-2* tube lens 2; *BS* bean splitter; *EP* eyepiece; *CCD* CCD camera

In this system, the scanning portion contains a dual spinning-disk arrangement in which the first disk has an array of 20,000 micro-lenses arranged in an Archimedes spiral. The micro-lenses of this disk receive the illumination light and are accurately aligned with a corresponding array of pinholes on the second, Nipkow, disk. The micro-lens array disk and the Nipkow disk are physically fixed at a distance equal to the focal length of the micro-lenses and are rotated together so as to scan the field of view at high speed. The typical speed of scanning of this dual disk system is 1,800 rpm (30 rps), which results in 1,200 pinholes scanning the sample at any given time. These spinning rates are 12 times the video rate of 30 fps, which results in a 12-frame average for each video image.

The constant pitch Archimedes spiral arrangement of the micro-lenses in the first disk and pinholes in the Nipkow disk creates even illumination across the

image field without creating scanning artifacts. Light from the laser or arc lamp illumination source is collimated and projected on to the micro-lens array disk. Light focused by the micro-lenses passes through a dichroic beam splitter mounted in the space between the micro-lens and the Nipkow disks and enters the corresponding pinhole in the Nipkow disk. Focusing the illumination light by the micro-lens disk prior to passing it through the Nipkow disk improves available illumination at the specimen by about 40%. The incident light is diffracted by the pinhole to fill the aperture of the objective lens where it is focused onto the focal plane of the specimen. Light emitted from the specimen is collected by the objective lens and then focused back on to the pinholes in the Nipkow disk. Transmission of the emitted light from the specimen through the same pinholes in the Nipkow disk eliminates out-of-focus signal and results in a confocal image.

Emitted light from the pinholes in the Nipkow disk is then deflected by a dichroic beam splitter positioned between the Nipkow disk and the upper micro-lens array disk and focused on the appropriate detector (Fig. 8.9). This arrangement of disks has several advantages, including the improved light efficiency described above. This has real advantages for real-time confocal imaging of live cells where fluorescence emission is often limiting. The improved light efficiency allows fluorescence imaging to be carried out at low intensity and power per unit area, thus reducing or minimizing photobleaching of probes and related phototoxic damage to living cells. By focusing the incident light onto the pinholes in the Nipkow disk, backscatter of the incident light at the surface of the Nipkow disk is also significantly reduced, thus improving the signal-to-noise (S/N) ratio of the confocal image. Improved speed of imaging is also possible with frame scan speeds as high as 1,000 fps being possible.

8.4.8 Slit-Scanning Systems

A modification of the pinhole type of spinning disk is the slit-scan spinning disk that Olympus has introduced in their disk scan unit (DSU) systems. The DSU systems offer a choice of five exchangeable disks with different slit widths for use with different objectives and specimen thicknesses. This addresses many of the problems discussed above concerning matching of objectives and pinhole aperture for optimum resolution. As discussed above for the swept-field slit-scanning systems, the PSF is affected when using slits rather than pinholes, so there is still some sacrifice of resolution, but the overall combined confocal effect and speed of imaging is superior to that of epifluorescence microscopes.

8.4.9 Image Collection in Spinning-Disk Systems

Images generated by spinning-disk systems can be viewed directly by looking through a port on the scan head, or captured by using the appropriate recording

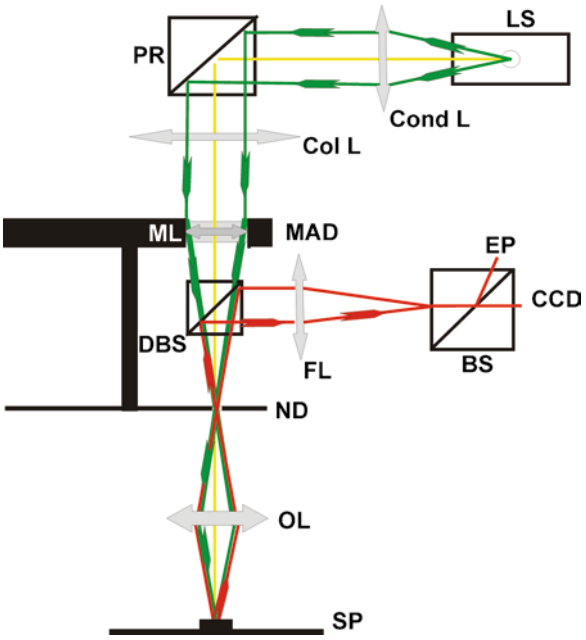

Fig. 8.9 Nipkow spinning disk microscope: Yokogawa design. This design represents a significant improvement over pervious spinning-disk microscopes. The principal improvement is the use of a tandem spinning-disk system in which the pinholes in the upper disk contain micro-lenses that focus the incident light on to the pinholes in the Nipkow disk. The diagram traces the ray path for incident and emitted light interacting with one micro-lens in the micro-lens array disk and one tandem pinhole in the Nipkow disk. *Green lines* – incident light from light source (LS); *red line* – emitted light by the specimen (SP); *yellow line* – optic axis of the microscope. Components: *LS* light source; *Cond L* condenser lens; *PR* 90° reflecting prism or front surface mirror; *Col L* collimating lens; *MAD* micro-lens array disk; *ML* micro-lens; *DBS* dichroic beam splitter; *ND* Nipkow disk with pinholes and tandem with micro-lens array disk; *OL* objective lens; *SP* specimen; *FL* field lens; *BS* beam splitter; *EP* eyepiece; *CCD* CCD camera

device. Since images are collected at high speed and may also have low S/N levels, CCD cameras are the most appropriate collection device. Although very reliable and inexpensive CCD cameras are available, imaging of live cells using fluorescence microscopy requires very sensitive and thus more expensive CCD cameras. Depending on the spinning-disk system, images may be generated at rates between 300 and 1,000 fps. The actual speed at which the instrument can capture images is dependent on the speed and sensitivity of the attached CCD camera and the intensity of the fluorescent emission signal from the specimen. Image collection using CCD cameras is discussed more fully in Chap. 6. Different experimental applications may require image acquisition at varying speeds or frame rates. The speed of the device is determined by the pixel read rate and the number of pixels that comprise the image.

References

Abbe E. 1884. Note on the proper definition of the amplifying power of a lens or lens system. *J Roy. Microsc. Soc*. **4**(2):348–351.

Centonze, V., and J. White. 1998. Multiphoton excitation provides optical sections from deeper within scattering specimens than confocal imaging. *Biophys J.* **75**:2015–2024.

Corle, T.R., Mallory, CL., Wasserman TD. 1991. Improved confocal scanning microscope. U.S. Patent 5,067,805 (Nov. 26, 1991).

Denk, W., J. Strickler, and W. Webb. 1990. Two-photon laser scanning fluorescence microscopy. *Science.* **248**:73–76.

Denk, W., D. Piston, and W. Webb. 1995. Two-photon molecular excitation in laser-scanning microscopy. *In* Handbook of Biological Confocal Microscopy, Second Edition. Pawley, J., editor. Plenum, New York, 445–458.

Gauderon, R., P. Lukins, and C. Sheppard. 1999. Effect of a confocal pinhole in two-photon microscopy. *Micros Res Tech.* **47**:210–215.

Genka, C., Ishida, H., Ichimori, K., Hirota, Y., Tanaami, T., Nakazawa, H. 1999. Visualization of biphasic Ca2+ diffusion from cytosol to nucleus in contracting adult rat cardiac myocytes with an ultra-fast confocal imaging system. *Cell Calcium.* **25**:199–208.

Gerritsen, H., and C. deGrauw. 1999. Imaging of optically thick specimens using two-photon excitation microscopy. *Micros Res Tech.* **47**:206–209.

Goodman, J.W. 1968. Introduction to Fourier optics. McGraw Hill, New York

Göppert-Mayer, M. 1931. Uber Elementarakte mit zei Quantenspruengen. *Ann Physik (Berlin).* **9**:273–294.

Ichihara, A., Tanaami, T., Isozaki, K., Sugiyama, Y., Kosugi, K., Mikuriya, K., Abe, M., Umeda, I. 1996. High-speed confocal fluorescence microscopy using a Nipkow scanner with microlens for 3-d imaging of a single fluorescent molecule in real time. *Bioimages* **4**:57–62.

Kino, G.S. 1995. Intermediate optics in Nipkow disk microscope. In: Handbook of Biological Confocal Microscopy. J.B. Pawley, ed. Plenum Press, New York. pp 155–165.

Kino, G.S., Xiao, G.Q. 1990. Rea-time scanning optical microscopes. In: Scanning Optical Microscopes. T. Wilson ed., Pergamon Press, London, pp. 361–387.

Nakano, A. 2002. Spinning-disk confocal microscopy – A cutting edge tool for imaging of membrane traffic. *Cell Struct. Funct*. **27**:349–355.

Nipkow, P. 1884. German Patent no. 30105. Germany.

Petrán M., Hadravsky, M., Egger, M.D., Galambos, R. 1968. Tandem scanning reflected light microscope. *J. Opt.Soc. Am*. **58**:661–664.

Petrán, M., Hadravsky M., Boyde, A. 1985. The tandem scanning reflected light microscope. *Scanning*, **7**:97–108.

Piston, D. 1999. Imaging living cells and tissues by two-photon excitation microscopy. *Trends Cell Biol.* **9**:66–69.

Tanaami, T., Otsuki, S., Tomosada N., Kosugi, Y., Shimizu, M., Ishida, H. 2002. High-speed 1 frame/ms scanning confocal microscope with a microlens and Nipkow disk. *Applied Optics*. **41**:4704–4708.

Xiao, G.Q., Corle, T.R., Kino G.S. 1988. Real time confocal scanning microscope. *Applied Phys Lett*. **53**:716–718.

Xiao, G.Q., & Kino, G.S. 1987. "A real-time confocal scanning optical microscope," Proc. SPIE, Vol **809**, Scanning Imaging Technology, T. Wison & L. Balk, eds 107–113.

Xiao, G.Q., Kino, G.S., Masters, B.R. 1990. Observation of the rabbit cornea and lens with a new real time confocal scanning optical microscope. *Scanning*. **12**:161–166.

Chapter 9
Setting the Operating Parameters

Robert L. Price

Keywords Averaging • Bit depth • Colocalization • Dynamic range • Laser • Look-up-table • Photobleaching • Pixels • Resolution • Signal to noise ratio

9.1 Introduction

The goal of this chapter is to systematically look at each decision made in obtaining images from a sample stained with single or multiple fluorochromes. While in this chapter most of the specific examples of choices made in setting instrument parameters are given by using images collected on a Zeiss LSM 510 META confocal microscope equipped with the following lasers: 405 nm blue diode, argon with peaks at 458, 477, 488 and 514 nm, 543 nm HeNe and 633 nm HeNe lasers, the basic choices made are the same regardless of the manufacturer of the system being used and the available hardware. When operating various confocal instruments, it is often simply a matter of identifying the terminology used, for example, pinhole versus iris or the name of a specific look up table (LUT), or finding where a particular software function is hidden in the multiple menus necessary to operate the system. Once the basic principals are understood, it is possible to quickly learn to operate any confocal microscope and to obtain publication quality images. Figure 9.1 illustrates a generalized flowchart that can be used to start an imaging session and to obtain the initial images. Detailed information on each of the steps involved is presented below.

R.L. Price (✉)
Department of Cell and Developmental Biology, School of Medicine, University of South Carolina, 6439 Garner's Ferry Road, Columbia, SC 29208, USA
e-mail: Bob.Price@uscmed.sc.edu

R.L. Price and W.G. (Jay) Jerome (eds.), *Basic Confocal Microscopy*,
DOI 10.1007/978-0-387-78175-4_9,

1. Turn on mercury or other imaging source for use in widefield imaging through the microscope. Allow several seconds for imaging source to stabilize.
2. Turn on the system hardware.
3. Turn on the computer and log in with username and password.
4. Open the operating software: This often takes a minute or more and involves a series of system self-checks to make sure the computer, system hardware, and microscope are communicating properly.
5. Open the confocal microscope operating software.
6. Activate appropriate lasers based on the fluorescence wavelengths that will be used during the imaging session. In most modern systems it is possible to activate only the lasers that will be used during the imaging session preserving hours on the other lasers.
7. Set up the light microscope parameters and obtain a wide field image of the sample
8. Select the AOTF, AOBS or other filters required for imaging the appropriate fluorescent wavelengths that will be used.
9. Set the scanning parameters including resolution, speed, line versus frame scanning, bit depth etc.
10. Set the image collection parameters such as pinhole diameter, detector gain and offset, Z-settings etc.
11. Store the final image in a format that will maintain information related to all operating parameters. Exporting images as TIF or other formats that are not default settings for the instrument may result in the loss of information related to the operating parameters such as lasers, laser power, pinhole settings etc.

Fig. 9.1 Generalized flow chart for starting an imaging session

9.2 Test Specimens and System Performance

As discussed in Chap. 1, Pawley (2000) posed the question, does a fluorescent micrograph reveal the actual location and number of labeled molecules in a cell or tissue, to members of his well-known confocal microscopy workshop. Based on the several factors that can affect the numerical values stored in a computer that represent a fluorescent micrograph (see Chap. 6), the conclusion was that all we "can really be sure of measuring with most confocal microscopes in the fluorescence mode is some feature of the number of photons collected at a particular time." In the previous chapters, we have addressed many of the factors, including fluorescence, the structure of digital images, specimen preparation, and system hardware that can affect these numerical values and the resulting quality and interpretation of the image.

In this chapter, we address the setup of the microscope operating parameters for image acquisition and how each affects the final image. Primary considerations when determining the setting of each of the adjustable parameters on an instrument include

X, Y, and Z resolution, signal to noise ratio (S/N), appropriate spectral resolution so no bleedthrough or spectral overlap exists, specimen damage, bit depth, and file size. Even with all of the variables present while imaging with a confocal microscope, it is possible for an investigator to obtain images on confocal instruments that are superior to widefield fluorescent images with relatively little training. However, minimally trained investigators seldom take full advantage of the superior imaging capabilities of confocal microscopes and rarely do they realize the compromises (Table 9.1) made in specimen damage and image quality when each instrument setting is altered. Improper setup of the system may also result in the collection of data artifacts that may not be recognized. It is only through a thorough understanding of the operation of each component of the confocal system that informed decisions can be made and optimal images obtained on a routine basis.

Zucker and Price (1999) have published an excellent article on methods for instrument maintenance and quality control to insure an instrument is operating at optimal specifications. While these topics are important and it is essential that attention is paid to these details, we will not go into extensive discussions concerning instrument maintenance and specifications here. Rather, this discussion focuses on the proper setup of an optimally functioning instrument for everyday imaging. Inherent in these discussions is the assumption that a core director or other personnel extensively trained in instrument maintenance are routinely checking and correcting instrument specifications and alignment.

For discussions below concerning parameters which affect image quality and proper setup of the confocal microscope, test specimens that consist of 4 μm beads,

Table 9.1 Advantages, disadvantages, and imaging compromises associated with the adjustment of confocal microscope operating parameters

Parameter	Advantage	Disadvantage
Increased laser output	Improved S/N ratio	Increased specimen damage
Decreased scan speed	Improved S/N ratio	Increased scan time and specimen damage
Line or frame averaging	Improved S/N ratio	Increased scan time and specimen damage
Increased pinhole size	Improved S/N ratio	Decreased contrast and resolution in x, y, and z
Increased number of pixels (smaller pixel size)	Improved resolution	Increased scan time; large file size
Increased amplifier gain	Fewer photons required	Poor S/N ratio
Increased amplifier offset	Improved gamma	Decreased contrast
Narrow band pass filter	Minimal bleedthrough	Decreased signal
Sequential imaging	Eliminates bleedthrough	Increased scan time and specimen damage
Simultaneous imaging	Decreased scan time and specimen damage	Increased bleedthrough of fluorochromes with overlapping emission spectra
Long wavelength fluorochrome	Improved depth of imaging	Decreased resolution
Short wavelength fluorochrome	Improved resolution	Decreased depth of imaging

filter paper stained with various fluorochromes, or Convallaria (Lily of the Valley) are used as examples. It is important to have test and reference specimens such as these which are relatively stable when exposed to a laser available for routine testing of instrument operation. Standard specimens are essential tools for training and as quality control assays to insure that the instrument is working properly. Often investigators blame poor image quality on the instrumentation when the actual problem is poor specimen preparation or operator error. Often, use of test specimens with known fluorescent characteristics to definitively show an instrument is working properly is the only factor that convinces an investigator that a problem may not lie with the instrument, but instead is a problem with specimen preparation or fluorophore specificity.

9.3 Definition of a Good Confocal Image

Even though a number of operating parameters on a confocal microscope can be adjusted, the goal should always be to set these operating parameters so that the digital image which is collected accurately represents the image as seen through the microscope.

A large number of operator decisions and compromises affect image resolution, S/N ratio, and qualitative and quantitative assessment of colocalization and structural information in a confocal image. Before discussing the changes that can be made in various operating parameters that affect specimen damage and image quality, reviewing the definition of a good confocal digital image is essential. As discussed in Chap. 6, an ideal confocal image is one that has appropriate resolution, a good (S/N) ratio so that little or no noise is apparent, good balance between contrast and brightness, and the use of the full dynamic range of the available pixel values. For an 8-bit image, this would represent pixel values between 0 and 255 and for a 12-bit image pixel values between 0 and 4,095. It may be desirable to leave 5–10 pixel values open on each end of the range for the application of histogram stretch functions for contrast enhancement. However, if any type of quantitative or semi-quantitative imaging is the goal of the study, analysis must be performed prior to the histogram stretch operation.

With the large number of specimen, hardware, software, and user definable factors that determine the quality of a confocal micrograph, it is essential that a mechanism be in place to insure quality images that include all available data without the introduction of artifacts can be routinely collected. Within the confocal software LUTs are available that take advantage of the ability of the human eye to detect colors more efficiently than gray tones. These LUTs set pixel values of zero to a specific color, typically blue or green, and pixel values of 255 in an 8-bit image to a contrasting color, such as red. All other pixel values are a shade of gray (Fig. 9.2). This allows the operator to quickly determine that the full range of pixel values is being used and that no detail is being lost on the low or high ends of the image histogram. Comparison of the gray tone images in Fig. 9.2b, d, and f shows the loss

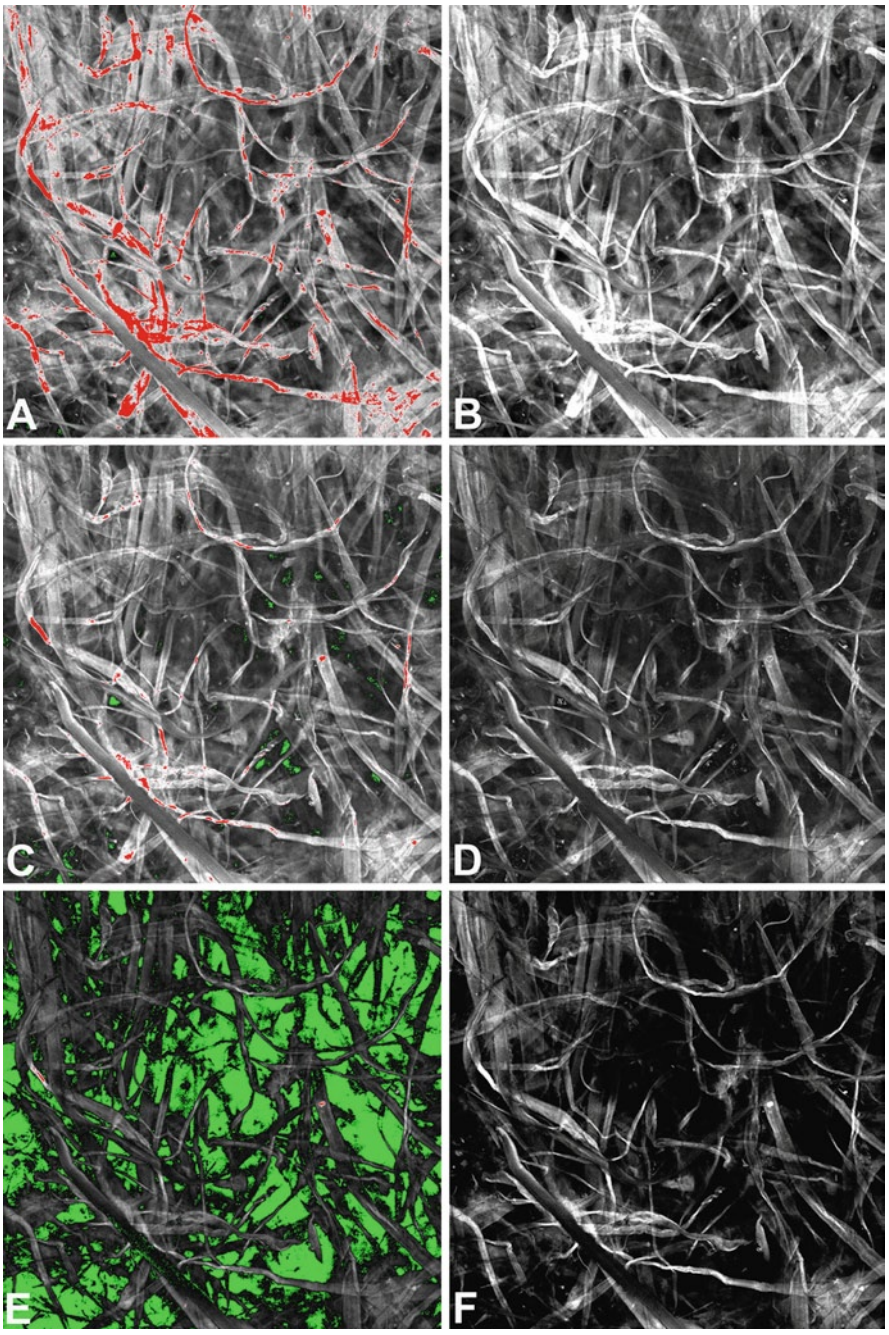

Fig. 9.2 Images of filter paper stained with a fluorescent dye to demonstrate the use of LUTs for setting the appropriate dynamic range in an 8-bit image. In images (**a**, **c**) and (**e**) the LUT is applied and pixel values of 0 are shown as *green*, pixel values of 255 are shown as *red*, and all other values are shown as a shade of *gray*. The goal is to set the pixel values in the image so that few *red* and *green* pixels are present as shown in panel (**c**). In (**b**, **d**) and (**f**) the corresponding *gray scale* images are shown demonstrating loss of fine detail in areas that were oversaturated (*red* pixels) or undersaturated (*green* pixels). The appropriate use of LUTs is required to avoid loss of fine detail in samples

of significant detail in both regions, where large numbers of red and green pixels are present. In the red region, details are lost since all pixels are saturated at the 255 range, and the entire region is shown as white. In the green range, details are lost since all pixels are undersaturated, and the entire region is shown as black. In the center images, the details of the fine paper fibers in the white and black regions are evident. Details on the use of LUTs to assist in the proper setup of confocal operating parameters are discussed below and examples showing the effects on the range of pixel values, S/N ratio, resolution, and other effects on image quality are illustrated as the operating parameters for the collection of an image are established.

9.4 The Opening Screen

From the opening screen (Fig. 9.3), it is possible to access multiple menus for the operation of the system and for data processing. Icons that users need to be aware of for normal operation of the instrument include the File, Acquire, 3D View, Laser, Microscope, Configuration, and Scan buttons. Each of these is discussed in detail below. Depending on the situation and level of training, the Maintain button may or

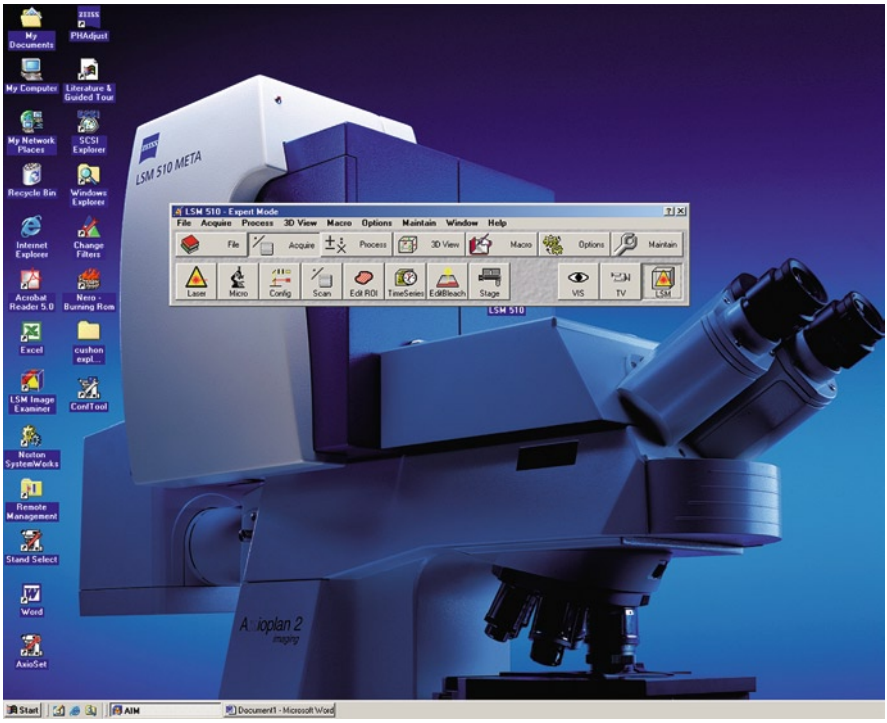

Fig. 9.3 The opening screen for the Zeiss LSM 510 META microscope

may not be accessible to everyday users. Typically, this has software for functions, such as alignment of pinholes and other routine maintenance functions. These should be checked on a routine basis, but many core facility directors discourage the everyday user from performing these duties. Other icons, such as the Edit region of interest (ROI), Time Series and Edit Bleach, as well as other functions such as FRET and FRAP software packages not shown here, may be options on systems which are not available on all instruments.

9.5 Starting the Lasers

With the Acquire Icon activated as shown in Fig. 9.4, access to the Laser, Microscope, Configuration, and Scan icons is possible. By activating the laser icon, it is possible to open a menu box that allows control of the individual lasers available on the microscope (Fig. 9.4). Within this menu box are the on/off controls for each of the four lasers available on this system. Only the lasers needed for a specific operating session need to be turned on. This saves laser life time on the lasers not needed for a specific experiment.

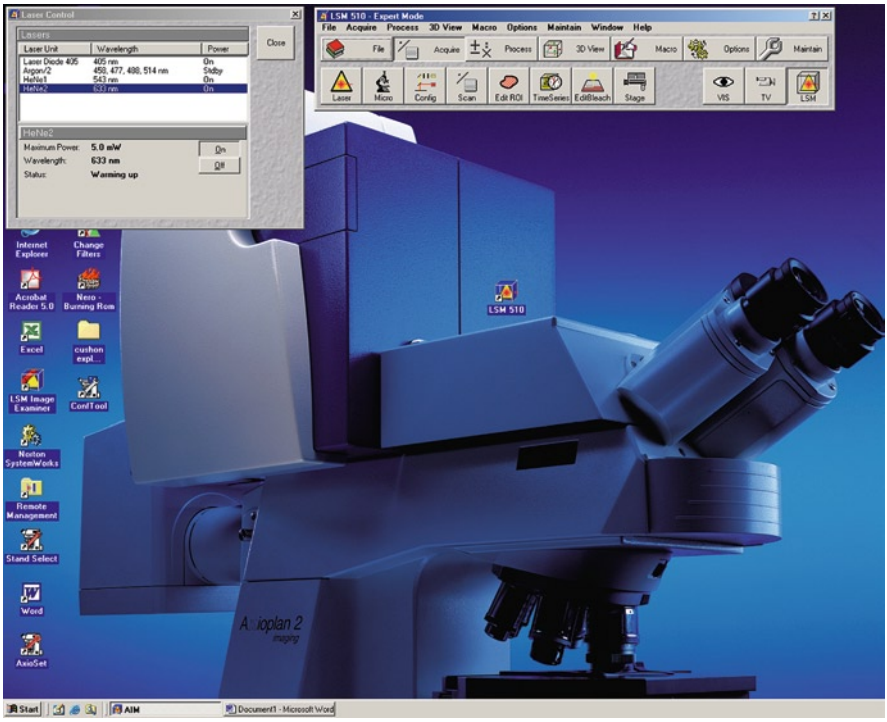

Fig. 9.4 Identification of available system lasers and starting those required for an operating session

The laser box also contains information concerning the peak excitation wavelengths available and the maximum power of each laser. Since not all systems are equipped with the same lasers, it is important to know the wavelength(s) of the lasers available when designing experiments so that a range of fluorochromes can be selected that best matches the available lasers. Many systems are only equipped with three lasers and may not have a laser, such as the 405 diode laser in the near UV or UV range. In our experience, considerable time and expense has been wasted by the selection of fluorochromes for which the specific system lacks the optimal laser for imaging the selected fluorochrome wavelengths. A common example is preparing specimens with DAPI, a very common stain for nuclei, when the system available to the investigator does not have a 405 nm laser. This makes DAPI an inappropriate fluorochrome for these systems.

New and improved lasers suitable for confocal microscopy are being introduced on a routine basis and information about laser wavelengths available for fluorochrome excitation is presented in Chap. 2. As noted above, one of the first choices to make in setting up an experiment is the selection of a series of fluorochromes for staining a sample that are excited at the optimal wavelengths of the lasers available on the confocal system. While it is often possible to excite a fluorochrome at a suboptimal wavelength, this typically involves the use of lasers at a high intensity which may result in specimen damage, such as quenching of fluorochromes in fixed samples and cell death in live cell imaging. Compromises in setup of the post excitation operating parameters, including opening the pinhole or increasing the sensitivity of the PMT, may also be required. These compromises result in poor resolution and S/N ratios. Whenever possible, using fluorochromes not ideally suited to the available lasers on a confocal system should be avoided

9.6 The Microscope Menu

The microscope menu box (Fig. 9.5) provides control over the various objectives and filters available on the light microscope associated with the confocal hardware. In fully integrated motorized systems, objectives and filters can be selected simply by clicking on the appropriate button to load the required hardware. In older systems, it may be necessary to manually change objectives and filters. Note that for the selection of filters (DAPI, FITC, and Rhodamine) in this figure that specific fluorochromes, such as Alexa 488 and Cy2, even though they may be more common for confocal imaging than those shown, are not referred to. This is often the case and the names of the filters here, as well as when the confocal system is configured, refers to families of dyes that fall within a certain range of excitation and emission characteristics. For instance, in this case, the FITC button is also used for Alexa 488, Cy2, and GFP and the Rhodamine button is also used for the Alexa 543 and Cy3 families of fluorochromes.

Also note that no filter combination is available for the far red dyes since these cannot be seen with the eye. This is one disadvantage of using these dyes since they

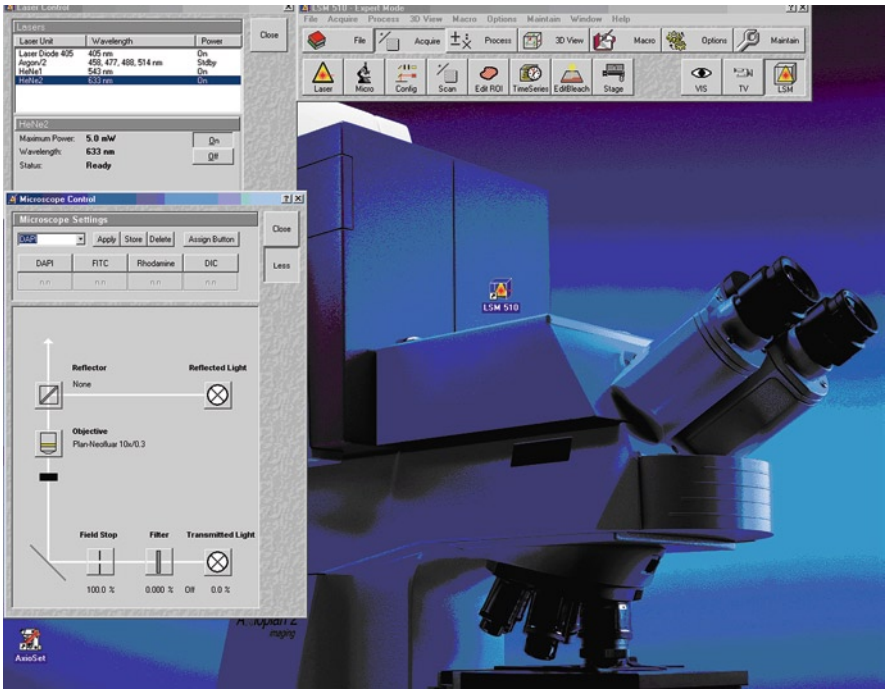

Fig. 9.5 Menu for control of the objectives and filters for the light microscope

can only be imaged while using the lasers. This disadvantage is often offset by the advantages of reduced specimen autofluorescence and slightly deeper imaging with the longer wavelengths in the far red range as discussed in Chap. 3.

Other buttons allow control of differential interference contrast (DIC) and transmitted light, as well as minimizing the size of the box with the “Less” button. This closes the lower portion of the box and leaves only the portion with the filters available. This is possible because there is redundancy in the program with more than one window of the software available for changing the objective lenses.

9.7 The Configuration Controls

The Configuration Control Menu (Fig. 9.6) contains the software necessary for setting up the confocal system for various types of imaging. As shown with the Channel Mode activated routine imaging for Single Track (simultaneous) or MultiTrack (sequential) imaging can be set up. The Lambda Mode and Online Fingerprinting are used to set up spectral imaging functions. For the purpose of the current discussion, our focus is on the use of Single and MultiTrack imaging protocols.

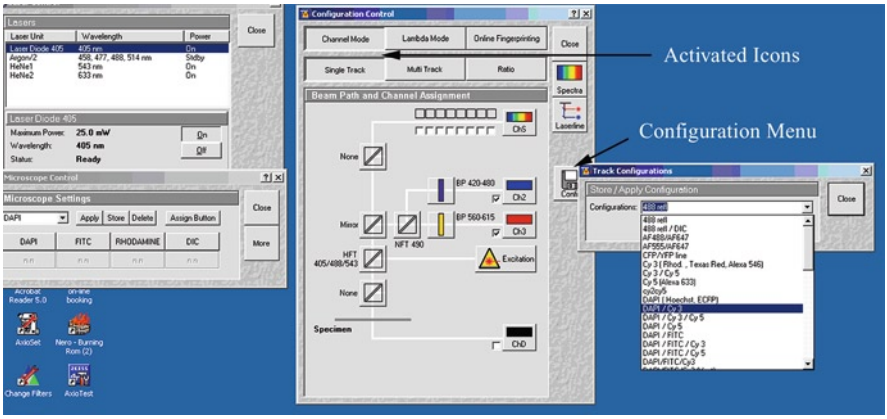

Fig. 9.6 Configuration control panel showing channel mode and single track configuration activated. Opening the configuration icon provides access to all single track configurations that have been written and saved

As discussed in Chaps. 3–5 on specimen preparation and labeling, several choices must be made concerning the fluorochromes used for staining based on their emission wavelengths. In addition to the considerations of labeling and bleedthrough, it is also important to make these choices based on the filter hardware available on the microscope. Chapter 3 provides information on the types of filters used in the separation of the excitation and emission wavelengths of light used. The various long pass, band pass, and dichroic filters available on a system are usually set at the time of instrument purchase. As with the selection of fluorochromes based on laser wavelengths available, data sheets for fluorochromes should be examined and compared with the available filter characteristics to insure that emission maxima and ranges for dyes selected closely match the filter sets available on the confocal system. Poor matching of fluorochrome emission maxima with available filters requires suboptimal settings in other components of the optical path during image acquisition. This results in increased specimen damage and inferior images with respect to S/N ratio and resolution. Fluorochromes should be selected and configuration protocols written based on matching the system hardware with the fluorochrome excitation and emission characteristics as closely as possible.

Protocols can be written and accessed under the Methods or Configuration icon in the software and available filters should be readily accessed through the software. In the LSM 510 software, available dichroic filters can be found by clicking on the buttons along the left side of the Beam Path and Channel Assignment window (Fig. 9.7). This opens a window with a list of dichroic filters that can be selected and assigned a spot in the optical path. Available band and long pass filters can also be selected by clicking on the filter position in front of each detector. This opens an additional window listing all filters available for the detector. Clicking on the selected filter assigns it to that detector (Fig. 9.7).

By selecting either Single Track or MultiTrack followed by selecting the Config button on the right side of the menu box, the Track Configurations menu can be opened.

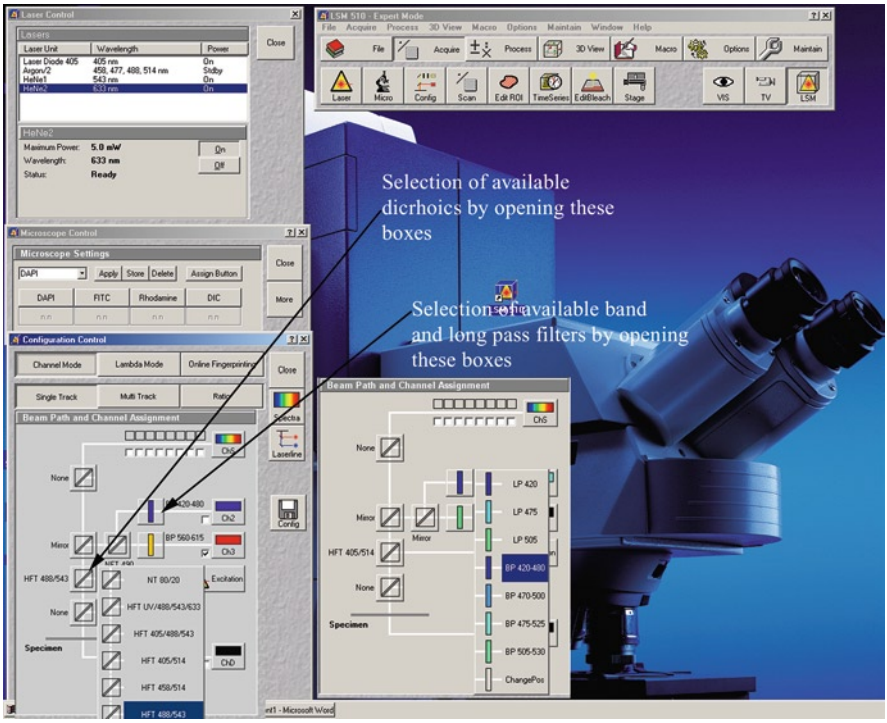

Fig. 9.7 Access to the available dichroic and long pass and band pass filters for the preparation of instrument configurations is provided by clicking on the indicated icons

This configuration menu contains all of the protocols that have been written for the instrument. By selecting a protocol, all laser settings, filters, detectors, and assigned colors for the various channels are loaded. As noted above for the microscope control, names are assigned based on families of dyes and as shown in Fig. 9.8, references to FITC include all fluorochromes that excite at 488 nm and emit around 514 nm.

9.7.1 Single Track (Simultaneous) Configurations

The path of excitation and emission photons can be followed by the diagram shown in the Beam Path and Channel Assignment Box. In the DAPI/Cy3 Single Track Configuration protocol shown in Fig. 9.6, excitation photons pass through a primary dichroic (HFT 405/488/543) which deflects them toward the specimen. Following laser interaction with the specimen, photons emitted from the fluorophores pass back through this dichroic and are deflected by a mirror toward the two active detectors (Ch2 and Ch3) as indicated by the checked boxes. Since this is a Single Track configuration, it is necessary to separate the photons emitted from DAPI (405 excitation and 480 emission) from those emitted by Cy3 (543 excitation and 570 emission).

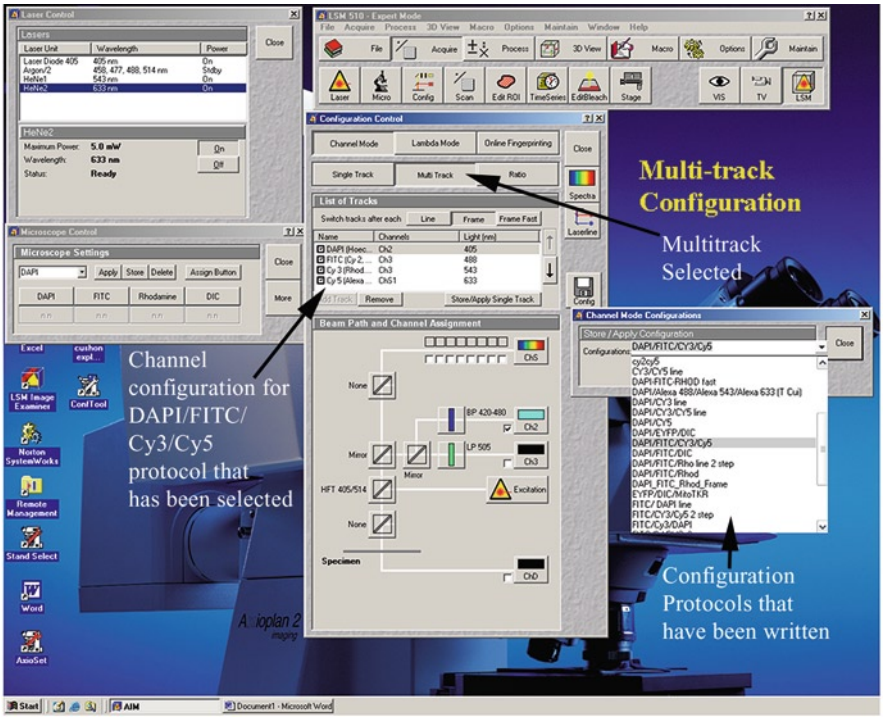

Fig. 9.8 Multitrack configuration mode and setup of the available tracks

To separate these emission wavelengths a secondary dichroic (NFT 490) is used to deflect light shorter than 490 nm toward the Ch2 detector while allowing photons with a wavelength longer than 490 to pass through to the Ch3 detector. Appropriate band pass filters are placed in front of each detector to further define the specific wavelengths of light used to form the image. In the case of Ch2, only light between 420 and 480 nm is allowed to pass through to the detector and that of Ch3 only light between 560 and 615 nm is allowed to pass through. The band pass filters effectively separate all photons into two distinct channels with no overlap or bleedthrough.

Although not shown in the diagram, in this model instrument pinholes are located in front of each detector. In other models of instruments, a pinhole may be placed in the optical path prior to light reaching the filtering mechanism.

9.7.2 MultiTrack (Sequential) Configurations

In many samples which require two or more labels, it is necessary to use fluorochromes which have overlapping emission spectra. In Fig. 9.8, a multitrack configuration is shown in which four tracks are being used. Note that in this protocol the Frame icon is

selected rather than Line. This indicates that an entire frame is scanned prior to changing the laser, Acousto-Optical Tuneable Filter (AOTF), and pinhole combinations for the next fluorochrome. If line were selected changes in the tracks collected would occur following the scanning of each line, but changes are limited only to the AOTF and Amplifier Offset (discussed later). The line function increases the speed of image collection along a single line of the image for potential detection of rapidly occurring events, but limits the selection of hardware between channels for image optimization. For normal imaging of fixed samples, frame imaging is usually selected.

To complete a laser scan in the MultiTrack frame configuration, each laser wavelength is imaged in sequence so only a single laser is active during each scan and four scans are required to complete the four channel image. By highlighting each of the fluorochromes in the box, full information concerning the filter combinations is provided. In the example (Fig. 9.8) shown, the DAPI track is highlighted and the information for the filters and mirrors in the optical path for DAPI are given as described above. By highlighting the other tracks, information on how these are set up is also available. With the setup of appropriate long and band pass filters, this mode of acquisition essentially eliminates bleedthrough problems when using fluorochromes that have overlapping emission spectra.

Most modern instruments include technology to further separate multiple or complex spectral patterns of fluorochrome emission. Many instruments capable of spectral imaging utilize a series of detectors that can be tuned to detect specific wavelengths of light. For example, the Zeiss LSM 510 Meta Detector consists of eight separate detectors that can be individually tuned to a minimum bandwidth of 10.7 nm per detector. While a bandwidth of 10.7 nm gives excellent spectral resolution, this usually provides minimal signal to the detector and may result in a poor S/N ratio. To accommodate the low signal, it may be necessary to adjust the detectors to allow multiple 10.7 nm bandwidths of light (i.e., 21.4, 32.1, etc.) through to the detector. Figure 9.9 illustrates the same four track protocol shown above and the use of the Meta Detector to detect signal in the far red emission range. In this case, the 633 laser is used to excite a Cy5 labeled specimen and emitted photons are allowed to pass through to the Meta detector. In the example shown, only the first channel (ChS1) is being used, and it is set to detect photons with wavelengths between 646.7 and 710.9 nm.

While in the above case the ChS1 detector was used as part of a four-color MultiTrack Configuration, the Meta Detector and other spectral imaging mechanisms may also be used to separate closely related excitation and emission spectra, such as those of GFP and YFP, when they are present in a sample. All manufacturers of systems are also rapidly developing hardware and software to address the ever increasing number of fluorochromes and potential combinations of fluorochromes investigators would like to image. Recently, companies have introduced hardware and software capable of imaging over extensive wavelength ranges (350 nm through 1,100 nm) with the detection of up to ten channels in a single image by using up to 34 spectral detectors.

Efforts are also being made to minimize or eliminate the number of filters in the optical path. Some recent systems have employed band pass sliders which do not

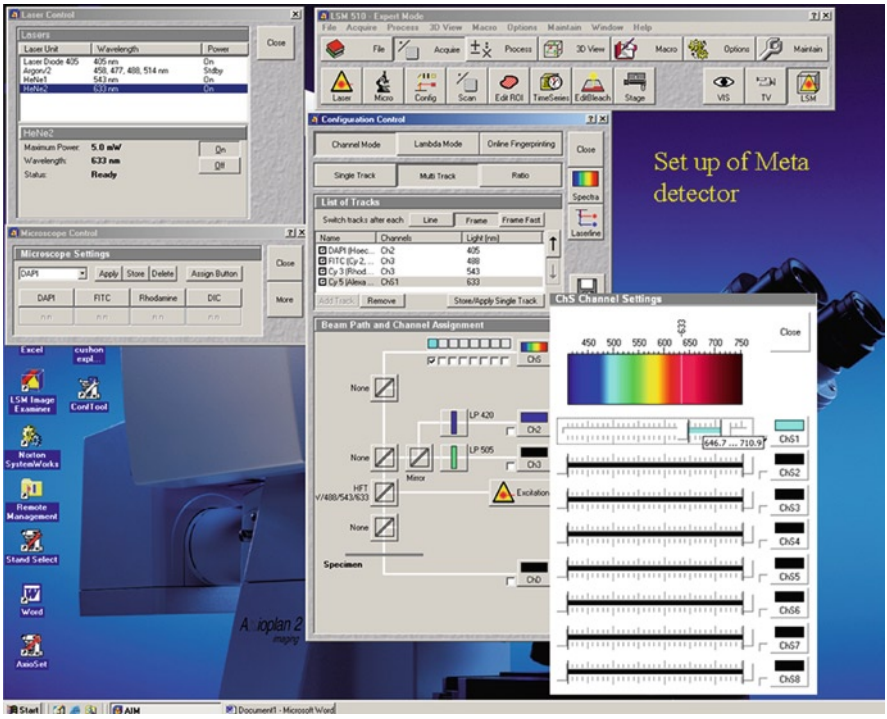

Fig. 9.9 Use of the Zeiss Meta detector for sequential collection of multiple channels from a sample

use the typical barrier filters. Another alternative to the use of multiple detectors and barrier filters to separate closely related fluorochromes is the AOBS spectral system, briefly described above, which has been developed and patented by Leica. The AOBS has many of the same advantages of the multiple detector philosophy and allows very accurate separation of closely related fluorochrome emissions. An additional advantage is that it is not necessary to have multiple filter sets in the system since the AOBS uses sound waves to separate multiple wavelengths of light. This eliminates the need to have multiple filter sets in a system and the requirement that a new set of filters be moved into place between collection of channels. This reduces vibration and misalignment of images.

9.7.3 Combined Single and Multiple Track Configurations

As discussed earlier, photobleaching and bleedthrough are often problems when imaging with the high intensity lasers of a single photon confocal microscope. Each additional scan increases the potential for specimen damage and many fluorochromes have overlapping emission spectra. To minimize the number of scans

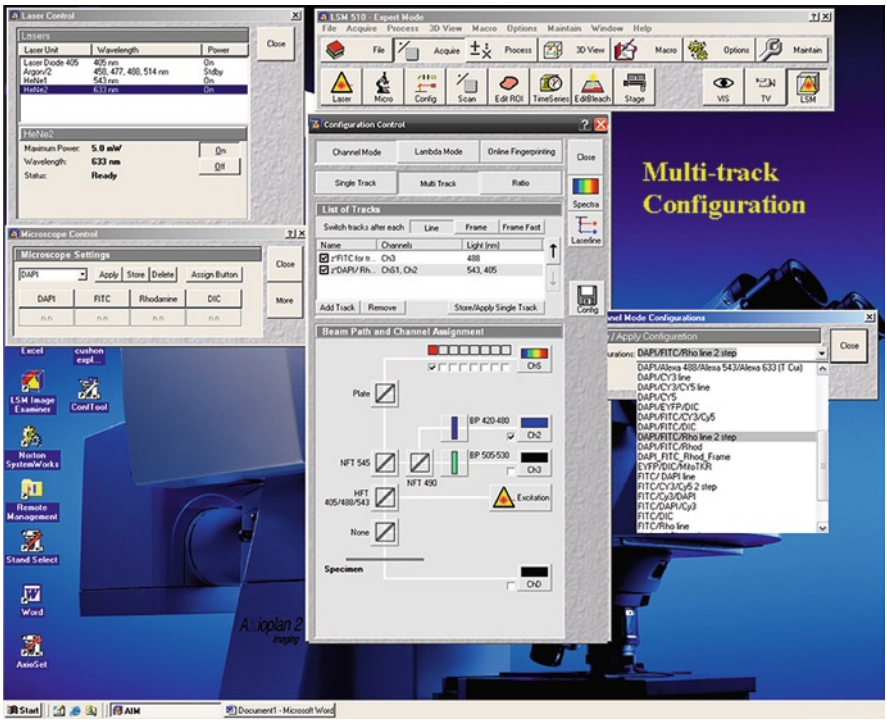

Fig. 9.10 The use of emission photon filtering mechanisms to combine single and multitrack protocols to minimize the number of scans and reduce the potential for photobleaching and bleedthrough

necessary to collect multichannel images, it is possible to combine simultaneous and sequential imaging protocols. An example of this is shown in Fig. 9.10, where the configuration menu indicates a DAPI/FITC/Rhodamine 2 step protocol. In this case, three fluorochromes are imaged only in two scans. Since there is little likelihood of DAPI and Rhodamine (Cy3, Alexa 543) emission spectra overlapping, these can be imaged simultaneously as described above for DAPI and Cy3. To avoid overlap of the FITC (Cy 2, Alexa 488) emission spectra with those of DAPI or Rhodamine, the second scan uses only the 488 laser and the appropriate mirrors and filters for this family of fluorochromes. This decreases the number of scans from three to two and reduces the potential for photobleaching while also eliminating the potential for bleedthrough.

9.7.4 Neutral Density and Acousto-Optical Tuneable Filters

It is essential to be able to attenuate the intensity of the laser light interacting with the specimen since allowing at or near 100% of the light to pass through to the specimen

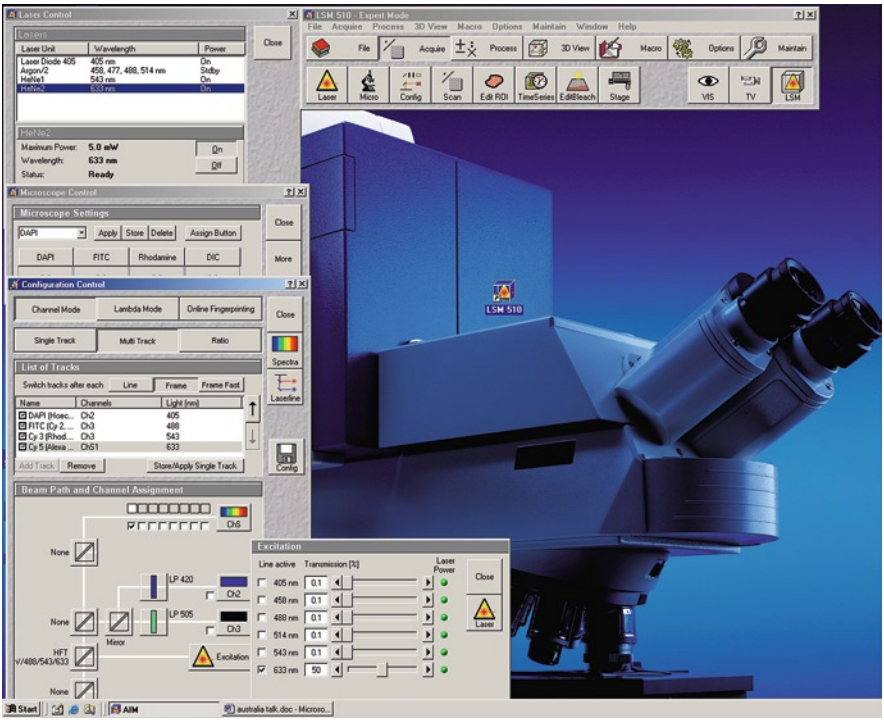

Fig. 9.11 The AOTF controls can be accessed by clicking on the excitation icon. With these controls, each laser on the system can be accessed and the percent of excitation light interacting with the specimen controlled

may result in extensive specimen damage and photobleaching. As discussed in Sect. 3.6, this is accomplished with either Neutral Density (ND) filters or AOTFs. For all of the protocols above, it is possible to use the AOTF to control the percent transmission from each of the lasers being used. Figure 9.11 shows the Excitation window open which allows each laser line available on the system to be independently selected and adjusted. For the Multitrack four-channel configuration shown, the Cy5 channel is highlighted and indicates that the percent transmission from the 633 laser is set at 50%. The transmission can be adjusted in 0.1% increments by sliding the bar or typing in the desired level. As indicated in Table 9.1, increasing the laser transmission improves the S/N ratio, but this also increases specimen damage.

9.7.5 Assignment of Colors to Channels

As discussed in Sect. 6.9, images stored by the computer are a series of binary numbers that represent 0–255 in an 8-bit image or 0–4,095 in a 12-bit image. The color images rendered by the computer that we see are colors assigned to each of these numerical values. By convention, we typically assign a color representative

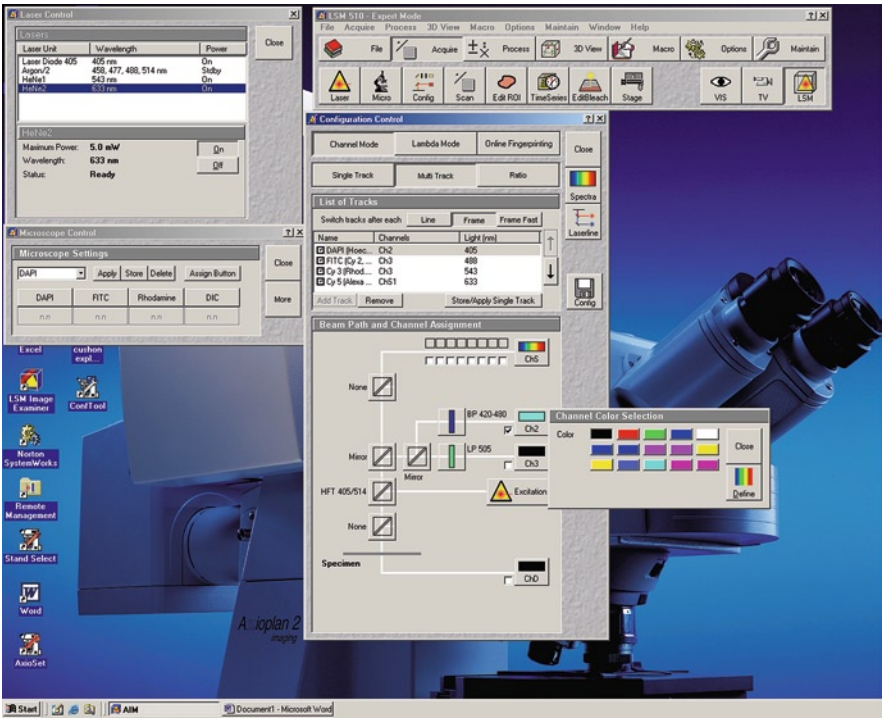

Fig. 9.12 Colors are assigned by the use of LUTs which can be accessed by clicking on the appropriate channel as shown for the Ch2 icon

of the region of the light spectrum the emission was generated from. For instance, in the multitrack configuration shown in Fig. 9.12, the Ch2 detector has been assigned to collect light from DAPI emission with the 420–480 band pass filter which is in the blue range. By convention, we assign a shade of blue to this detector. However, by clicking on the Ch2 icon, we can open an LUT and we could have easily assigned red, green, or any other color to the image.

A note of interest is that green and red are traditionally assigned as the colors for fluorochromes that emit in the 525 and 560 nm ranges. This is occasionally a problem during imaging and presentations since 7–10% of males are red-green color blind. When presenting confocal data sets which use red or green, it is often helpful to indicate the appropriate colors for these individuals during presentations.

9.7.6 A Word of Caution on Configuration Menus

All of the optical path components in the Configuration Control menu are user definable so additional protocols can be written and stored in the software for future use. A precaution here is that in multiuser situations, since these Configurations are user

definable, protocols should be routinely checked to insure no changes have been made and saved by previous users. Settings should also be stored in a separate area limited to Administrator access for future use. Most systems also have a reuse function so that if a protocol has been used to collect an acceptable image the same protocol may be used for the collection of similarly prepared images during future imaging sessions. Since no two specimens are identical, fine adjustments in settings are usually required. Caution must also be used in comparison of images collected during different operating sessions as laser conditions and other operating parameters change over time. However, established Configuration protocols and Reuse functions are very useful in rapidly establishing instrument settings to obtain an image when starting a session.

9.8 The Scan Control Menu: Selection of Image Collection Parameters

After configuring the system lasers and filters, it is necessary to set the parameters for how the image is collected. This involves selection of the image X, Y, and Z resolution, scan speed, bit depth, zoom, detector settings, etc. At this point in the decision-making process, it is advantageous to collect images with knowledge concerning the end point of the experiment and how the data is presented. It will save considerable time and effort after the images are collected if minimal work in Photoshop or other image enhancement programs is required for image adjustments after collection. For example, is the experimental end point a qualitative assessment of structural components at a relatively low magnification, or is it a quantitative colocalization experiment? If recurring organized structures, such as myofibrils, are present in a cell, is it possible to compose groups of images prior to collection so that orientation of the recurring components will all be collected in the same direction? This saves time rotating images postcollection for presentation purposes.

If decisions are not possible concerning the end point of the experiment at the time of image collection, then a rule of thumb to follow is to collect big and work small (Commandment #8: resolution is a one-way street). Once an image is collected, it is not possible to improve the resolution or to increase the bit depth. However, if images are collected at high resolution and bit depth, it is possible to selectively reduce the data (i.e., number of Z-sections) while working with images in enhancement and analysis programs. However, it is essential that the original files be archived if data reduction processes are used to insure no significant loss of information occurs.

9.8.1 Scan Control Mode Functions

Figure 9.13 shows the Scan Control window with both the Mode and Channels windows open for convenience. Typically, one or the other is open and the user toggles back and forth between the menus. Under this menu, there is again a choice

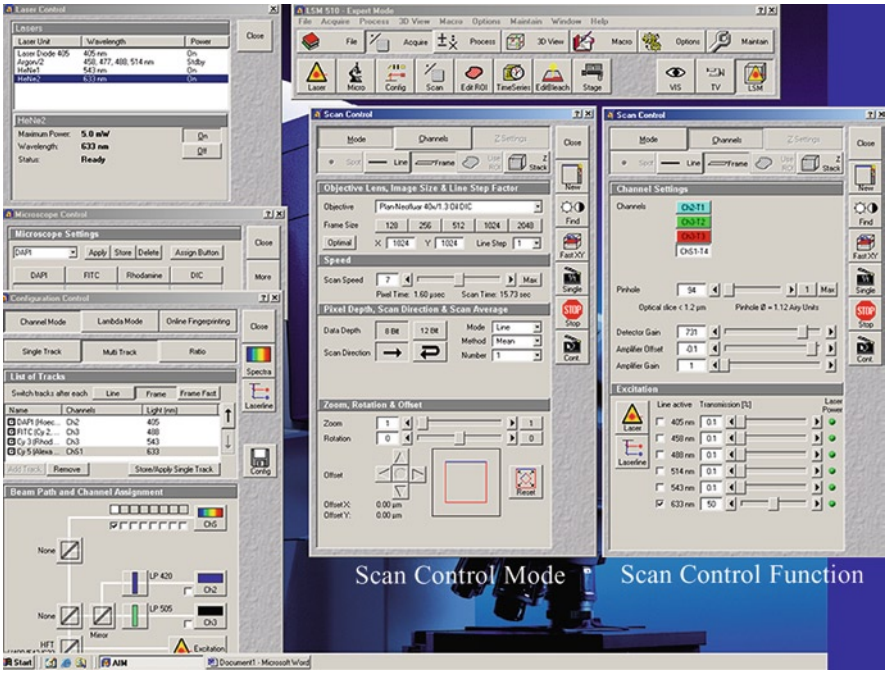

Fig. 9.13 Scan control mode and channels menus open showing the necessary controls for establishing the parameters for image collection

between Line and Frame scanning. In this case, Line scanning results in a single line being scanned which may assist with setting up image parameters along a region of interest. In Frame scanning, as above, entire frame is scanned from top to bottom and the process then repeated. In the Spot scan mode, a single spot is scanned. The Z-stack functions are discussed separately following the setup description for the Mode and Channels window functions.

As shown in Fig. 9.13, the multitrack four color configuration discussed above is active and the boxes next to all four laser lines are checked. In this scenario, if a scan is started, all four tracks will be imaged sequentially. In many cases, it is advantageous to focus, frame an image in the X–Y plane, and set up the start and end optical planes of a Z-series by using a single channel. This is possible by deselecting three of the lasers and working in only one track at a time. As described below, this is also necessary for the use of LUTs and rapid setup of imaging parameters to insure the use of the full dynamic range of the image as shown in Fig. 9.2.

Along the right side of the Scan Control windows are several icons that allow scanning in Find, Fast, Single, and Continuous modes. When first starting an operating session, the Find mode is useful as the instrument rapidly detects a signal and displays a low resolution image. This allows the operator to quickly establish a "ballpark" range for setting up the imaging parameters. In the Fast X-Y mode, the instrument also scans rapidly at a decreased resolution. The Fast X-Y is typically

used for framing and focusing the specimen. The Single Mode is used to collect the final image which will be saved. In the Continuous Mode, the sample continues to be scanned at the selected resolution and speed until the Stop icon is selected. The Continuous Mode should be used when setting up the scan speed, detector settings, etc., that are used to collect the final image. Caution should be used in the Continuous Mode since considerable specimen damage may occur during multiple scans.

9.8.2 Scan Control Mode: Objective Lens, Image Size, and Line Step Factor

Many operating programs provide some redundancy for ease of operation. For example, even though it is possible to select the objective that is used in the Microscope Control box, it is also possible to select the objective lens of choice in the scan control software. A word of caution is that in some older systems if the microscope and software are not automated it may be necessary to manually indicate the objective being used to insure proper calibration of the system for determining pixel dimensions and the addition of scale bars to the images. It is also essential that instruments be routinely properly serviced and calibrated since scale bars and other image measurement functions are dependent upon calibration of the objective magnification with the data readout for these measurements.

Frame size, or the number of pixels per frame in the X and Y directions, is selected by default based on the objective lens selected, but can be manually changed. As discussed in Chap. 7, the final resolution of the image is determined at this point. With respect to confocal imaging, several choices must be made in selection of the appropriate resolution to minimize specimen damage and optimize image quality. Modern confocal systems give several choices of pixel resolution that range from low resolution images that include relatively few pixels (128×128) to high resolution images ($2{,}048 \times 2{,}048$) and in some instruments as high as $4{,}096 \times 4{,}096$. The effect of pixel size on image quality was shown in Fig. 6.3. Ideally, selection of pixel resolution should be based on the Nyquist Theorem as discussed in Chap. 6. However, increasing the number of pixels in an image increases the amount of time required to scan a specimen which may result in increased specimen damage. For example, in the Zeiss LSM 510 META system scanning at a resolution of 512×512 at a scan speed of 9 (see below) results in a pixel dwell time of the laser of 0.8 μs and a total time to collect a single channel frame of 983 ms. At the same scan speed, an increase in image resolution to $2{,}048 \times 2{,}048$ results in the same pixel dwell time, but since many more pixels are present the time to collect a single channel frame increases to 15.73 s. Although resolution is improved significantly, the increased time may result in photobleaching damage which prevents imaging multiple optical planes in a Z-series and much longer overall time to collect the images.

File size and image processing capabilities must also be considered when selecting image resolution. While confocal systems are typically equipped with computers containing large data storage and processing capabilities, many offline processing systems do not have the storage and RAM capabilities to work with the large data sets collected with confocal microscopes. For example, a single channel image collected at a pixel resolution of 1,024 × 1,024 is slightly over 1 Mb in size. However, most confocal data sets are multichannel. A four-channel image collected at a resolution of 1,024 × 1,024 is over 4 Mb in size. If a large Z-series is collected in four channels, each optical section then requires over 4 Mb of storage and data sets of multiple channels and optical slices rapidly approach a gigabyte or more in size. This often challenges the image processing capability of standard office and home computers. Even though data storage is inexpensive, processing capabilities of available offline computers should also be considered when collecting large data sets.

The Line Step icon allows selection of the number of lines in the Frame which is imaged. At a setting of 1, all lines based on the resolution selected are scanned. For example, at a Frame Scan of 1,024 × 1,024, all 1,024 lines are scanned. At a Line Step of 5, only every fifth line is scanned and information between lines 1 and 5 is interpolated to form the final image. This again significantly increases the speed of scanning at the expense of computer interpolation to form the final image (Fig. 9.14). At a Line Step of 1, Frame Scan of 1,024 × 1,024, and Scan Speed of 9, the pixel dwell time is 1.6 μs and the time to collect the entire frame is 3.93 s. By increasing the Line Step to 5, the frame collection time is reduced to 786 ms, and when the Line Step is 10 the time is further reduced to 393 ms. Thus, by adjusting the Frame Size and Line Step image acquisition times can be significantly reduced for the collection of images from live samples or from those that photobleach rapidly.

While the difference in actual time to collect a single frame may seem small, when imaging events in live cells, or when imaging preserved samples that are rapidly photobleaching, increased scan speeds to reduce the exposure of a sample to the high intensity lasers may mean the difference between being able to collect meaningful data, although at reduced resolution, and not being able to collect the data necessary to complete an experiment.

9.8.3 Scan Control Mode: Scan Speed

Selection of scan speed is a critical component in establishing S/N ratio and in controlling photobleaching. A slow scan speed allows the laser to remain in contact with a point in the specimen for a longer period of time resulting in the generation of a larger number of photons, or improved signal. However, this is at the expense of increased photobleaching which may be a problem in some samples. In Fig. 9.13, a scan speed of 7 has been selected with a frame size of 1,024 × 1,024. With these operating conditions, the pixel dwell time is 1.6 μs, and it takes 3.93 s

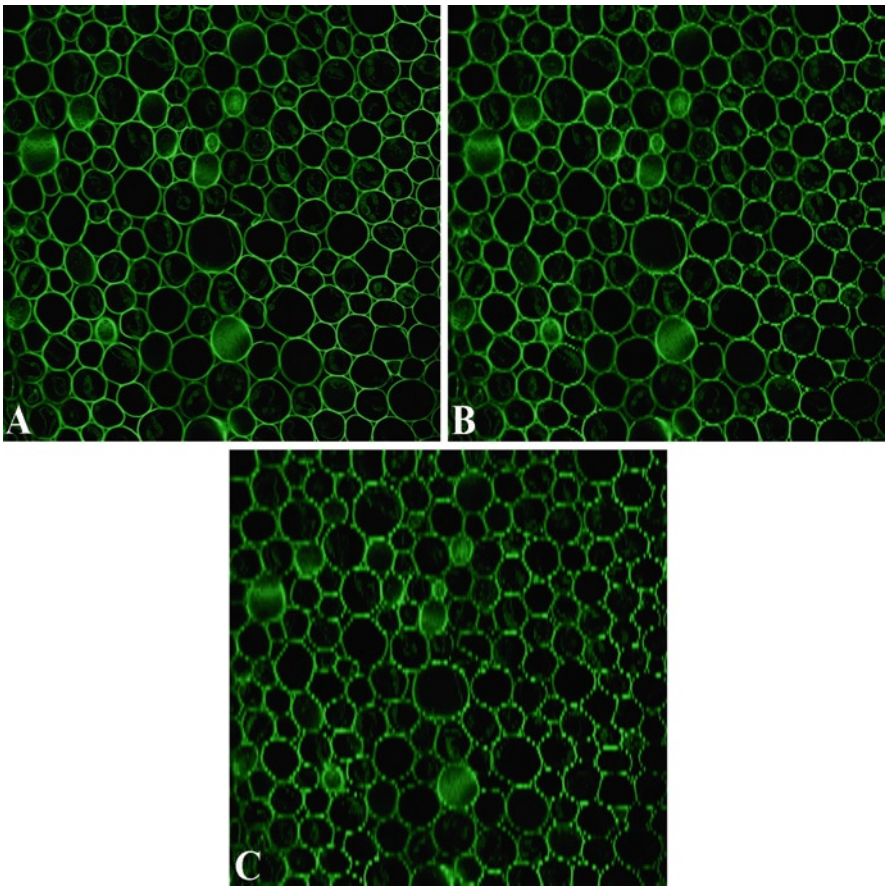

Fig. 9.14 Changing the line step function from a setting of 1 (**a**) to 5 (**b**) and 10 (**c**) reduces the time necessary to scan an image but decreases image resolution since not as many lines are scanned

to collect a single frame of one color. In the example shown, a multitrack configuration requiring four scans is selected so the time to scan a single optical section of four colors with these conditions is 15.73 s. If the scan speed is increased to 9, the pixel dwell time decreases to 0.8 μs and the time necessary to collect a single frame of one color decreases to approximately 1.97 s. With the above conditions, if a Z-series consisting of 50 optical slices with four colors is collected at a scan speed of 7, it will take approximately 13 m of scanning to collect the data set, while at a scan speed of 9 the same number of images can be collected in only 6.5 m. As described above, in single photon confocal imaging the laser interacts with a large volume of the specimen during each scan. This may result in excessive bleaching and loss of signal in optical planes above and below the focal plane of the specimen if the sample is not protected against photobleaching with mounting media, such as DABCO as described in Chap. 4.

While the time necessary to collect a data set should not be a major consideration in most imaging protocols, by knowing the options available on an instrument and compromises that are made in specimen damage and image quality, both instrument access and operator time can be used efficiently. If photon emission from the sample is sufficient to collect an image with a good S/N ratio, a faster scanning rate can be used saving both operator and instrument time. This allows optimal use of the specimen and instrument.

9.8.4 Scan Control Mode: Scan Averaging and S/N Ratio

Even with the best of specimens and operating conditions most confocal images have the potential to contain noise in the image as a result of the electronics present in the hardware. This is most easily observed in dark areas of the image that contain little or no fluorochrome. In a single pass of the laser, some pixels in these areas have a bright appearance that is above the zero value set for black. This can be seen in comparison of the left and right images in Fig. 9.15, where bright pixels can be seen inside the cells and outside the section of the Convallaria sample in the left image. In live imaging, the brightness of these pixels changes with each pass and as the laser passes a second and third time the same pixel may have values that range from zero to high enough to show a bright spot in the image background. Shifting of the value of these pixels during subsequent scans indicates electronic noise in the image. If noise becomes a severe problem, it adversely affects image quality, and if a pixel is bright enough it may affect quantitative assessment of the data.

Since electronic noise is random, it is unlikely that the same pixel experiences a noise event in subsequent scans. Imaging several lines or frames and averaging each pixel value reduces the background level by decreasing pixel values where noise has occurred. Two methods for averaging are available. In the line average as shown in Fig. 9.15, each line is scanned the set number of times and the average value obtained for each pixel position assigned to the final image. As an example, if an averaging function of 8 is selected as shown in Fig. 9.15 and one of the scans has a noise value of 24 while the remaining scans have a pixel value of 0, the average pixel value assigned to that location in the image is 3. This should fall at the end of the image histogram reserved for histogram stretch functions and result in a black image pixel.

By clicking on the Average Mode Box, Line Averaging can be changed to Frame Averaging. In this Mode, the averaging of pixel values occurs after the completion of each frame scan. In the above case where any scan could have had a pixel value of 24 and all other scans had a value of 0, the final pixel value would be 3. However, in frame scanning, if the noise value of 24 occurred in a later scan, the final pixel value would be averaged from that point.

A common question is if averaging improves image quality why shouldn't several more frames be included while collecting images? In the above example,

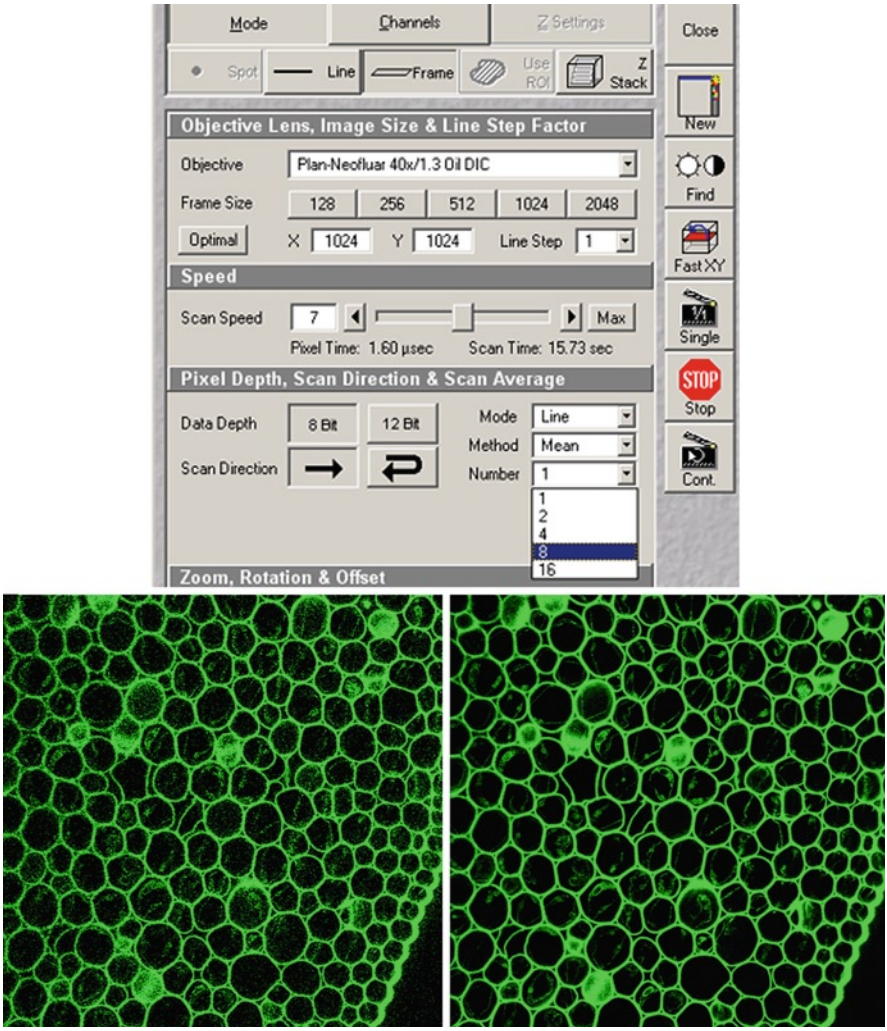

Fig. 9.15 Averaging images results in an improvement in S/N ratio. The image on the *left* was not averaged resulting in a number of bright pixels inside the cells of the Convallaria and in the region outside of the sample. These bright pixel values represent noise since there is no labeling in these regions. By averaging the collection of eight scans, the noise is integrated out resulting in an image with a much improved S/N ratio as shown by the image on the *right*

an averaging function of eight scans was selected which reduced the noise in the pixel from a value of 24 to 3. If the number of scans was doubled to 16 under the same operating conditions, the average pixel value for the location would have only dropped to 1.5. Both values are at the low end of pixel values in the image and would be detected by the eye as a black pixel. Several factors enter

into the decision on the number of scans to average. The improvement in an image is directly proportional to the square root of the number of scans averaged. Thus, if an image is averaged 16 times, the image is improved by a factor of 4. If the image is scanned four times, it is improved by a factor of 2. However, to get the improvement in S/N ratio from 4 to 2, it takes four times as long to scan a frame which significantly adds to the total number of scans and time the specimen is exposed to the laser. For example, at a scan speed of 7 averaging two frames requires 7.9 s to collect a 1,024 × 1,024 image. Increasing the averaging function to 8 requires 31.5 s to complete the data collection for a single channel of the image.

As a rule of thumb, if possible all images should be averaged at least by a factor of 2 to reduce noise. In samples where S/N ratio is a significant problem and the fluorochromes are stable, averaging of more frames improves the image quality, but the compromise of S/N ratio versus sample stability and time should always be a primary consideration when establishing the number of frames averaged. (Table 9.1)

9.8.5 Scan Control Mode: Summing and S/N Ratio

In addition to averaging the line or frame scan, it is also possible to sum the pixel values from multiple scans (Fig. 9.16). This can be advantageous when imaging samples with a low signal, but several precautions are in order. First, by adding pixel values, it is possible to misrepresent the data and make it appear as though much more fluorescence is present than can be seen through the microscope. This can be particularly misleading when comparing data from different data sets if different values for summing are used on the different samples. Second, areas of the image can quickly reach maximum pixel values (255 or 4,095) resulting in the loss of fine details in the image in areas where all pixels are white as shown in Fig. 9.2. Third, noise values are also summed. While this may not be a factor at a specific pixel location, overall summed images appear noisier due to the likelihood of noise occurring at multiple pixel locations during several scans as shown in the bottom image of Fig. 9.16. Fourth, as above with the averaging function, scan times can be significantly prolonged resulting in specimen damage.

9.8.6 Scan Control Menu: Bit Depth

As discussed in Chap. 6, pixel bit depth is also an important consideration when scanning a specimen. Many systems have the option of scanning at 8 or 12 bit levels of information (Fig. 9.13). While intuitively one might always want to select the

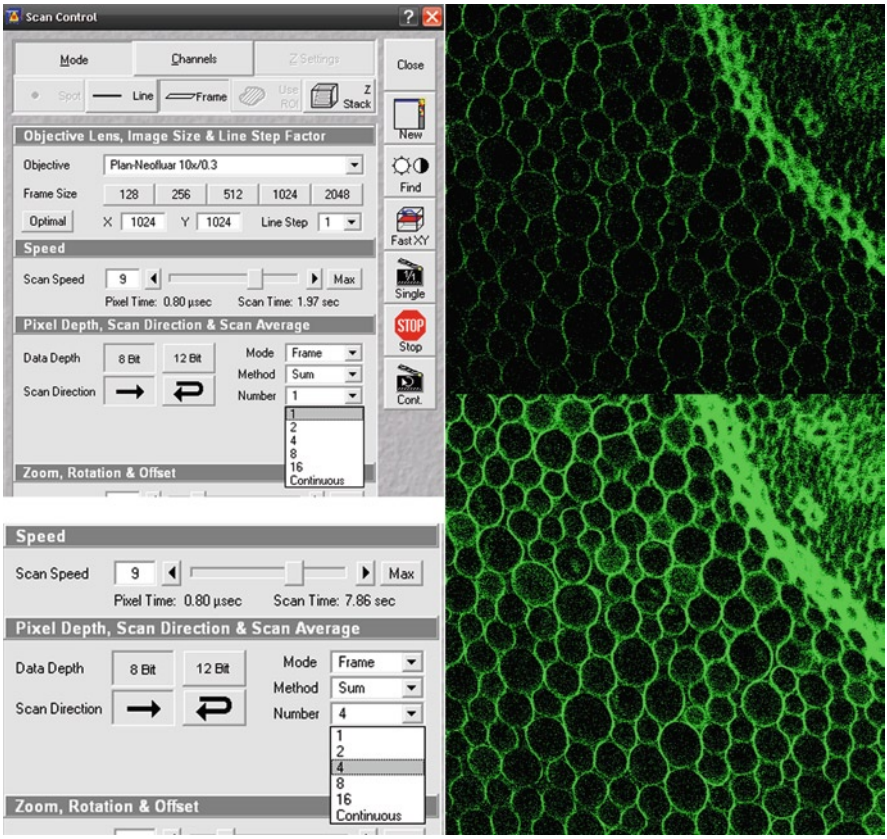

Fig. 9.16 Summing of images results in an overall improvement in signal but the noise level also increases as shown in a comparison of the *top* image which was collected with a single scan and the *bottom* image which represents a summed image of four scans

option to scan for the collection of 12 bits to increase the information available in an image, many of the above considerations on file size should be considered. File size of a single optical section can double in size when scanning at bit depths of 8 and 12, respectively. For example, when exported as a Tif file, file size for an 8-bit image collected at 1,024 × 1,024 was 3,077 kb. With the same imaging parameters but collected at 12 bits, the exported Tif file was 6,153 kb in size. When imaging multiple channels in a large Z-series, this may become a major factor in being able to process images in many enhancement and analysis programs.

The major advantage of scanning at a bit depth of 12 is the increased information available in the data set for quantitative experiments. However, if the end point of the experiment is a qualitative assessment of the data, scanning at a bit depth of 8 typically provides more information than the human visual system can interpret and is an option to reduce file size.

9.8.7 Scan Control Mode: Unidirectional Versus Bidirectional Scanning

We have already identified several mechanisms available in the scan control menu for increasing scan speed that may be used to image events that occur fairly rapidly. During standard scanning of a sample, a unidirectional scan pattern is used in which the laser is scanned from side to side across the sample and is then blanked as it returns. All of the scanning times identified above are based on a unidirectional scan pattern. To decrease the amount of time it takes to scan an entire frame, it is also possible to use a bidirectional scan pattern in which the beam is not blanked, but scans across the sample in both directions. This results in some image distortion which must be corrected by adjusting the scan correction X and Y controls as shown in Fig. 9.17. However, bidirectional scanning reduced the scan time in half as shown in Fig. 9.17 in which unidirectional scanning at a speed of 7 resulted in a frame collection time of 3.93 s and a bidirectional scan resulted in a frame collection time of only 1.97 s.

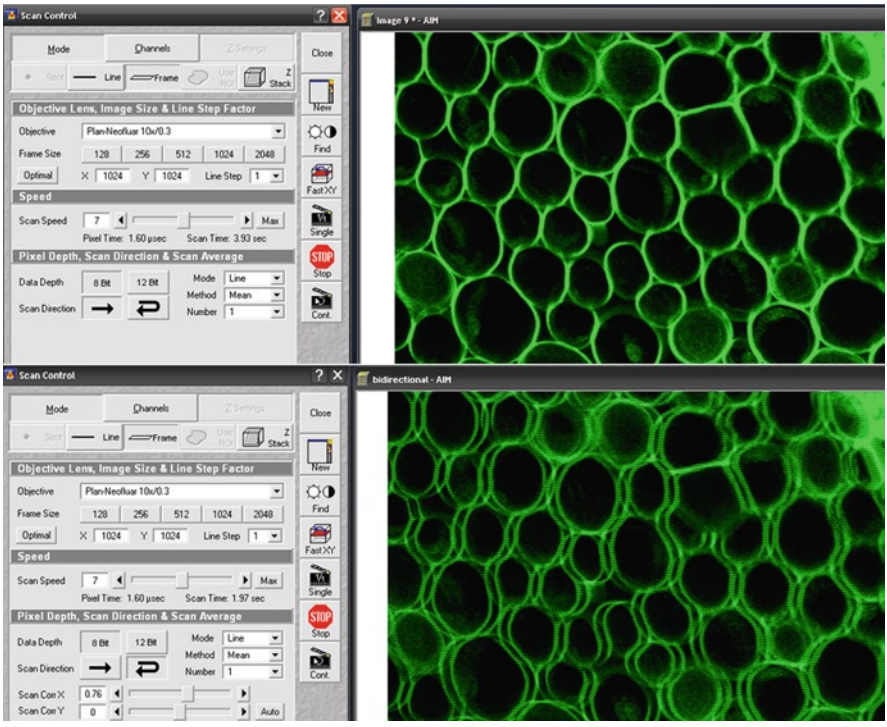

Fig. 9.17 Bidirectional scanning reduces scan time in half, but introduces distortion in the image as shown in the *bottom* panel. This distortion must be corrected by the use of the scan correction X and Y controls to bring the image back into register as shown in the *top* panel

9.8.8 Scan Control Mode: Region of Interest Scanning

An additional method of imaging rapidly occurring events is to scan small regions of the sample with the AOTF as discussed in Sect. 3.6.2 and shown in Fig. 3.14. ROI scanning utilizes the AOTF controls of the laser to scan a specific area of the sample rather than scanning an entire frame. In Fig. 3.14, a circular ROI and a hand-drawn ROI are scanned while the areas outside of the selected ROIs are not scanned. This is an excellent mechanism to minimize specimen damage outside the ROI and to increase scan speed, which depends on the size of the ROI. Total scan time also depends on the above factors, such as scan speed and resolution.

9.8.9 Scan Control Mode: Zoom, Rotation, and Offset

The Zoom, Rotation, and Offset functions are valuable when framing a specimen and when electronically increasing or decreasing the magnification of a sample. Figure 9.18a show images at a zoom of 1.0 but rotated approximately 90° to frame the image differently. This is often useful when organizing a plate of images collected from different samples so all orientation of structures is the same. By increasing the zoom factor above 1.0 as shown in Fig. 9.18b, it is possible to increase the magnification of the image by scanning a smaller area of the sample and projecting onto the fixed sized PMT. Once the image is zoomed, it is also possible to move across the sample to image different regions. The area of the sample scanned is indicated in the box in the Zoom, Rotation, and Offset window. However, increasing the zoom factor by a large degree may introduce some blurring of edges as shown in the top panel of Fig. 9.18c which is zoomed to a factor of 4×. When an increase in magnification of this order is necessary, pixel resolution can be increased with the limitations of file size and scan times as noted above. However, if a large increase in magnification is needed, this should be performed by using an objective of higher magnification rather than electronically. Finally, it is also possible to electronically decrease the magnification to scan a larger area of sample as shown in the bottom panel of Fig. 9.18c, where the scan was performed at a zoom of 0.7×. This function can be very useful when collecting low magnification survey images and when magnifications intermediate between available objectives are beneficial.

9.9 Scan Control Channel Functions

The Scan Control Channel menu provides control for adjustment of the pinhole and detector settings. For ease of use, there is also redundant control for the AOTF functions which are also found in the Configuration Control menu.

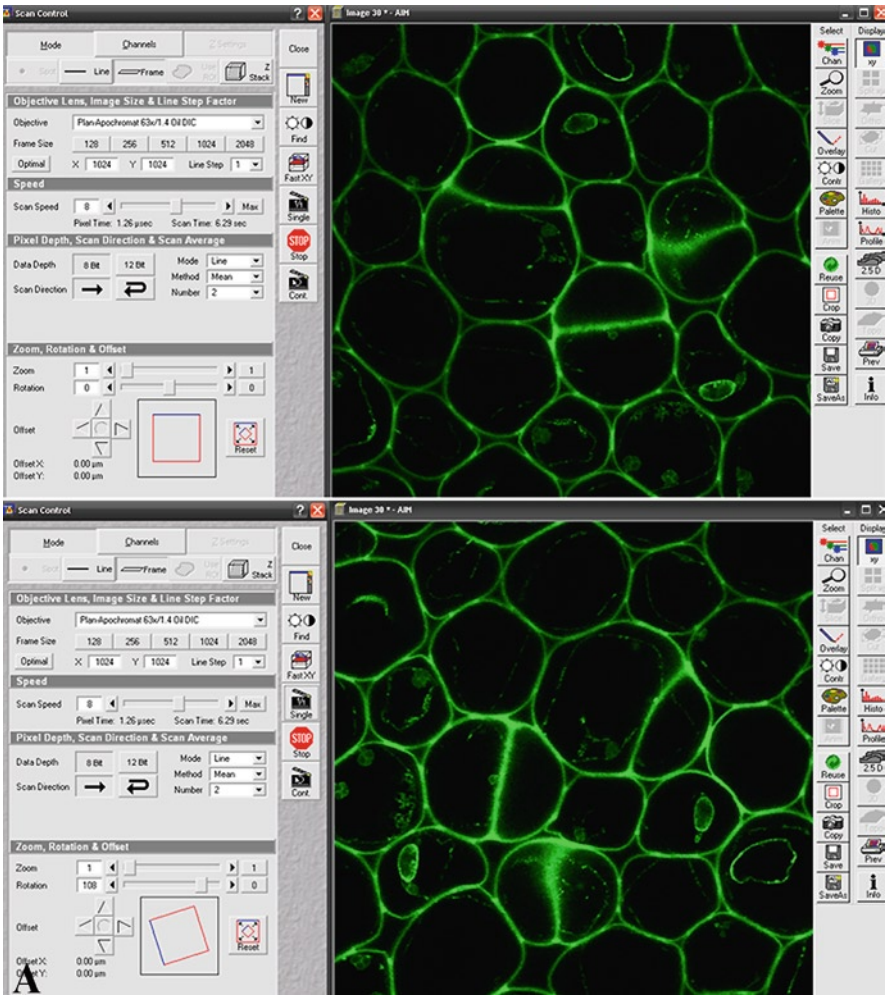

Fig. 9.18 The zoom, rotation, and offset functions can be very useful for electronically adjusting the magnification and framing of an image for presentation purposes. (**a**) Image rotation for framing. (**b**) Image zoom by a factor of 2 and scanning of different regions based on the area of the PMT used as shown by the position of the red box in the Zoom, Rotation, and Offset window. (**c**) High levels of zoom may result in loss of image sharpness as shown by the zoom factor of 4 in the top panel while lower magnification can also be obtained by setting the zoom factor below 1 as shown in the bottom panel

9.9.1 Scan Control Channel: Pinhole Settings in a Single Channel Image

Setting the pinhole diameter is one of the most important decisions made when imaging a sample. Adjustment of the pinhole can directly affect image resolution, S/N ratio, quantitative analyses of structure size, and interpretation of colocalization

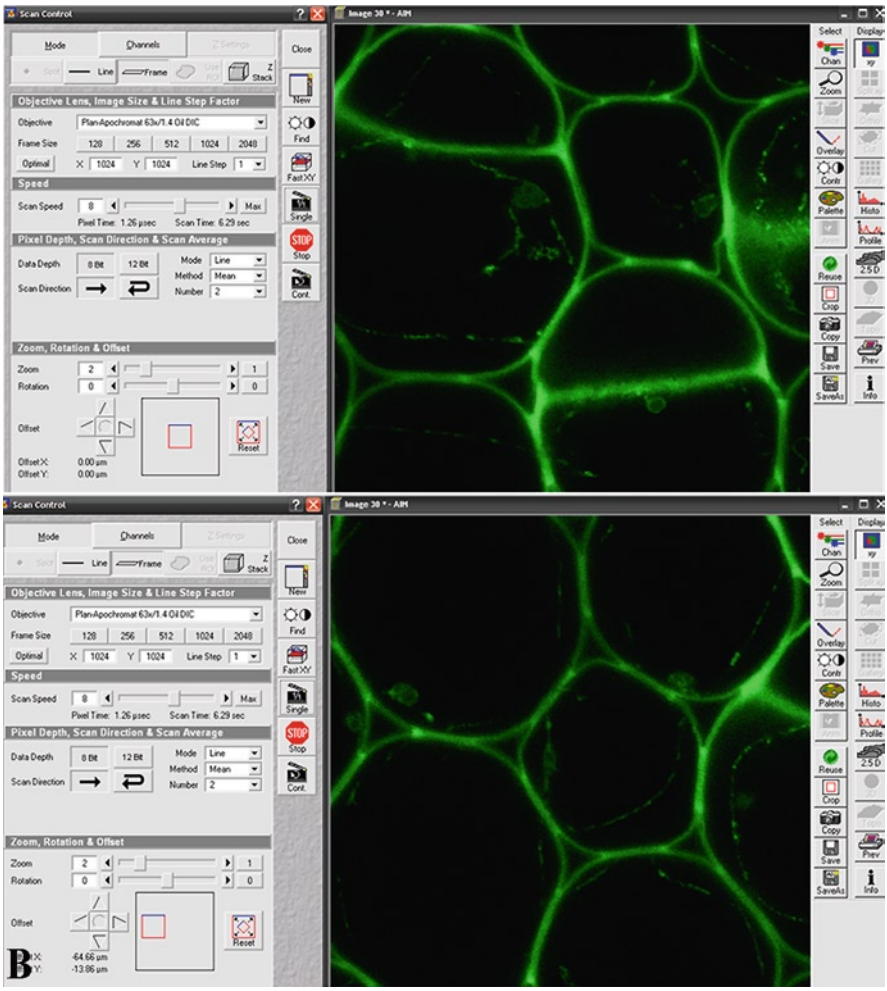

Fig. 9.18 (continued)

data. Since the effects of pinhole diameter adjustment occurs after the interaction of the laser with the specimen, effects on specimen damage are indirect. For example, increasing the size of the pinhole improves the S/N ratio and allows reduced laser intensity and/or scan time which can protect the specimen from laser damage. However, this results in less than optimal resolution if the pinhole size is larger than 1 AU (see Chap. 7 for discussion of resolution and Airy Units (AU)).

Figure 1.3 illustrates the differences in contrast, brightness and resolution between images of the same sample collected with a wide field fluorescent microscope and a confocal system. As discussed in Chap. 1, images collected by wide-field fluorescence imaging include photons from the entire thickness of the sample. This results in a large percentage of the photons in the final image being collected

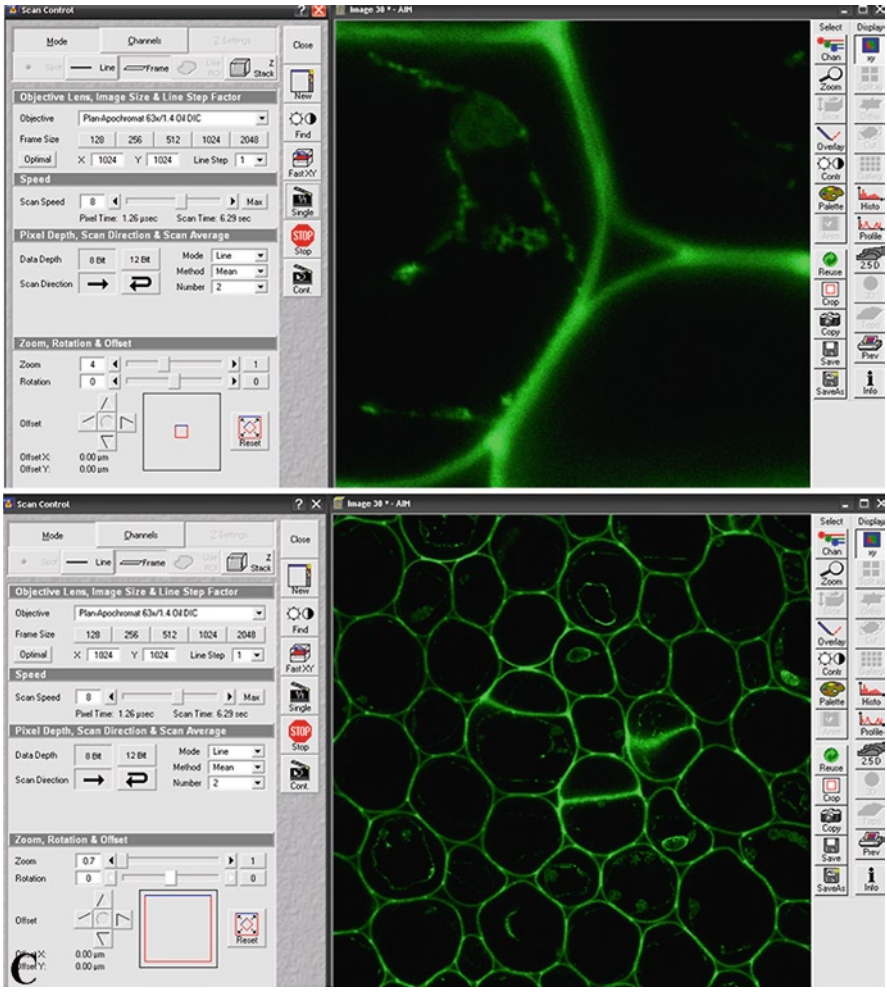

Fig. 9.18 (continued)

from out of focus regions of the sample. When the pinhole of the confocal system is set to 1 AU, the resulting image is of optimum resolution and contrast with respect to focused information being collected from the sample. If all other factors are held constant, opening the pinhole increases the signal (brightness) of a confocal image, but decreases contrast and Z-resolution due to inclusion of information in the image from out of focus areas of the sample.

This is illustrated in Fig. 9.19 which shows images collected at pinhole diameters of 1 and 2 AU. Note that in this example all detector and laser settings were held constant. At 1 AU, the signal is set relatively low to demonstrate that by increasing the diameter of the pinhole more signal is present and the image is brighter. As the pinhole diameter doubles, the optical slice thickness also increases

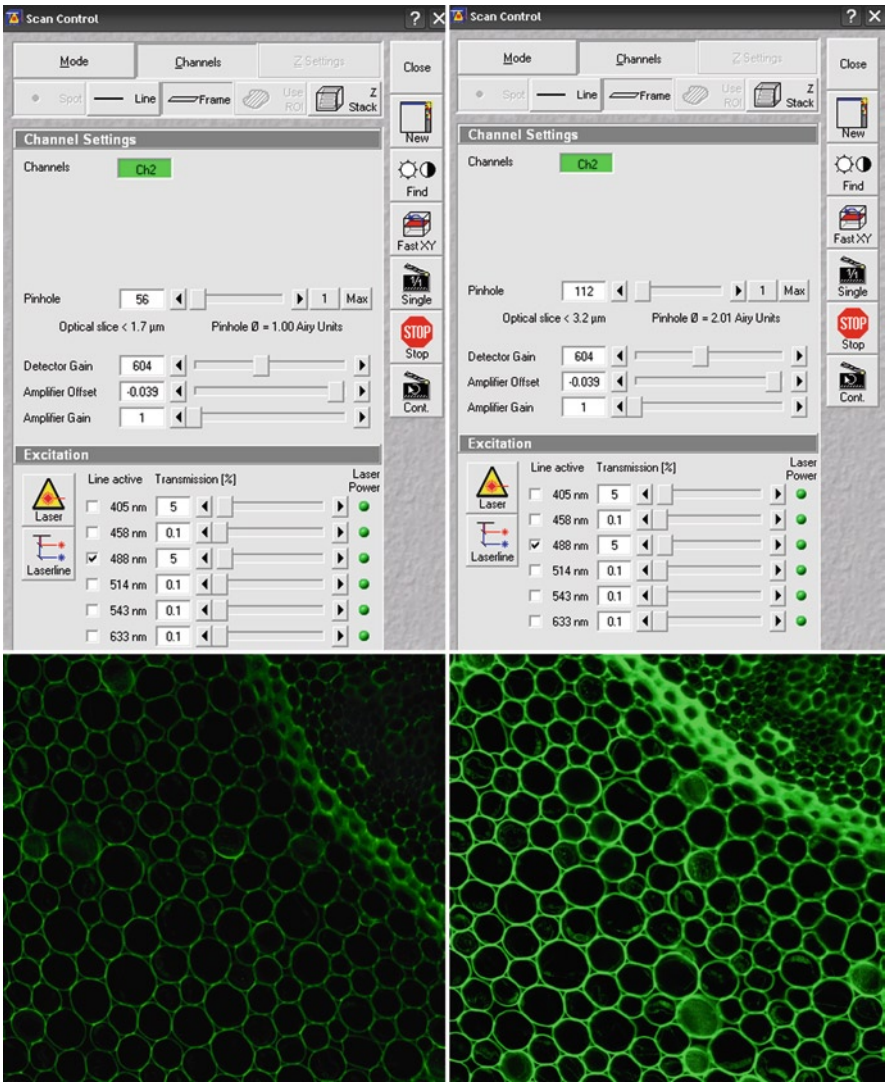

Fig. 9.19 Comparison of image brightness and resolution when collected at pinhole settings of 1 AU (*left*) and 2 AU (*right*). Opening of the pinhole results in increased signal, but the additional photons come from out of focus planes resulting in some loss of resolution which is noticeable along the cell walls of the Convallaria. Opening the pinhole from 1 to 2 AU results in an increase in the optical slice thickness (Z-resolution) from 1.7 to 3.2 µm

from 1.7 to 3.2 µm allowing photons from out of focus regions of the sample to contribute to the final image. Although some of the signal is contributed from out of focus regions, even when using suboptimal settings of the pinhole (above 1 AU), image resolution and contrast are greatly improved over that of widefield images.

Adjusting the pinhole above 1.0 AU can also be useful for improving the S/N ratio of samples that have low levels of fluorescence or are sensitive to moderate to high levels of laser exposure. By increasing the pinhole to an AU above 1.0 to improve the S/N ratio, laser intensity can be decreased and scan speed increased. Both factors protect the specimen from the effects of photobleaching and involve some of the many compromises in confocal imaging as shown in Table 9.1.

9.9.2 Pinhole Settings in a Multichannel Image

When collecting multichannel images in systems with multiple pinholes, artifacts introduced in colocalization and multichannel volumetric studies as a result of changes in pinhole diameter are often not recognized. As discussed in Chap. 2, fluorochromes have different physical properties associated with their specific wavelengths. This affects resolution in the X–Y and Z dimensions. As wavelength changes with the selection of different fluorochromes, if the pinhole diameter for each channel is set at 1 AU for optimal contrast and resolution as shown in Fig. 9.20, the optical slice thickness or Z resolution varies in each channel due to the properties of the various wavelengths of light being used. For example, for the image shown, if the pinhole is set at 1 AU for each of the four channels used in collecting an image with the 63 × 1.4 NA objective with the 405, 488, 543, and 633 lasers available on the Zeiss LSM 510 META system used in these studies, resulting optical slice or Z-thicknesses are 0.6, 0.8, 0.8, and 1.0 μm, respectively. This would result in a study where each channel in the image would consist of different optical slice thickness and could lead to the wrong interpretation of colocalization data or result in difficulty performing 3D reconstructions of Z-stacks.

In this situation, a recommendation is to image all channels at the same Z resolution. This may sacrifice image contrast and resolution since some images are collected with a pinhole setting of larger than 1 AU as shown in Fig. 9.21. In this situation, it was necessary to set the pinhole at 1 AU for the image collected in the 633 channel as above, but to maintain an optical slice of 1 μm in all channels it was necessary to increase the pinhole to 1.2 AU for the 543 channel, 1.42 AU for the 488 channel, and 1.7 AU for the 405 channel. In this situation, it is best to set the optimal contrast and resolution (1 AU) for the longer wavelengths of photons being used. If the short wavelengths of light are set at 1 AU, the pinhole may be very small for the longer wavelengths which can adversely affect the S/N ratio.

9.9.3 Scan Control Channel: Detector Gain and S/N Ratio

In the above examples, all detector and laser settings were held constant while only the pinhole diameter was increased to improve the S/N ratio. The compromise made was the loss of resolution (Table 9.1). If high resolution is essential, it is also possible to increase the brightness of the image by adjusting the Detector Gain so

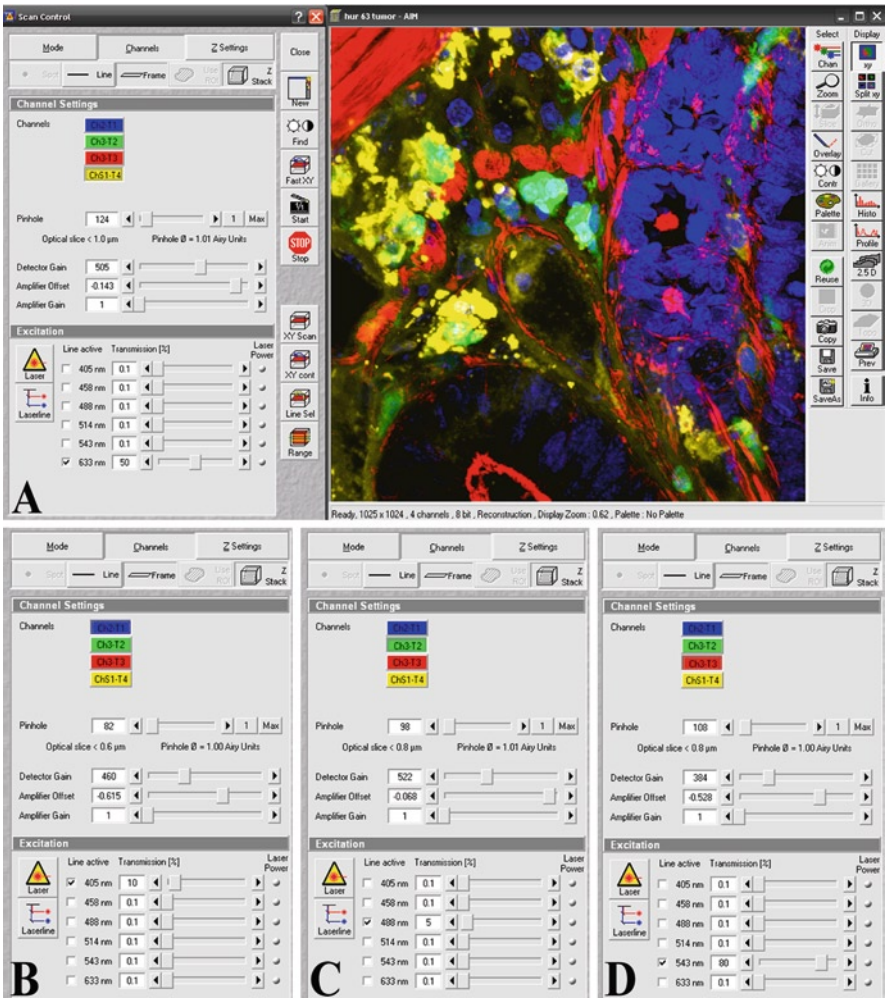

Fig. 9.20 In multichannel images, if the pinhole is held constant, optical slice thickness will vary which can affect interpretation of colocalization data and reconstruction of Z-series. (**a**) Image data for the 633 nm laser channel at 1 AU and optical slice thickness of 1.0 mm. (**b**) Image data for the 405 nm laser channel at 1 AU and optical slice thickness of 0.6 m. (**c**) Image data for the 488 nm and (**d**) for the 543 nm laser channels where optical slice thickness is 0.8 mm

that it takes fewer photons to saturate the PMT as shown in Fig. 9.22, where the gain was increased from a setting of 604 to 700 which results in a much brighter image when all other parameters are held constant. The disadvantage of increasing the detector gain is that fewer photons (signal) are required to form the image which may result in a poor S/N ratio as shown in Fig. 9.15. If a poor S/N ratio results, it may still be possible to average the image as shown in Sect. 9.8.4 to improve image quality. Even though a poor S/N ratio may result, increasing the gain is a

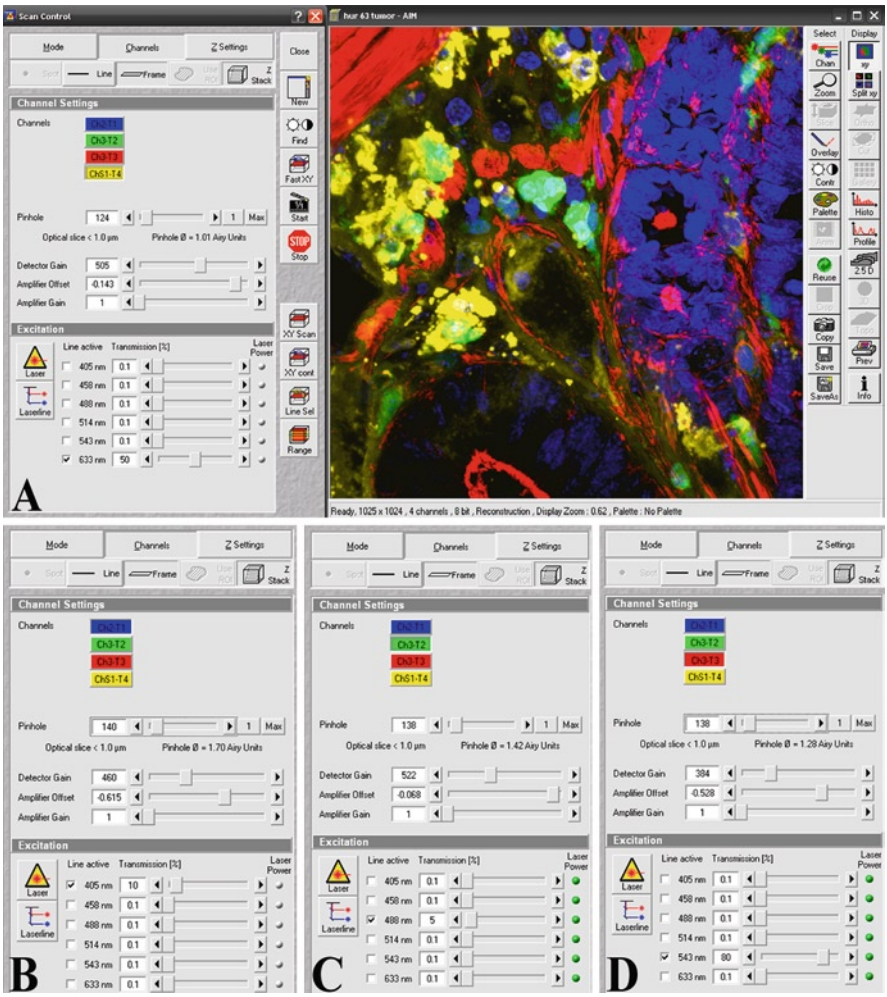

Fig. 9.21 To maintain an optical slice thickness of 1.0 µm, it is necessary to increase the pinhole diameter as laser wavelengths change as shown for the 633 (**a**), 405 (**b**), 488 (**c**) and 543 (**d**) nm lasers

compromise that can be made to improve the brightness of the image and allow scan speed and/or laser intensity to be reduced as a mechanism to protect the sample from photobleaching (Table 9.1).

9.9.4 Scan Control Channel: Laser Transmission and S/N Ratio

If it is not possible to increase Pinhole Diameter or Detector Gain to produce an image with sufficient signal, another option is an increase in the number of

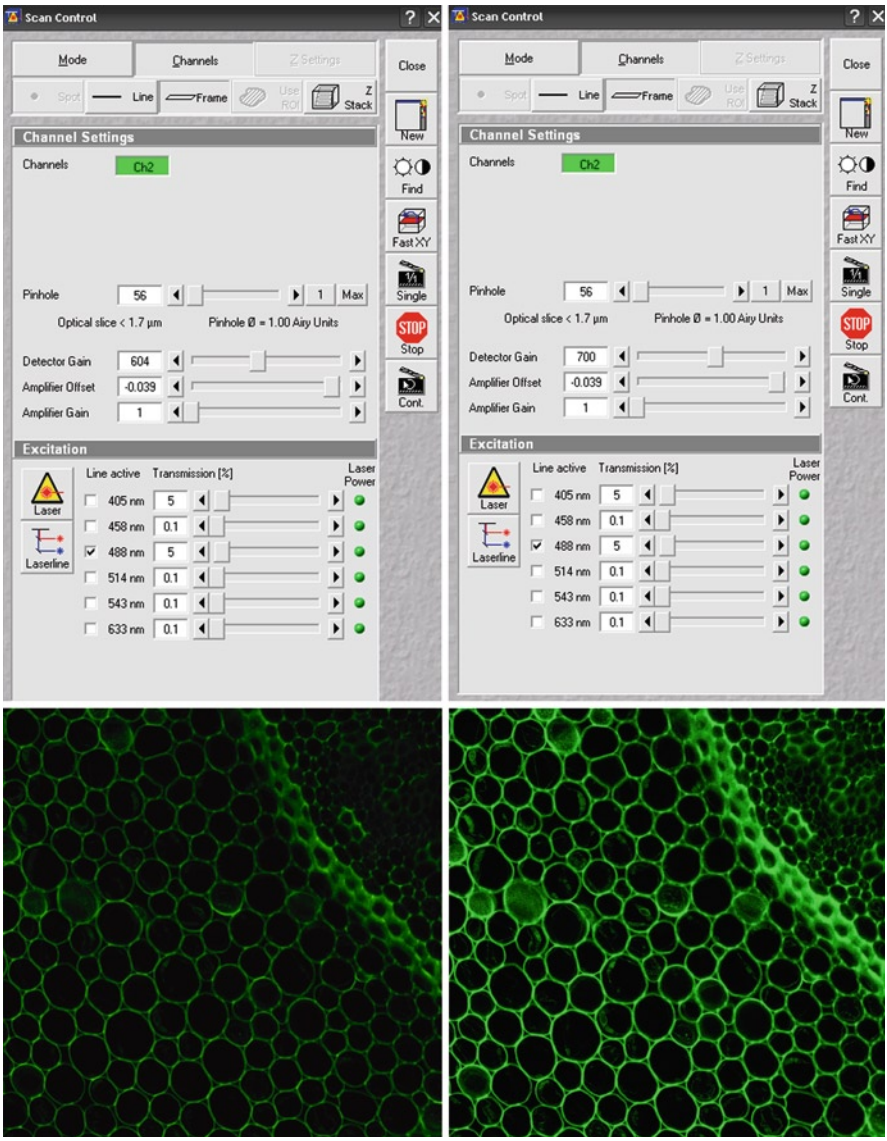

Fig. 9.22 The PMT may be made more sensitive to light level by increasing the detector gain. As the gain is increased, fewer photons (signal) are required to saturate the detector and thus the S/N ratio is decreased and a noisy image may result

excitation photons from the laser which are allowed to interact with the specimen. This is accomplished by adjusting the transmission percentage with the AOTF as shown in Fig. 9.23, where the AOTF was adjusted from a Transmission

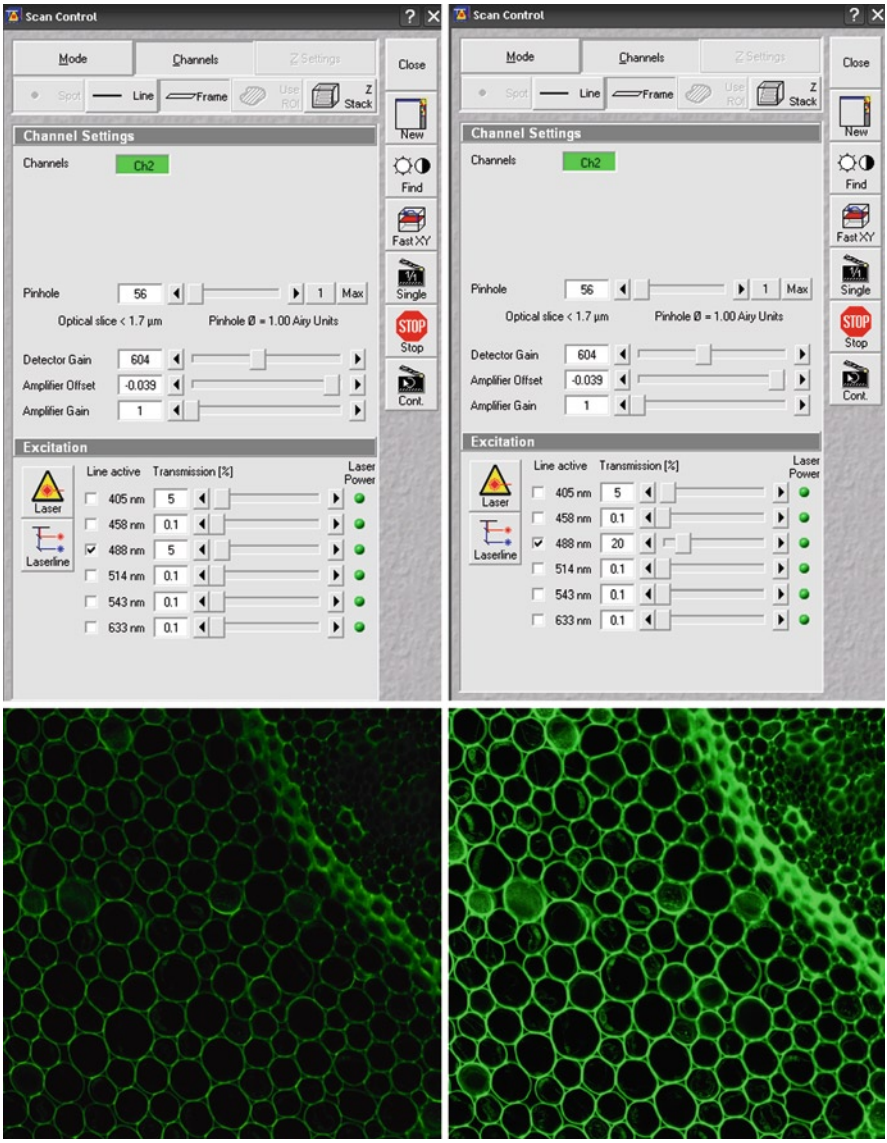

Fig. 9.23 Increasing laser transmission may also be used to improve signal in the image, but this is at the expense of increased specimen damage. The left panel shows an image collected at a laser transmission of 5% and the right pane an image at a laser transmission of 20%

of 5–20% to improve the signal in the image. The compromise for the increased signal is an increase in specimen damage as a result of photobleaching or cell death (Table 9.1).

9.9.5 Scan Control Channel: Amplifier Offset and Gain and S/N Ratio

Improper adjustment of the signal level with the pinhole, detector gain, and/or laser transmission may result in large numbers of pixels in the black (0) range if the signal is too low, or conversely a large number of white (255) pixels if the signal is too high. The amplifier offset and gain functions may be used to adjust the black-level of an image to bring out information in regions with low pixel values. The amplifier settings should be used in conjunction with the pinhole, PMT, and laser settings to establish imaging conditions in which the full dynamic range of pixel values are present in an image as shown in Fig. 9.2 and discussed in more detail in the next section the use of LUTs.

9.10 Image Enhancement and Analysis Software

At this point, a basic understanding of how to collect an image has been presented. Before going further, a discussion of the available software for setting up an image correctly and the subsequent enhancement and analysis of the image is necessary. Figure 9.24a shows a two channel (red and green) image of Convallaria in the image window with image enhancement and analysis software functions located on the right side of the window. Figure 9.24b shows an enlargement of the text for the various software functions. In this version of software, these functions are organized into five columns: Select, Display, Overlay, Channels, and Slice. By choosing an icon in the Select Column, one can open the other columns or perform the selected function, such as saving an image. For example, using the mouse to select the Chan icon opens up the Channels Column to provide access to each of the channels in the image by then selecting the red, green, or mono (grayscale) icon. Clicking on the same icon a second time closes the icons in the selected column. The following sections discuss each of these software functions in detail.

All confocal software programs have the same basic functions as shown in the five columns in this program. In some, individual windows must be opened to access the functions while in others they remain open. For the most part, it is simply a matter of becoming familiar with the location of various functions within the programs.

9.10.1 Enhancement and Analysis: Channels and Image Presentation

With the Channels Icon activated as shown in Fig. 9.24, each channel can be accessed by clicking on the appropriate color. Note that, as for the situation with the lasers, the colors represent pseudo colors. It is possible to change the color of

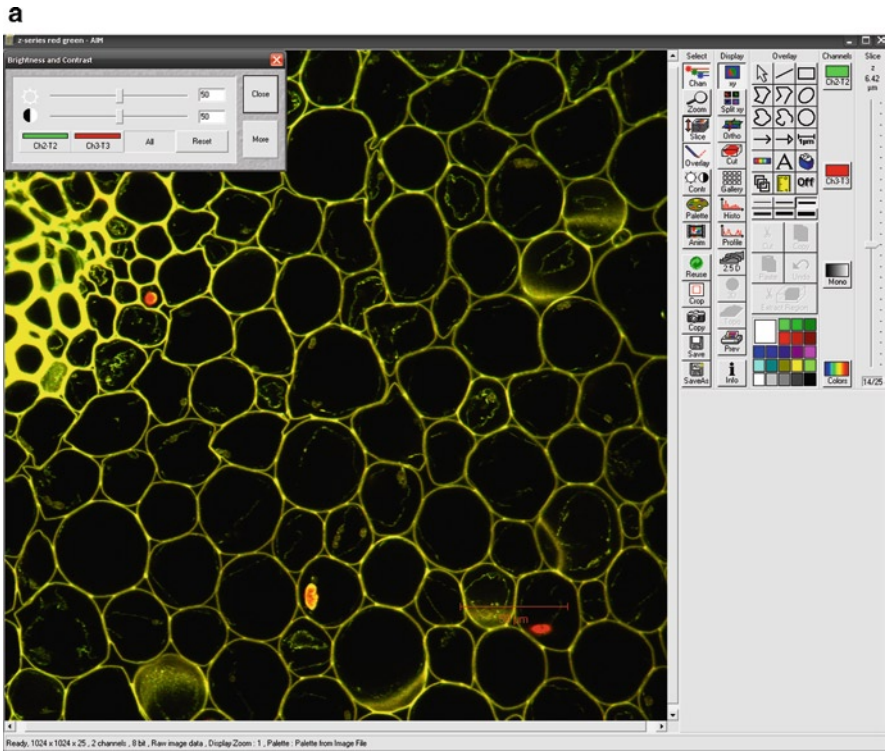

Fig. 9.24 Overview of the image display, analysis, and enhancement functions in the software using a *red/green* Convallaria example. (**a**) shows the image and controls while (**b**) shows an enlargement of the controls referred to in the text

each channel by clicking on the color which opens a color LUT which can be used to change the assigned color. Worth noting is that changing the color of the image here affects only the active image. Changing the color of the image at the level of the PMT as shown earlier affects all images collected with that particular laser.

By activating the Display XY icon in the second column, all channels in the image are merged into a single image as shown in Fig. 9.24. By activating the Split XY icon in the second column, each channel is shown individually and a merged channel is shown in the last position (Fig. 9.25). The Zoom icon allows the size of the window and image to be adjusted in various frames.

9.10.2 Enhancement and Analysis: The Z-Slice Icon

When activated, the Z-slice icon provides access to the Ortho, Cut, Gallery, and Animate icons in the Display Column as well as the Z-Slice bar in Column 5. The Z-slice bar allows the selection of each image in the Z-series for further analysis.

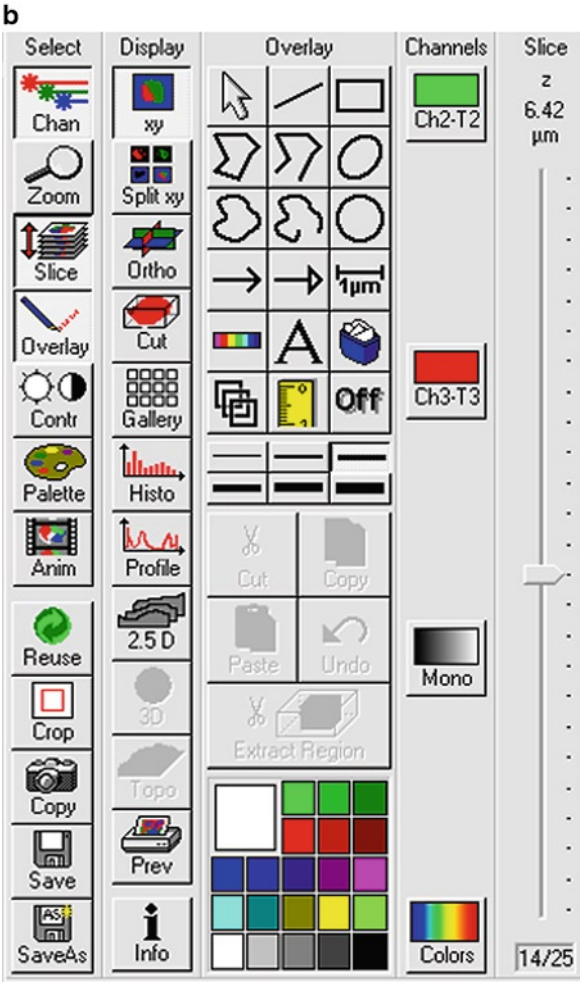

Fig. 9.24 (continued)

For example, section 14 of 25 is shown in Fig. 9.24b which allows analysis of this image separate from the other images in the Z-series. These functions are discussed further in the section on collection and analysis of Z-stacks.

9.10.3 Enhancement and Analysis: The Overlay Icon

The overlay icon provides several functions for annotating images, including text, arrows, and scale bars. Several controls within the overlay function allow adjustment of colors, fonts, line size, etc. In Fig. 9.24, the Overlay menu has been used to add a scale

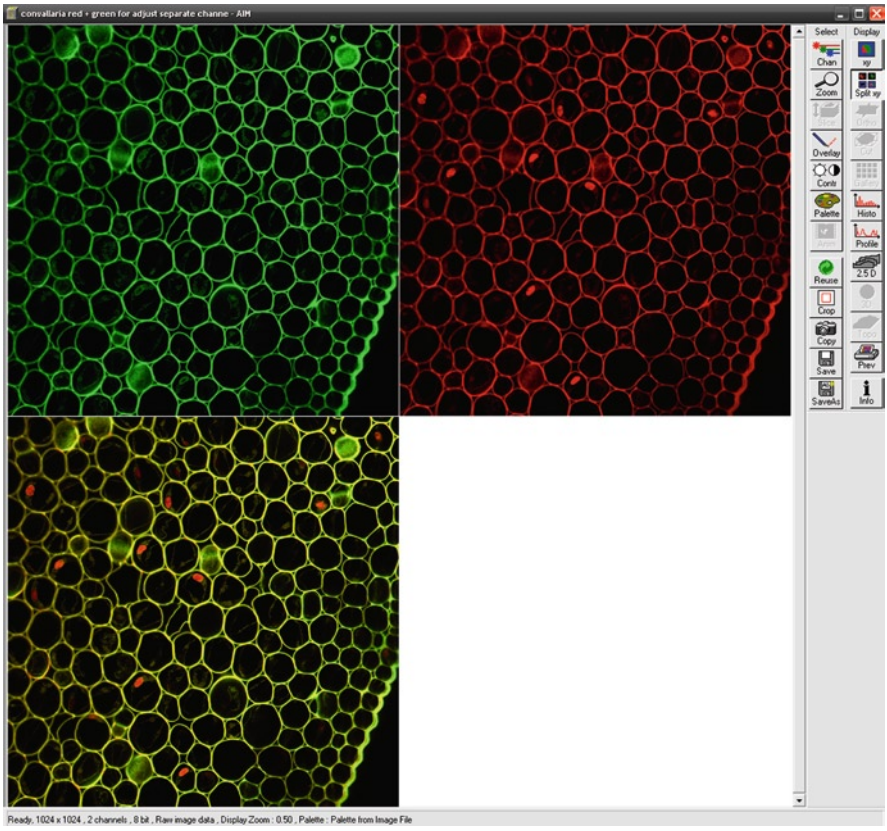

Fig. 9.25 Individual channels and a merged image can be seen by selecting the split XY icon in the display column as shown in Fig. 9.24b. In the example shown, the *green* and *red* channels are shown in the *top* panel and the merged panel on the *bottom left*. If additional channels are imaged, additional windows showing each channel will also be opened

bar to the image. While many of these functions are useful when viewing images, it is often beneficial to add annotations in programs, such as Photoshop, Image Pro, Metamorph, or Image J, following the final setup of images for presentation.

9.10.4 Image Enhancement and Analysis: The Contrast (and Brightness) Icon

Selecting the Contrast and Brightness icon (Fig. 9.24) opens a window shown in the upper left of the image which allows adjustment of single and combined (All) channels of the image. As noted in the chapters on digital imaging, care should be taken when adjusting the contrast and brightness of an image and often these functions should be

avoided since gamma adjustment in programs, such as Photoshop, provide better controls for adjustment of pixel values. It is also important when adjusting individual channels to make sure relationships between pixel values in different channels are not altered. It is very easy when adjusting a single channel to increase the brightness and/or contrast to the point where other channels in the image are either blocked or become more prevalent. In the next section, the proper method of setting the correct dynamic range (pixel values) in an image is discussed extensively. If done properly, adjustments in image contrast and brightness to improve the appearance of an image should be minimal or not required.

9.10.5 Image Enhancement and Analysis: Setting the Dynamic Range of Pixels in an Image

At this point, we have presented several mechanisms to improve the S/N ratio present in an image as well as several compromises that must be considered with respect to specimen damage versus image quality (Table 9.1). If the definition of a good confocal image is one that utilizes the full dynamic range of pixel values in the available bit depth of an image, how can the operator quickly and efficiently set up the microscope to reach this goal as shown in the image of filter paper in Fig. 9.2?

As mentioned above, all confocal programs include an LUT which takes advantage of our ability to distinguish color. Figure 9.24 shows a portion of the image enhancement and analysis window open in the LSM 510 software and the location of the Palette icon under the Select column on the right of the image. Selecting this icon provides access to the available LUTs in the software as shown in Fig. 9.26. In the Zeiss software, the appropriate LUT is the Range Indicator, although on other instruments this is named something else. These LUTs assign a color (in this case red) to all pixels above a certain color, a different color (blue) to all pixels below a certain value, and a gray tone to all pixels that fall between the upper and lower limits.

In Fig. 9.26a, a four channel image of mouse small intestine is shown with the Palette Window open next to the image. It is important to use the LUTs on all channels in an image to insure that all are collected correctly. In Fig. 9.26b, the green, red, and yellow channels are turned off and the Range Indicator LUT is selected so the dynamic range of the pixels in the blue channel, which is DAPI staining for nuclei, can be seen. As shown, a few red (255) pixels are present on the brightest nuclei, and all other nuclei are a shade of gray. Areas outside the nuclei either appear black or blue representing pixels of very low intensity values since DAPI is specific for nuclear staining. In this case, the lumen of the gut, where no signal should be present, has been set for pixel values of 0 (blue) and other regions slightly above blue to avoid the loss of all signals in some of the nuclei that are not stained as well. Levels of red and blue pixels can be adjusted by the several choices of laser intensity, PMT, and pinhole detector settings discussed above. Any choice that increases signal increases the number of red pixels and any choice that decreases signal increases the number of blue pixels while decreasing the number of red pixels. All compromises

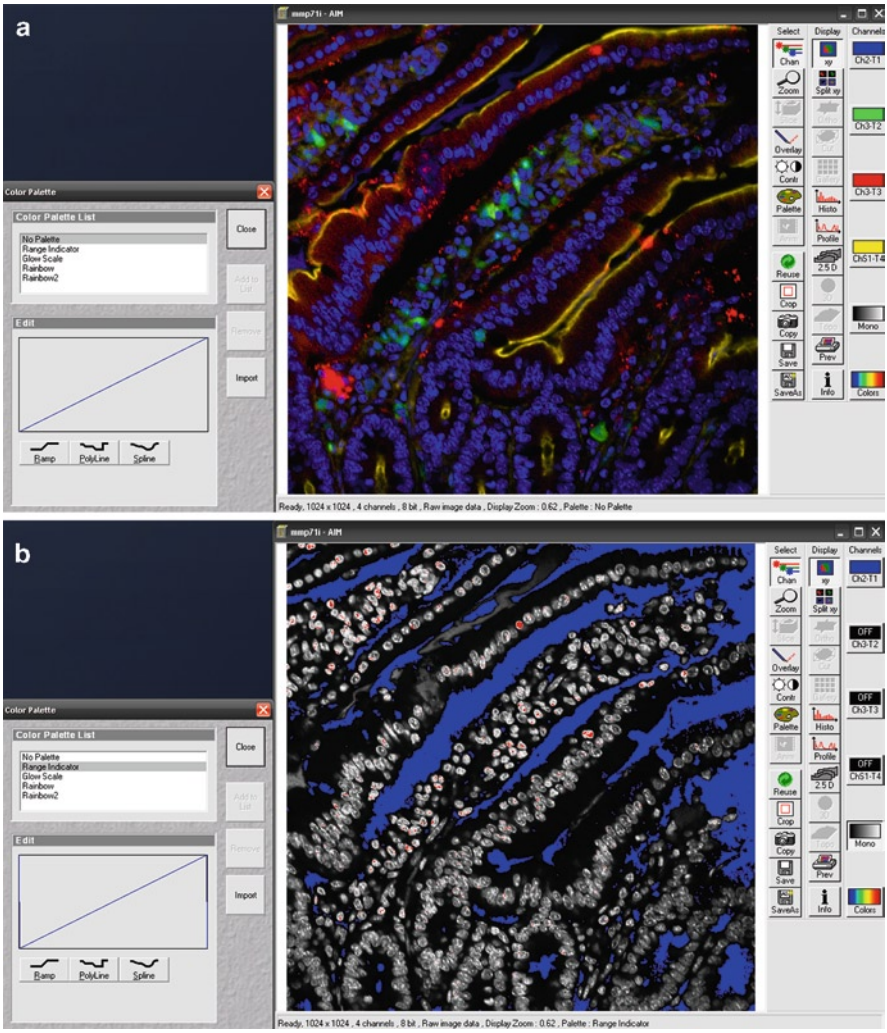

Fig. 9.26 The use of color LUTs or palettes to set the proper dynamic range in images. In (**a**), all four channels are shown in a section of mouse small intestine. In (**b**), only the *blue* channel is shown, and the range indicator palette has been applied, so all pixels of intensity value 0 are seen as *blue*, and all pixels of intensity value 255 are seen as *red* to take advantage of the eye's ability to distinguish color better than *gray* values. The proper dynamic range in an image should include a small number of *blue* and *red* pixels with all others being seen as a shade of *gray*

in setting up the system for image quality versus specimen damage (Table 9.1) come into play at this point when establishing the operating parameters.

Once the dynamic range for the blue channel is set, it is deactivated and one of the other channels set using the Range Indicator Palette. Setting the LUTs for qualitative imaging in this manner is to some extent an art and knowledge of the specimen is

essential. For instance, when imaging a DAPI-stained sample to identify nuclei as shown, we know that DAPI only stains the nucleus. In cases such as this, it may be appropriate to have more 0 value pixels in regions which are known not to stain with DAPI.

While the use of LUTs to set the qualitative properties of an image is important, it is absolutely essential that they are used when quantifying images. Figure 9.27 shows a series of images collected from a 4 μm bead in which the laser intensity and detector settings are identical, but the pinhole is opened from a value of 1 AU through 2, 4, and 8 AU. When measured at 1 AU, the diameter of the beads is 4 μm as expected. As the pinhole is opened the apparent diameter nearly doubles from 4 to 7.5 μm. The appearance of three distinct beads is also lost as the boundaries of the beads run together. The same effect can be generated by leaving the pinhole constant and adjusting either the laser intensity or the PMT gain settings. It is essential

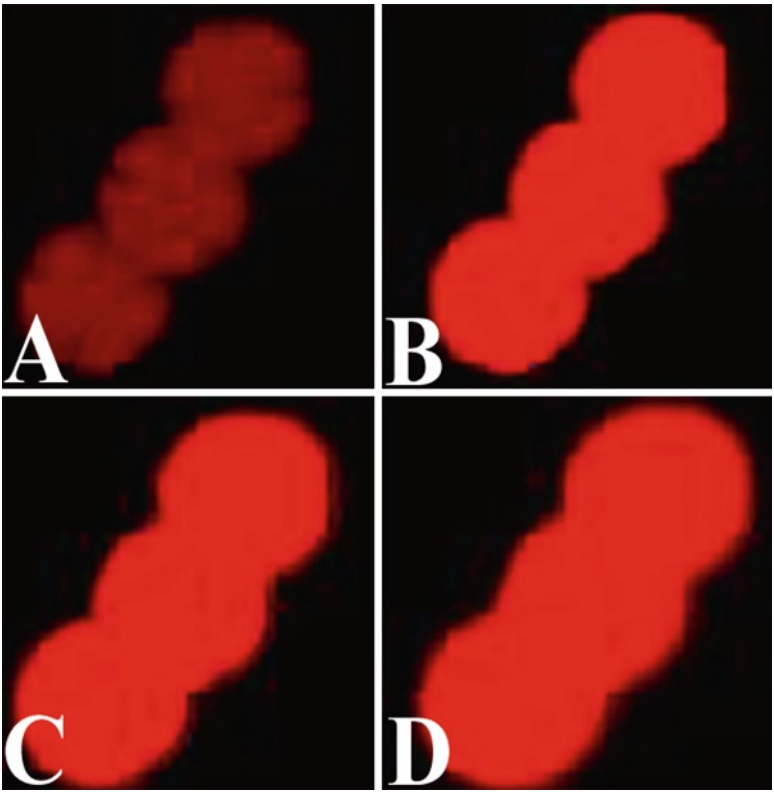

Fig. 9.27 It is essential to use the available LUTs to set imaging parameters correctly. In the example shown, 4 μm fluorescent beads were imaged under the same conditions with the exception that the pinhole was opened 1 AU (**a**), 2 AU (**b**), 4 AU (**c**), and 8 AU (**d**) which increased the brightness and apparent dimension of the beads. The same effect can be seen by improperly setting the dynamic range with the laser intensity and detector controls

that time be taken when setting up imaging parameters to insure that measurement artifacts are not introduced into the image through improper setup of the instrument hardware.

9.10.6 Image Enhancement and Analysis: Histogram Functions

The use of LUTs is an excellent mechanism for setting up qualitative imaging parameters for the overall image. However, at times it may be desirable to also quantify the pixel values in an image for area and colocalization functions, with the caveat that has been mentioned several times that absolute quantification of fluorescence is a difficult task. If quantification is the end point one should definitely utilize LUT as one mechanism for standardizing image collection. As discussed in Chap. 6, once the quanta are defined in a digital image, it is possible to further analyze the data by creating histograms of pixel distributions. In Fig. 9.28, the Histogram icon is activated in the Display column and the frequency of each pixel value in the red and green channels of the Convallaria image is shown. With the Step value set to 1, the Low Threshold to 0 and the High Threshold to 0, all pixel values from 0 to 255 are included in the analysis. In addition, at the bottom of each graph, the minimum and maximum values found in the image are shown. The table includes the number of pixels found at each value for both channels. Although not included here, it is also possible to determine the area (μm^2) occupied by each pixel value. All of this data can be included in a table format which can be saved as text (*.txt) files and exported to spreadsheets, such as Excel, to facilitate quantitative analysis.

A variety of additional histogram analysis functions are often included in confocal programs. Figure 9.29 illustrates a different analysis of the above data by eliminating black (0) pixels from the analysis, binning remaining pixel values into groups of 10, and by thresholding all pixel values below 20 into a single bin at the left of the histogram and all pixel values above 200 in the red channel into a single bin on the right of the histogram. Pixels thresholded below 20 are now shown as blue in the image and those above 200 are shown as red. Even though the histograms in both Figs. 9.28 and 9.29 were generated from the same image, the shape of the histogram and potential conclusions regarding the pixel intensity data have been changed significantly.

The above examples provide data for the overall distribution of pixel values in an image. At times, it is also beneficial to know the exact pixel values at specific locations within an image either during or after collection. In Fig. 9.30, the Profile icon is activated which provides several additional mechanisms for the analysis of pixel intensity distribution and for the measurement of structures. In the example shown, a Profile line has been drawn across several cells in the Convallaria sample and an Intensity graph of the green (Channel 2) and red (Channel 3) channels along the line mapped. The Profile line can be drawn across any region of an image. In the example shown, pixel values (0–255) for both channels are shown on the *Y*-axis

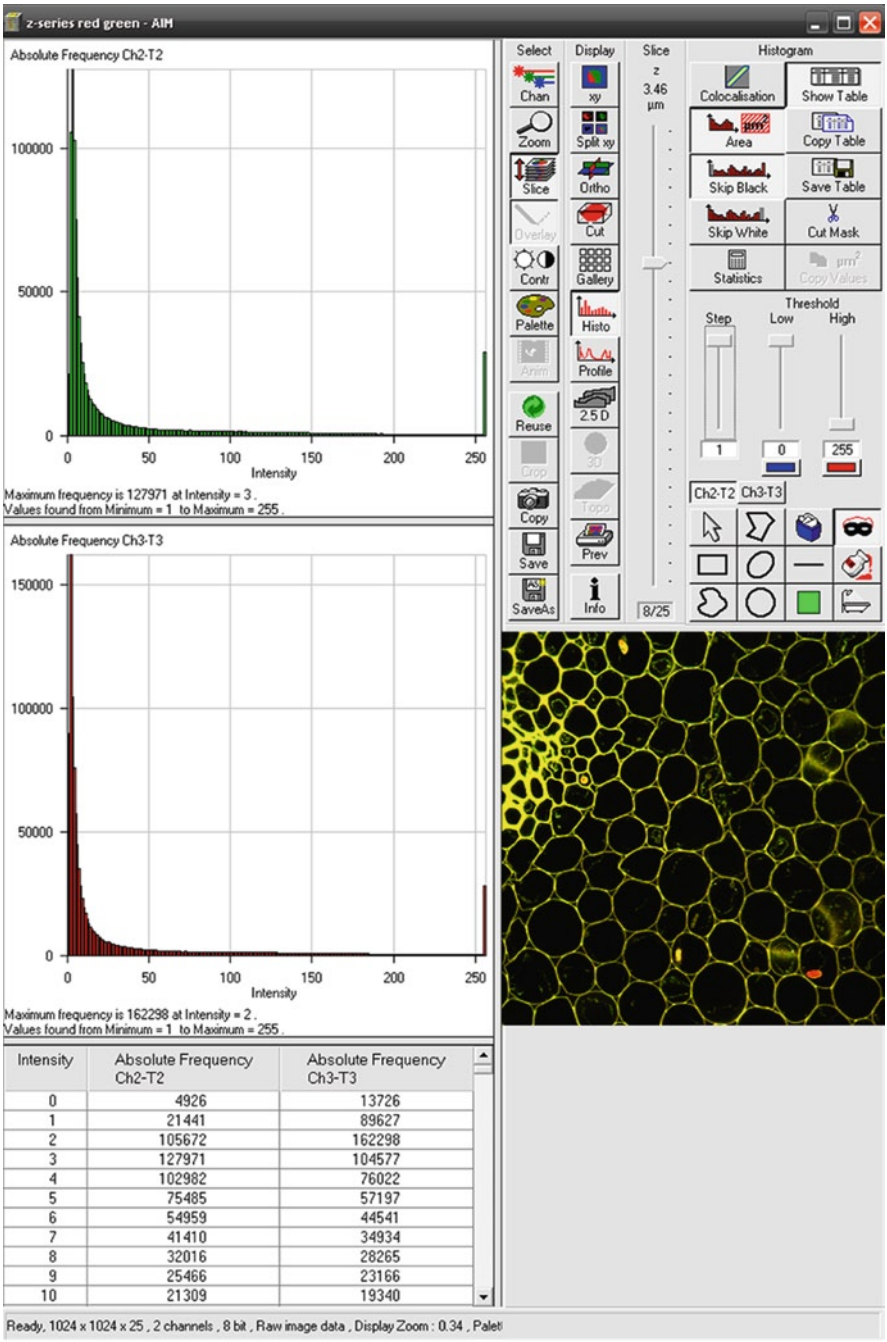

Intensity	Absolute Frequency Ch2-T2	Absolute Frequency Ch3-T3
0	4926	13726
1	21441	89627
2	105672	162298
3	127971	104577
4	102982	76022
5	75485	57197
6	54959	44541
7	41410	34934
8	32016	28265
9	25466	23166
10	21309	19340

Fig. 9.28 Histogram analysis of pixel intensity values in the *red* and *green* channels of a Convallaria image showing the distribution of each value and a table that includes all data. Minimum and maximum intensity values are also given at the *bottom* of each graph

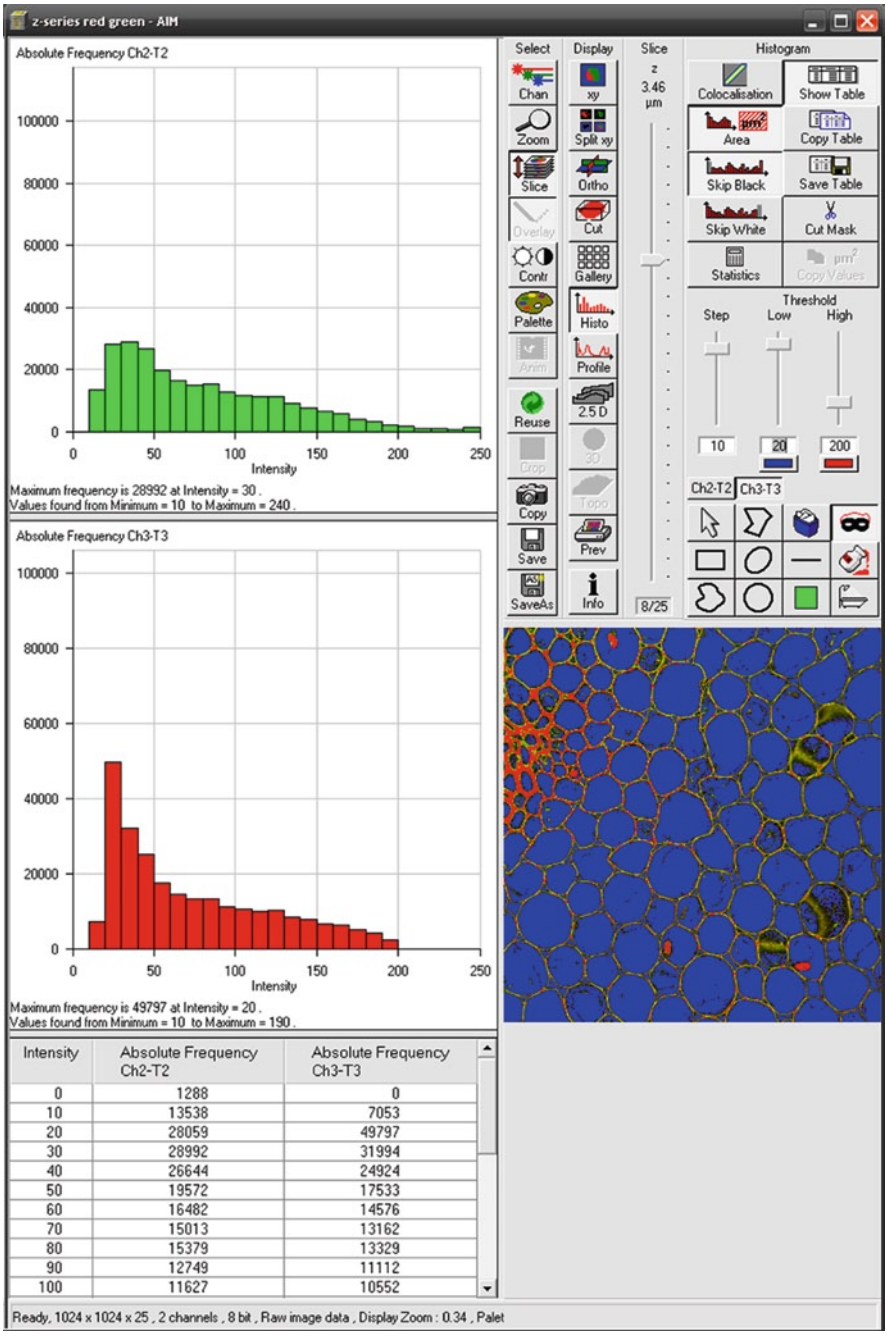

Intensity	Absolute Frequency Ch2-T2	Absolute Frequency Ch3-T3
0	1288	0
10	13538	7053
20	28059	49797
30	28992	31994
40	26644	24924
50	19572	17533
60	16482	14576
70	15013	13162
80	15379	13329
90	12749	11112
100	11627	10552

Fig. 9.29 Histogram analysis on the same image shown in Fig. 9.28, but in this case the step has been set to 10, so pixel intensity values are binned and the threshold *low* and *high* values in the *red* channel have been set at 20 and 200. This eliminates all pixels below an intensity value of 20 and above an intensity value of 200 from the *red* channel analysis. Care must be taken when analyzing pixel intensity distribution data to analyze all channels identically

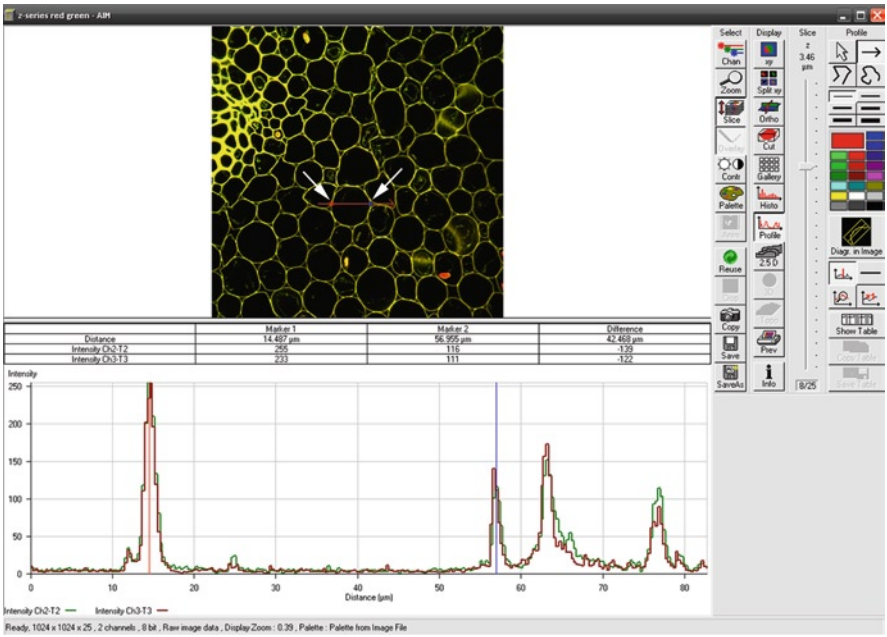

Fig. 9.30 Use of the line profile function to determine pixel intensity values in a specific region of the image and distance across a cell of the Convallaria sample. The line profile allows calipers (*blue* and *red* targets indicated by *arrows*) to be placed on an image and distance between the targets displayed in table format

and the distance across the line in μm is shown on the *X*-axis. The Intensity Profile shows that at most pixel positions values for both channels peak as the line crosses a cell wall and is near zero inside the cells. In addition to lines, boxes or other shapes can also be used to determine pixel values in specific regions of the image.

The profile line can also be used to determine 2D length measurements made by selecting the measurement tool in the Profile icon window. In the example shown in Fig. 9.30, the red and blue targets indicated by the arrows are placed on the edge of a cell and the pixel intensity values and distance between the lines are given for these positions in the Table. The cell being measured is 42.47 μm in diameter. This data can also be exported in table format to Excel spreadsheets facilitating the analysis of large numbers of measurements.

9.10.7 Image Enhancement and Analysis: Colocalization

The Profile lines in the above examples give some indication that pixels in the green and red channels of the Convallaria cell walls are colocalized since, for the most part, both peaks occur at the same position along the line. To further analyze

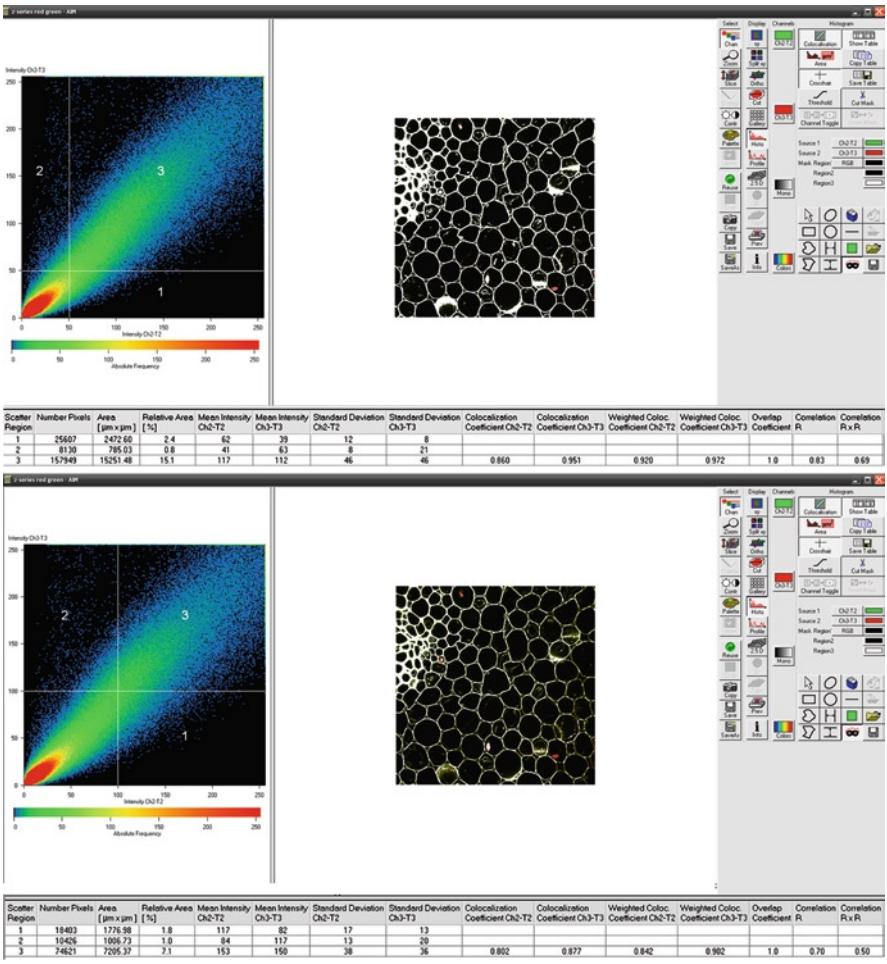

Fig. 9.31 Confocal microscopy frequently involves analysis of colocalization of signal from multiple fluorochromes at a single pixel or voxel location in an image. However, these studies can be somewhat subjective based on selection of pixel values as shown by the different colocalization coefficients when threshold values of 50 (*top panel*) and 100 (*bottom panel*) are selected

colocalization, it is possible to generate scatter plots of pixel values and to determine the number of pixels in an image that have overlapping signals. In Fig. 9.31, a scatter plot is shown in which the colocalization of pixels with values above 50 in the green (channel 2) and red (channel 3) channels is determined. Pixels present in Region 1 are those that have only signal from the green channel and those from Region 2 have signal from only the red channel. Pixels that have a threshold value of 50 or below (primarily black pixels in the image) fall in the region without a number in the bottom left corner of the scatter plot are not included in the analysis. Pixels in Region 3 are those that have values above 50 in both the green and red

channels and are thus determined to be colocalized signal. Note that the selection of the threshold levels, and the resulting determination of colocalization, can be relatively subjective.

The attached tables generated by the software provide a range of statistics used to analyze the image. The colocalization coefficient is a measure of the number of pixels with colocalization when compared to the total number of pixels above the threshold value of 50 or 100. A value of 0 indicates that no pixels have a value of 50 in both channels and a value of 1.0 indicates all pixels in both channels have a value above 50. The weighted coefficient compares the summed pixel values in the channels and provides more weight to pixels with high numerical values (bright pixels) than those with low numerical values. Values of 0 and 1.0 again indicate either no colocalization or 100% colocalization. The Correlation R provides information on the intensity distribution within Region 3. If all pixels have the same intensity value, a straight line would result and the value would be either 1.0 or −1.0. This value is dependent on the setup parameters as noted above. If the channels are set with different image parameters as discussed above when using the Palette LUT, then intensities in one channel may artificially be much different than the other channel. The correlation RXR is an analysis independent of signal intensities in the two channels. As above, a value of 0 indicates that no pixels are colocalized and a value of 1.0 indicates that all pixels are colocalized.

A frequently asked question when working in multiple channels is if two labeled molecules can be considered colocalized based on the observation that red pixels plus green pixels result in yellow pixels (North 2006; Barlow et al. 2010). In the report generated by Barlow et al. (2010), they note that in three high impact journals, Cell, Nature and Science that of a total of 185 published papers with micrographs 96 reported colocalization based on red-green-yellow merge images and only 6 papers reported a quantitative analysis of colocalization. As noted in several examples throughout this book, many factors affect the intensity, resolution, and location of the pixels and voxels in the images generated by confocal microscopy. It is very important that a well-designed quantitative statistical analysis of colocalization is performed prior to concluding that biological molecules are indeed colocalized (Boltes and Cordelieres 2006; Barlow et al. 2010; Manders et al. 1993; Zinchuk et al. 2007).

9.10.8 Image Enhancement and Analysis: Other Display Modes

A number of additional display modes, such as the 2.5D Filled Rainbow display of pixel values from an image of Convallaria (Fig. 9.32), are available in the Display Column. Many of these have specific and useful functions in the analysis of pixel and voxel intensity display and analysis of images for presentation and publication purposes. These display modes vary from manufacturer to manufacturer and are not discussed in detail here.

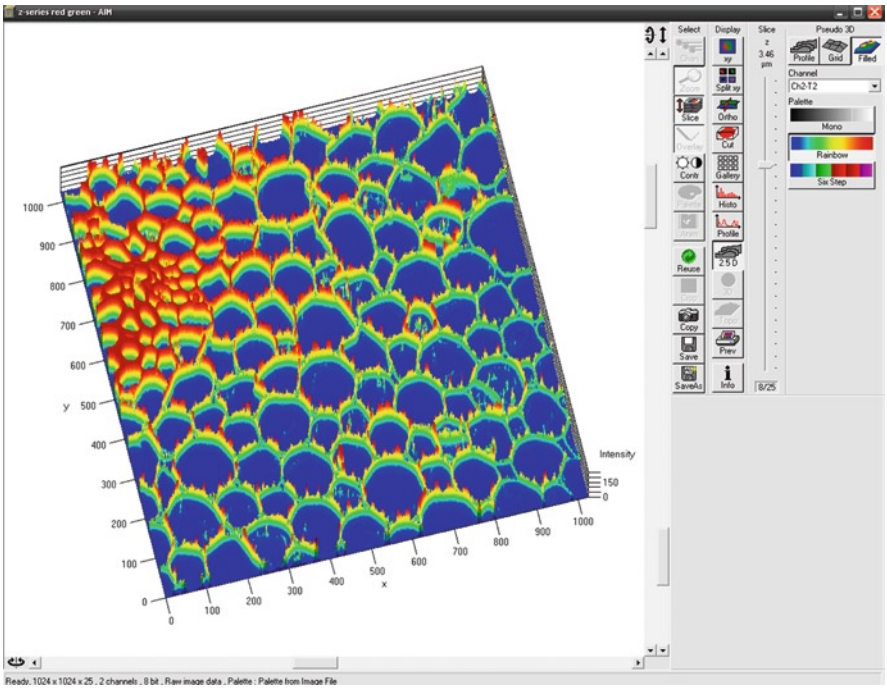

Fig. 9.32 Several additional display modes, including the 2.5D filled rainbow image of Convallaria, are available in the various software programs

9.10.9 Image Enhancement and Analysis: The Reuse and Info Icons

In the Select Column, a very useful icon is the Reuse function (Fig. 9.24). At any time, an image is open by clicking the Reuse icon all operating parameters that were used to collect an image can be reloaded. This becomes useful when questions arise about system configuration or if a current image just does not look as "good" as one that was collected previously.

The Reuse function is based on information stored along with the image in the proprietary format of the manufacturer. This information can be accessed by clicking on the Info icon in the Display column and includes all of the information on the settings of the hardware and software that was used during collection of the image, including lasers, detectors, resolution, pixel dwell time, etc. (Fig. 9.33). It is important to note that for most systems this information is only carried along with images saved in the proprietary formats of the manufacturer. As discussed in Chap. 6, when images are exported to other formats, such as TIF, this information is lost. If an original image with the information is opened, the Reuse Icon can be activated and this will load all parameters used to collect the image. Archiving an original

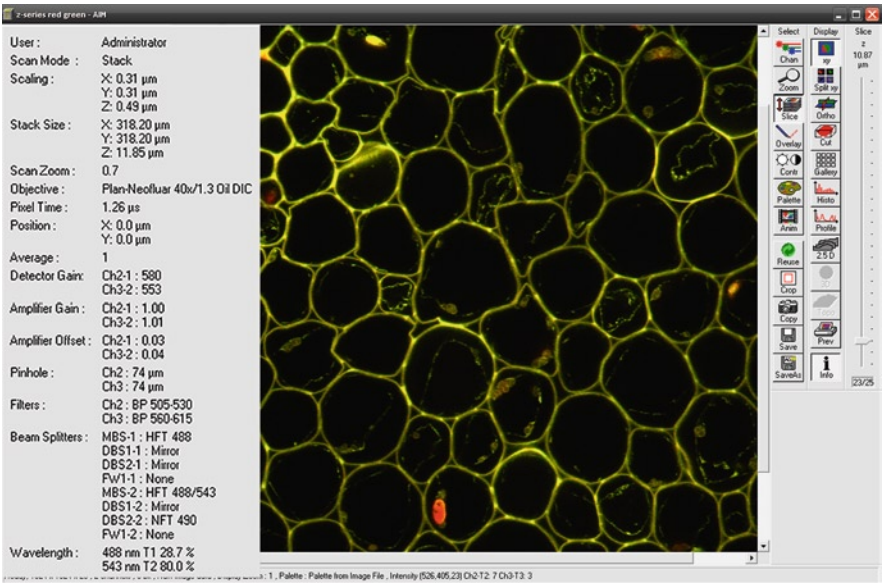

Fig. 9.33 By activating the Info icon, all information concerning operating parameters can be accessed and the Reuse icon can then be used to set up identical operating parameters

image with this information is important for accessing the Reuse function for the collection of images with the same operating parameters in the future, but perhaps more importantly, it is essential in the event the parameters used to collect an image are subsequently questioned by reviewers of manuscripts or others trying to repeat an experiment (Fig. 9.33).

9.11 Scan Control Function: Collection of Z-Stacks

One of the most common uses and largest advantages of confocal imaging is the collection of Z-series data stacks in which every optical section through a sample is in focus and the data set can be reconstructed for presentation in 3D and animated images. This section is presented near the end of this chapter since all of the considerations above on image collection and display are essential in the proper collection and analysis of a Z-series data set. Compromises based on the desire to collect as much data as possible versus specimen stability, time, and file size are often necessary. By understanding these compromises, informed decisions can be made to avoid oversampling of data while making sure adequate amounts of data are collected to complete an analysis. Once an operator understands all of these considerations and compromises necessary for the collection of a single optical section,

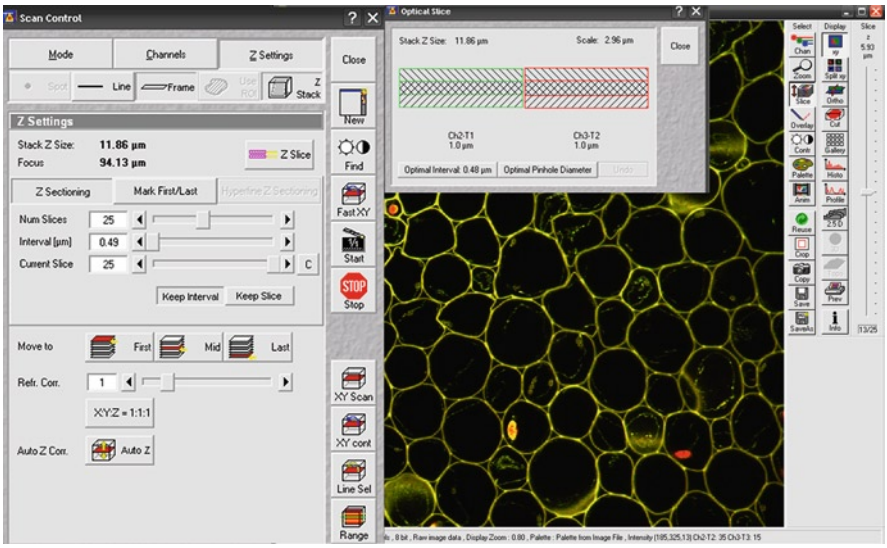

Fig. 9.34 Access to the software for setup of Z-series collection is through the scan control Z-settings icon

setting up Z-series imaging is relatively simple. Figure 9.34 shows the Scan Control Z-stack icon activated which opens the software for the collection of Z-stacks.

In the Z-Stack window (Fig. 9.34) with the Z-sectioning icon activated information concerning the size of the Z-series (11.86 µm in this example), the current focus position of the microscope stage (94.13 µm), the number of slices in the Z-series (25), the interval between the slices (optical slice thickness – 0.49 µm), and the current slice being imaged in the window (25) are displayed. Note that the interval was selected by the software as the optimal optical slice thickness to match the Nyquist-Shannon conditions discussed in Chap. 7. These values can be adjusted, but if thinner this will result in oversampling and larger file sizes than necessary and if thicker it will result in undersampling and problems in the analysis of colocalization and 3D rendering as discussed in Chap. 10. A final consideration in optical slice thickness is that in some cases 3D reconstructions benefit from having the same voxel dimensions in the X, Y, and Z axes as discussed in Chap. 10. If this is the case, the X-Y-Z=1:1:1 icon can be selected and all dimensions set the same. Again, Nyquist-Shannon considerations need to be taken into account when selecting this icon.

Activation of the Mark First/Last icon allows the microscope stage to be set at the beginning and end of the Z-series. Note that collection of images above and below the region of interest should be avoided. In single photon confocal microscopy, remember that photobleaching occurs both above and below the optical slice being recorded, so the collection of additional slices outside the region of interest can add significant time, file size, and specimen damage during collection.

For example, to collect this two channel 25 section Z-series takes approximately 3.5 m of scan time at a scan speed of 9 on this instrument. This is ample time for photobleaching to occur if the sample is not protected and may result in problems collecting sufficient signal during the later scans.

Activation of the Z-Slice icon opens the Optical Slice Window shown on the bottom left. At this point, a final decision to determine if the optimum pinhole (best resolution and contrast in each channel) or the same optical slice (necessary for colocalization and 3D analysis) is used to collect the Z-series. As shown here, the same optical slice thickness of 1.0 μm was selected, so the colocalization and 3D reconstruction images discussed in this chapter could be collected.

When imaging thick specimens, a choice is often necessary on where to set the optimal signal based on the use of the LUTs as discussed earlier. If the optimal signal is set at the Mid-point of the series, signal from the first section is often too bright and signal from the last section is often minimal making reconstructions difficult. The low signal from the deepest sections may be a result of a phenomenon termed Z-drop which involves penetration of the laser into the sample and the ability of emitted photons to exit the sample and be collected. Many factors, including excitation and emission wavelengths, photobleaching and refractive index mismatch, as discussed in several places throughout this book, may affect Z-drop. Selection of the Auto Z Corr icon automatically adjusts the Detector Gain, AOTF transmission, and Amplifier Offset and Gain by linear interpolation between the initial and end collection values to minimize the Z-drop effect.

9.11.1 Suggested Sequence for Collection of a Z-Series

A suggested sequence for setting up the collection of a Z-series is as follows:

1. If working in multiple channels, choose a single channel to establish the first and last sections that will be used in the collection of the Z-series. If working in a multitrack configuration, this can be done by checking only a single laser line as discussed in the multitrack configuration section. Typically, the laser line chosen should be the longest wavelength for the specific specimen being used and the pinhole should be set to 1 AU in the Channels Menu. If this step is performed on the short wavelengths, the pinhole size in the long wavelengths may be very small and limit the available signal.
2. Focus to the optical plane of interest and obtain an acceptable image. It is not necessary at this point to fully adjust the dynamic range of the image. If Z-drop is a problem, it may be desirable to use the first section as the optical plane of interest, so the Auto Z Correction can be applied.
3. Operate at a fast scan speed with the average or sum function set to 1, so changes in the image focal plane can be rapidly observed.
4. Use the focus controls to move to the first section of interest in the sample and mark this position as the starting point in the Z-series. Remember that while

collecting data, specimen damage occurs above and below the plane being imaged so only the sections of interest should be collected.
5. Use the fine focus controls to focus in the opposite direction until the last section in the data set is reached. Set this as the last or end point in the data set. This establishes the size of the Z-stack.
6. Rapidly set the optimal gain, offset, and laser settings by the use of the LUTs as discussed above.
7. Determine if the data stack is collected using the optimal pinhole setting or the optimal interval (optical slice thickness) for each section and start the acquisition.

9.11.2 Presentation of Z-Stack Data

All confocal systems have some basic software applications for the presentation of Z-stacks and some of these 3D reconstruction capabilities are discussed here. However, these are limited when compared to advanced programs, such as AMIRA and others, which are discussed in Chap. 10. On the right side of Fig. 9.34 is a Z-slice bar which allows individual images in the data set to be seen and analyzed. In the example, slice 13 of 25 is shown. Scrolling through the images can be done by moving the slider or automatically by clicking on the Animate icon. It is also possible to show all images in a Gallery format as shown in Fig. 9.35 by selecting the Gallery icon or to select subsets of the image for processing with the Subset icon.

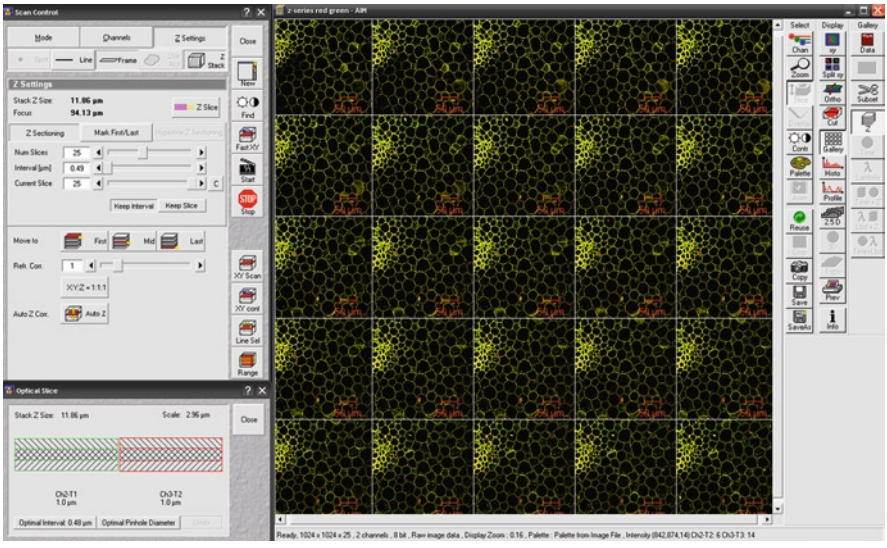

Fig. 9.35 All images in the series can be observed in the gallery mode

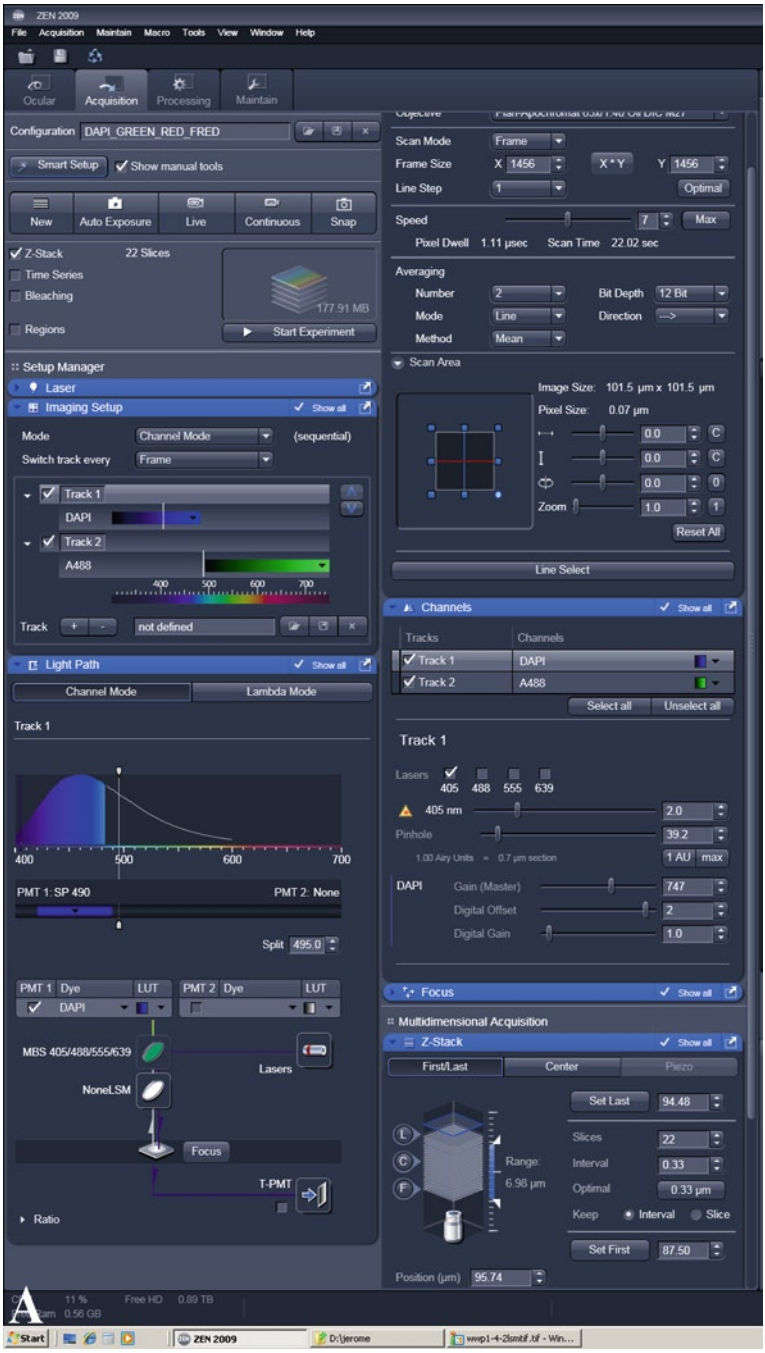

Fig. 9.36 The new Zeiss Zen 2009 operating software. It was necessary to split the window into (**a**, **b**) for presentation purposes, but all information is open in a single window on the monitor making access to the various menus more easily accessible than that in the LSM 510 software. However, setup and operation are very similar

Projection of the data set in several formats can be accomplished by selecting the Projection icon on the Menu bar. This opens a series of windows that allow projection of the data set in several formats, including flat, orthographically, and as a rotating movie. It is also possible to threshold various pixels and to change the transparency of layers to enhance images as they are projected. These topics are discussed in detail in Chap. 10 on 3D reconstructions and volumetric analysis.

9.12 Other Confocal Microscope Operating Programs

As noted earlier, if the basic operating principals are learned and applied, it should be possible to collect publication quality images on any confocal microscope after a short period of time. For the most part, it is simply a matter of learning where the programers have placed the various functions for the proper collection and setup of images. In fact, as confocal software has evolved operation of confocal systems has become much easier and more intuitive than it is in the version of the Zeiss LSM 510 META program presented here. Figure 9.36 presents the main window in the

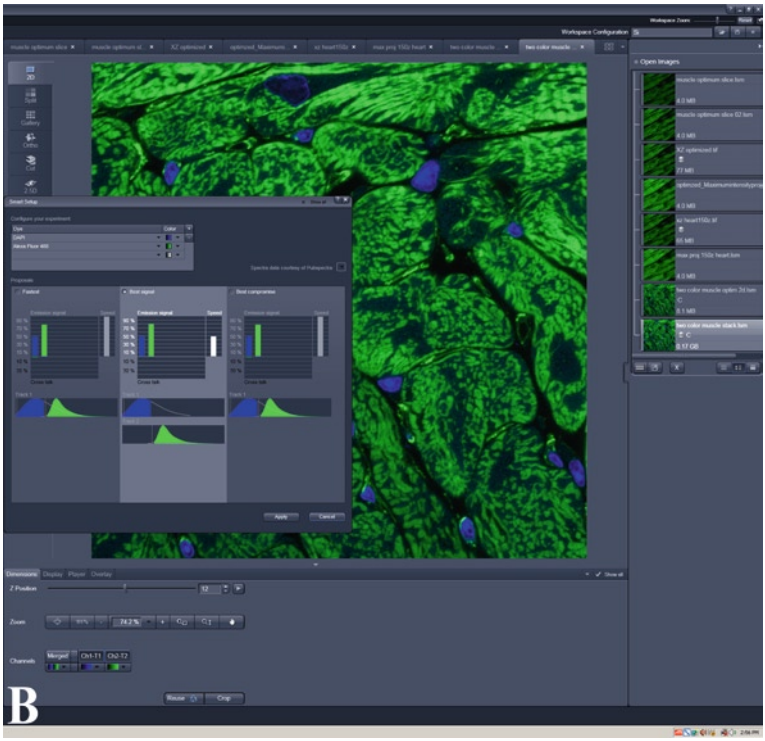

Fig. 9.36 (continued)

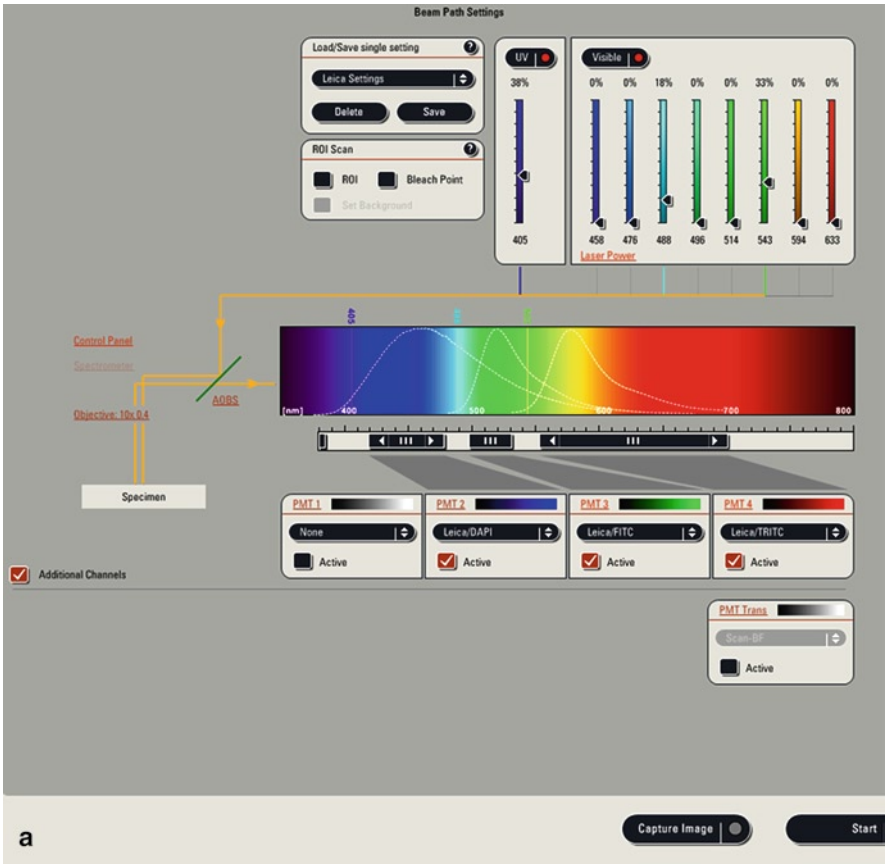

Fig. 9.37 Operating software for the Leica TCS SP5 AOBS confocal microscope. (**a**) shows the beam path setting diagram for selection of wavelengths for each PMT and (**b**–**d**) show the setup software for sequential imaging (**b**), XY imaging (**c**), and collection of a Z-series (**d**)

newest Zeiss operating software, the Zen 2009 program. Figures 9.37 and 9.38 show the Leica and Nikon operating software. As can be seen from all, it is simply a matter of the organization of the various windows for access to the controls necessary to perform good confocal microscopy.

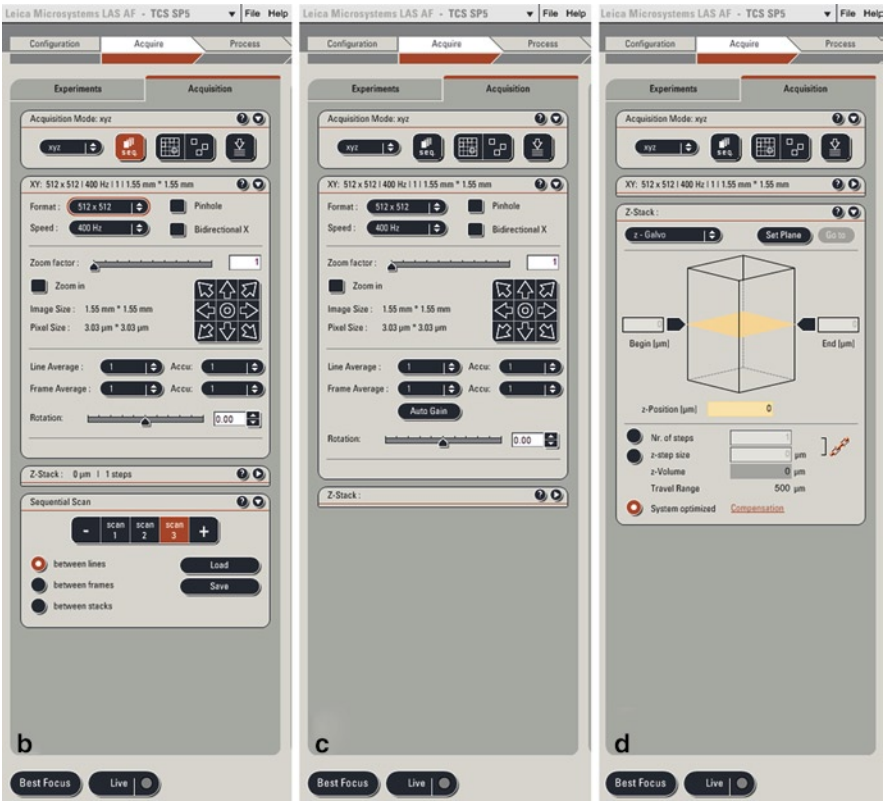

Fig. 9.37 (continued)

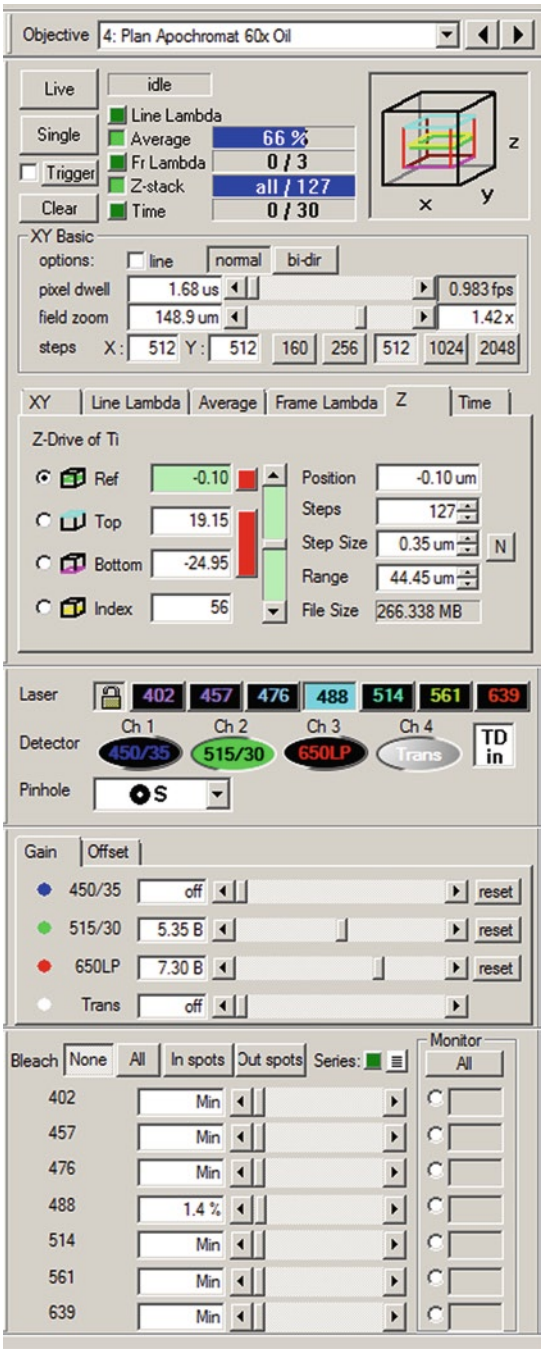

Fig. 9.38 The basic operating software for the Nikon C1Si confocal system showing the organization of windows for the collection of XY and Z images, the laser, detector, and AOTF settings

References

Barlow, AL, MacLeod, A., Noppen, S., Sanderson, J., and Guerin, JG. 2010. Colocalization analysis in fluorescence micrographs: Verification of a more accurate calculation of Pearson's Correlation Coefficient. Microsc Microanal 16(6):710–724.

Boltes, S and Cordelieres, FP. 2006. A guided tour into subcellular colocalization analysis in light microscopy. J Microsc 224:213–232.

Manders, EMM., Verbeek, FJ., and Aten, JA. 1993. Measurement of co-localization of affects in dual-colour confocal images. J Microscopy 169:375–382.

North, AJ. 2006. Seeing is believing? A beginners guide to practical pitfalls in image acquisition. J Cell Biol 172:9–18.

Pawley, J. 2000. The 39 steps: A cautionary tale of quantitative 3-D fluorescence microscopy. Biotechniques. 28:884–888.

Zinchuk, V., Zinchuk, O., and Okada, T. 2007. Quantitative colocalization analysis of multicolor confocal immunofluorescence microscopy images: Pushing pixels to explore biological phenomena. Acta Histochem Cytochem. 40:101–111.

Zucker, RM and Price, OT. 1999. Practical confocal microscopy and the evaluation of system performance. Methods 18:447–458.

Chapter 10
3D Reconstruction of Confocal Image Data

Thomas C. Trusk

Keywords 3D reconstruction • Image contrast • Histogram • Pixel • Resolution • Segmentation • Volume render • Voxel

10.1 Introduction

The main advantage of the confocal microscope is often said to be the ability to produce serial optical sections of fluorescent samples, ultimately for the purpose of reconstructing microscopic objects in three dimensions (Carlsson and Aslund 1987). There are many ways, and reasons, to reconstruct confocal image data. As an example, consider the sample of embryonic mouse heart shown in Fig. 10.1 reconstructed using a variety of three-dimensional (3D) techniques. This chapter will introduce these methods and discuss topics such as (a) why one might want to undertake this task, (b) some definitions of the representation of 3D space using images, (c) the different types of 3D representations that can be made, and (d) the necessary steps to make useful reconstructions. Along the way, the limitations and potential pitfalls that arise will be discussed.

10.2 Why Reconstruct?

Reconstructing image data into 3D representations is a fairly recent activity made necessary by the invention of devices that virtually deconstruct their subjects by scanning serial planes at different depths. Positron emission tomography scanners,

T.C. Trusk (✉)
Department of Regenerative Medicine and Cell Biology, Medical University of South Carolina, BSB 643, 173 Ashley Avenue, Charleston, SC 29425, USA
e-mail: truskt@musc.edu

R.L. Price and W.G. (Jay) Jerome (eds.), *Basic Confocal Microscopy*,
DOI 10.1007/978-0-387-78175-4_10,

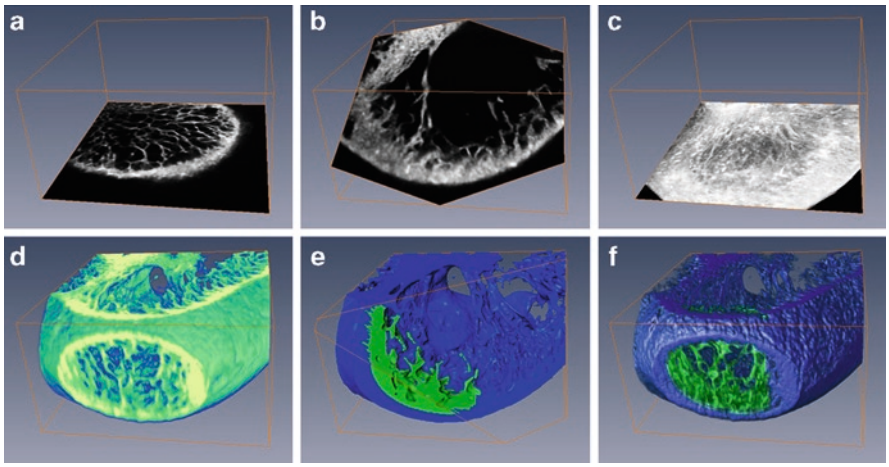

Fig. 10.1 Sample 3D reconstructions. The left ventricle of an embryonic mouse sampled in a confocal microscope. The 3D image data set is contained inside the *orange box* where only the first confocal optical slice is shown (**a**). Methods which sample the 3D data set include (**b**) an oblique slice; (**c**) a maximum projection through the *z*-axis; (**d**) a simple volume render; (**e**) a surface render manually segmented to highlight interior features; and (**f**) a volume render using complex lighting and segmentation information derived from (**e**)

computed axial tomography scanners, magnetic resonance imagers, ultrasonic imagers, and confocal microscopes are all examples of devices that can collect these 3D image data sets. Before these devices were available, building accurate 3D models of microscopic biological specimens had always been a daunting task; that is, until powerful computers and sophisticated software were introduced. Instead of using scissors, cardboard, wax, modeling clay, or Styrofoam, it is now possible to sit in front of a computer workstation and construct, in a fraction of the time, a model that can be displayed in multiple forms and used to convey a wide variety of useful information.

Historically, the primary reason to reconstruct in 3D has been to display the morphology of the subject. In many cases, the 3D shape of the microscopic object may be completely unknown, or some experimental condition may influence its structure. It might also be helpful to reconstruct the various compartments of the subject and divide it into organs, tissues, cells, organelles, and even domains where some fluorescently labeled protein might be expressed. These arrangements often produce clues concerning function (for example, see Savio-Galimberti et al. 2008). The value of a computerized 3D reconstruction is that the finished reconstruction can be viewed at different angles, including visualizations from perspectives impossible to achieve in the confocal microscope. Furthermore, most 3D software applications provide tools to produce digital movies, including interactive surface slicing, transparency, or subregion coloration in the models. These animations can be invaluable in conveying the structure of the subject.

3D reconstructions can be used to provide a substrate for the superimposition of other information (Hecksher-Sorensen and Sharpe 2001). For instance, the multiple channels used in confocal microscopy can be used to highlight the domain of proteins bound to fluorescent markers emitting different colors. Depending on the experimental question, these domains may be expected to be mutually exclusive, or partially (or even completely) correlated within the structure of the subject. In another example, quantitative information (such as cell density or rate of cell proliferation) may be overlaid as a coded color scheme onto a reconstructed object and provide a visualization of that property throughout the sample (Soufan et al. 2007).

Finally, once a fully segmented, surface-rendered reconstruction has been made, it is a simple matter to extract quantitative information from the sample. This includes counting objects, determining volumes, measuring surface areas, or quantifying the spatial arrangements of parts (such as measuring distances or angles between features).

10.3 Defining the 3D Space Using Images

The 3D Cartesian coordinate system (Fig. 10.2) provides a convenient space within which to reconstruct image data. The Cartesian system consists of three physical dimensions – width (x), length (y), and height (z), that are perpendicular to each other (a relationship termed orthogonal) and are typically oriented with the

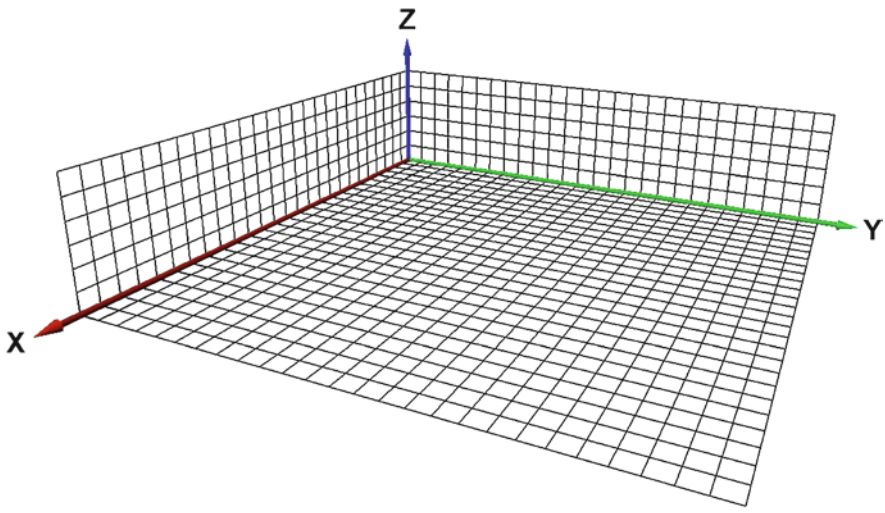

Fig. 10.2 The 3D Cartesian system. A mathematical model of 3D space. Every position in the space is defined by its location along one of three axes (x, y, and z)

z-dimension pointing up. Individual images are considered orthogonal slices through the *z*-dimension, and the pixel plane of each image is defined in the *x*- and *y*-dimensions. Figure 10.1a is an example of an orthogonal slice. Planes cut through the Cartesian space that are not perpendicular to a major axis are said to be oblique, as in the slice shown in Fig. 10.1b.

10.3.1 Perspective

When an observer views a 3D scene consisting of objects of equal size, objects that are far off in distance will appear smaller than objects closer to the viewer. An artist (and a computer) will enhance the perception of depth in rendering a scene by drawing objects "in perspective," as if the drawing was traced on a window through which the viewer was looking. In Fig. 10.3a, rays exit the object and project directly to the viewer. The object is drawn on the display such that the back face of the box appears smaller than the front face. In an orthographic projection (Fig. 10.3b), all rays passing through the scene toward the display are parallel, and the object on the display does not appear in perspective. These types of renderings are sometimes useful, as in architecture, where object size comparisons are more important than the perception of depth. Most 3D software suites can draw objects on the screen with or without perspective, as the viewer chooses. The perception of depth in a scene is quite helpful to the viewer, especially when objects may be moving in dynamic displays or animations. Objects drawn orthographically and rotated often appear to switch rotation direction suddenly.

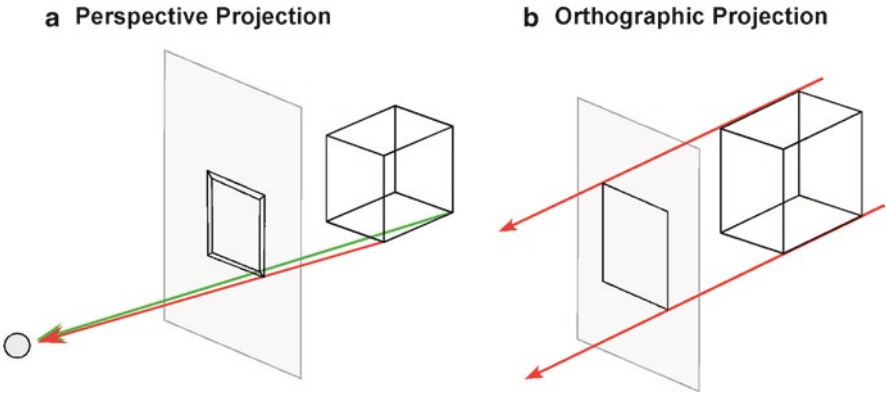

Fig. 10.3 Perspective vs. orthographic projection. For objects drawn on a screen in perspective (**a**), all rays project from the object to the viewer. The more distant back face of the box appears smaller than the front face. In an orthographic projection (**b**), all rays projected from the object to the display screen remain parallel, and the perception of depth in the scene is lost

10.3.2 Voxels

A single confocal "optical slice" has a "thickness" in the *z*-dimension that is defined by the microscope optics and the confocal pinhole. Recall that increasing the diameter of the pinhole allows extra light from above and below the focal plane to contribute to the light gathered at each pixel. On the contrary, a single "image" is infinitely thin along the *z*-dimension (see Fig. 10.4). Confocal *z*-series images are typically collected at evenly spaced intervals, and when the images are re-stacked at the correct *Z* distance, the empty space between the images is readily apparent.

In order to fill the space between images, it is necessary to expand the concept of a two-dimensional (2D) image pixel into a 3D volumetric voxel. This is demonstrated for a single voxel in Fig. 10.5. The grid of 2D image pixels is stretched in the *z*-dimension to produce 3D voxels. Each voxel has the same dimensions of single image pixels in the *x*- and *y*-dimensions, and the distance between consecutive images in the *z*-dimension. Thus, the volume of each voxel is defined as the area of each pixel (*X* multiplied by *Y*) multiplied by the distance between optical slices (*Z*). This voxel volume is the smallest unit of volume that can be measured in that image data set.

One can easily imagine that voxels are the "bricks" used to construct a 3D model. Each voxel has not only spatial dimensions, but also a single unique brightness value inherited from its basis pixel. In an 8-bit sensitivity system, this value

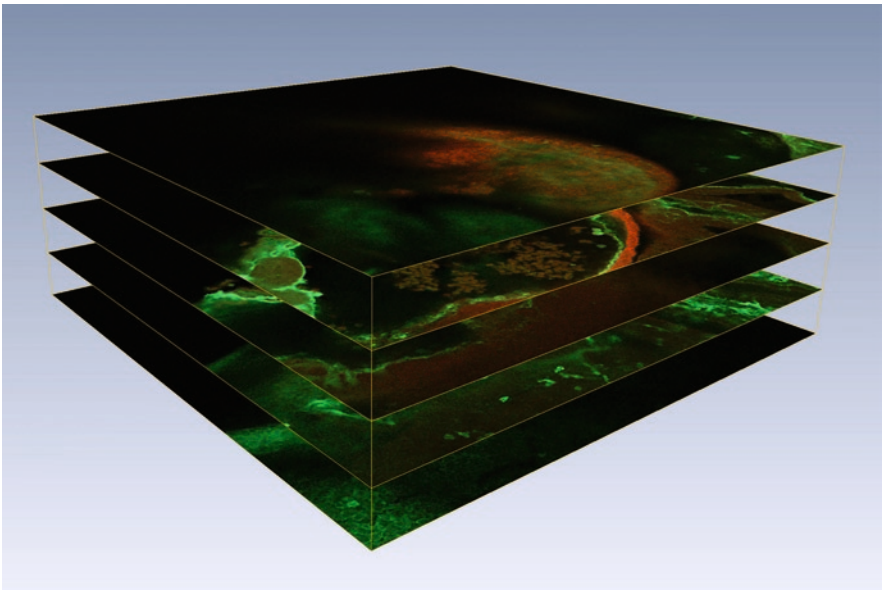

Fig. 10.4 A single image has no depth. Five evenly spaced confocal slices demonstrating the infinitely thin nature of image data in the depth (*z*) plane

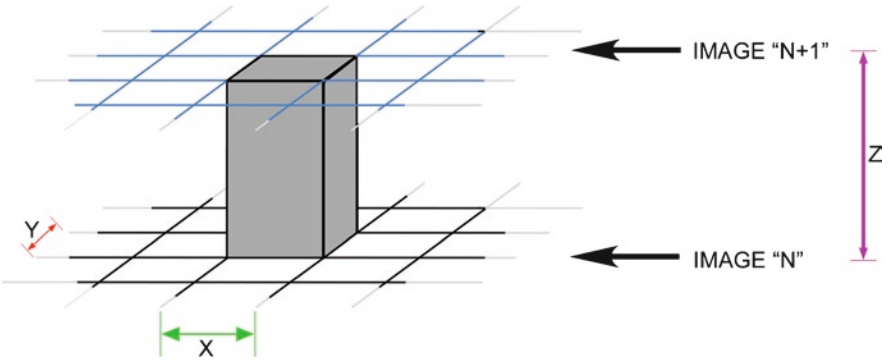

Fig. 10.5 Definition of a voxel. A portion of two consecutive images from a confocal series is shown. Image pixel dimensions were *X* units by *Y* units, and images were collected every *Z* units. A single voxel is the space defined by the pixel dimensions and the distance between consecutive images

will range from 0 to 255, and is constant within the confines of a single voxel. Much like the bricks used to construct buildings, the voxels in a 3D image data set are all the same shape and size, and each voxel has only one homogeneous color.

10.3.3 Resolution

The shape of individual voxels in an image data set is determined by the resolution of the system. Some confocal microscope software controls will, by default, choose to slice a sample optically using a *Z* distance that is as close as feasible to the pixel size. This would result in voxels that are nearly cubic, where *x*-, *y*-, and *z*-dimensions are approximately equal. This is desirable for many reasons. First, cubic voxels more easily reconstruct 3D features correctly, no matter what orientation they may have. For example, if you were to choose to use bricks to build a sphere, what shape brick would make the best representation? Figure 10.6 displays surface reconstructions of the same sphere rebuilt with different shape voxels, and demonstrates the effect of increasing the voxel *z*-dimension (or slice thickness) on the surface of reconstructed objects.

Most mathematical functions used in 3D reconstruction and visualization are much more efficient when the data set uses isotropic or cube-shaped voxels. Using extremely anisotropic voxels can lead to inaccuracies in many measurements, especially surface area, and produce 3D visualizations that lose resolution when viewed from particular angles (see Fig. 10.7).

One solution offered in 3D reconstruction software is to resample the image data into near-cubic dimensions. That is, the original data will be interpolated to fit a cubic voxel model. However, this approach only helps in the calculation efficiency and does not improve the visualization of the sample. Resampling the data into

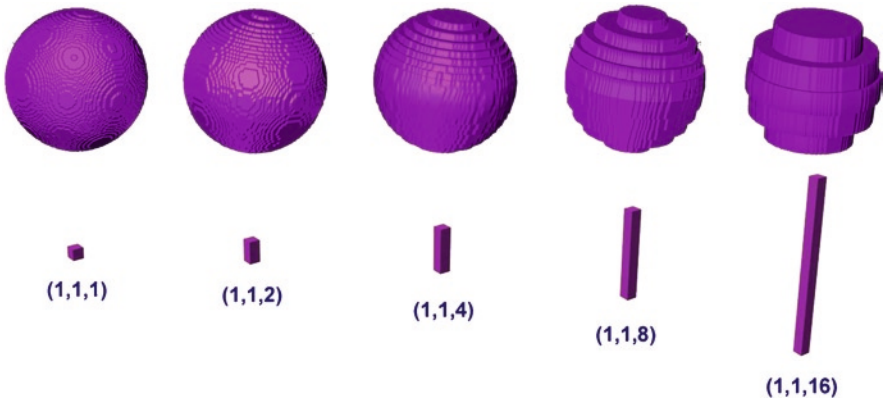

Fig. 10.6 Effect of voxel shape on surface reconstruction. The same spherical object is surface reconstructed with voxels of increasing *z*-dimension. The voxel shape used is shown (much magnified) below each rebuilt sphere with the voxel dimensions in *x*-, *y*-, and *z*-axis. The *leftmost* sphere was rebuilt using cubic voxels

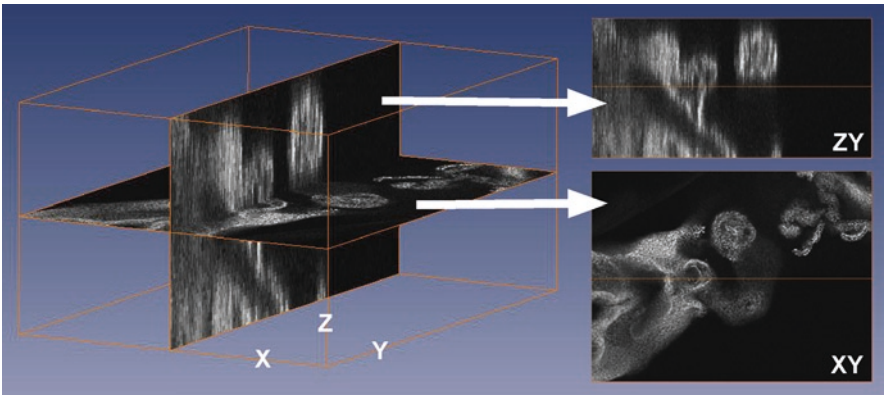

Fig. 10.7 Effect of voxel shape on 3D visualization. A confocal 3D image data set is sliced in the *XY* plane (as originally collected by the confocal system) and in the *ZY* plane. Voxel *x*-, *y*-, and *z*-dimensions in micrometer (μm) are 2.4, 2.4, and 12

larger voxels can be quite helpful if the computer memory is insufficient, but resampling into smaller voxel sizes will only make the volume take up more memory and not increase visible resolution at all. It is worth noting that resolution decisions are best made at the microscope when acquiring images, and this is demonstrated in Fig. 10.8. The same epithelial cell was captured using a 20× lens, a 40× lens, and a 40× lens with a digital zoom of 5 (for an effective 200× magnification). The actual collected pixel sizes were 0.73, 0.37, and 0.07 μm for the 20×, 40×, and 200× images, respectively. In each image, a white box identifies the same mitochondria,

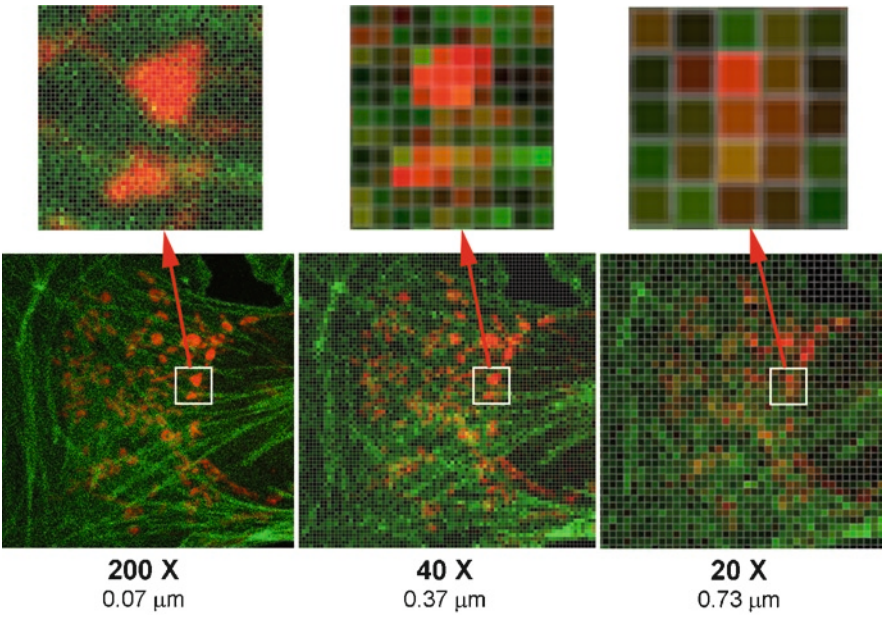

Fig. 10.8 Changing resolution. A bovine epithelial cell acquired on a confocal microscope using increasing objective power to improve resolution. The actual pixel dimension resolved is given for each image in µm. The *white box* region in each image has been magnified to reveal actual image pixels

and the image data inside have been magnified to show individual image pixels. It should be easy to discern that the visual information obtained at 20× would be difficult to resample (or subdivide) into the higher resolution information seen at higher optical magnifications. This demonstration of resolution in the *x*- and *y*-dimensions also applies to the resolution in the *z*-dimension.

Resolution in the *z*-dimension is set at the confocal microscope by choosing an appropriate distance between optical slices. For 3D reconstruction work, a good rule of thumb is to slice optically at a distance between one and five times the size of pixels in the images. Oversampling the object by slicing at smaller intervals is easier to correct later by resampling. If you are worried about data sets that are too large or take too long to collect, consider that the cost of data storage is essentially free. Returning the sample to the microscope later is always risky as fluorescence may have waned or the tissue may have deteriorated.

10.4 Types of 3D Reconstruction

3D image data sets can be reconstructed and visualized in a variety of ways. These 3D models range in complexity from projections, a common function within most confocal system software suites, to surface reconstructions, which often require

additional software. More recent confocal microscopes now include a sophisticated selection of reconstruction routines as part of the operating software, or possibly as optional additions. There are three basic methods used to present a 3D data set: projections, volume renders, and surface reconstructions. The following will briefly describe how each type is calculated.

10.4.1 Maximum Projections

A projection is a single 2D image generated using data from the entire 3D image set. In the case of fluorescent images, this consists of finding the brightest or maximum pixel value at each pixel address from each image in the entire data set, and projecting it onto a result image (see the example in Fig. 10.1c). While the obtained image itself is not a 3D object, it conveys a visualization of the entire object from a particular viewpoint. Typically, the viewpoint used has been orthogonal, or along a principal axis (*x*, *y*, or *z*), which simplifies the mathematics of calculating a projected image.

Consider the simple 3D data set in Fig. 10.9. Three optical slices, each a 3 by 3 pixel image, are projected along *z*-axis (red) and *x*-axis (green) projection lines. The brightest pixel encountered along each line is placed in the result image. Note that these projection lines are parallel to each other; thus they produce an orthographic rendering of the data, as previously discussed. As such, projected images tend to lack a perception of depth.

An illusion of depth can be partially elicited by making a projection animation (or multi-frame movie) where the object appears to rotate in place, either in complete circles, or by alternately rocking the object clockwise and counterclockwise. These animations are generated by mathematically rotating the object a few degrees and recalculating the maximum pixels encountered along parallel rays projected toward the result image (see Fig. 10.10). When the frames are collected into a movie and played in sequence, the projected object appears to rotate. Recall that the resolution along the *z*-axis (as seen through the microscope) is always best, and that resolution is reduced when the data are viewed along the *x*- or *y*-axis. This is why projected images tend to appear to lose clarity as the object rotation exceeds 30–45° away from perpendicular to the *z*-axis. For this reason, most animations are made to show the object shifting rotation between ±30° of tilt.

A common mistake is to slice the confocal sample at step sizes ten or more times the size of individual pixels. This will produce a 3D data set that will lose resolution too rapidly as the object is rotated. The illusion of depth is also lost when the number of slices is very small when compared to the pixel dimensions of each image. For example, ten *z*-slices taken at 1,024 × 1,024 resolution will make disappointing rotation animations. The best projection animations use 3D data sets with *z*-slice intervals close to *xy* pixel size (that is, near *cubic voxels*), and small rotation factors between projection animation frames (about 1° of rotation for each frame).

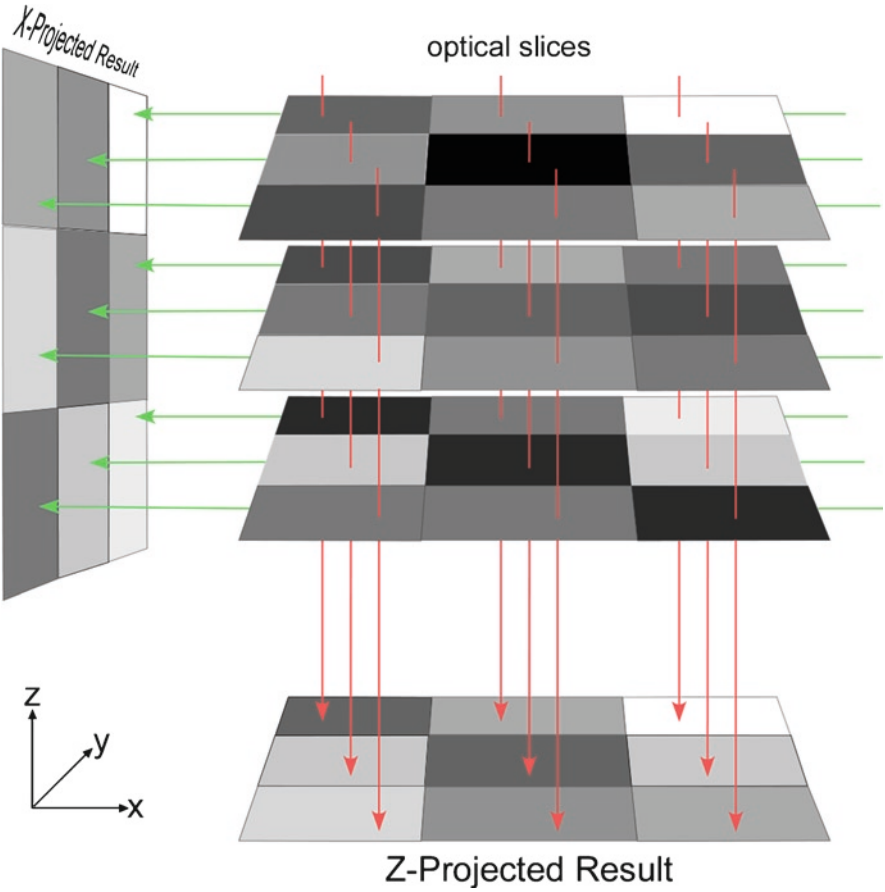

Fig. 10.9 Projected images. Three optical slices, each 3 × 3 pixels, are projected along the *z*-axis (*red lines*) and the *x*-axis (*green lines*). The maximum (or brightest) pixel values along each projection line are placed in the resulting projected image

Maximum projections are the most commonly seen 3D reconstructions, and all confocal software systems routinely generate orthogonal views at the press of a button. Procedures for making projection animations are also widely available. Projections work best as orthogonal visualizations of 3D fields with little depth and provide the "all-in-focus" micrographs difficult to obtain on wide-field fluorescent microscopes. However, be warned that maximum projections can also be misleading. When the object is hollow with internal structure, like the heart ventricle shown in Fig. 10.1c, the external signal will mask the interesting internal features. More importantly, maximum projections of multichannel image sets will mix colors by addition. Red and green channel signals that lie along similar projection lines, but are not otherwise co-localized, will produce yellow objects in the result image. This could lead to misleading conclusions.

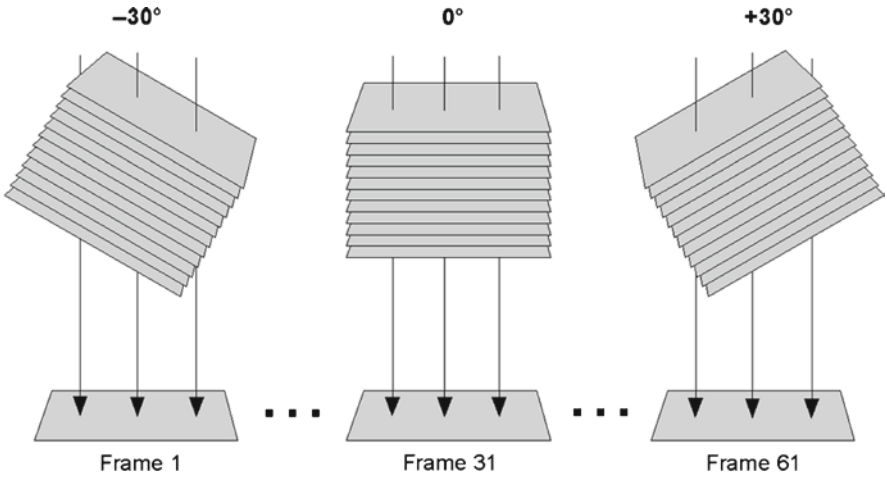

Fig. 10.10 Maximum projection animation. A 61-frame animation is made by rotating a 3D image data set 1° before each maximum projection result frame is calculated. When the frames are collated into a movie, the projected image appears to rotate in place

10.4.2 Volume Rendering

As acquired in the confocal microscope, each voxel can be described with certain *x*-, *y*-, *z*-spatial coordinates, and a fluorescent intensity recorded in each channel. In order to visualize a 3D data set in proper perspective, we need to render an image on the display in a manner which will allow internal structure to be correctly observed. One way to accomplish this is to assign each voxel an additional attribute of transparency. This attribute is termed alpha in imaging technology, and it has an inverse commonly used in 3D rendering called opacity, i.e., a voxel of 100% opacity has no alpha transparency. Alpha ranges from 0 to 1, thus opacity is 1-alpha.

By now you should be familiar with the concept of pseudo-coloring images using color look-up tables. For 3D renderings, alpha becomes a fourth attribute, and voxel pseudo-color values are often referred to as RGBA tuples, referring to the 4 values assigned to each voxel. A typical RGBA look-up table is shown in Fig. 10.11 for two possible voxel values. In fluorescent images, the background is typically dark (not fluorescent). Since we wish to see through nonfluorescent regions, we assign the most transparent alpha values to the darkest image pixels. In this particular example, we choose to make brighter image values to produce more saturated yellow voxels that also become less transparent (or more opaque) as intensity increases. This RGBA table will produce brightly stained fluorescent objects as yellow structures and leave the unstained background transparent.

In the process of calculating a volume rendering, imaginary projection rays proceed from the display screen and completely penetrate the 3D data set. If the

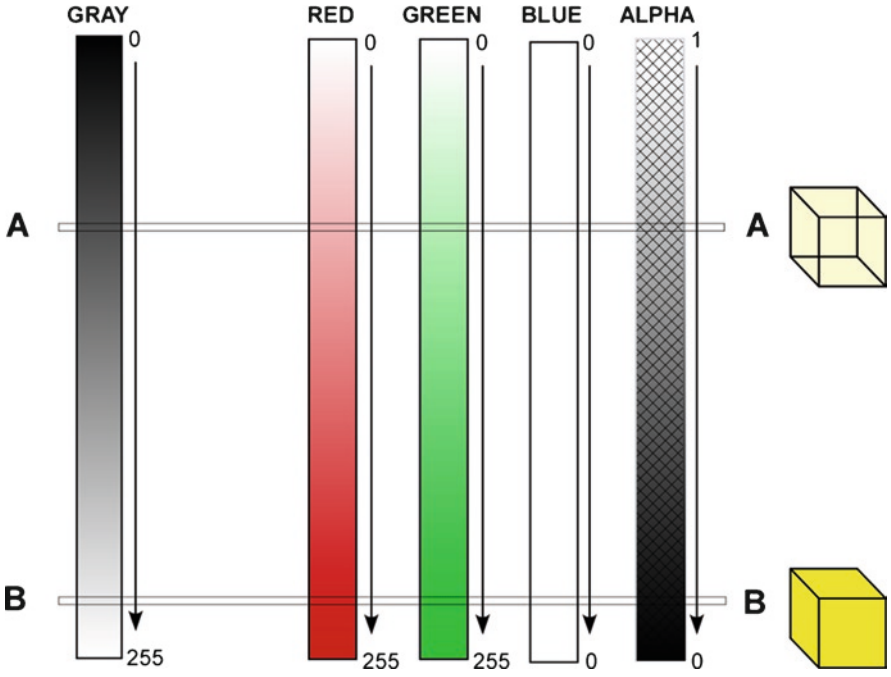

Fig. 10.11 RGBA look-up table. An 8-bit look-up table is used to convert *gray* values from a voxel into the corresponding *red*, *green*, *blue*, and *alpha* (transparency) values used for display. *Red* and *green table* values range from 0 to 255, *Blue* is 0 across the range, and *alpha* ranges from 1 (transparent) to 0 (opaque). The *gray* values at A and B are converted in the mixed RGBA values and displayed in voxels at the *right*. The darker value at A mixes *red* and *green* to produce a transparent weak *yellow* voxel, while the brighter value at B produces a more saturated and opaque *yellow* voxel

display is to be orthographic, the rays remain parallel from the display through the object. For displays remaining in perspective, the rays appear to originate from the viewer and are not parallel. The number of rays possible can be quite high, but only enough are needed to fill each pixel on the display screen. As this limited number of rays pass through the object, the software has the choice of using all of the data, where calculations are made from every voxel the ray passes through, or the data can be interpolated by averaging across a select number of neighboring voxels to speed up the process for more dynamic displays.

The first steps in the process of calculating voxel values used along a projection ray are shown in Fig. 10.12. Consider a small sample, a $3 \times 3 \times 3$ volume. The volume is shown in the brick model in (a), and in another conceptual format, the cell model in (b). In the cell model, voxels are viewed as the vertices of a 3D grid. A single projection ray is shown in (c) as it passes through the volume and intersects the display pixel where the result will be seen. As the ray passes through the volume, it passes through several cells, each defined by the 8 voxels in the cell corners. The intensity value used for each cell is calculated using trilinear interpolation,

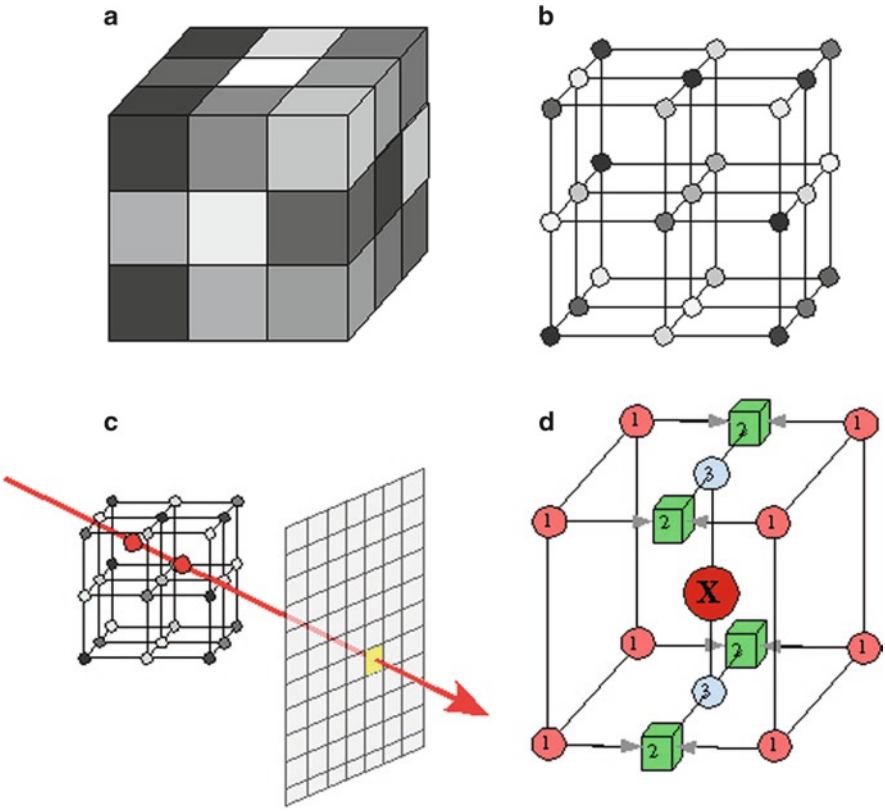

Fig. 10.12 Voxel averaging. A simple 3×3×3 volume shown using the brick model (**a**) and the cell model (**b**). In the cell model, voxels are viewed as the vertices of a 3D grid. A single projection ray is shown in (**c**) as it passes through the volume and intersects the display pixel where the result will be viewed. As the ray passes through the volume, it passes through cells, each defined by the 8 voxels in the corners. The intensity value used for each cell is calculated using trilinear interpolation, as shown in (**d**). In the first approximation, four pairs of corner voxels are averaged, then those four values are averaged, and then finally the last pair are averaged

as shown in (d). In the first approximation, four pairs of corner voxels are averaged, then those four values are averaged, and then finally the last pair is averaged. The final value is converted using the look-up table into an RGBA tuple. This process is repeated for all cells along the projection ray, and the final step is to composite all of these tuples into a single value to be displayed.

In compositing these values, calculations usually proceed from the back of the object space to the front, toward the viewer. As the ray first strikes the object, it has the color or intensity value of the background. The intensity passing through each cell in turn is modified according to the formula

$$\text{Intensity}_{\text{out}} = \text{Intensity}_{\text{in}} \times (1 - \text{alpha}_{\text{cell}}) + (\text{Intensity}_{\text{cell}} \times \text{alpha}_{\text{cell}}),$$

and this process continues until the ray leaves the object, where the final intensity$_{out}$ is placed in the display pixel.

Most modern computer video display adapters are now capable of performing much of these 3D rendering computations very rapidly. This makes it possible for most modern desktop computers to perform volume renders as quickly as expensive graphic workstations of the recent past. The addition of hardware accelerators dedicated to 3D texture mapping, mainly used in modern gaming software, has also made it possible to generate even more complex volume texture renderings. For these methods, each cell can be given attributes beyond color intensity and transparency, such as texture-mapping, specular or diffuse reflection, shadowing, and other lighting effects (as shown in Figs. 10.1f and 10.20c).

Volume-rendering animations more faithfully display internal structure compared to maximum projection animations, and are less likely to generate false-positive conclusions regarding co-localization. However, a single frame volume render of a multichannel 3D data set can be just as misleading regarding co-localization as a maximum projection of the same data set. Depending on the software, multichannel volume renders will often mix RGBA tuples for the final display image, or may choose to display one channel as masking another. It is best not to rely on one visual aspect when ascertaining co-localization.

10.4.3 Surface Reconstruction

In image-based reconstruction, a surface is a 3D polygonal boundary surrounding voxels of special interest. These voxels can be defined by setting a single intensity threshold value, or by including a specific range of intensity values. Alternatively, individual voxels can be selected manually (in a process called segmentation) for inclusion into a surface boundary. A mathematical routine called the Marching Cubes algorithm is typically used to define a surface in 3D space.

As an introduction to 3D surfaces, consider the simpler 2D isosurfaces used to map intensity values in single images. We are used to seeing contour lines mapping altitude or isotherm lines showing temperature differences on weather maps. In Fig. 10.13a, the color-coded isolines surround pixels of a narrow range of intensity values. In 3D space, the isolines become surfaces which divide 8-voxel cells (as described above in volume rendering) to isolate voxels either by intensity or by segmentation. For example, given a threshold value of 100, the voxels of the single cell shown in Fig. 10.13b require the green surface to divide the 4 voxels of intensity 200 from the 4 voxels of intensity 40. This is how the Marching Cubes algorithm functions, evaluating every cell in the volume so as to place boundaries sufficient to isolate voxels which either exceed a selected threshold, or which have been manually selected. There are 256 possible solutions to an 8-voxel cell analysis, but given rotational symmetries, this number can be reduced to only 15 potential answers (Fig. 10.13c). After cleaning up some

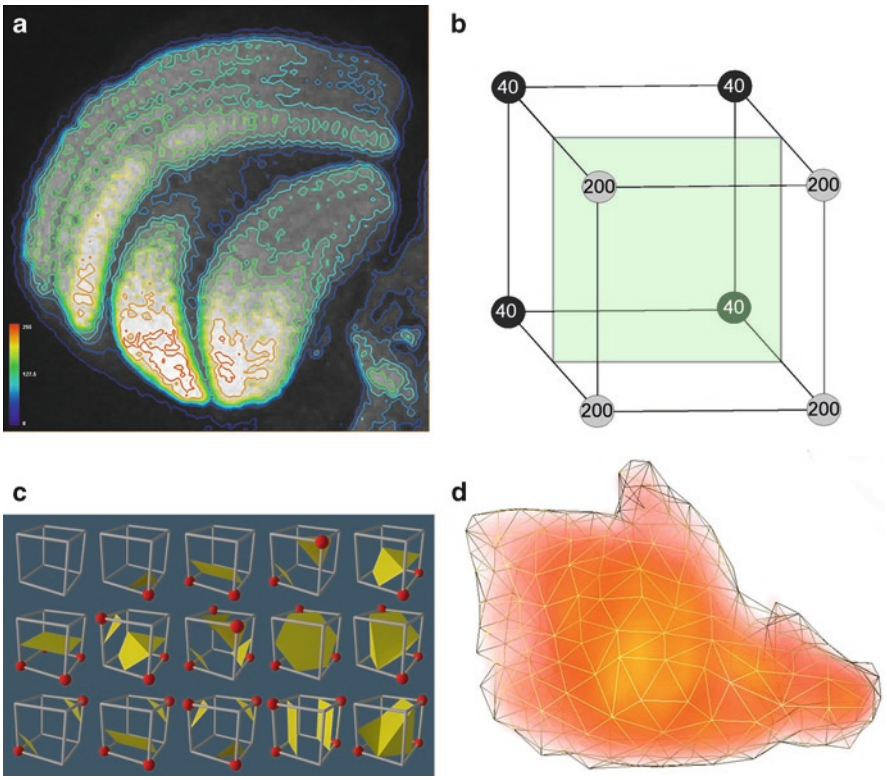

Fig. 10.13 Surface reconstruction. (**a**) Intensity isolines in a 2D image. (**b**) A single 8-voxel cell is subdivided by a *green* surface boundary based on voxel intensities above 100. (**c**) The 15 possible solutions to the Marching Cubes algorithm. (**d**) A 3D polygonal wireframe surface bounding volume-rendered voxels

inconsistencies and imposing some rules governing maximal surface folding, the algorithm produces a set of vertices defining a mesh of triangles which enclose the selected voxels (d).

The number of triangle faces produced by the Marching Cubes algorithm depends on the voxel resolution. An ideal solution contains just enough faces to enclose the 3D region of interest efficiently. However, the speed of rendering a surface is directly related to the number of faces to draw. Most efficient surfaces have less than 40,000 faces; yet the first approximation of the Marching Cubes algorithm will often yield over a million faces. The face count can be reduced by either averaging across 2 or more voxels before executing the Marching Cubes algorithm, or by using a surface simplification routine on the final surface.

A variety of choices are available when rendering a surface to the display (Fig. 10.14). Drawing the mesh of triangles that connect the vertices defining the surface produces a wireframe (Fig. 10.14a) which is transparent. Triangles can be filled with

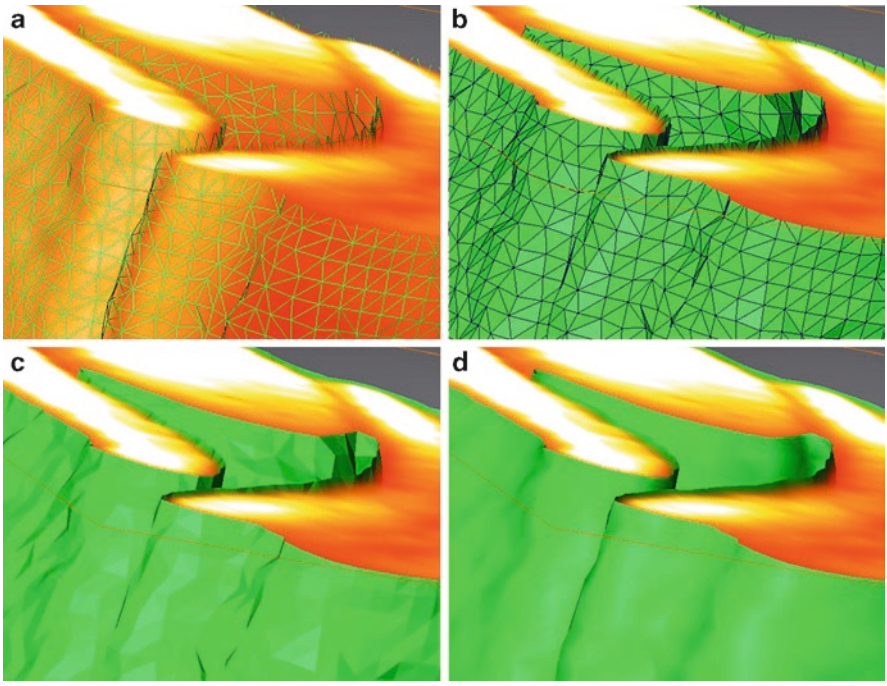

Fig. 10.14 Surface rendering. A portion of a folded surface reconstruction rendered as a wireframe (**a**), a wireframe filled with *green* (**b**), a *green* surface without the wireframe (**c**), and a *green* surface with reflection normals moved to the center of vertices (**d**)

a chosen solid color (Fig. 10.14b), and the wireframe triangles can be hidden (Fig. 10.14c). This reveals the faceted reflections of the light bouncing off the triangles. This facet effect is caused by the 3D lighting calculations of the display system, which depend upon a surface normal that has been generated for each surface triangle. The normal is a spatial vector pointing away from the center of each triangle, and this vector is orthogonal to the plane of each triangle. The normal guides light in the scene directly to the triangle face, where it is reflected, producing a faceted appearance. This reflection can be removed by forcing the rendering engine to use normals centered on the triangle vertices rather than the center of triangle faces, which produces reflections of a smoother, more natural surface (Fig. 10.14d).

Surface reconstructions produce virtual representations of objects in 3D. While they appear less like the original object compared to projections and volume renderings, the segmentation process for surface reconstructions is a necessary first step to quantify anything in the data set. The process of segmenting data set voxels based on intensity (or some other specific criteria) provides a framework for calculating volumes (the number of voxels multiplied by the volume of a single voxel), and counting objects (the number of independent regions with directly connected voxels). Surface areas are easily determined by adding together the areas of triangles enclosing virtual objects of interest.

10.5 The Steps to Reconstruction

Three possible reconstruction pathways are shown in Fig. 10.15. Each path is based on the main types of reconstruction that can be produced, and the flow chart points out the main steps that will be required to achieve the desired result. Note that the results obtained in more complicated reconstructions may contribute to other types of visualizations. The steps to reconstruction can be reduced to seven basic processes that must be followed in order, but it should be clear that not every step is required to produce a 3D visualization.

Most 3D reconstruction software systems perform similar functions (Clendenon et al. 2006; Rueden and Eliceiri 2007), but it is beyond the scope of this chapter to produce a guide to reconstruction for each system. As is generally true with software, the more you pay, the more power you get. Each system should have a user guide to the functions, and with luck, some tutorials designed to reduce the learning

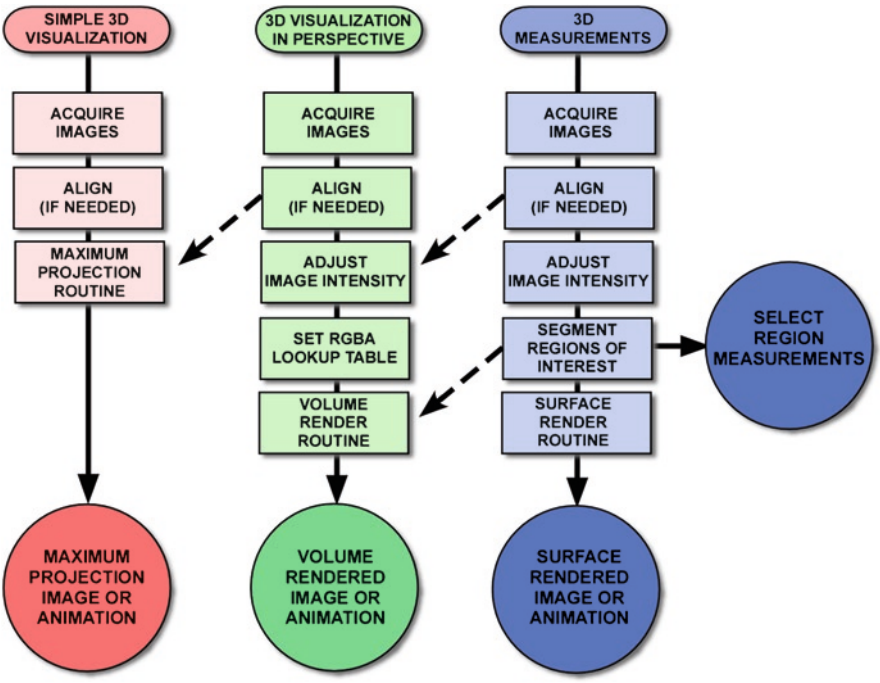

Fig. 10.15 The reconstruction process flowchart. The steps required to reconstruct will depend upon the type of result desired. (*Red*) Simple 3D visualizations generated using maximum projection methods only require a confocal *z*-series. (*Green*) Volumes rendered in perspective may need some intensity adjustment and the assignment of a suitable RGBA look-up table. (*Blue*) Surface reconstructions and any 3D measurements will require segmentation of the volume into regions of interest. The *dashed arrows* between pathways indicate that results from one path can contribute to other types of reconstruction. For example, the segmentation output of a surface reconstruction can be used to assign textures to multiple regions of a volume render (instead of using an RGBA look-up table)

curve for novice users. This section will present a more philosophic approach to 3D reconstruction, and attempt to describe the generic steps for performing this complicated task.

10.5.1 Planning

When building (or rebuilding) any structure, it is always helpful to have a plan. In 3D reconstruction, this means gathering as much information about the sample as is feasible and to have some idea of what the final product will include. For example, what is the approximate real size of the largest and smallest features to be reconstructed? That information will guide the microscopist to select an objective with enough resolving power and sufficient field of view. In some cases, there is no objective that will work well for both resolution and view field. This is typically true when the entire object is too large to fit in the view of an objective needed to resolve the smallest features of interest. In those situations, it is best to use the higher power objective for the best resolution of the smaller features. The microscopist should then plan to collect overlapping fields of view in acquisition and then realign all the parts into one complete data set.

There should be specific goals in place. Ask yourself which products will result from the reconstruction? Are you attempting to visualize the sample from unique 3D perspectives? Will you need to subdivide the structure into components to study how they fit together? Do you wish to quantify some spatial characteristics of your sample? The answers to these questions will determine which tasks you must perform, and will lead you to an efficient path to your goals.

10.5.2 Acquisition

Most of the content of this book is aimed at improving the readers' ability to acquire quality confocal images, but it is worth repeating that collecting the best data set possible will greatly influence the reconstruction process. All of the issues previously discussed apply, especially maximizing contrast and resolution in the images. The basic rule is to enhance the visualization of the regions of interest as much as possible.

Your raw image data will be collected using your specific model confocal microscope's software system. Every manufacturer's software suite saves *z*-series image stacks in a different format, so it is important to understand how your system stores these images. Furthermore, every 3D reconstruction program reads these image stacks in a different manner, so you must also be prepared for the possibility that you might need to reformat your original data in order to move it into the 3D software. Hopefully, your 3D software can read the raw data format of your confocal microscope, but if not, the best solution is to export *z*-series into TIFF format images using filenames that are in the correct order when alphabetically sorted. If you must export TIFF images, you must also keep different confocal channel

images in separate, appropriately named folders. As explained elsewhere in this book, it is best to avoid using JPEG format when moving 3D data sets.

Another consequence of exporting TIFF images is that spatial information may not be read with the data into the 3D software. If you plan to produce quantitative information using physical units, be prepared to know the pixel size and *z*-slicing distance. Most 3D systems ask for the size of a single voxel as an *x*, *y*, *z* input. Be sure to report all of these values in the same units (e.g., μm).

10.5.2.1 Deconvolution

Deconvolution of confocal image data may seem unnecessary, but this process can actually remove a noticeably large proportion of the background noise, especially in the *z*-plane, and greatly assist in later reconstruction steps. Deconvolution should really be considered an adjustment method, but because its implementation has more stringent image acquisition requirements, it is best to mention it here. Any discussion on the process of deconvolution would be beyond the scope of this chapter, so the reader is greatly encouraged to consider recent papers for a general introduction (Biggs 2004, 2010; Feng et al. 2007; McNally et al. 1999).

10.5.3 Alignment

One of the more difficult and tedious tasks in reconstruction is aligning the serial slices of the 3D image set. When serial tissue slices from a microtome are mounted, stained, and photographed, the slices must be returned to their original positions by transforming the images (moving in *x*- and *y*-directions, and rotating). Often, the process of cutting the tissue will change the shape of serial slices as the sample is dragged across a sharpened knife. For confocal data, this step is completely unnecessary. The sample remains intact, the serial slices are obtained optically, and every image is collected in perfect alignment to the entire sample.

However, circumstances do arise when it becomes necessary to align multiple confocal data sets into one large data set. Consider the case where larger features of interest cannot fit into the field of view of the objective required to resolve the smallest regions of interest. In these situations, the entire range of features can be obtained by tiling 3D image sets together. Many modern confocal microscopes come equipped with automated *x*–*y* stages and software which will stitch together neighboring *Z*-series into large 3D image data sets.

10.5.4 Adjustment

Typically, if you were careful setting the gain and offset during acquisition, your confocal images should need little adjustment beyond minor changes in brightness

or contrast. Please keep in mind the guidelines for scientific data as applied to images, such as those defined by the Microscopy Society of America (Mackenzie et al. 2006). However, it might be necessary to adjust the intensity values in the images to enhance the differentiation of regions of interest for thresholding or manual segmentation procedures to follow. Always remember that it is important to keep a record of these procedures and to report them in any scientific reports so that your results are repeatable.

Most 3D software suites provide image adjustment functions that will alter the brightness data in the images either in individual slices, across all slices, or even using 3D kernels as image filters. These functions are strictly to be used to help differentiate regions of interest when necessary. Some "automatic" segmentation routines work best when the regions of interest have sharp boundaries based on intensity, and these functions can often help the efficiency of those routines. When manual segmentation procedures will follow, these adjustment routines greatly assist the observer in finding regional boundaries.

As an example, consider the application of the histogram equalization function. Histogram equalization is often used to increase contrast in an image by "equalizing" the frequency of pixel intensities across the available range. The effect of typical unrestrained histogram equalization is shown in Fig. 10.16a, b. For confocal images, this type of equalization tends to emphasize the out-of-focus epifluorescence, which tends to defeat the purpose of optical slicing. A better solution is to apply the histogram equalization function repeatedly over smaller, more contextual regions of the image in a procedure called local adaptive histogram equalization. This not only greatly maximizes contrast, making hidden regions more visible, but also greatly enhances the background noise and produces shadows at image intensity edges (Fig. 10.16c).

10.5.4.1 Contrast-Limited Adaptive Histogram Equalization

This is a procedure originally developed for medical imaging and can be quite helpful in enhancing low-contrast images without amplifying noise or shadowing edges. Briefly, contrast-limited adaptive histogram equalization (CLAHE) works by limiting the amount of contrast stretching allowed in small local areas based on the contrast already present. So in regions where the intensity is uniform, the amount of equalization is reduced and the noise is not emphasized. The CLAHE effect is typically set by variably adjusting the degree of contrast stretching to be applied in local areas, and this is demonstrated in Fig. 10.16d–f. For the purpose of regional segmentation, the adjusted image in Fig. 10.16d would be far easier to differentiate than the original for both automatic and manual procedures.

10.5.4.2 *Z*-Drop

The sample itself will often interfere with both excitation light on the way in and emission light on the way out (Guan et al. 2008; Lee and Bajcsy 2006; Sun et al. 2004). The effect of this is to produce an image set where the average intensity of

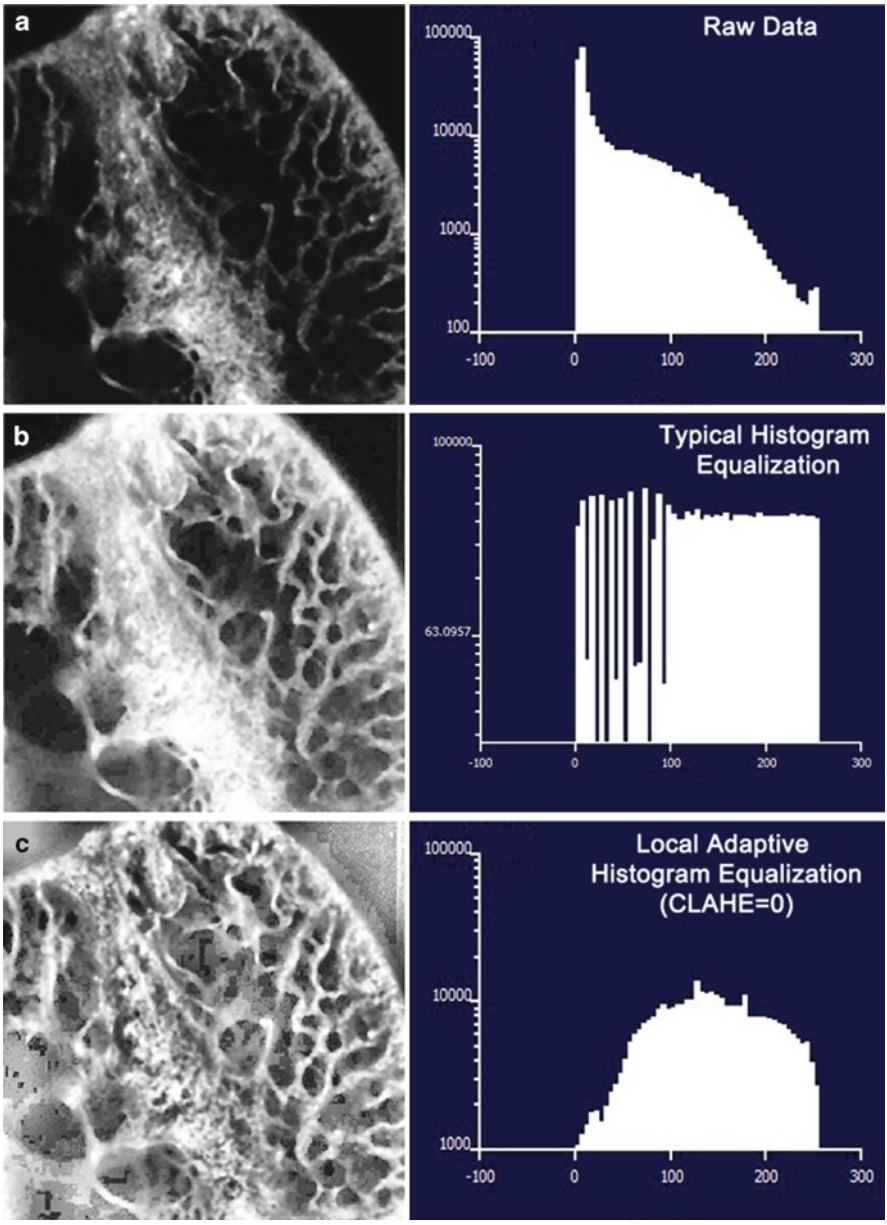

Fig. 10.16 Image adjustment. Histogram equalization. (**a**) A raw image and the corresponding histogram. (**b**) The result of a typical unrestrained histogram equalization. (**c**) Local adaptive histogram equalization without contrast limit. The effect of increasing the contrast limit in adaptive histogram equalization to 5 (**d**), 10 (**e**), and the maximal 15 (**f**)

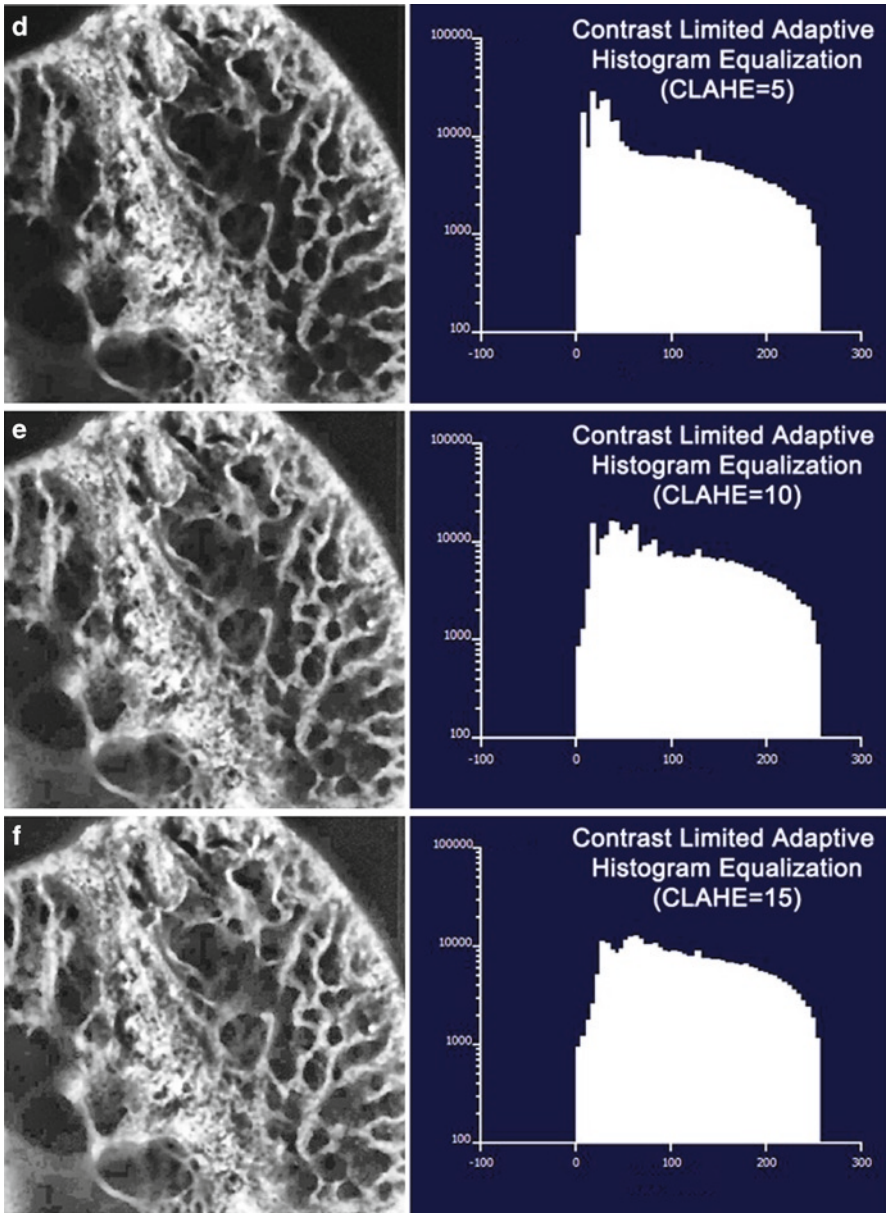

Fig. 10.16 (continued)

each optical slice appears to be reduced in deeper *z*-sections (a phenomenon termed *z*-drop, see Fig. 10.17). Most automated segmentation routines used threshold-based rules based on voxel intensity; thus it would be desirable that voxel intensity within regions of interest be uniform throughout the sample. Many 3D reconstruction systems offer routines to correct for *z*-drop as an adjustment procedure.

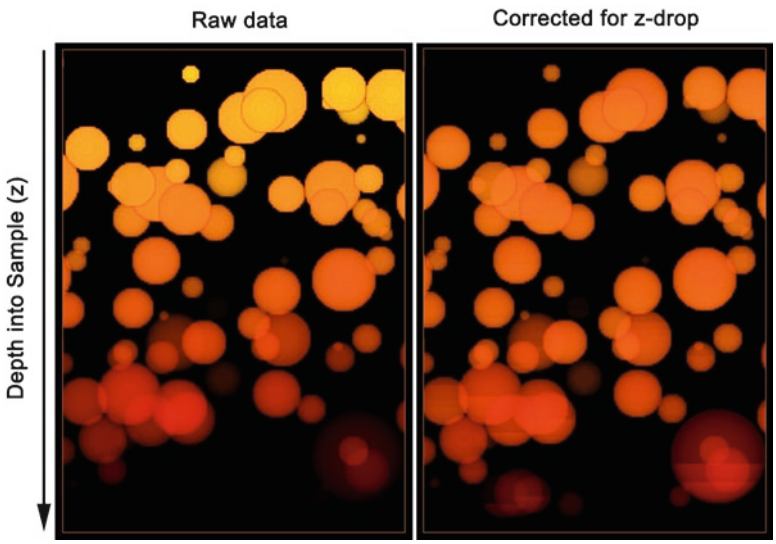

Fig. 10.17 Correcting for *Z*-drop in confocal data. Volume rendering (*XZ* view) of confocal data set showing the effect of *z*-drop through the depth of the sample (*left*). Following correction (*right*), voxel intensities have been adjusted so that average intensity is more nearly constant with depth

It is often possible to correct *z*-drop in the acquisition process by systematically adjusting laser intensity or detector gain (or both) as deeper optical slices are collected. Many confocal microscope control systems include a routine which will adjust these settings with optical depth, usually based on linear models of the *z*-drop effect.

10.5.5 Segmentation

Segmentation is the process of dividing the image data set into regions of interest. This is often the most time-consuming task and typically requires a great deal of expertise. It is worth noting here that segmentation is required in order for any measurements to be collected. In the simplest case, a confocal data set collected in a single fluorescent channel can be divided into two regions: fluorescent signal and background. Segmenting this channel using a fast, automated method is a matter of choosing a threshold intensity value that discriminates between these regions. However, the selection of a single threshold value that will apply across every optical slice is often thwarted by effects such as noise or *z*-drop. When such problems cannot be otherwise corrected in acquisition or by adjustment, manual segmentation methods are usually necessary. In this simple case, that may involve selecting a different threshold appropriate for each optical slice (to subvert conditions such as *z*-drop), or manually editing the results of an automatic segmentation to remove artifacts.

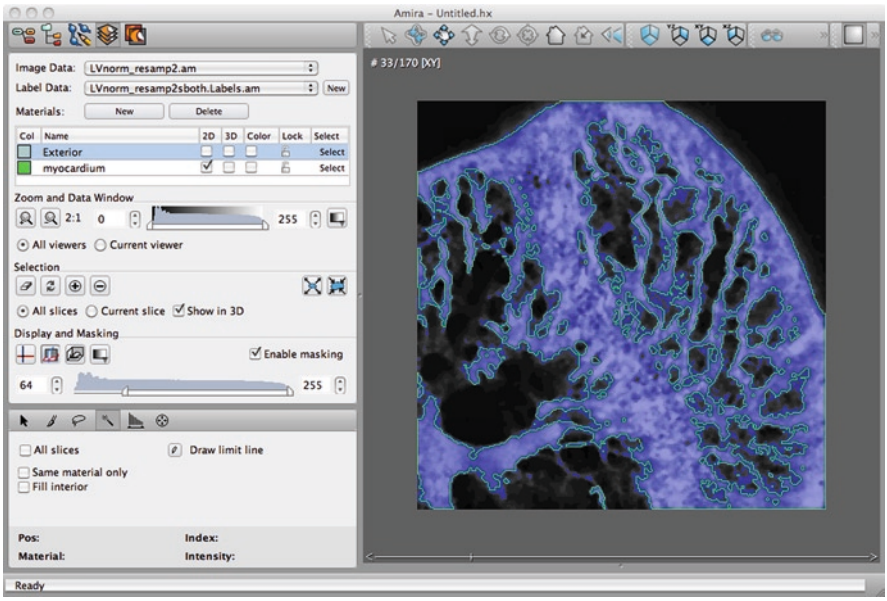

Fig. 10.18 Segmenting confocal data based on threshold. The segmentation editor in Amira (http://www.visageimaging.com) was used to locate voxels with intensity values between 64 and 255 (see the Display and Masking section on the *left*). The selected voxels are assigned to the Material "myocardium" and outlined in *green*. Although only one slice is shown, the selection was completed on all 170 optical slices simultaneously

An example of a segmentation editor is shown in Fig. 10.18. This routine is from the 3D software Amira (http://www.visageimaging.com) and offers a slice-by-slice view of the data from any perspective in addition to a selection of automated and manual selection tools. In the sample shown, a threshold has been set in the Display and Masking Section to select all voxels (in the entire confocal data set) with an intensity greater or equal to 64. Those voxels were then placed in a material named "myocardium" and outlined in green. These material data are saved in a separate Label Data file associated with the Image Data.

Once the nonfluorescent background has been isolated from the fluorescent signal, further refinements are possible. For the sample data shown in Fig. 10.18, it was decided to further segment the fluorescent signal into two histologically relevant regions: trabecular myocardium and compact myocardium. Obviously, these regions cannot be isolated based on voxel intensity, so manual segmentation by an experienced observer is required. In Fig. 10.19, the "myocardium" material was renamed "compact myocardium," and a second material "trabecular_myocardium" has been defined and color-coded red. The background material "Exterior" was locked (to prevent any changes), and a large paintbrush was used on each optical slice to select voxels from the green regions that belong in the red material. For 170 optical slices and with a trained observer, this procedure took about 2 h.

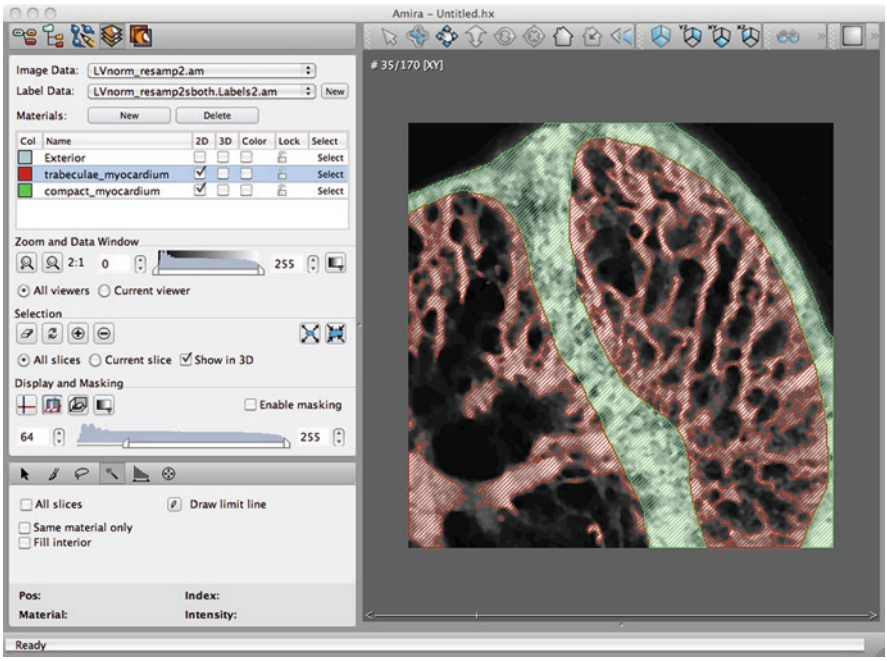

Fig. 10.19 Segmenting confocal data based on manual selection. The automatically segmented data in Fig. 10.18 was further separated into trabecular (*red*) and compact (*green*) myocardium on each optical slice by manual selection using the drawing tools

More sophisticated approaches to segment confocal data automatically have been reported (Lin et al. 2003; Losavio et al. 2008; Rodriguez et al. 2003; Yi and Copplino 2006), and some have even been made available in some specialized 3D software programs. These methods are usually based on finding the edges of regions based on voxel intensity, and some use filters based on the shape and size of the regions they expect to locate. As such, these routines require the image data to have the best contrast available (the data use most of the available brightness spectrum), and the resolution should be optimal (and probably even deconvolved). While these routines can save time, the results will still contain errors and require some manual editing.

10.5.6 Modeling and Visualization

Most modern computers can now render 3D models practically in real time; thus visualized results are often rendered repeatedly until the desired results are obtained. These computational speeds also make it easier to render animation frames, where the subject changes position or rotates in the field of view in a

series of predetermined steps. Nearly all 3D software programs offer methods of generating animations in avi or mpeg format, or can generate a folder full of single frames suitable for import into digital movie applications such as Adobe Premiere.

The amount of information conveyed in a 3D visualization can be augmented with just a little extra work. Consider the data from the confocal data set from the previous segmentation example now portrayed in Fig. 10.20. In (a), the middle 50 optical slices are shown as a maximum projection image generated immediately after acquisition. If all 170 optical slices had been included in the projection, the interior detail of the trabecular myocardium inside the ventricle would have been obscured (see Fig. 10.1c). In Fig. 10.20b, all of the data are visualized in a volume render using an RGBA look-up table which renders the background noise as transparent. The more intense voxels are rendered more opaque. The 3D nature of the sample is more apparent, and the trabecular myocardium can now almost be differentiated from the compact myocardium. In (c), the volume render has made use of the segmentation data to color code the two histological types of myocardium, and the discrimination of trabeculae inside the ventricle wall composed of compact myocardium is clear. Note that (c) is not a surface reconstruction, but a special volume render utilizing the segmentation data to color code voxels, and adding diffused lighting and specular effects.

While single images of 3D models are easy to publish, often it is of value to share a model which can be viewed from multiple angles. This has typically involved supplying a supplementary animation file with a guided tour of the object as directed by the film maker. It is now possible to include 3D objects entirely within the Adobe Acrobat PDF file format (http://www.adobe.com) such that the data can be interactively manipulated by anyone with the PDF file (Ruthensteiner and Hess 2008). Note that only surface reconstruction data (not volume renders) can be imported into PDF files, as of the writing of this chapter.

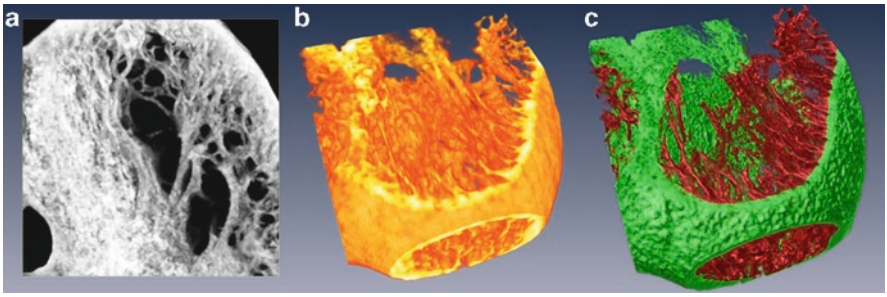

Fig. 10.20 Reconstruction models. (**a**) Projected data from the middle 50 slices (of 170). (**b**) Volume rendering of all 170 optical slices. (**c**) Volume rendering using manual segmentation to highlight trabecular (*red*) and compact myocardium (*green*)

10.5.7 Measurement

Measurements obtained from 3D data sets are based on the spatial dimensions of single voxels in the data. For example, if the size of a single voxel is $1 \times 1 \times 1$ mm, then the smallest volume that can be measured is a single voxel, or 1 mm^3. To determine the volume of a fluorescent object in an image data set, it is necessary to identify (segment) and then count the voxels in that object. The total volume will then be the voxel count multiplied by the volume of a single voxel.

The calculation of surface area will require a surface reconstruction. In this case, the individual triangles within the surface will each have unique areas determined by the *x*, *y*, and *z* coordinates of the three vertices of each triangle. The planar areas of each triangle are calculated and summed to produce a total surface area. (One can appreciate why surface calculations proceed more slowly when there are millions of triangles.)

The segmentation data of Fig. 10.19 were used to make the surface reconstructions shown in Fig. 10.21. Figure 10.21a is a surface model of the voxels contained in both segments. For segmented data and surface reconstructions, it is possible to

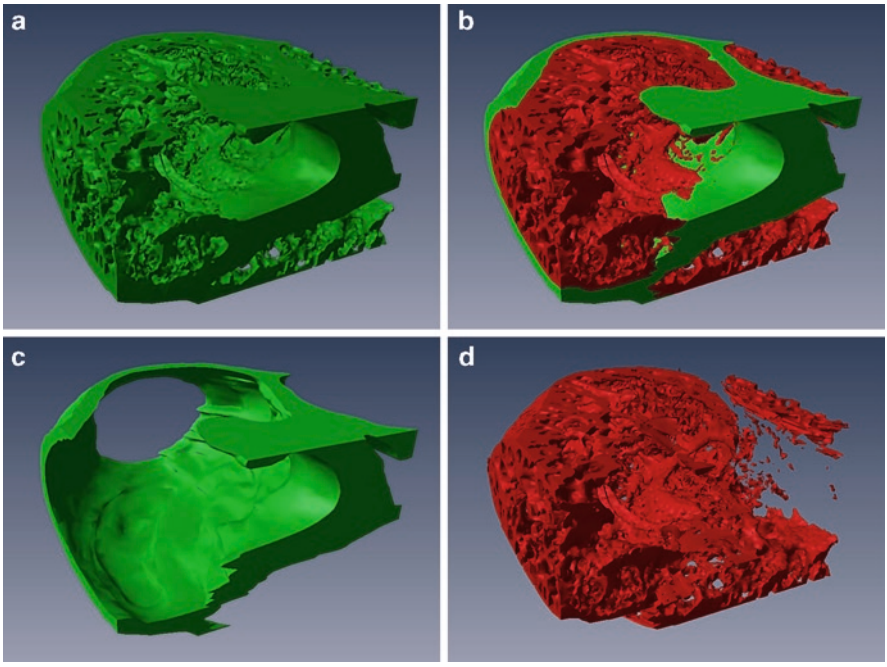

Fig. 10.21 Surface reconstructions from segmented confocal data. (**a**) Surface from threshold-based automatic segmentation. (**b**) Surface from data in (**a**) manually segmented into trabecular (*red*) and compact (*green*) myocardium. Segmented regions of interest allow separate rendering (**c**, **d**) and measurement

model the segments together (Fig. 10.21b) or independently (Fig. 10.21c–d). The volume and surface area measurements for the defined segments are shown in Table 10.1.

Most 3D software systems with measurement capabilities will further subdivide each material into regions based on voxel connectivity. That is, an isolated island of contiguous voxels is considered a region separate from other voxel regions. Material statistics can be gathered for materials based on regions, which is useful for counting cells, or nuclei, or any other objects that exist as isolated fluorescent entities.

Figure 10.22a shows a field of fluorescently stained nuclei that were segmented using an automatic threshold, and then surface rendered (Fig. 10.22b). Material statistics generated on this segmentation yields the data in Table 10.2, where the nuclear material has been analyzed based on region (the table is abbreviated). The analysis provides a total count of the regions, revealing that 139 isolated regions were identified. The volume; voxel count; x, y, z center coordinates; and mean voxel intensity within each region are provided. The data can be exported for more complex analyses. Note that these data from Amira are sorted by volume. It is a task

Table 10.1 Measurements from 3D reconstructed confocal data

Material	Voxel count	Volume (m^3)	Surface area (m^2)
Exterior	7,083,350	0.760	
Trabecular myocardium	1,838,729	0.197	21.4
Compact myocardium	2,219,041	0.238	7.3
Total	11,141,120	1.196	

Voxel size = 5.08 × 5.08 × 4.14 μm
Total data set is 256 × 256 × 170 voxels

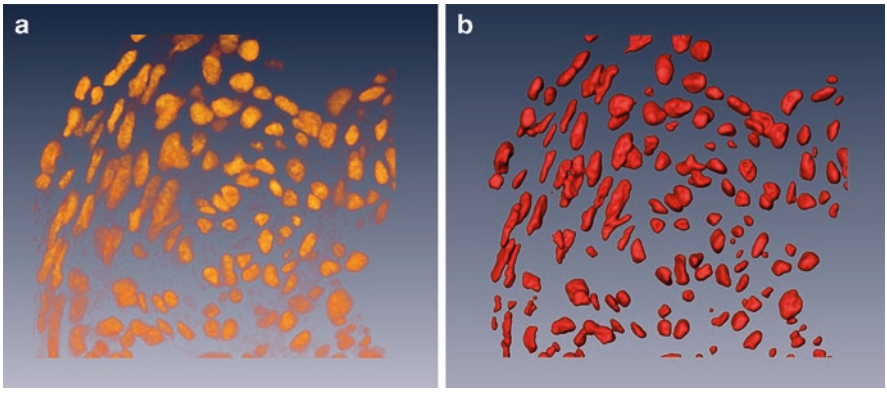

Fig. 10.22 Counting nuclei in segmented confocal data. (**a**) Voxel rendering of a field of stained nuclei. (**b**) The nuclei were segmented using an automated threshold for surface reconstruction. Material statistics for the regions in this segmentation report volume, spatial location, and fluorescence intensity data for each nucleus (see Table 10.2)

Table 10.2 Regional measurements

Number	Region	Voxel count	Volume	Center *X*	Center *Y*	Center *Z*	Mean
1	Exterior 1	2,196,590	116,823.1	93.6	119.4	5.3	13.0
2	Nuclei 139	13,248	704.5	44.7	133.3	6.2	78.6
3	Nuclei 138	13,229	703.5	122.8	96.4	5.5	81.3
4	Nuclei 137	9,868	524.8	104.0	111.3	5.6	87.6
5	Nuclei 136	9,134	485.7	93.1	92.6	6.2	89.2
6	Nuclei 135	8,511	452.6	62.9	114.3	5.5	71.9
7	Nuclei 134	8,500	452.0	80.5	105.9	5.1	79.1
8	Nuclei 133	8,015	426.2	72.0	83.7	5.7	82.0
9	Nuclei 132	7,334	390.0	78.5	92.4	5.6	84.9
10	Nuclei 131	7,048	374.8	77.6	123.0	5.6	73.6
…	…	…	…	…	…	…	…
138	Nuclei 3	19	1.0	41.4	149.6	6.83	59
139	Nuclei 2	19	1.0	93.7	72.6	2.9	57
140	Nuclei 1	19	1.0	82.3	91.4	8.8	62

left to the experimenter to decide if the smallest regions (nuclei with volumes of 1 μm^3) are noise.

The measurement routines in most 3D software systems will provide the basic data described here. Some provide more sophisticated tools, but these systems tend to be more expensive and will have highly specialized functions that are of little use to everyone. Thus, the last advice this chapter can offer is that the user should have some knowledge of the type of quantitative measures needed and to select carefully a software package that will fulfill the research requirements.

References

Biggs, D.S., *3D deconvolution microscopy.* Curr Protoc Cytom, 2010. **Chapter 12**: p. Unit 12 19 1–20.

Biggs, D.S.C., *Clearing up deconvolution.* Biophotonics International, 2004(February): p. 32–37.

Carlsson, K. and N. Aslund, *Confocal imaging for 3-D digital microscopy.* Appl. Opt., 1987. **26**(16): p. 3232–3238.

Clendenon, J.L., J.M. Byars, and D.P. Hyink, *Image processing software for 3D light microscopy.* Nephron Exp Nephrol, 2006. **103**(2): p. e50–4.

Feng, D., D. Marshburn, D. Jen, R.J. Weinberg, R.M. Taylor, II, and A. Burette. *Stepping into the third dimension.* J Neurosci, 2007. **27**(47): p. 12757–60.

Guan, Y.Q., Y.Y. Cai, X. Zhang, Y.T. Lee, M. Opas. *Adaptive correction technique for 3D reconstruction of fluorescence microscopy images.* Microsc Res Tech, 2008. **71**(2): p. 146–57.

Hecksher-Sorensen, J. and J. Sharpe, *3D confocal reconstruction of gene expression in mouse.* Mech Dev, 2001. **100**(1): p. 59–63.

Lee, S.C. and P. Bajcsy, *Intensity correction of fluorescent confocal laser scanning microscope images by mean-weight filtering.* J Microsc, 2006. **221**(Pt 2): p. 122–36.

Lin, G., U. Adiga, K. Olson, J.F. Guzowski, C.A. Barnes, and B. Roysam *A hybrid 3D watershed algorithm incorporating gradient cues and object models for automatic segmentation of nuclei in confocal image stacks.* Cytometry A, 2003. **56**(1): p. 23–36.

Losavio, B.E., Y. Liang, A. Santamaría-Pang, I.A. Kakadiaris, C.M. Colbert, and Peter Saggau, *Live neuron morphology automatically reconstructed from multiphoton and confocal imaging data.* J Neurophysiol, 2008. **100**(4): p. 2422–9.

Mackenzie, J.M., M.G. Burke, T. Carvalho and A. Eades. *Ethics and digital imaging.* Microscopy Today, 2006. **14**(1): p. 40–41.

McNally, J.G., T.S. Karpova, J.A.Cooper, J.-A. Conchello. *Three-dimensional imaging by deconvolution microscopy.* Methods, 1999. **19**(3): p. 373–85.

Rodriguez, A., D. Ehlenberger, K. Kelliher, M. Einstein, S.C. Henderson, J.H. Morrison, P.R. Hof and S.L. Wearne, *Automated reconstruction of three-dimensional neuronal morphology from laser scanning microscopy images.* Methods, 2003. **30**(1): p. 94–105.

Rueden, C.T. and K.W. Eliceiri, *Visualization approaches for multidimensional biological image data.* Biotechniques, 2007. **43**(1 Suppl): p. 31, 33–6.

Ruthensteiner, B. and M. Hess, *Embedding 3D models of biological specimens in PDF publications.* Microsc Res Tech, 2008. **71**(11): p. 778–86.

Savio-Galimberti, E., J. Frank, M. Inoue, J.I. Goldhaber, M.B. Cannell, J.H.B. Bridge, and F.B. Sachse. *Novel features of the rabbit transverse tubular system revealed by quantitative analysis of three-dimensional reconstructions from confocal images.* Biophys J, 2008. **95**(4): p. 2053–62.

Soufan, A.T., G. van den Berg, P.D. Moerland, M.M.G. Massink, M.J.B. van den Hoff, A.F.M. Moorman and J.M. Ruijter. *Three-dimensional measurement and visualization of morphogenesis applied to cardiac embryology.* J Microsc, 2007. **225**(Pt 3): p. 269–74.

Sun, Y., B. Rajwa, and J.P. Robinson, *Adaptive image-processing technique and effective visualization of confocal microscopy images.* Microsc Res Tech, 2004. **64**(2): p. 156–63.

Yi, Q. and M.G. Coppolino, *Automated classification and quantification of F-actin-containing ruffles in confocal micrographs.* Biotechniques, 2006. **40**(6): p. 745–6, 748, 750 passim.

Chapter 11
Ethics and Resources

W. Gray (Jay) Jerome and Robert L. Price

Keywords Colocalization • Ethics • Gamma • Histogram stretch • Nyquist • Pixels

11.1 Introduction

In the opening paragraph of this text we noted that often students and technologists use the confocal microscope to collect images without a full understanding of how the system works. Unfortunately, an additional factor affecting image collection is that often the students and technologists are given a preconceived idea of what the final image or data should look like.

11.2 Imaging Ethics

This is not a new problem as illustrated by a quote from the book *The Microscope Made Easy* (shortened title) by Henry Baker (1742): "When you employ the microscope, shake off all prejudice, nor harbor any favorite opinions; for, if you do, 'tis not unlikely fancy will betray you into error, and make you see what you wish to see." With the sophistication of today's microscopes and the power of digital imaging techniques, accurate presentation of data and avoiding the temptations of seeing what we wish to see and of "cleaning up" images have never been more important. As noted by North (2006) "All data are subject to interpretation"

R.L. Price (✉)
Department of Cell and Developmental Biology, School of Medicine, University of South Carolina, 6439 Garner's Ferry Road, Columbia, SC 29208, USA
e-mail: Bob.Price@uscmed.sc.edu

R.L. Price and W.G. (Jay) Jerome (eds.), *Basic Confocal Microscopy*,
DOI 10.1007/978-0-387-78175-4_11, © Springer Science+Business Media, LLC 2011

and many errors are introduced in complete innocence. A perfect example, as discussed throughout this text and by North, is whether the presence of yellow in a red/green merged image represents true colocalization. Hopefully, at this point it is recognized that many factors affect and alter the colors (signal) in a fluorescence image.

Unfortunately, it is not always in complete innocence that images are used inappropriately. The number of cases involving questionable images has been on a consistent upward trend since the first Department of Health and Human Resources Office of Research Integrity (ORI) Annual Report reporting period of 1989–1990 when only 2.5% of the cases involved questionable images (Krueger 2005). Perhaps the most famous case of unethical use of digital images is that of Woo Suk Hwang's manipulation of digital images of stem cells in his 2005 Science paper (Hwang et al. 2005). Other examples of questionable image manipulation, including confocal images, have been reported as detailed in the 2008 ORI annual report (Federal Register Volume 73 Number 196 page 58968). The 2009 ORI Annual Report further indicates that 68% of the cases opened by the ORI involve cases of questioned images (Krueger 2009).

With the ease of image collection in confocal microscopy continual diligence in handling confocal digital images through the various steps of collection and processing in Photoshop, AMIRA and other programs is essential. Our images are our data and just as it would not be acceptable to vary or alter pipetting volumes when loading a Western blot, it is not acceptable to vary or alter pixel data. Equally important is that early in training all are taught the importance of maintaining detailed laboratory notebooks for experiments, but few are taught the importance of the proper handling and archiving of digital images. An article by Goldenring (2010) emphasizes the importance of keeping original image files collected from the microscope and for maintaining nonflattened archival Photoshop files of all image manipulations. It was only through proper archiving of all images and image processing that Dr. Goldenring and members of his laboratory were able to disprove reviewer and editorial charges of misconduct regarding confocal images.

11.3 Journal and Office of Research Integrity Guidelines

Most journals have published guidelines for acceptable processing of digital images. The ORI has also published a series of guidelines for handling digital images that are essential for acquisition and publication of confocal images (http://ori.dhhs.gov/products/RIandImages/guidelines). While many of these topics have already been discussed, because of the importance of the topic, some redundancy is justified and the full list of 12 guidelines is given here. Expanded discussions of each topic are available on the ORI website.

1. Treat images as data: Scientific digital images are data that can be compromised by inappropriate manipulations.

2. Save the original: Manipulations of digital images should always be done on a copy of the raw image. The original must be maintained.
3. Make simple adjustments: Simple adjustments to the entire image are usually acceptable. Reasonable adjustments using software tools like brightness and contrast, levels, and gamma are usually appropriate.
4. Cropping is usually acceptable. Legitimate reasons for cropping include centering an area of interest, trimming empty space around the edges of an image, and removing debris from the edge of an image. Questionable forms of cropping include editing which can create bias such as removal of dead or dying cells leaving only healthy cells. Motivation for cropping should always be a primary consideration. Is the image being cropped to improve its composition or to hide something?
5. Comparison of images should only involve images that have been collected under identical conditions of preparation and acquisition, and any postimaging processing should be identical for all images involved.
6. Manipulation should be done on the entire image. It is not acceptable to alter one area of an image to enhance a specific feature.
7. Filters such as smoothing and sharpening functions degrade data and are not recommended. If filters are used this needs to be reported in the Methods and Materials sections of the paper.
8. Cloning or copying pixels from other images or a different area of the same image should not be done. Copying pixels to create structures in an image which did not exist is research misconduct.
9. Intensity measurements are difficult to perform and must be done on image pixels collected and processed in an identical manner. Measurements should always be performed on the raw data.
10. Avoid the use of lossy image compression formats. TIFF (Tif) is the most widely accepted format for images but always check the journal format prior to submitting images. In general, the JPEG format should never be used for collection of scientific images.
11. Confocal images include *X*, *Y*, and *Z* dimensions and digitally altering the size (magnification) in any of these directions will alter the data. Care must be taken to sample or collect images according to the Nyquist theorem. If doubt exists concerning Nyquist sampling then oversampling should be performed.
12. Altering the number of pixels in an image to make images fit a page can result in software interpolation of data which will create a new resolution and possibly intensity value for pixels. This can result in aliasing artifacts.

As noted by Rossner and Yamada (2004) each image should be an accurate representation of what was observed through the microscope. Manipulating images to make them more convincing can change data that others might be interested in or interpret differently.

11.4 Microscopy Society of America Statement on Ethical Digital Imaging

All of the above considerations have led the Microscopy Society of America to issue a Statement on Ethics in Digital Imaging:

> Ethical digital imaging requires that the original uncompressed image file be stored on archival media (e.g., CD-R) without any image manipulation or processing operations. All parameters of the production and acquisition of the files, as well as any subsequent processing steps, must be reported to ensure reproducibility.
>
> Generally acceptable (non-reportable) imaging operations include gamma correction, histogram stretching, and brightness and contrast adjustments. All other operations (such as unsharp masking, Gaussian blur, etc.) must be directly identified by the author as part of the experimental methodology. However, for any image data that is used for subsequent quantification, all imaging operations must be reported.

If care is taken in the preparation and collection of confocal images as discussed in the previous chapters and all of the above guidelines are followed for processing confocal images, few problems concerning the ethics of how your data was collected and processed should arise. Always remember the Confocal Commandments and keep an original unaltered archived file of your data and work from a copy.

11.5 Available Resources

There are a number of websites maintained by manufacturers that are excellent resources for fluorescence and confocal microscopy. Among these are:

Nikon Microscopy U: http://www.microscopyu.com/articles/confocal/
Olympus Microscopy Resource Center: http://www.olympusmicro.com/primer/techniques/fluorescence/fluorhome.html
Zeiss Online Campus: http://zeiss-campus.magnet.fsu.edu/tutorials/index.html

The Confocal Microscopy List Serve (confocalmicroscopy@lists.umn.edu) is dedicated to topics in confocal imaging while the Microscopy Society of America also maintains a List Serve (http://www.microscopy.com/) that addresses topics in confocal as well as all other forms of microscopy.

There are also a number of books available which cover many aspects of confocal imaging. However, many of these are relatively old and/or cover various techniques and applications rather than basic information on how to operate a confocal system. The rate at which confocal technology is being developed also makes it difficult to keep up with advances in confocal microscope hardware. A chronological listing of some of the books that we have found very useful is:

John K. Stevens, Linda R. Mills, and Judy E. Trogadis (Eds). 1994. Three Dimensional Confocal Microscopy: Volume Investigation of Biological Systems. Academic. 507pp (Good practical information; nice section on spinning-disk microscopes).

Ming Gu. 1996. Principles of Three-Dimensional Imaging in Confocal Microscopes. World Scientific Publishing Company, Inc. 352pp (Very technical but good for advanced students).

Stephen W. Paddock (Ed). 1999. Confocal Microscopy (Methods in Molecular Biology Volume 1212). Humana. 464pp (Very good practical protocols as well as basics. A new version is scheduled to be released in November of 2010).

Alberto Diaspro (Ed). 2001. Confocal and Two-Poton Microscopy: Foundations, Applications and Advances. Wiley. 576pp (Excellent treatise of some advanced confocal imaging techniques).

Brian Matsumoto (Ed). 2002. Methods in Cell Biology volume 70: Cell Biological Applications of Confocal Microscopy Second Edition. Academic. 507pp (Information on system hardware and applications to some specific biological organisms and systems.)

Alan Hibbs. 2004. Confocal Microscopy for Biologists. Springer 474pp (Good for beginners and advanced; great appendix of information; live cell imaging).

James B. Pawley (Ed). 2006. Handbook of Biological Confocal Microscopy, 3rd Edition. Springer 988pp (A very good comprehensive review of advanced confocal microscopy).

Hopefully, the book you are currently reading will be added to your list of useful resources for confocal imaging.

References

Baker, H. 1742. The Microscope Made Easy; or I. The nature, uses, and magnifying powers of the best kinds of microscopes described… for the instruction of such, particularly, as desire to search into the wonders of the minute creation… II. An account of what surprising discoveries have been already made by the microscope… And also a great variety of new experiments and observations… London, R. Dodsley. 311pp.

Goldenring, JR. 2010. Innocence and due diligence: Managing unfounded allegations of scientific misconduct. Academic Medicine 85(3):527–530.

Hwang et al., 2005. Patient specific embryonic stem cells derived from human SCNT blastocysts. Science 308:1777–1783.

Krueger, J. 2005. Confronting image manipulation of digital images in science. ORI Newsletter 13(3):8–9.

Krueger, J. 2009. Incidences of ORI cases involving falsified images. ORI Newsletter 17(4):2–3.

North, AJ. 2006. Seeing is believing? A beginners' guide to practical pitfalls in image acquisition. J Cell Biol. 172(1):9–18.

Rossner, M and Yamada, KM. 2004. What's in a picture? The temptation of image manipulation. J Cell Biol. 166(1):11–15.

Glossary (Terms are Defined with Respect to Confocal Imaging)

Acousto-optical beam splitter (AOBS)	A form of AOTF that replaces the dichroic filters in Leica confocal systems, making it possible to work with a larger variety of excitation and emission wavelengths without the changing of multiple filters.
Acousto-optical tuneable filters (AOTF)	Typically a tellurium dioxide or quartz crystal whose optical properties (refractive index) can be controlled by varying the acoustic waves it is exposed to. As the refractive index is altered, the wavelengths of light present are split or combined into specific bandwidths which can be selected for use in the confocal microscope.
Affinity	A measure of the strength of antibody:antigen binding.
Alexa Fluor dyes	A family of dyes produced by molecular probes that has excellent photostability for use in confocal imaging. Dyes are available for a wide range of excitation and emission ranges that span the visible spectrum.
Alpha value	Measure of voxel opacity or transparency when creating and analyzing 3D reconstructions. An alpha value of 0 creates opaque voxels, while an alpha value of 1 creates transparent voxels.
Analog image	An image in which gray or color tones are continuous in infinitely small increments.
Anti-fade reagent	Various reagents such as DABCO and other mounting media that inhibit or stop the photobleaching of fluorochromes when they are excited by high-intensity lasers.
Antibody	A protein produced as an immune response by a host which recognizes and can attach to the antigen which elicited the immune response. By attaching fluorescent markers to the antibody, specific labeling of the antigen can be achieved.

R.L. Price and W.G. (Jay) Jerome (eds.), *Basic Confocal Microscopy*,
DOI 10.1007/978-0-387-78175-4, © Springer Science+Business Media, LLC 2011

Antigen	A specific molecule or group of molecules which is capable of eliciting an immune response from a host, resulting in the production of antibodies. Attachment of fluorochromes to the antigen, or to antibodies which recognize the antigen, allows the precise localization of the antigen in cells and tissues.
Autofluorescence	Fluorescence in a sample that may arise from endogenous substances (NADH) or frequently from fixation with aldehydes. In fluorescence microscopy of biological samples, autofluorescence is most often a problem when using an excitation wavelength around 488 nm.
Avidity	The number of binding sites for a target molecule that a label possesses.
Background	Spurious information in an image that may result from autofluorescence or from noise introduced by the detector and electronics of the system. Autofluorescence typically shows as nonspecific fluorescence across the range of the specimen, while electronic noise typically shows as bright pixels in areas where no labeling or sample fluorescence is present.
Band-pass or Emission filter	See "Emission filter."
Binning	Grouping together of adjacent imaging elements (photodiodes) in a CCD camera to increase speed of imaging or intensity of the signal. Binning results in the loss of resolution, which creates a compromise situation between performing high-resolution and fast imaging.
Bit-depth	An expression of the number of gray tones or colors available in an image. An 8-bit image (2^8) has 256 available values and a 12-bit image (2^{12}) has 4,096 available values.
Bleed-through	Term used to describe spectral overlap of photons emitted from two or more fluorochromes labeling the same sample. This may make it difficult to determine which fluorochrome contributed the signal affecting localization and quantification of sample fluorescence.
Brightness	A measure of how light or dark a pixel appears. A brightness value of 0 is black and a brightness of 255 in an 8-bit image is white.
Cartesian coordinate system	System used for reconstruction of data sets in which the *x*-, *y*-, and *z*-axis are all perpendicular to each other.
Charge-coupled device (CCD) camera	A photodiode-based detection system frequently used for wide-field fluorescence and spinning disk confocal systems due to its ability to capture images rapidly. However, rapid capture is often at the expense of resolution.

Chromatic aberration	The result of shorter wavelengths of light (blue) being focused closer to the surface of a lens than longer (red) wavelengths of light. If objective lenses are not corrected for chromatic aberration, significant artifacts in interpretation of confocal co-localization data may result.
CMYK color space	A subtractive color scheme comprised of cyan, magenta, yellow, and key (black). When no colors are present, a pixel is white. When all colors are present, the pixel is represented as black.
Co-localization	The presence of signal from two or more fluorochromes in the same pixel or voxel of information.
Confocal microscope	A microscope in which an aperture is placed in front of the detection device to block out-of-focus light from contributing to the final image. When used properly, this results in all planes of the final image being in focus.
Correction collar	A collar on a microscope lens which allows the optical elements to be slightly rotated to correct for spherical aberration resulting from refractive index mismatch due to incorrect coverslip thickness or differences between sample and mounting media refractive indices.
Cyanine dyes	A family of fluorescent synthetic dyes named based on the number of methine of trivalent functional CH groups present in the structure of the molecule. Thus, Cy3 has three methine groups and Cy5 has five methine groups. The photostability and specific excitation and emission values associated with each member of the Cy family make the dyes very useful in multilabeling confocal microscopy experiments.
1,4-Diazabicyclo[2,2,2] octane (DABCO)	A common anti-fade reagent that can be mixed into mounting media such as PBS glycerine to protect the sample from photobleaching.
Deconvolution	A mathematical method to recover lost signal and resolution in an image based on the pattern of light spread from a point source of emission.
Depth of field	The range to which the specimen can be moved in the *Z*-direction while remaining in acceptable focus.
Depth of focus	The distance (depth) in the *Z*-direction that information around a point in the sample is still in acceptable focus. Depth of focus is dependent on the wavelength of the imaging source, numerical aperture, and refractive index.
Dichroic (dichromatic) filter	A filter that is capable of reflecting light of one range of wave lengths, while allowing other wavelengths of light to be transmitted through. In confocal imaging, dichroics are typically used to reflect excitation photons toward the sample, while allowing emission photons to pass through to the detector.

Differential interference contrast (DIC)	A high-contrast, high-resolution imaging mode based on the use of polarized light for working with live cells and unstained tissues.
Digital image	An image that consists of discrete elements (pixels or voxels) that have values of one unit or a multiple of that unit (1, 2, 3, etc.). For example, it is not possible to have an element with a value of 1.1 because this value is not a whole multiple.
Digitization	The process of converting an analog image comprising a continuous series of numerical values into a digital image that has discrete whole number values.
Dipping lens	A microscope objective designed to be used without the presence of a coverslip. This allows the lens to be placed directly into the cell culture dish. Although dipping lenses typically have a low numerical aperture, they have a long working distance, making them ideal for direct imaging of cells in a dish.
Dry lens	A microscope objective designed to be used without an immersion fluid such as water or oil.
Emission filter	Filter which determines the wavelengths of photons that will be allowed to pass through to the detector. • Short pass – short-pass emission filters allow all photons shorter than a specific wavelength to pass through to the detector. • Band pass – band-pass emission filters allow photons between two specific wavelengths to pass through to the detector. • Long pass – long-pass emission filters allow photons longer than a specific wavelength to pass through to the detector.
Epifluorescence microscope	Fluorescence imaging system in which both the excitation and emission light pass through the objective lens. The various wavelengths of light are separated by excitation and emission filters.
Epi-illumination	The system in which excitation photons are focused onto the specimen with an objective lens rather than a condenser lens, and the emitted light travels in the direction opposite to that of the excitation light.
Epitope	The region of the antigen that conveys specificity to the antibody. Epitopes are often sensitive to fixation and processing, thus making identification of the antigen by the antibody difficult and resulting in reduced intensity of labeling.

Excitation filter	Filter used to control the wavelength and intensity of the excitation photons.
Fixative (precipitating)	Chemical which preserves cell structure by dehydration and precipitation of cell components, typically proteins. Most are organic solvents such as alcohols and acetone which remove lipids, but significantly affect 3D architecture due to removal of water, resulting in shrinkage of the sample.
Fixative (cross-linking)	Most commonly members of the aldehyde group of chemicals which preserve tissue structure by forming molecular bridges between amino groups.
FLIM (fluorescent lifetime imaging microscopy)	Imaging method based on the length of time a fluorescent molecule remains in the excited state, making it possible to distinguish dyes in the same wavelength range and to separate emission from autofluorescence. Lifetimes may vary and are affected by a variety of environmental factors, making it possible to study many factors that affect living cells.
Fluorescence	Emission of photons following absorption of energy of a shorter wavelength.
Fluorescence lifetime	The delay in emission of a photon from the time a photon is absorbed by a fluorochrome.
Fluorescence recovery after photobleaching (FRAP)	The technique in which a specific region of a cell is exposed to a high-intensity laser, resulting in photobleaching. The region is then monitored to determine the time required for fluorescence to return. This provides a measure of dynamic events that may occur within the cell.
Fluorescence resonance energy transfer (FRET)	The technique in which energy from one excited fluorochrome (donor) is transferred to and excites a fluorochrome associated with a second molecule (acceptor). Excitation of the acceptor occurs only if molecules are closely associated (less than 10 nm), giving a measure of the distance between the two molecules.
Fluorochrome	Molecule which absorbs a photon of light of a specific wavelength and, after a brief interval, emits some of that energy in the form of a photon of a different wavelength.
Fluorophore	Fluorochrome linked to a biologically active substance such as protein, DNA, or RNA.
Focal length	The distance from the surface of the lens to the point or plane in the specimen where the light is focused. Focal length is dependent on several factors including refractive index and chromatic and spherical aberrations.

Focal plane	The plane of the specimen which is in focus.
Formaldehyde	A common fixative in which the aldehyde groups bind to amine groups in proteins. Paraformaldehyde is the crystaline powder form, while formaldehyde is a gas.
Formalin	A 40% solution of formaldehyde.
Full-width half maximum (FWHM)	The width of an emission peak at half its height. Often used for describing characteristics of fluorophore emission and emission filter specifications.
Gamma	The relationship between the gray level that is detected and that which is rendered in the final image. A gamma of 1 indicates that the detected and rendered gray levels are identical. Gamma relationships are not linear. At a gamma of 0.5 pixel values of 0 and 255 remain as 0 and 255 but an input pixel value of 50 has an output pixel value of 113.
Gamma correction	The inverse of gamma. Gamma correction can be used to restore the original image pixel values.
Green fluorescent protein (GFP)	One of a family of naturally occurring fluorescent proteins that can been incorporated into the genomic structure of cells and used as a locator molecule in fluorescence microscopy. Excitation of GFP is in the blue range and emission in the green range. Other fluorescent proteins such as red and yellow variants also exist with specific excitation and emission ranges.
Histogram equalization	An image processing procedure in which pixel values in a digital image are remapped so that all intensity values are equally represented in the image. The effect is to maximize contrast (and noise) in the image.
Histogram stretch	In an 8-bit image, the darkest pixel value will be assigned to 0 and the highest pixel value assigned to 255, so that all 256 available values are utilized to improve the contrast of the image. The histogram is stretched to use the full dynamic range.
Hue	Defines the color of a pixel or voxel. All blue pixels have the same hue.
Immersion lens	Lens designed to be immersed in a fluid such as water, glycerin, or oil to minimize the refractive index mismatch of components in the optical path. Immersion lenses differ from dipping lenses in that they are designed to be used with a coverslip in place.

Interpolation	A method of resampling data sets by the computer. Often used to create near-cubic voxels to facilitate 3D reconstructions.
Jablonski diagram	Diagram of energy absorption and emission from a fluorochrome.
Joint photographic experts group (JPEG)	A compressed generic image file format useful for digital transfer of images and incorporation of images into programs such as Powerpoint. JPEG files are a lossy format and should not be used for data analysis or for final storage of scientific images.
Kernel	A grouping of pixels or voxels used for image enhancement, analysis, and reconstruction. For example, a group of three pixels in the *X*-direction and three pixels in the *Y*-direction would represent a 3×3 kernel.
LASER	Acronym for light amplification by stimulated emission of radiation. Lasers produce an intense monochromatic beam of coherent collimated light that is useful in confocal imaging.
Light-emitting diodes (LED)	High-performance stable light sources with relatively nar row emission spectra which can be used to excite fluorochromes in epifluorescent and spinning disc confocal systems.
Ligand	A substance that is capable of binding to and activating a cell receptor. With respect to confocal and fluorescence imaging, ligands may be conjugated to fluorescent molecules and attachment to receptors detected.
Look-up table (LUT)	A table of alternate values (typically colors) that will be used to display pixels of certain values to be re-assigned a specific color. Often used as an aid when setting optimal ranges of pixel values for display of a confocal image.
Luminance	A measure of the perceived brightness. Luminance considers the color sensitivity of the human eye to certain colors such as yellow-green, which the eye is sensitive to, compared to blue, which the eye is not very sensitive to.
Magnification	The extent to which a sample is enlarged when comparing the actual size and the size in the final image.
Marching Cubes algorithm	A computer graphics algorithm used to define a surface in 3D space by the use of voxels. Based on assigned criteria such as threshold values, the algorithm can be used to define specific structures in a region of interest for reconstruction of a 3D data set.

Maximum projection	A method of projecting multiple confocal slices and flattening into a single image. Pixel values at each location in all images of the Z-series are compared and the maximum value kept and projected into the final 2D image.
Molar extinction coefficient	A measure of the quantity of light absorbed as a function of the path length of the excitation light and the concentration of the fluorochrome. A molecule with a high molar extinction coefficient is more likely to exhibit fluorescence.
Multiphoton (two-photon)	Systems that use the additive energy of long-wavelength energy photons to excite fluorochromes rather than the short-wavelength high-energy photons used in single-photon confocal systems. Multiphoton systems provide the distinct advantages of reduced specimen damage and deeper specimen imaging.
Multitrack (sequential) imaging	See "Sequential imaging."
Neutral density (ND) filter	A filter that is used to reduce the intensity of light (number of photons) from the laser prior to interacting with the specimen. In most modern high-end systems, the ND filter is replaced with an AOTF which provides additional control over the intensity and wavelengths of light used to excite a specimen.
Numerical aperture	A measure of the resolving power and light-gathering capacity of a lens given by the equation $NA = n \sin \theta$, where n represents the refractive index of the medium and θ represents the half angle of the light entering the lens. As NA increases, the light-gathering capacity and resolution of the lens improve.
Nyquist theorem	A simplified explanation of the Nyquist theorem useful for confocal imaging is that to resolve a structure, it must be sampled at least twice in the data set. This is important in both 2D and 3D imaging space but becomes very important in 3D reconstructions and sampling when collecting *Z*-series data sets where *Z*-resolution is easily adjusted with the pinhole settings. Oversampling may result in very large data sets and extensive collection times, while undersampling will require computer interpolation when generating 3D reconstructions.
Objective lens	The primary image-forming lens and a key component of the optical path in a confocal microscope. High-quality objective lenses corrected for flat-field imaging and chromatic and spherical aberrations are essential for confocal imaging.

Oblique planes	Data presentation in which image planes are not perpendicular to the major *x*-, *y*-, and z-axis used when the original image data are collected.
Orthographic projection	3D data representation in which all projection rays passing through the data remain parallel and without reference to the viewer so objects do not appear in perspective. This results in same sized objects appearing identical, regardless of the distance they may be from the viewer.
Orthogonal planes	Data presentation in which planes are perpendicular to each other. In imaging, this refers to image planes perpendicular to any of the *x*-, *y*-, and *z*-axis used when the original image data was collected.
Perspective projection	3D data representation in which rays from objects in a scene project directly toward and converge at the viewer. This results in objects appearing to decrease in size as they increase in distance from the viewer.
Phase contrast microscopy	An imaging mode useful for unstained cells in which small phase shifts of the light occur as it passes through the specimen. Based on optical components added to the light path, the phase shifts can be used to introduce contrast to transparent specimens.
Photobleaching	Chemical or mechanical destruction of a fluorophore due to high-energy photons from the excitation source. Photobleaching results in an irreversible reduction in the number of photons emitted and can be a major concern for several fluorophores used in single-photon confocal imaging.
Photomultiplier tube (PMT)	The primary type of detector used in single and multiphoton-based confocal scanning laser microscopes. PMTs are highly sensitive detectors capable of detecting and proportionally amplifying relatively few photons emitted from a sample.
Photon	The elementary particle of light or quantum of electromagnetic radiation. Photons exhibit specific wavelength and particle properties that allow separation into specific bands of light useful for excitation and emission of fluorophores used in confocal imaging.
Pinhole (also referred to as an aperture or iris in some systems)	A small opening that restricts the passage of light waves to only those that are in focus at the opening.
Pixel	Discrete 2D picture elements which comprise a digital image. Pixels have a 2D address within an image (*x*, *y* location) and an intensity value (i.e., 0–255).

Plan objective	An objective lens corrected for flat-field imaging so no curvature of the lens is present. Plan objectives are important in confocal imaging since curvature may result in multiple focal planes and loss of signal due to the confocal effect of the pinhole.
Planck's Law	The radiation energy of a photon is inversely proportional to its wavelength.
Quantum dots	Photostable fluorescent semiconductor nanocrystals with high quantum yield that absorb light and emit light at a longer wavelength similar to standard organic fluorochromes.
Quantum efficiency	See "Quantum yield."
Quantum yield	A measure of the efficiency of a fluorochrome presented as a ratio of the number of photons emitted relative to the number of photons absorbed. Thus, it is a measure of the efficiency of fluorescence, and a quantum yield of 1.0 would be a perfect emitter with one photon emitted for each photon absorbed.
Quenching	The reversible reduction in number of photons emitted from a fluorophore. A number of factors including excitation, changes in solution chemistry, and interaction with surrounding molecules may result in quenching.
Refractive index	A measure of the speed of light as it passes through various media. As light passes through a vacuum, the refractive index equals 1.0. As light passes through various other media, the speed, and thus the refractive index, varies and is presented as a ratio of the speed through the vacuum compared to the speed to the specific medium. For example, the refractive index through water is 1.33. With respect to confocal imaging, this term refers to a measurement of how the wavelength of photons is affected as they pass through components of the optical path.
Refractive index mismatch	As light passes through the various components in the optical path of a confocal microscopy, the speed, and thus the refractive index, varies. Refractive index mismatch refers to this variation in the speed of light as it passes along the optical path and can result in significant deterioration of the image due to chromatic and spherical aberrations.
Resolution	The ability to distinguish two points or objects within a sample clearly. Based on the Nyquist theorem, the two points must be sampled twice to be able to resolve them.

RGB color space	An additive color mechanism in which images are comprised of red, green, and blue. When all three colors are present, a white pixel results. When none are present, a black pixel results.
RGBA tuples – (red, green, blue, alpha)	Coding of voxel values in each of the four channels for display of 3D data sets and reconstructions.
Saturation (color)	Determines how intense the color appears. A fully saturated color is brilliant, while a less saturated color appears faded.
Saturation (pixel/voxel)	A pixel or voxel that has the highest value available. For an 8-bit image, this would be 255 and for a 12-bit image, this would be 4,095.
Segmentation	Process of dividing an image data set into regions of interest based on selection of pixels or voxels which meet the specific criteria.
Sequential imaging	A method of collecting multichannel images in which each fluorescent channel is collected separately. Hardware and software settings are changed between collection of each channel to avoid overlap or bleed-through of signal into multiple channels.
Signal-to-noise (*S*/*N*) ratio	A measure comparing the amount of signal (photons) detected and noise that is produced by the detector.
Simultaneous imaging	Set up of the operating hardware and software so that more than one channel of fluorescence is detected in a single pass of the laser(s). This results in a multichannel image but care must be taken to avoid bleed-through of one channel into neighboring channels.
Single-photon confocal microscopes	Confocal systems that use a high-intensity laser of short wavelengths as the excitation source, resulting in a single excitation photon producing an emitted photon of a longer wave-length.
Single track imaging	See "Simultaneous imaging."
Spectral imaging	Imaging mode where the available wavelengths of light are divided into several channels so that closely related fluorophores such as green and yellow fluorescent proteins can be separated. Spectral imaging is also often used to separate autofluorescence from true signal produced by a fluorophore.
Spherical aberration	Image defects introduced when light rays from the peripheral and central regions of the objective lens are focused in different planes. In confocal imaging, spherical aberrations can result in significant loss of signal from regions of the image, since out-of-focus light is eliminated by the pinhole.

Spinning disk confocal microscopes	A group of instruments that use a rapidly spinning disk with several microlenses rather than a laser scanned point by point to form the confocal image. Spinning disk systems are usually preferred for rapid or live cell imaging protocols.
Stoke's shift	The difference in wavelength from the light absorbed by fluorochrome and the light that is emitted following excitation.
Surface render	Technique used for visualizing the surface of a 3D data set. The Marching Cubes algorithm is used to segment voxels based on a threshold intensity or selected value.
Tagged image file format (TIF)	Very good uncompressed generic image format readable by most computers. The TIF format is probably the most accepted format for scientific images.
Threshold	An assignment of a particular value to a group of pixels or voxels for the purpose of image enhancement and analysis. For example, a group of pixels that fall between the values of 0 and 50 may all be assigned a value or thresholded at a value of 50.
VaLaP	A 1:1:1 mixture of petroleum jelly (Vaseline), lanolin, and histology paraffin that can be used to support and seal cover glasses for imaging.
Vital dyes	Stains that are minimally or nontoxic to living cells when used in low concentrations. Many are useful as they change emission spectra or emission intensity when the intracellular environment is altered.
Volume render	Technique used to display a 3D data set in a manner which will allow the internal structure present in the volume to be observed. Voxels are displayed after assigning transparency (alpha) values to certain voxel intensities so that less intense voxels do not hide brighter voxels.
Voxel	A discrete volume element which consists of x, y, and z dimensions. Isotropic voxels have equal dimensions in all three planes, while anisotropic voxels have different dimensions in at least one of the planes. Voxels have a 3D address within a 3D space (x, y, and z location) and an intensity value.
Wide-field fluorescence microscope	A microscope system in which fluorophores in the entire volume of the specimen are excited at the same time, and the resulting image included signal from both the focal plane of interest and the out-of-focus planes above and below the focal plane.

Working distance	The distance from the surface of the objective lens and the coverslip (or specimen if using a dipping lens) when the specimen is in focus.
Z-drop	A phenomenon resulting in loss of intensity of pixels in deeper sections of a sample due to poor laser photon penetration or ability of photons emitted from a fluorochrome to pass through the sample and be collected.
Z-series	A series of images collected through the depth of the sample. Sample depth is typically along the *z*-axis.

Index